PHOTOSPHERIC ABUNDANCE ANALYSIS OF LOW MASS PRE-MAIN SEQUENCE STARS

Thesis by

Deborah Lynne Padgett

In Partial Fullfillment of the Requirements
for the Degree of
Doctor of Philosophy

California Institute of Technology
Pasadena, California

1992
Submitted October 31, 1991

Acknowledgements

Successful completion of a Ph.D. thesis is necessarily a team effort. For this project, I have been privileged to work with people from both coasts of the U.S. (3 coasts including Hawaii!), as well as a talented observing staff in Chile. A great number of people have contributed to this effort over the years, and I am endebted to all of them.

At Caltech, I owe a great deal of thanks to Bev Oke, who first introduced me to observing at Palomar, supported me with research assistantships for several years, and has had the patience to see me through this project. Although much of Bev's most recent work involves distant clusters of galaxies, his scientific interests have been broad enough to encompass my interest in T Tauri stars as well. He is a consummate observer and instrumentalist, and I have benefited enormously from my association with him.

I am also deeply endebted to Ann Boesgaard, who has also advised me on this thesis from the beginning. Ann provided the inspiration for this project during her stay at Caltech and has continued to provide input during the entire process, including a set of incredibly detailed and useful comments on the lithium chapter. Her encouragement has been much appreciated. I am also grateful for her support in 1988 which enabled me to work at the Institute for Astronomy in Oahu for a month; I will never forget that trip or those lovely islands... Ann also introduced me to George Herbig, the father of all modern T Tauri star studies, with whom I had a most interesting discussion about the nature of the T Tauri phenomenon. Her intervention also allowed me to attend a Workshop on the Lithium Problem, which was very useful for directing my thoughts about lithium in pre-main sequence stars.

During my years at Caltech, I was very fortunate to have been awarded time at both the Palomar and Las Campanas Observatories. Observing trips have been

a highlight of my graduate career, as well as the fulfillment of childhood fantasies for a little girl who had a Tasco refracting telescope at age six. At Palomar, I thank Mike Doyle, Dave Tennant, and John Henning, who were all friendly and extremely helpful, especially at those rare instances when something went awry. I am also indebted to Fred Harris for keeping the CCDs up to snuff, and I enjoyed his good humor when I worked on Bev Oke's CCD testing project one spring. At the 60-inch, thanks go to Skip and Will, whose stories about dune buggies and pot-bellied pigs made the nights seem short. Of course, I have great appreciation for Juan, the guardian spirit of the 200-inch. It has been a privilege to work with him. Gratitude is also due to the people who made my two trips to Las Campanas so successful. I especially thank Angel, my principal night assistant in Chile, who drove me to the La Serena bus depot after a long night of observing in 1988. Las Campanas Observatory is a first class operation, and I have enjoyed observing there immensely.

Working with the folks at JPL has been another great benefit of my graduate years at Caltech. I have enjoyed the courses taught by Charles Elachi, and I am in his debt for getting me involved in the LDR project. Thanks go to Paul Swanson for making me feel like a member of the LDR design team; I hope the project goes forward soon. Being adjacent to JPL during two Voyager flybys has been fantastic. I will never forget those nights at South Mudd with Dave Stevenson and Steve Squyres doing instant science as the images rolled in. Thanks go as well to the planetary science students who have been friendly over the years: Mark Hofstadler, Bill Anderson, Julie Moses, Walter Kiefer, Rich Acterberg, and many others.

Although my interest in planetary science has been a long-term affair, living in California has given me a new and intense interest in geology. Thanks go to Bob Sharp for leading the most enjoyable course I took at Caltech and being an all-around great guy. Gene Shoemaker convinced me that at least some geologists are crazy with his rock climbing antics at Meteor Crater; he and Caroline also helped me find an asteroid, which, alas, has never been seen again. I also thank Arden Albee for leading several field trips which combined remote sensing and desert camping.

Many people in Robinson have enriched my Caltech experience. Thanks go to Wal Sargent, Jeremy Mould, Nick Scoville, and Anneila Sargent for some interesting classes and discussions. In the graduate classes prior to mine, Alain Porter was an excellent instructor for the use of the 60-inch CCD camera. John Biretta provided invaluable assistance in helping a UNIX user to adjust to VMS in the early days. Dave Hough organized the P.J. trip to Yosemite, which showed me that valley at peak loveliness in the late spring. Jim McCarthy helped me to use the echelle spectrograph he built, and Kent Budge also assisted me in learning how to observe with the 60-inch echelle. Thanks to fellow classmates Chuck Steidel (who was also a comrade at Princeton), Blaise Canzian, and Steve Myers, an O.K. guy despite his early exposure to James Van Allen. I was also fortunate to share the department with youngsters Alain Picard, Helen Johnston, Rich Rand, MingShen Han, Josh Roth, Chris Tinney, Irwin Horowitz, and Chris Wilson who accompanied me on several enjoyable trips outside of the L.A. area. Irwin also helped to motivate Karl and myself to get involved in S.E.D.S. again after the Challenger accident - thanks, Irwin. Outside of the department, Lois Banta, Bridget Jenson, and Zhou Ping Li were good roommates, and my deepest thanks go to fellow Princetonian Mark Looper for being such a good friend.

Because of my untimely contraction of Lyme Disease in 1989, I was unable to finish this thesis before arriving at my postdoctoral position at the Five College Astronomy Department. I am very much in debt to Steve and Karen Strom for their patience and useful commentary on my thesis project. Without their understanding, it would have been extremely difficult for me to finish this thesis. I also thank Susan Edwards and Tony Readhead for their encouragement during this difficult time.

My family have been extremely supportive during my graduate career. I am deeply appreciative of the love and encouragement provided by my parents, grandparents, and other relatives both before and during this thesis project.

My experience at Caltech has been most closely shared by Karl Stapelfeldt, my best friend and companion for over 11 years. Karl has been with me through every

step of the Ph.D. process, and his contributions to this work are beyond estimation. I feel incredibly fortunate to have so close a kindred spirit as colleague and husband.

To my family: past, present, and future

Photospheric Analysis of Low Mass Pre-Main Sequence Stars

Ph.D. Thesis of

Deborah Lynne Padgett

Abstract:

The atmospheres of low mass pre-main sequence stars are extremely valuable tools for probing the composition of the star-forming interstellar medium. This thesis investigation uses photospheric abundance analysis techniques to determine metal abundances both for individual weakly active T Tauri stars and the molecular clouds with which these stars are associated. Using the high resolution echelle spectrographs of the Palomar 1.5m and the Las Campanas Observatory 2.5m telescopes, high signal-to-noise ratio spectra have been obtained for 53 low mass pre-main sequence stars in six major northern and southern hemisphere star formation regions. Spectra were also taken of 14 main sequence stars with known effective temperatures and metallicity to serve as spectral standards. Equivalent widths of a large number of Fe I absorption lines have been measured, as well as lines of Ca I, Al I, V I, Ni I, Ti I, K I, and Li I. Temperature-sensitive line ratios of neutral iron and vanadium calibrated against the spectral standards are used to derive effective temperatures for 30 weak-line T Tauri stars, which are much improved over the low resolution spectral classifications found for these objects in the literature. Microturbulent velocities have also been found for 16 of the pre-main sequence stars in the sample. Several stars with abnormally high microturbulences for their spectral

type have been found.

Using these improved stellar parameters, metallicities of a large number of T Tauri stars have been determined for the first time. Abundance analyses of iron, aluminum, calcium, nickel, and titanium are performed on 30 low mass, pre-main sequence stars. In the star-formation regions of Taurus-Auriga, Orion, Chamaeleon, and Ophiuchus, which each contributed five or more association members to the young star survey, bulk metallicities have been determined. The results indicate that the current metal abundances in these clouds are near or slightly above solar values. Cloud material metallicities are then used to calibrate ultraviolet line-of-sight metal depletion studies for the Orion and ρ Ophiuchi clouds.

The final chapter of this work is a lithium abundance analysis for the entire sample of 53 pre-main sequence stars. Statistics performed on a subset of 37 T Tauri stars without veiling give a mean lithium abundance of 3.60 $\pm$ 0.07 on the logarithimic scale relative to $\log N(H) = 12$, and a few stars have derived abundances in excess of 4.0. The *mean* lithium values among pre-main sequence stars are considerably higher than the *maximum* values of 3.1 - 3.2 derived for young main sequence cluster stars, indicating that the processes of lithium destruction are quite rapid for low mass stars during the transition onto the main sequence. Although an appreciable spread in lithium abundances are found among the stars in each pre-main sequence star association, no significant difference in mean or maximum lithium abundances are seen between the clusters.

Table of Contents

Chapter I.

Thesis Introduction

T Tauri stars were first designated as a class by Joy (1945), who noted both their irregular variability and strong hydrogen emission lines as defining characteristics. Ambartsumian (1947) first suggested that T Tauri stars are extremely young low mass stars which are still contracting on their way to the main sequence. Subsequent investigations have proven that this hypothesis is correct. Probably the most persuasive evidence is the correspondance between the location of T Tauri stars above the main sequence on the Hertzsprung-Russell diagram and theoretical pre-main sequence evolutionary tracks (Cohen and Kuhi 1979). The position of the stars on these tracks suggest that most T Tauri stars are less than 10^7 years old and have masses $\leq 3\ M_{\odot}$. Another indication of youth is the fact that T Tauri stars are spatially and kinematically associated with dark molecular clouds. Figure 1 is a plot of T Tauri star location mapped over contours of photographic extinction for the Taurus-Auriga cloud complex (Herbig 1977). The presence of T Tauri stars on the cloud boundary, as well as many more deeply embedded infrared sources inside, implies that the surrounding pre-main sequence objects were formed from the cloud material. In addition, low mass pre-main sequence stars all have an exceptionally strong absorption line of neutral lithium at 6707 Å. Figure 2 compares the 6700 Å region of KM Orionis (top), a pre-main sequence star with spectral type K2, to HR 1136 (bottom), a solar metallicity main sequence K0 star. The lithium line is extremely deep in the T Tauri star and completely absent in its main sequence counterpart. Among low mass stars, a large abundance of lithium implies youth since this element is very rapidly fused into helium at the temperatures found in

stellar atmospheres. Therefore, T Tauri stars are the best stellar indicators of the lithium abundance in the interstellar medium.

Low mass pre-main sequence stars have been the subject of intense observational scrutiny during the past several decades. However, most of the attention has been directed at the most unusual members of this stellar population, the extreme or "classical" T Tauri stars (CTTS). The optical spectra of such objects are every bit as exotic as those of active galactic nuclei, with bright emission lines of hydrogen, ionized calcium and iron, and often other metallic species apparent even on underexposed spectrograms. The only spectral indication that such objects are actually stars is the presence of a stellar absorption line spectrum of spectral class G - M sometimes nearly hidden beneath the emission lines and excess non-photospheric continuum emission. Indeed, some of the most extreme T Tauri stars such as AS 353 A have long been classified as "continuum" stars since the absorption features which are ordinarily used to determine the stellar temperature are too weak to be seen except on good quality high resolution spectra (Basri and Batahla 1990). It is no surprise that such objects are considered unappealing subjects for photospheric compositional analysis!

Fortunately for the current thesis investigation, the classical T Tauri stars only account for about 1/3 of the presently known population of solar-type pre-main sequence stars (Montmerle and André 1989). The remaining objects are known as "weak-line" T Tauri stars (Strom *et al.* 1989) because their spectra show only weak emission in the hydrogen Balmer series and the Ca II H and K lines. They were originally designated as "naked" T Tauri stars (Walter *et al.* 1988), although the latter appellation is not quite correct since infrared and submillimeter observations have since shown that many of these stars do possess substantial amounts of circum-

stellar material in the form of dust (Strom *et al.* 1989; Beckwith, Sargent, and Chini 1990). Unlike the CTTS, most of which were discovered by Hα or Ca II objective prism surveys, many weak-line pre-main sequence stars have been found in X-ray images of prominent star-formation regions by the *Einstein* satellite. Their great brightness at X-ray wavelengths is thought to reflect a high level of surface magnetic activity which is similar to solar activity, although several orders of magnitude greater in scope. Despite their lack of emission lines, veiling continuum, and very large infrared excesses, WTTS lie in the same region of the HR diagram as their more exotic relatives, the classical T Tauri stars; therefore, these two sub-classes are considered to be coeval, although some of the least active WTTS are among the oldest low-mass pre-main sequence stars ($\approx 10^7$ yr old). Weak-line T Tauri stars are also found near or within dark clouds and have strong lithium resonance lines which are further indications of their youth. However, there is as yet no extensive database of high resolution, high signal-to-noise ratio spectra of weak-line T Tauri stars as there is for both northern and southern hemisphere CTTS. Line abundance analysis of WTTS absorption spectra promise insights into the composition and photospheric peculiarities of solar-type stars still contracting toward the main sequence, without the difficulty of accounting for the exotic properties of the more active PMS stars.

Figure 3 is a comparison of Palomar 60-inch echelle spectra in the 6700 Å region for the extreme CTTS AS 353 A (spectral type K2 according to Basri and Bertout 1990) and the weak-lined pre-main sequence K0 star NTTS 042417. The striking difference in absorption line depth between these two stars is due to the non-photospheric "veiling" continuum in the spectrum of AS 353 A. In addition, the CTTS spectrum has a broad He I emission feature at 6678 Å that is absent in LkCa 15. The Li I line at 6707Å is present in both spectra, although it is very

much weaker for AS 353A. Recent studies have shown that the excess or "veiling" continuum emission observed in CTTS is nearly featureless (Hartigan *et al.* 1989; Basri and Batalha 1990; Hartigan *et al.* 1991), in contrast to earlier investigations which suggested that it might be a continuous forest of chromospheric emission lines partially filling in the absorption spectrum (Finkenzellar and Basri 1987). These observations have provided further evidence for models of T Tauri star activity based on circumstellar disk accretion (Bertout 1989) rather than the theory favored in the early 1980's that required a deep chromosphere to generate emission lines and excess continuum (Calvet *et al.* 1983). In the disk activity theory, non-photospheric continuum emission originates in the high-temperature boundary layer between the slowly rotating stellar surface and an accretion disk in Keplerian rotation. Emission lines may be formed by interaction of the disk with a substantial stellar wind. Unlike the deep chromosphere model, disk accretion provides an explanation of why infrared excesses in pre-main sequence star spectral energy distributions are so often correlated with the degree of veiling (Hartigan *et al.* 1991). One implication of the disk activity theory is that T Tauri star photospheres may be analogous to those of main sequence stars in temperature structure. The deep chromosphere hypothesis predicts that T Tauri stars should have a shallower temperature gradient in their photospheres in order to fill in the stronger absorption features with emission (Basri 1988). One way to test these theories is to compare neutral iron absorption line equivalent widths of WTTS and standards of the same spectral type; if a shallow photospheric gradient is present in the PMS star, its strong iron lines will have lower equivalent widths than the main sequence counterpart. This type of analysis is performed in Chapter III. Although several researchers have already attempted lithium abundance analyses of T Tauri stars utilizing standard model photospheres (Strom *et al.* 1989; Maguzzu and Rebolo 1989; Basri, Martin, and

Bertout 1991), the current study intends to test the validity of these models by using them in an iron abundance analysis for a large number of PMS stars. Since the abundance of iron should not differ between cluster members formed from the same interstellar cloud, reasonably consistent iron abundances among WTTS in the same star forming region would provide further evidence of the normality of T Tauri star photospheres.

Weakly active T Tauri stars show promise as compositional probes of the presently star-forming interstellar medium. Although O and B stars have also been used in this capacity for elements such as carbon and oxygen (Pagel and Edmunds 1981; Rana 1991), the intense radiation field and high temperatures of such stars make abundance determinations extremely dependent on customized models and non-LTE corrections. In addition, the cosmologically important element lithium is completely ionized in hot stars and, thus, unobservable. As the youngest population of optically visible solar-type stars, WTTS photospheric abundances should provide measurements of current metallicity inside star-forming clouds. At the present time, the youngest star cluster with measured metallicities is the α Persei cluster with an age of about 3 x 10^7 yr (Boesgaard and Friel 1990). One of the goals of this thesis investigation is to determine the metallicities of several pre-main sequence star associations in order to provide a current value of the galactic metallicity, as well as the variations which may occur due to incomplete mixing of chemically enriched material into all interstellar clouds. Because T Tauri stars are still associated with the molecular clouds from which they formed, their photospheric abundances can be compared to ultraviolet line-of-sight gas phase abundances of the cloud itself in order to derive the depletion of various metallic elements onto interstellar dust grains. At the present time, all depletions are referenced to solar abundances since the actual metallicities of most clouds remain unknown.

The current lithium abundance in the interstellar medium is a matter of extreme importance to astrophysics. Because lithium was one of very few elements synthesized in the "Big Bang", knowledge of the primordial lithium abundance provides one of the very few observational constraints on various cosmologies. Although there is some question as to whether the present interstellar medium lithium abundance is primordial or enriched by galactic chemical evolution, many researchers have been in hot pursuit of the current lithium value for over a decade. However, lithium is an extraordinarily fragile element which can be fused into helium at temperatures existing in the convection zone of low-mass stars. For this reason, stars like the Sun have very little lithium remaining in their atmospheres. Generally, only the youngest solar-type stars have substantial lithium abundances as measured by the Li I λ6707 line; thus, pre-main sequence stars are the natural sites to search for the "cosmic" Population I value. Accurate temperatures and microturbulences, derived from high quality spectra of a large number of T Tauri stars in the course of the present study, will permit a comprehensive survey of lithium abundances in several star-formation regions.

The primary observational task of this thesis investigation is to obtain high signal-to-noise, high resolution spectra of a large number of T Tauri stars in several different star forming regions. Having achieved this goal (discussed in Chapter II), line ratios from these spectra will be calibrated against ratios from spectral standards to determine effective temperatures for the pre-main sequence samples with much greater accuracy than the currently available low-resolution spectral types in the literature (Chapter III). Equivalent widths of Fe I, and several other metallic species will be measured and used to derive the stellar microturbulences (Chapter III) and metal abundances (Chapter IV). Finally, all these quantities will be applied in the determination of the lithium abundances for the entire sample of pre-main se-

quence stars (Chapter V). It is hoped by this author that the current study will help to establish low mass, pre-main sequence stars as valuable compositional probes of the ISM and as the youngest solar-type cluster stars, rather than as the class of exotic objects which they have been catagorized as for so long.

REFERENCES

Ambartsumian, V. A. 1947, in *Stellar Evolution and Astrophysics*, Acad. Sci. Armenian SSR, Erevan.

Basri, G. 1988, in *The Impact of Very High Signal to Noise Spectroscopy on Stellar Physics*, I.A.U. Symposium No. 132, eds. G. Cayrel De Strobel and M. Spite, Kluwer Academic Publishers: Dordrecht, p. 345.

Basri, G., Batalha, C. 1990, *Ap.J.*, **363**, 654.

Basri, G., Martin, E., Bertout, C. 1991, submitted to A.A..

Beckwith, S., Sargent, A. I., Chini, R. S., Gusten, R. 1990, *A.J.*, **99**, 924.

Bertout, C. 1989, *Ann.Rev.Astron.Ap.*, **27**, 351.

Boesgaard, A. M., Friel, M. J. 1990, *Ap.J.*, **351**, 467.

Bonsack, W. K., Greenstein, J. L. 1959, *Ap.J.*, **131**, 83.

Calvet, N., Basri, G., Kuhi, L. V. 1983, *Ap.J.*, **277**, 725.

Cohen, M., Kuhi, L. V. 1979, *Ap.J.Supp.*, **41**, 743.

Finkenzeller, U., Basri, G. 1987, *Ap.J.*, **318**, 823.

Hartigan, P., Hartmann, L. W., Kenyon, S. J., Hewett, R., Stauffer, J. R. 1989, *Ap.J.Supp.*, **70**, 899.

Hartigan, P., Kenyon, S. J., Hartmann, L. W., Strom, S. E., Edwards, S., Welty, A. D., Stauffer, J. R. 1991, FCAD preprint.

Herbig, G. H. 1977, *Ap.J.*, **241**, 747.

Kenyon, S. J., Hartmann, L. W. 1987, *Ap.J.*, **323**, 714.

Maguzzu, A., Rebolo, R. 1989, *Mem.S.A.It.*, **60**, 105.

Montmerle, T., André, P. 1989, in *Low Mass Star Formation and Pre-Main Sequence Objects*, ESO Conf. Proceedings No. 33, ed. B. Reipurth, pp. 408-422..

Pagel, B. E. J., Edmunds, M. G. 1981, *Ann.Rev.Astron.Ap.*, **19**, 77.

Rana, N. C. 1991, *Ann.Rev.Astron.Ap.*, **29**, 129.

Strom, K. M., Strom, S. E., Edwards, S., Cabrit, S., Skrutskie, M. 1989, *A.J.*, **96**, 297.

Strom, K. M., Wilkin, F. P., Strom, S. E., Seaman, R. L. 1989, *A.J.*, **98**, 1444.

Walter, F. M. 1987, *P.A.S.P.*, **99**, 31.

Walter, F. M., Brown, A., Mathieu, R.D., Myers, P.C., Vrba, F.J. 1988, *A.J.*, **96**, 297.

FIGURE CAPTIONS

Figure 1. Positions of low mass, pre-main sequence stars plotted on contours of $A_{pg} = 1.5$ in the Taurus-Auriga molecular cloud. Galactic coordinates are indicated along the margins. Reprinted from Figure 4, Herbig (1977).

Figure 2. Comparison between Li I λ6707 spectral regions for KM Orionis (top), a K2 pre-main sequence star, and HR 1136 (bottom), a K0 main sequence standard. The lithium resonance line is extremely prominent in KM Ori, but completely absent in HR 1136 since it has fused into helium during the longer lifetime of this star. The weak line at 6707 Å in HR 1136 is probably Fe I λ6707.

Figure 3. Comparison between the 6700 Å spectral regions for AS 353 A (top), a K2 classical T Tauri star with a large non-photospheric ("veiling") continuum, and NTTS 042417 (bottom), a K0 weak-line T Tauri star with no veiling. The absorption lines of AS 353 A are much shallower than those of the weak-line star, despite the more active star's cooler photosphere.

Figure 1

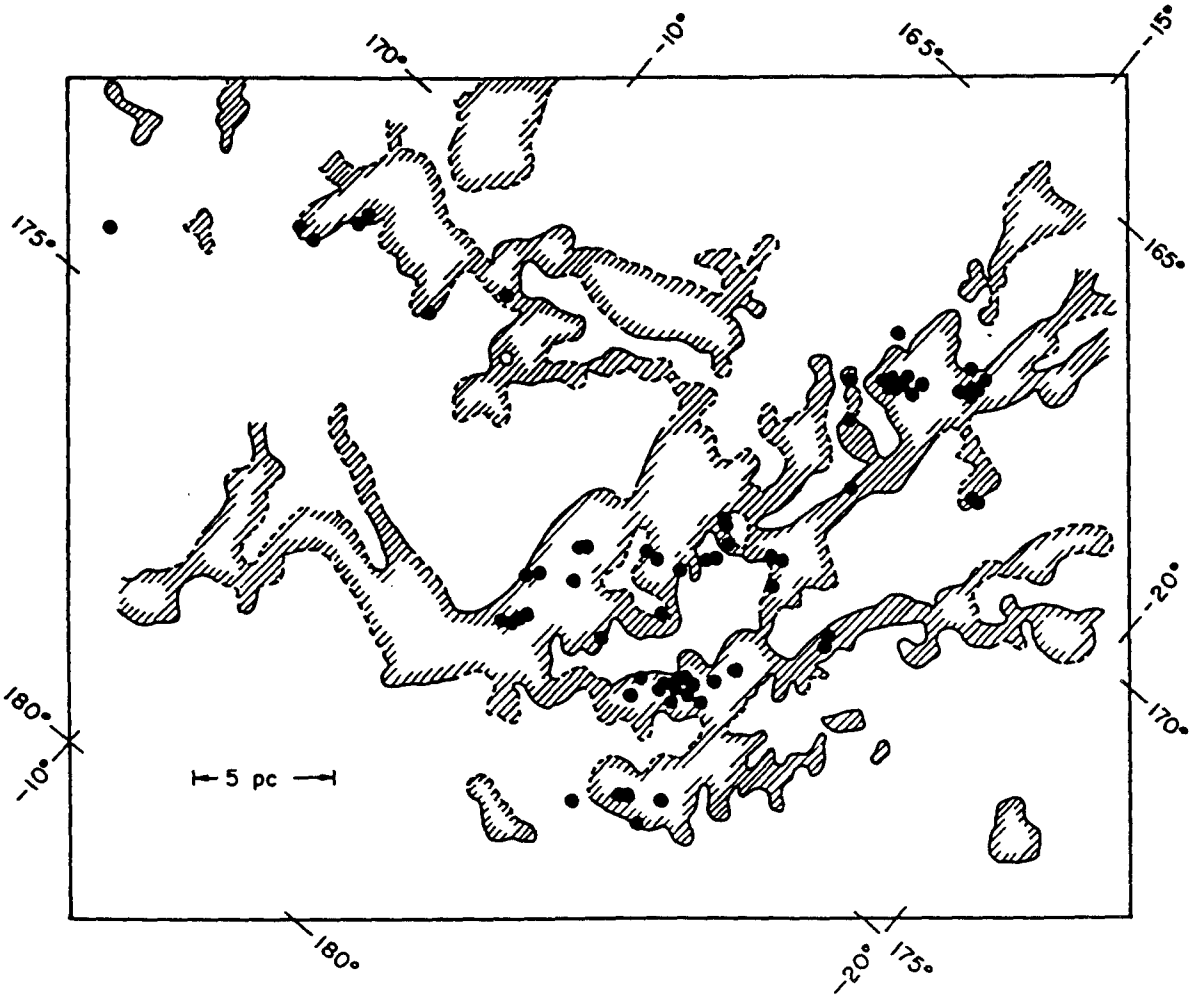

Figure 2

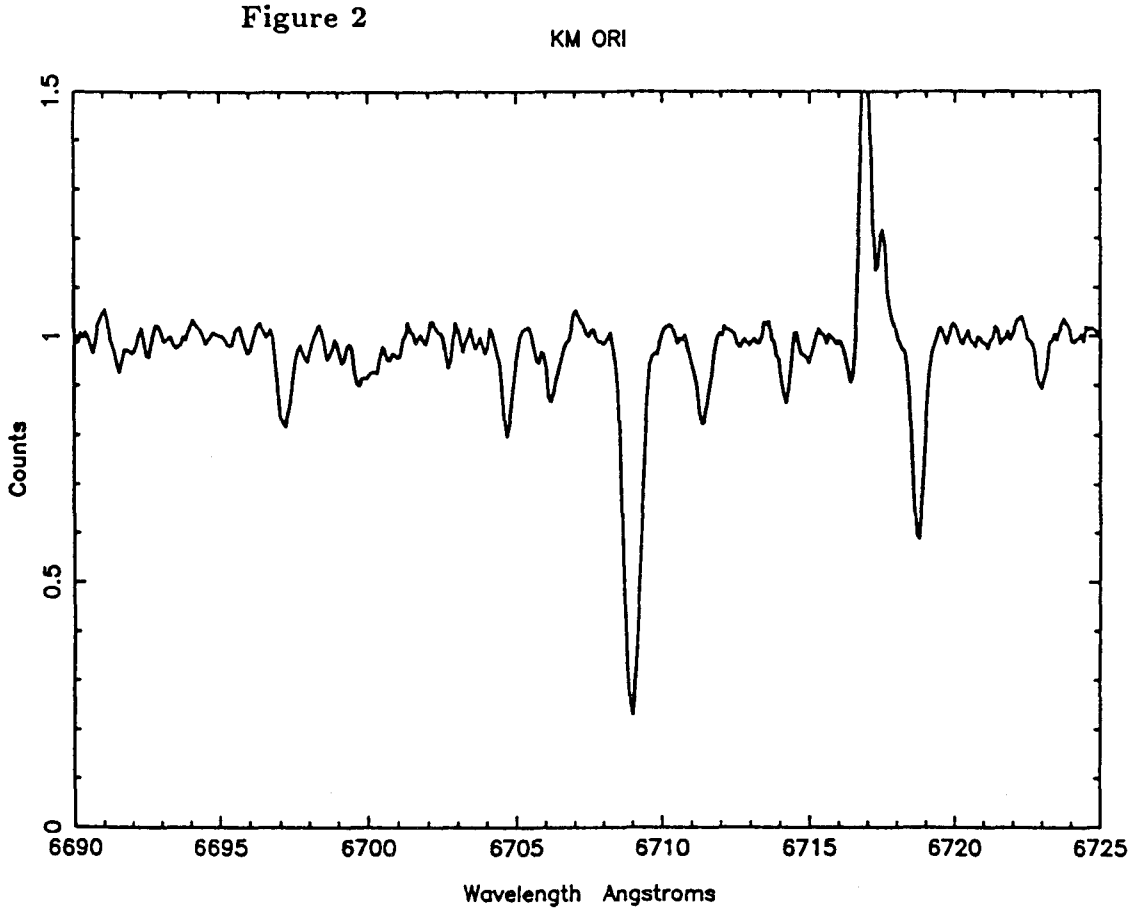
KM ORI
Counts
0
0.5
1
1.5
6690
6695
6700
6705
6710
6715
6720
6725
Wavelength Angstroms

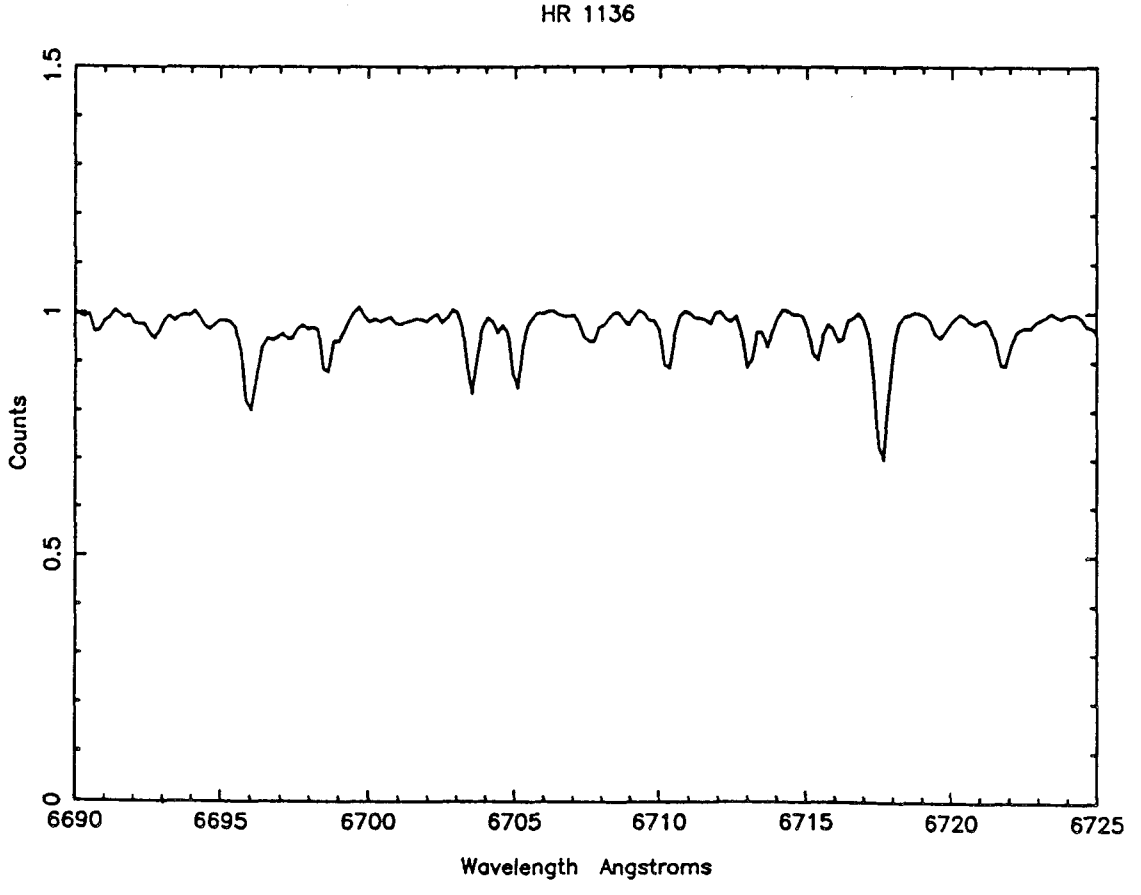
HR 1136
Counts
0
0.5
1
1.5
6690
6695
6700
6705
6710
6715
6720
6725
Wavelength Angstroms

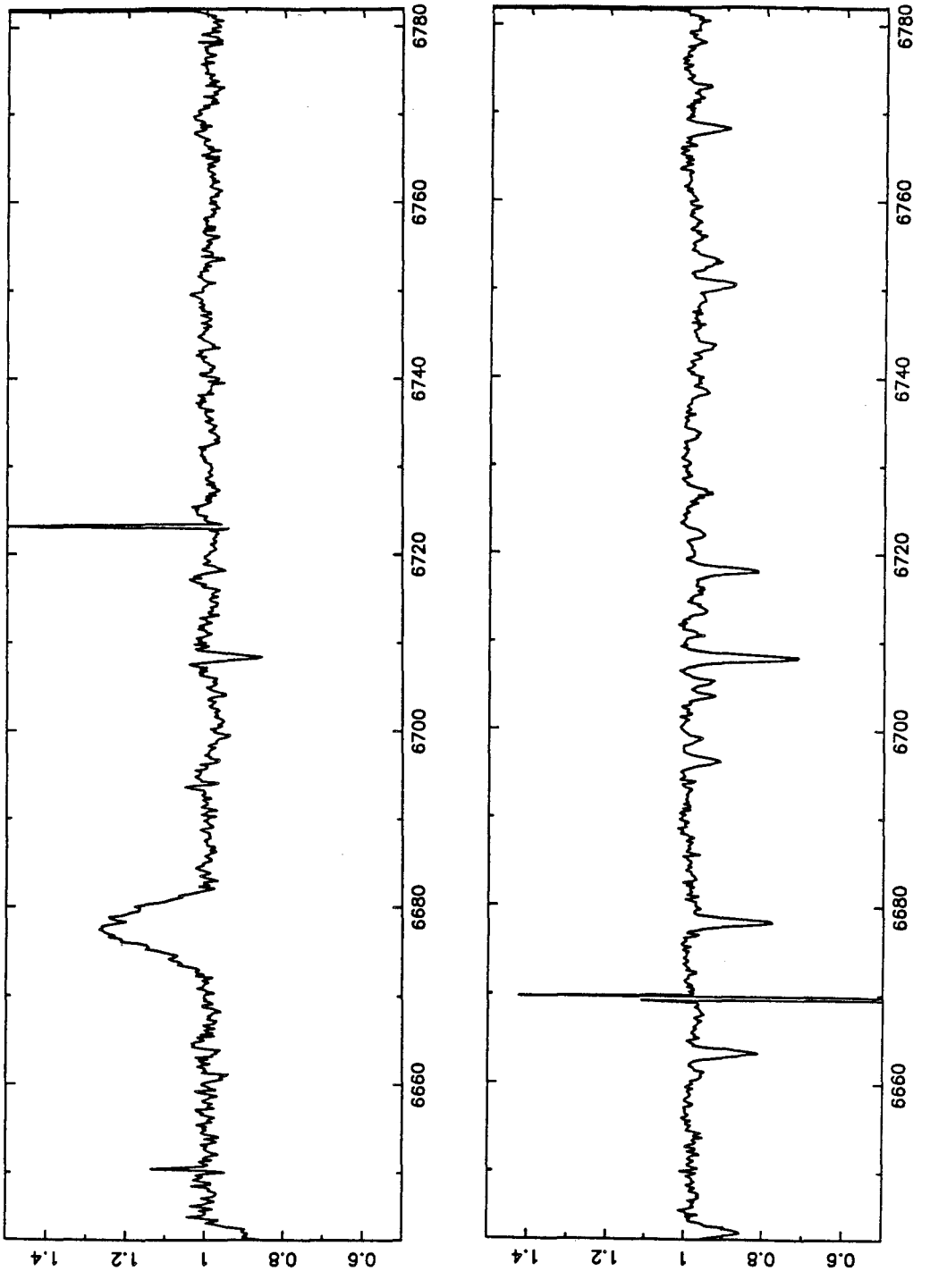

Figure 3

Chapter II.

Observations and Reductions

I. Introduction

Over the past decade, a number of moderate to high resolution spectral studies of T Tauri stars have appeared in the literature. Many have concentrated on analysis of the velocity structure and time variability apparent in the emission spectra of active classical T Tauri stars (Ulrich *et al.* 1983; Appenzeller, Jankovics, and Krautter 1983; Appenzeller, Jankovics, and Jetter 1986; Appenzeller, Reitermann, and Stahl 1988; Schwartz and Heuermann 1981; Bertout *et al.* 1982; Mundt and Giampapa 1982; Boesgaard 1984; Edwards *et al.* 1987; Cabrit *et al.* 1990; etc.). Some others are surveys of v sin i among low mass, pre-main sequence stars (Vogel and Kuhi 1981; Bouvier *et al.* 1986; Hartmann *et al.* 1986; Hartmann, Soderblom, and Stauffer 1987; Hartmann and Stauffer 1989; Duncan 1991), most of which require only low signal to noise ratio in the continuum. Only quite recently have a few high resolution, high S/N investigations of PMS star absorption spectra been published. Finkenzellar and Basri (1987), Hartigan *et al.* (1989), Hartigan *et al.* (1991), and Basri and Bertout (1990) have each presented high quality spectral data used for "veiling" continuum analysis in active T Tauri stars. Some of the spectra produced in the course of these investigations have been of sufficiently high resolution ($R \geq 2 \times 10^4$) and signal-to-noise (≥ 50 in the continuum) ratio to permit line abundance analysis of the lithium resonance line at 6707 Å, and a few such analyses have been performed using modern instrumentation (Strom *et al.* 1989b; Duncan 1991; Basri, Martin, and Bertout 1991; Maguzzu and Rebolo 1989). However, since Bonsack and Greenstein (1959), there has been only one study of elemental abun-

dances other than lithium in the atmosphere of a T Tauri star (Franchini, Castelli, and Stalio 1991). The purpose of the current observational effort was to obtain high resolution, high S/N spectra of enough PMS stars to adequately sample the abundances of metallic elements and lithium in several star-formation regions. Using the Palomar 1.5m (P60) and Las Campanas 2.5m echelle spectrographs, 53 T Tauri stars have been observed in pursuit of this goal.

II. Selection of Objects

In order to fulfill the objectives of this thesis investigation, the stars chosen for analysis were subject to a number of instrumental and scientific selection criteria. All spectra were obtained with either the Palomar 1.5m echelle or the Las Campanas 2.5m echelle spectrographs. The requirement for high signal to noise ratio data in the stellar continuum constrained the sample to stars with $m_v \leq 13$ for both instruments. The weak-line T Tauri star TV Orionis with $m_v \approx 13.5$ is the only exception to this rule, and the S/N of its spectrum is consequently lower than that of any other object in the study. The most desirable stellar subjects for line abundance analysis also have almost no broadening due to stellar rotation. Rotational broadening tends to blend weak absorption features together, resulting in a depression of the effective continuum level and thus causing underestimates of line equivalent widths for stars with large $v \sin i$ (≥ 30 km s^{-1}). Surveys of PMS star $v \sin i$ (Vogel and Kuhi 1981; Bouvier *et al.* 1986; Hartmann *et al.* 1986; Hartmann, Soderblom, and Stauffer 1987; Hartmann and Stauffer 1989; Duncan 1990) indicate that most T Tauri stars have $v \sin i \geq 10$ km s^{-1}, with the mean value around 20 km s^{-1}. An upper limit of $v \sin i = 35$ km s^{-1} was placed upon stars chosen for this study. At the time of observation, $v \sin i$ data on PMS stars in Orion and all southern sky SFR was unavailable in the literature, so many stars were eliminated

on the basis of trial spectra taken at the 2.5m Las Campanas echelle. Another requirement for the sample was that the stars have spectral types between G0 and K7 so that a grid of stellar photospheric models with effective temperatures between 4000 and 5800 K provided by Gustafsson (1988) could be used in the abundance analyses. The most important constraint used in selection of T Tauri stars for the current study is the lack of strong emission lines or photospheric veiling of any type. Prior to the utilization of X-ray surveys in locating PMS star candidates (Walter *et al.* 1988; Feigelson and Kriss 1989), objective prism plates centered around Hα were used almost exclusively to discover new T Tauri stars (Schwartz 1977). The result of this strategy was that most of the known low-mass pre-main sequence stars known prior to 1980 were of the active or "classical" type, especially the brightest members of the class. However, the x-ray studies revealed a new population of T Tauri stars with weak emission features (H$\alpha \leq 10$ Å) and no photospheric veiling: the "naked" or "weak-line" T Tauri stars. It is from the latter category that the bulk of PMS sample was chosen. The data compiled in the Herbig and Bell Catalogue of Orion Population Stars (HBC; 1988) was consulted for most of the star selections.

Another thesis objective involved observing an adequate sample of PMS stars in each of several star formation regions (SFR) in order to characterize the elemental abundances in different molecular clouds. Large separations between T Tauri star associations were desirable although observations were difficult for SFR beyond 500 pc due to the faintness of low mass stars at such distances. A few spectra were taken of stars in NGC 2264 (900 pc) and Cygnus (1 Kpc), but not enough bright objects were found in either region to fulfill the minimum "cluster size" of five PMS objects. In Lupus, one of the closest SFR (150 pc; Krautter 1989), there are very few stars with spectral types earlier than K7 and thus fitting the temperature criterion of

this study. The only star observed in that region was RY Lupi, a star famous for its quasi-periodic variability (Gahm *et al.* 1988). Spectra were also obtained for one star (AS 507) in the Cepheus SFR.

Most of the PMS sample stars are part of the Taurus-Auriga, Orion, Chamaeleon, or Ophiuchus T associations. Taurus-Auriga is perhaps the best studied of all star-formation regions due to its convenient location in the northern sky and proximity to the Solar System (160 pc; Strom, Strom, and Margulis 1989). The observational database on this region is impressively large (Cabrit *et al.* 1990; Basri, Martin, Bertout 1991; Walter *et al.* 1988; etc.). Taurus-Auriga and Lupus share the characteristic that only low-mass stars appear to be forming in the molecular cloud. However, the lack of O and B stars in these regions mean that very few ultraviolet line-of-sight studies to determine the gas phase abundances in these clouds have been attempted. Eight WTTS in Taurus-Auriga were observed for this investigation. The Orion Molecular Cloud at about 490 pc (Strom, Strom, and Margulis 1989) also has a large number of weak-line PMS stars (Parenago 1954); however, the v sin i data on these stars is less complete than for Taurus-Auriga. Lithium abundances have been derived for a large number of stars in L1641 using moderate resolution spectra (Strom *et al.* 1989a). UV depletions of metallic elements have been studied along the line-of-sight to η and π^5 Orionis (Shull 1979). Seven Orion stars are included in the PMS metallicity sample and a total of 12 were analyzed for lithium abundance. The six Chamaeleon stars observed are all associated with the Chamaeleon I dark cloud. The distance to this star-forming region is a matter of controversy in the literature. Estimated distances vary from 140 pc (Whittet *et al.* 1987) to 215 pc, the value favored by Hyland, Jones, and Mitchell (1982), Jones *et al.* (1985), and Gauvin and Strom (1991). Pre-main sequence evolutionary tracks for this cloud indicate that the stars range in age from about 10^5 to 10^7 years,

and the luminosity function appears similar to the ones found for L1641 in Orion and the Taurus-Auriga cloud (Gauvin and Strom 1991). No depletion studies are yet available for the Chamaeleon SFR. Six stars were observed in Ophiuchus, of which 5 were analyzed for metal abundances. The Ophiuchus star-forming region is located in midst of the Sco-Cen OB association (Wilking and Lada 1983). The distance to the best known part of this SFR, the ρ Oph cloud, is about 160 pc (Bok 1956; Bertiaud 1958; Whittet 1974). The PMS stars SR 9 and SR 4 are within the bounds of the ρ Oph cloud; the others observed in this survey are nearby. Like Orion, the Ophiuchus cloud complex appears to be a site of bimodal star formation (Wilking and Lada 1983). A large number of ultraviolet depletion studies have been performed in the area; the most recent is Snow, Joseph and Meyer (1986).

The list of observed PMS stars are presented in Table 1. As the table indicates, more stars were analysed for lithium abundances than for metallicity since the Li I λ6707 line is very strong in T Tauri stars and therefore is more easily measured than the weaker metal lines. The spectral classifications given in Table 1 are low-resolution spectral types catalogued by Herbig and Bell (1988) (HBC). High resolution spectroscopic temperature determinations for many of these stars are presented in Chapter III. All positions and other stellar parameters are from the HBC, except for the equivalent widths of Hα λ6562, which were measured using the techniques described in Section IV.

III. Observations

A. Palomar 1.5m echelle observations

Thirty PMS stars and 14 standard stars were observed using the Palomar 1.5m (P60) echelle spectrograph. This instrument uses an unthinned TI 800 x 800

CCD (Palomar CCD9) as detector. The spectral resolution is $\lambda/\Delta\lambda$ = 38,800 per pixel, which coupled with the 1.5 pixel FWHM of the instrumental profile yields an effective resolution of $\approx$ 26,000. Use of the 1.4" slit lowers the actual resolution to about 20,000. The CCD sensitivity is optimized for 4000 - 7000 Å. The spectral coverage extends to beyond 9500 Å, but is non-continuous past 7000 Å. Due to the redness of PMS stars, reasonable S/N was only obtained for wavelengths longer than 4600 Å for the stars in the current sample. The P60 echelle throughput is an impressive 11% at 6000 Å, which makes it competitive in speed with less efficient spectrographs on much larger telescopes (McCarthy 1988).

P60 echelle observations occurred on the nights of December 28 - January 4, 1988 and October 29 - November 4, 1988. Wavelength calibrations were performed at the beginning and end of each run using a thorium-neon arc source. At the time of observation, the arc lamp was not internally installed, so the entire instrument had to be removed for this calibration. Comparison between the thorium-argon arcs taken at the beginning and end of the run show that the wavelength calibration remained stable throughout the run. The 1.4 arcsec slit was used throughout the run. Multiple flat fields were taken and averaged once per night using an internal continuum lamp. Table 2 summarizes the results of the Palomar run, including the signal-to-noise ratio per pixel of the observations.

B. Las Campanas 2.5m echelle spectrograph

Twenty PMS stars in the Orion, Monoceros, Chamaeleon, and Ophiuchus SFR were observed with the Las Campanas 2.5m echelle spectrograph. The detector for this instrument is the "2-D Frutti", a 2-dimensional photon counting array using several image tubes to amplify the spectrum. This spectrograph is much more

sensitive in the blue than the P60 echelle, providing reasonable S/N spectra to 3700 Å; however, its long wavelength limit is 7000 Å, which excludes the neutral potassium line at 7699 Å. Depite the instrumental profile FWHM of nearly 4 "pixels" using a 1.5" slit, the effective resolution of the Las Campanas echelle is about 30,000, somewhat better than the P60 echelle. Unfortunately, this instrument is slow compared to the P60 spectrograph because of its photon-counting detector, requiring in excess of 4 times the exposure time of the P60 echelle to obtain similar S/N despite the larger telescope size. In addition, count rates are limited to less than 20000 counts/sec to avoid saturation of the image tubes. In order to avoid this problem, neutral density filters must be introduced into the optical path for objects brighter than $m_v = 11.5$. Thus, spectra of very bright ($m_v \leq 8$) spectral standards cannot be obtained with this instrument because of the limited number of neutral density filters that are available to attenuate the signal.

The Las Campanas data was collected during two observing runs: January 23 - 27, 1988 and February 21 - March 4, 1989. A single flat field was accumulated over the course of each run by exposing the detector to an internal LED. Since the image tubes are sensitive to pointing changes due to a residual magnetic field in the dome structure, the average of an internal thorium-argon arc taken before and after each spectrum was used for wavelength calibration. Table 2 also describes the data obtained with the Las Campanas 2.5m echelle.

IV. Reduction of Echelle Spectra

The echelle spectral reduction software written by Jim McCarthy (1988) for P60 echelle data was used in the initial reduction of both the P60 and Las Campanas 2.5m echelle data. These routines are an extension of the *Figaro* data re-

duction package written by K. Shortridge. Echelle spectra generally consist of a large number ($\approx$ 40) of sections or "orders" of spectra about 100 Å in length, but only cover about 4 pixels in the cross-dispersion direction. The raw orders are usually somewhat curved, especially in the case of the Las Campanas spectra which suffers from time-variable s-distortion due to the image tubes in its detector (McCarthy 1988). To rectify the echelle orders, the *Figaro* routine SDIST is used to fit the shape of about 10 interactively designated orders with a polynomial curve. The program stores the fitting data in a file called SDIST.DAT that is utilized by CDIST to "straighten" all the orders. The P60 data only required one SDIST fit per observing night to properly rectify the data; the Las Campanas 2.5m spectra needed separate fits for each exposure. The prrogram ECHTRACT was then used to flatten the spectral images, subtract the scattered light, and reduce the two dimensional spectra to an array in which the orders occupy exactly one row each. The P60 echelle images were thus reduced to 40 x 800 (# orders x pixel length of order) arrays; the Las Campanas reduced spectra are 40 x 1512. Wavelength fitting was performed with ECHARC. ECHARC requires interactive line identifications for up to 10 orders of a thorium-argon arc; using that data and a catalogue of Th-Ar emission line positions, ECHARC automatically finds many other lines (typically 1200) and produces a wavelength fit based on this information. Again, the P60 data were easily fit with this method using 5 interactively fit orders and showed no time variability in wavelength calibration, while the Las Campanas data required ten interactively fit orders to obtain a proper wavelength fit. A warning for future users is that ECHARC is very sensitive to the parameters chosen for the wavelength fit, especially for Las Campanas echelle spectra, and may require considerable trial and error experimentation before a proper fit is generated. This step was by far the most time-consuming part of the data reduction. The wavelength fits were applied

to the stellar spectra with ECHXREBIN. The final step in the initial reduction was to attempt continuum normalization using ECHYCONT and ECHXCONT. The first of these programs worked reasonably well in smoothing out large scale variations in the cross-dispersion direction. However, ECHXCONT, which was written to fit O and B star spectra with a few broad lines, proved inadequate in providing continuum fits for G and K stars with their multitude of narrow metallic lines. Therefore, the final stage of the spectral data reduction was performed using the *IRAF* data reduction package.

Continuum flattening, co-addition of spectra, and equivalent width measurements were done using the NOAO *IRAF* routines in the task *onedspec*. After extracting individual spectral orders from the 2-D *Figaro* echelle data files and reading them into *IRAF* format, the continuua were normalized using the CONTINUUM command. This routine requires a choice of fitting function (bicubic spline was chosen in this case), as well as upper and lower limits for rejection of points used in the fit. For the current set of spectra, an upper limit of 3σ and lower limit of 1.6-1.8σ yielded fits which pass through the middle of the noise in the continuum and properly reject points within absorption or emission features for use in the continuum fit. Some of these normalized PMS spectra are shown in Figure 1. *IRAF* routines were also used for co-addition of some spectra taken on different nights and for smoothing some of the noisier Las Campanas echelle data (by 1/2 x FWHM of instrumental profile). Equivalent widths were measured using the "e" command ("equivalent width") in SPLOT for isolated lines. This technique simply integrates the area underneath and between two interactively designated continuum points. The "d" command ("deblend") was utilized for slightly blended line pairs; it derives line parameters by interactively fitting the sum of gaussians to a blend. The equivalent widths of Fe I, Al I, Ca I, Ti I, and Ni I are given in Table 3 for the 30

PMS stars included in the metallicity survey. Equivalent widths of Li I λ6707 are presented in Chapter V. Figure 1 (6 pages) shows seven wavelength regions for 6 PMS stars in the current T Tauri sample. The top three spectra on each page of the figure are P60 echelle data; the bottom three were obtained with the Las Campanas echelle spectrograph. Figure 2 (4 pages) is an atlas of line identifications for the K2 weak-line T Tauri star KM Orionis. The feature identifications were made using the Ultrecht Solar Atlas (Minnaert *et al.* 1965). KM Ori has the largest equivalent width of Li I λ6707 for its spectral type of any star observed in the survey.

Theoretically, the signal-to-noise ratio in the continuum is related to the formal equivalent width uncertainty by the equation:

$$< \delta W_\lambda^2 >^{\frac{1}{2}} \simeq 1.6\epsilon(w\delta x)^{\frac{1}{2}}$$

where w $\equiv$ FWHM instrumental profile, δx $\equiv$ spectral resolution in Å per pixel, and $\epsilon \equiv (S/N)^{-1}$ (Cayrel 1988). For wδx = 0.2 Å/pixel and S/N = 100, the formal equivalent width uncertainty is about 7 mÅ. However, a much larger potential uncertainty is due to the improper placement of the continuum. This step is critical, since a 1% continuum placement error can change W_λ by 5% or more (Basri, Martin, and Bertout 1991). Normalization errors of this type can be caused by improper subtraction of scattered light, small wavelength undulations in the continuum which are improperly normalized, or simply by overlapping weak spectral features that cause the apparent continuum to be depressed relative to the actual continuum level. Although the exact magnitude of this uncertainty will vary from star-to-star, repeated observation of the same star on different nights suggests that a 12 - 15 % equivalent width uncertainty is reasonable for the current data set.

Several subsets of the observational sample of 53 pre-main sequence star spectra are utilized in the following three chapters. The 30 star sample used in the

effective temperature, microturbulence (Chapter III), and metallicity (Chapter IV) determinations consist of mostly WTTS with low v sin i and/or high S/N spectra. An expanded sample of 37 WTTS and CTTS without veiling which includes some low S/N spectra is used in the statistical lithium study of Chapter V. Finally, lithium abundances and lower limits are presented in Chapter V for all 53 stars, including some active CTTS with veiling.

V. Summary

High resolution spectroscopic observations have been obtained for 44 low mass pre-main sequence stars in six star-formation regions. The observation and reduction techniques are discussed for spectra taken at both the Palomar 1.5m echelle and Las Campanas 2.5m echelle. Sample spectrograms are plotted for 6 of the PMS stars, and an atlas of line identifications is presented for the K2 PMS star KM Orionis in the region from 5900 - 6740 Å.

REFERENCES

Appenzeller, I., Jankovics, I., Krautter, J. 1983, *A.A.Supp.*, **53**, 291.

Appenzeller, I., Jankovics, I., Jetter, R. 1986, *A.A.Supp.*, **64**, 65.

Appenzeller, I., Reitermann, A., Stahl, O. 1988, *P.A.S.P.*, **100**, 845.

Basri, G., Batalha, C. 1990, *Ap.J.*, **363**, 654.

Basri, G., Martin, E., Bertout, C. 1991, Submitted to *A.A.*.

Bertiaud, F. C. 1958, *Ap.J.*, **128**, 533.

Bertout, C., Carrasco, L., Mundt, R., Wolf, B. 1982, *AA*, **47**, 419.

Boesgaard, A. M., 1984, *A.J.*, **89**, 1635.

Bok, B. J. 1956, *A.J.*, **61**, 309.

Bonsack, W. K., Greenstein, J. L. 1959, *Ap.J.*, **131**, 83.

Bouvier, J., Bertout, C., Benz, W., Mayor, M. 1986, *Ap.J.*, **330**, 350.

Cabrit, S., Edwards, S., Strom, S. E., Strom, K. M. 1990, *Ap.J.*, **354**, 687.

Cayrel, R. 1988, in *The Impact of High S/N Spectroscopy on Stellar Physics*, I. A. U. Symposium 132, eds. G. Cayrel De Strobel and M. Spite, (Kluwer Academic Pub.: Dordrecht), p. 345-353.

Cohen, M., Kuhi, L. 1979, *Ap.J.Supp.*, **41**, 743.

Duncan, D. K. 1991a, STScI preprint.

Duncan, D. K. 1991b, STScI preprint.

Edwards, S., Cabrit, S. Strom, S. E., Heyer, I., Strom, K. M., Anderson, E. 1987, *Ap.J.*, **321**, 473.

Feigelson, E. D., Kriss, G. A. 1989, *Ap.J.*, **338**, 262.

Finkenzeller, U., Basri, G. 1987, *Ap.J.*, **318**, 823.

Franchini, M., Castelli, F., Stalio, R. 1991, *AA*, **242**, 449.

Gahm, G. F., Fischerström, C., Liseau, R., Lindroos, K. P. 1988, Stockholm Observatory preprint, submitted to A.A..

Gauvin, L. S., Strom, K. M. 1991, *FCAD* preprint.

Gustafsson, B. 1988, personal communication.

Hartigan, P., Hartmann, L. W., Kenyon, S. J., Hewett, R., and Stauffer, J. R. 1989, *Ap.J.Supp.*, **70**, 899.

Hartigan, P., Kenyon, S. J., Hartmann, L. W., Strom, S. E., Edwards, S., Welty, A. D., Stauffer, J. R. 1991, *FCAD* preprint.

Hartmann, L., Hewett, R., Stahler, S., Mathieu, R. D. 1986, *Ap.J.*, **309**, 273.

Hartmann, L. W., Kenyon, S. J. 1990, *Ap.J.*, **349**, 190.

Hartmann, L. W., Soderblom, D. R., Stauffer, J. R. 1987, *A.J.*, **91**, 575.

Hartmann, L. W., Stauffer, J. R. 1989, *A.J.*, **97**, 880.

Herbig, G. H., Bell, R. 1988 *Publ. Lick Obs.* 1111.

Hyland, A. R., Jones, T.J., Mitchell, R. M. 1982, *M.N.R.A.S.*, **201**, 1095.

Jones, T. J., Hyland, A. R., Harvey, P. M., Wilking, B. A., Joy, M. 1985, *A.J.*, **90**, 1192.

Krautter, J. 1989, in *Low Mass Star Formation and Pre-Main Sequence Objects*, ESO Conf. Proceedings No. 33, ed. B. Reipurth.

Maguzzu, A., Rebolo, R. 1989, *Mem. S. A. It.*, **60**, 105.

McCarthy, J. A. 1988, Ph.D. Thesis, Caltech.

Minnaert, M., Mulders, G. F. W., Houtgast, J. 1965, *Photometric Atlas of the Solar Spectrum*, D. Schnabel, Amsterdam.

Montmerle, T., Andre, P., 1989 in *Low Mass Star Formation and Pre-Main Sequence Objects*, ESO Conference Proceeding No. 33, ed B. Reipurth, p. 408-422.

Mundt, R., Giampapa, M. S. 1982, *Ap.J.*, **256**, 156.

Parenago, P. 1954, *Trudi Sternberg Astr. Int.*, 25.

Schwartz, R. D. 1977, *Ap.J.Supp.*, **35**, 161.

Schwartz, R. D., Heuermann, R. W. 1981, *A.J.*, **86**, 1526.

Shull, J. M. 1979, *Ap.J.*, **233**, 182.

Snow, T. P., Joseph, C. L., Meyer, D. M. 1986, *Ap.J.*, **303**, 433.

Steenbock, W., Holweger, H. 1981, *AA*, **99**, 102.

Sternik, M. 1991, private communication.

Strom, K. M., Wilkin, F. P., Strom, S. E., Seaman, R. L., 1989a, *A.J.*, **98**, 1444.

Strom, K. M., Strom, S. E., Edwards, S., Cabrit, S., Skrutskie, M. F. 1989b, *A.J.*, **97**, 1451.

Strom, S. E., Strom, K. M., Margulis, M. 1989, in *Low Mass Star Formation and Pre-Main Sequence Objects*, ESO Conf. Proceedings No. 33, ed. B. Reipurth.

Strom, S. E., Edwards, S., Skrutskie, M. F. 1989, *Cool Stars, Stellar Systems, and the Sun*, ed. G. Wallerstein, p. 275.

Schwartz, R. D., Heuermann, R. W. 1981, *A.J.*, **86**, 1526.

Ulrich, R. K., Shafter, A. W., Hawkins, G., Knapp, G. 1983, *Ap.J.*, **267**, 199.

Vogel, S. N., Kuhi, L. V. 1981, *Ap.J.*, **245**, 960.

Walter, F. M., Brown, A., Mathieu, R. D., Myers, P. C., Vrba, F. J. 1988, *A.J.*, **96**, 297.

Whittet, D. C. B. 1974, *M.N.R.A.S.*, **168**, 371.

Whittet, D. C. B., Kirrane, T. M., Kilkenny, D., Oates, A. P., Watson, F. G., King, D. J. 1987, *M.N.R.A.S.*, **224**, 497.

Wilking, B. A., Lada, C. J. 1983, *Ap.J.*, **274**, 698.

Table 1

Name	HBC	RA (1950)	Dec (1950)	m_v	$W_{H\alpha}$ Å	$v\sin i$ km s^{-1}	SpT	Li only?
Orion PMS								
AN Ori	150	05 33 14.56	-05 30 04.2	11.32	$\leq$26	hi	K0,1	Y
KM Ori	122	05 32 28.48	-05 25 07.9	11.55	4.1	12	K1	N
LL Ori	126	05 32 38.18	-05 27 13.5	11.66	47	med	K2,3	Y
LX Ori	133	05 32 45.89	-05 41 28.7	12.09	26	low	K3	N
TV Ori	147	05 33 08.55	-05 03 07.9	13.40	6.9	low	K6	N
P1270	109	05 31 19.68	-05 59 12.9	12.11	8.0	16	K1	N
P1404	113	05 31 49.28	-05 38 43.6	11.50	13	27	G5	N
P1724	452	05 32 36.51	-05 10 07.3	10.55	-	hi	G8n	Y
P2252	479	05 33 24.83	-05 06 56.7	11.52	6.6	med	G7	Y
P2441	167	05 34 22.70	-04 27 26.9	10.76	11	18	G5	N
P2494	487	05 34 42.93	-06 08 01.6	10.74	-	low	K0	Y
V466 Ori	100	05 30 34.84	-05 28 28.6	12.28	21	22	K1	Y
San 6	182	05 39 25.38	-08 01 56.7	11.85	49	low	K3,5	Y
HD245059	443	05 31 49.26	+10 05 10.9	9.82	0.5	med	K3	N
Lupus								
GQ Lup	250	15 45 58.3	-35 29 58	11.40	36	low	K7	Y
HK Lup	616	16 05 00.9	-38 56 44	12.88	27	$\leq$15	K7,M0	Y
RY Lup	252	15 56 05.0	-40 13 36	10.41	6.3	25	K0,1	N
RU Lup	251	15 53 24.3	-37 40 35	10.52	118	low	K	Y
Chamaeleon								
CS Cha	569	11 01 07.8	-77 17 25	11.63	23	low	K5:	N
CV Cha	247	11 10 53.8	-76 28 01	10.96	53	32	G8	N
SZ Cha	566	10 57 05.7	-77 01 17	11.99	2.5	med	K0	N
Sz 19	245	11 05 57.5	-77 21 50	10.68	20	32	G2	N
Sz 41	588	11 10 50.2	-76 20 45	11.60	-	low	K0	N
LHα332-20	244	10 57 50.8	-76 45 33	11.24	39	37	K2	Y
Ophiuchus								
He 3-1126	608	15 55 38.9	-22 48 46	10.5:	13	low	G5	N
SR 9	264	16 24 38.88	-24 15 23.3	11.38	8.2	16	K5,7	N
SR 4	259	16 22 54.87	-24 14 01.5	12.89	84	9	K6,7	Y
Wa Oph/1	630	16 08 14.75	-18 57 02.2	11.65	0.7	low	K2	N
Wa Oph/2	633	16 09 05.0	-18 59 12	11.65	-	low	K1	N
Haro 1-14/c	644	16 28 03.9	-23 58 12	12.29	-	low	K3	N

Table 1 (continued)

Name	HBC	RA (1950)	Dec (1950)	m_v	$W_{H\alpha}$	$v\sin i$	SpT	Li only?
Tau-Aur								
NTTS035120 NE	353	03 51 20.8	+31 54 18	12.31	-	$\leq$10	G5	N
NTTS035135 SE	355	03 51 35.0	+25 28 22	12.67	-	26	K0	N
NTTS042417	388	04 26 21.89	+24 26 30.0	10.34	-	16	K1	N
NTTS043124	407	04 31 23.7	+18 23 55	12.67	-	$\leq$10	G8	N
NTTS045251	427	04 52 51.0	+30 16 20	11.60	0.5	$\leq$10	K7	N
LkCa 15	419	04 36 18.40	+22 15 12.7	12.09	28	13	K5	N
LkCa 19	426	04 52 25.90	+30 13 10.8	10.85	0.9	19	K0	N
UX Tau A	43	04 27 09.96	+18 07 21.0	10.69	8.2	26	K2	N
BP Tau	32	04 16 08.61	+28 59 15.3	12.09	61	$\leq$10	K7	Y
DS Tau	75	04 44 39.07	+29 19 56.2	11.90	73	$\leq$10	K5	Y
T Tau	35	04 19 04.21	+19 25 05.4	9.90	43	20	K0	Y
V773 Tau	367	04 11 07.29	+28 04 41.2	10.62	0.4	hi	K3	Y
Cygnus								
LkHα191	301	20 57 17.76	+43 45 20.4	12.8	24	low	K0	N
LkHα228	295	20 22 46.22	+42 06 17.4	13.2	17	low	K1,2	N
V1057 Cyg	300	20 57 06.24	+44 03 46.4	11?	-	med	Ge	Y
Other Stars								
AS 507	741	23 18 58.99	+73 57 41.0	10?	13	med	G5,8	N
G-G 405	209	06 36 56.61	+09 01 39.3	12.38	39	low	K3,5	N
IP Mon	227	06 38 16.13	+09 35 37.1	13.19	15	$\leq$25	K3	Y
MO Mon	238	06 38 46.4	+09 29 53	13.54	53	$\leq$30	K2	Y
SS Mon	230	06 38 21.21	+10 29 34.3	12.61	17	hi	K3	Y
V360 Mon	231	06 38 21.28	+09 39 15.7	13.29	5	$\leq$25	F8e	Y
W134 A,B*	536	06 38 14.06	+09 58 12.3	12.44	-	low	G5	Y

* Double-lined spectroscopic binary.

Table 2

Star Name	Instrument	Date	Exp. Time (hours)	S/N*
Orion PMS				
AN Ori	P60 echelle	11/1/88	0.5	65
KM Ori	LC echelle	1/25/88	1.0	39
	LC echelle	2/27/89	1.0	50
LL Ori	P60 echelle	11/2/88	0.5	57
LX Ori	LC echelle	1/26/88	1.0	33
TV Ori	LC echelle	1/26/88	1.0	18
P 1270	LC echelle	1/24/88	2.5	35
P 1404	LC echelle	1/23/88	2.5	37
P 1724	P60 echelle	10/31/88	0.5	140
P 2252	P60 echelle	11/2/88	1.0	-
P 2441	LC echelle	1/24/88	3.5	42
P 2494	P60 echelle	10/31/88	0.5	-
V466 Ori	P60 echelle	11/1/88	1.0	74
San 6	P60 echelle	10/29/88	1.5	106
HD245059	P60 echelle	10/29/88	0.5	137
Lupus				
GQ Lup	LC echelle	1/24/88	1.8	-
	LC echelle	2/27/89	1.0	32
HK Lup	LC echelle	1/24/88	1.5	-
RY Lup	LC echelle	1/26/88	0.8	40
	LC echelle	2/27/89	1.0	53
RU Lup	LC echelle	1/23/88	1.0	-
Chamaeleon				
CS Cha	LC echelle	2/22/89	4.0	76
CV Cha	LC echelle	1/26/88	0.75	-
	LC echelle	2/24-25/89	3.0	88
SZ Cha	LC echelle	2/23-3/4/89	6.5	100
Sz 19	LC echelle	1/25/88	2.0	42
	LC echelle	2/27/89	1.25	30
Sz 41	LC echelle	2/24-27/89	3.5	60
LHα332-20	LC echelle	1/23/88	2.0	-
Ophiuchus				
He 3-1126	LC echelle	2/24-3/2/89	3.4	58
SR 9	LC echelle	2/26-3/4/89	4.75	66
SR 4	LC echelle	2/27-3/2/89	4.64	-
Wa Oph/1	LC echelle	2/22-3/3/89	3.6	83
Wa Oph/2	LC echelle	2/25-3/1/89	4.5	71
Haro 1-14/c	LC echelle	2/27-3/3/89	4.25	71

Table 2 (continued)

Star Name	Instrument	Date	Exp. Time	S/N*
Tau-Aur				
NTTS035120 NE	P60 echelle	10/29/88	2.0	88
NTTS035135 SE	P60 echelle	11/1-4/88	3.0	105
NTTS042417	P60 echelle	10/29/88	0.5	146
NTTS043124	P60 echelle	10/31/88	2.0	67
NTTS045251	P60 echelle	10/31/88	1.0	102
LkCa 15	P60 echelle	10/31/88	1.0	80
LkCa 19	P60 echelle	10/29/88	0.5	126
UX Tau A	P60 echelle	1/2/88	1.5	-
BP Tau	P60 echelle	10/31/88	1.7	107
DS Tau	P60 echelle	11/4/88	2.0	70
T Tau	P60 echelle	12/31/87	1.5	121
V773 Tau	P60 echelle	10/29/88	0.5	81
Cygnus				
LkHα191	P60 echelle	10/31/88	3.0	73
LkHα228	P60 echelle	10/31-11/1/88	5.0	85
V1057 Cyg	P60 echelle	10/29/88	0.75	110
Other Stars				
AS 507	P60 echelle	10/29/88	1.0	170
G-G 405	P60 echelle	11/2/88	1.0	88
IP Mon	P60 echelle	1/2/88	2.5	69
MO Mon	LC echelle	10/29/88	0.75	22
SS Mon	P60 echelle	10/31/88	1.5	22
V360 Mon	P60 echelle	10/31-11/1/88	4.0	70
W134 A,B	P60 echelle	11/2-4/88	3.7	-

* Signal-to-noise ratio per pixel. S/N per spectral resolution element is about twice the given value for Las Campanas echelle data.

Table 3

Star Name	Al I 6696	Al I 6698	Ca I 6122	Ca I 6166	Ca I 6471	Ca I 6717	Ni I 6108	Ni I 6643	Ni I 6767	Ti I 5966	Ti I 5978	Ti I 6261	Ti I 6743
Orion PMS													
KM Ori	0.103	0.070	0.396	0.144	0.209	0.194	0.115	0.195	-	0.108	0.075	0.173	0.106
LX Ori	0.118	0.046	0.400	0.108	0.172	-	0.107	0.170	-	0.079	0.097	-	0.092
TV Ori	0.127	0.097	0.567	0.077	0.161	0.289	0.079	0.272	-	0.124	0.094	-	0.195
P1270	0.120	0.053	0.348	0.130	0.171	0.182	0.092	0.132	-	0.084	0.064	0.152	0.096
P1404	0.056	0.045	0.216	0.093	0.120	0.165	0.056	0.113	-	-	-	-	-
P2441	0.066	0.042	0.186	0.070	0.114	0.165	0.061	0.108	-	0.059	-	0.099	0.038
HD245059	0.079	0.033	0.467	0.126	0.206	0.211	0.097	0.151	0.135	0.067	0.072	0.094	0.080
Chamaeleon													
CS Cha	0.121	0.053	0.656	0.142	0.192	0.226	0.106	0.109	-	0.104	0.088	0.112	0.064
CV Cha	0.117	0.048	0.330	0.096	0.127	-	0.083	0.112	-	0.084	0.081	-	-
SZ Cha	0.085	0.044	0.371	0.094	0.162	0.199	0.085	0.117	-	0.074	0.112	0.150	0.068
Sz 19	0.097	0.057	0.252	0.077	0.107	0.152	0.052	0.131	-	-	0.036	0.037	-
Sz 41	0.119	0.051	0.488	0.155	0.201	0.204	0.105	0.160	-	0.128	0.067	0.234	-
Ophiuchus													
He 3-1126	0.064	-	0.288	0.072	0.123	0.165	0.098	0.092	-	0.062	0.044	-	0.080
Haro 1-14/c	0.107	0.062	0.588	0.160	0.193	0.234	0.102	0.206	-	0.100	0.130	0.072	0.141
Wa Oph/1	0.099	0.063	0.514	0.132	0.184	0.188	0.105	0.160	-	0.065	0.097	-	0.047
Wa Oph/2	0.097	0.038	0.409	0.052	0.146	0.206	0.097	0.109	-	0.104	0.075	0.175	0.053
SR 9	0.110	0.063	0.513	0.136	0.188	0.239	0.102	-	-	0.096	0.103	0.207	0.122
Tau-Aur													
NTTS035120	0.053	-	0.204	0.079	0.114	0.135	0.037	0.091	0.091	0.033	0.037	0.031	0.024
NTTS035135	0.086	0.049	0.375	0.144	0.145	0.180	0.050	0.157	0.113	0.039	0.082	0.062	0.040
NTTS042417	0.093	0.038	0.347	0.093	0.166	0.209	0.083	0.121	0.095	0.057	0.067	0.075	0.064
NTTS043124	0.080	0.045	0.411	0.118	0.155	0.181	0.084	0.130	0.150	0.084	0.044	0.093	0.062
NTTS045251	0.114	0.066	0.797	0.183	0.222	0.303	0.094	0.157	0.160	0.145	0.140	0.238	0.126
LkCa 15	0.110	0.062	0.606	0.186	0.177	0.235	0.096	0.121	0.117	0.097	0.081	0.172	0.146
LkCa 19	0.100	0.038	0.487	0.125	0.226	0.245	0.096	0.154	0.156	0.098	0.094	0.120	0.115
UX Tau A	0.093	0.027	0.373	0.106	0.198	0.217	0.080	-	-	0.114	0.070	0.089	-
Cygnus													
LkHα 191	0.073	0.037	0.390	0.075	0.200	-	0.103	0.154	0.133	0.079	0.084	0.142	0.067
LkHα 228	0.033	0.015	0.186	0.034	0.130	0.107	0.051	0.124	0.080	0.047	0.021	-	-
Other Stars													
AS 507	0.083	0.034	0.322	-	0.108	0.214	0.090	-	0.118	0.080	0.064	0.080	0.068
G-G 405	0.081	0.038	0.380	0.082	0.176	0.196	0.095	0.173	0.108	0.101	0.071	0.079	0.082
RY Lup	0.091	0.054	0.329	-	0.145	0.193	0.099	0.100	-	0.074	0.067	-	-

Table 3 (continued)

Fe I 6056	Fe I 6165	Fe I 6173	Fe I 6187	Fe I 6200	Fe I 6219	Fe I 6229	Fe I 6246	Fe I 6290	Fe I 6335	Fe I 6336	Fe I 6393	Fe I 6469	Fe I 6581	Fe I 6703	Fe I 6705	Fe I 6726	Fe I 6750
0.100	0.067	0.153	0.105	0.125	0.171	0.083	0.189	0.123	0.196	0.190	0.235	0.080	0.040	0.075	0.079	0.070	-
0.105	-	0.138	0.097	-	0.171	-	0.185	0.088	0.209	0.177	0.238	0.093	0.062	0.083	0.062	0.083	-
-	0.082	0.102	-	0.151	0.177	0.103	0.230	0.148	0.251	0.205	0.295	0.075	-	0.082	0.055	0.107	-
0.102	0.104	0.118	0.038	0.141	0.176	0.080	0.202	0.093	0.190	0.197	0.244	0.086	0.052	0.114	0.089	0.090	-
0.070	0.058	0.075	0.078	0.098	0.091	0.061	0.196	0.082	0.151	0.160	0.209	0.074	-	0.030	0.072	0.066	-
0.062	0.079	0.105	0.054	0.095	0.104	0.041	0.135	0.076	0.134	0.122	0.131	0.080	0.020	0.037	0.066	0.056	-
0.120	0.050	0.096	0.068	0.140	0.205	0.062	0.268	0.104	0.189	0.204	0.290	0.069	0.049	0.067	0.057	0.079	0.144
0.100	0.049	0.114	0.096	0.130	0.170	0.076	0.213	0.073	0.178	0.177	0.227	0.081	0.062	0.081	0.056	0.064	-
0.093	0.066	0.067	0.071	0.096	0.137	0.069	0.135	0.067	0.144	0.163	0.216	0.067	0.041	0.073	0.077	0.054	-
0.132	-	0.097	0.036	0.042	0.152	-	0.196	0.074	0.176	0.177	0.229	0.085	0.052	0.096	0.059	0.051	-
0.081	0.033	0.087	0.040	0.077	0.086	0.055	0.186	-	0.140	0.132	0.183	0.079	0.052	0.056	0.057	0.032	-
0.092	-	0.120	0.069	0.105	0.177	0.080	0.230	0.098	0.214	0.199	0.274	0.087	0.066	0.101	0.066	0.058	-
0.076	0.056	0.116	0.085	0.094	0.107	0.051	0.181	0.109	0.145	0.212	0.134	0.091	0.061	0.066	0.043	0.044	-
0.085	0.100	0.131	0.079	0.154	0.174	0.099	0.202	0.110	0.197	0.188	0.259	0.077	0.078	0.081	0.081	0.071	-
0.086	0.030	0.132	0.088	0.168	0.164	0.058	0.220	0.112	0.217	0.237	0.224	0.067	0.079	0.087	0.071	0.062	-
0.092	0.059	0.140	0.070	0.122	0.164	0.074	0.280	0.087	0.213	0.190	0.204	0.079	0.059	0.078	0.067	0.071	-
0.088	0.117	0.128	0.088	0.134	0.162	0.097	0.209	0.115	0.184	0.218	0.241	0.078	0.112	0.077	0.061	0.073	-
0.102	0.054	0.093	0.054	0.102	0.100	0.050	0.147	0.040	0.122	0.139	0.221	0.058	0.038	0.031	0.044	0.064	0.057
0.128	-	0.098	0.075	0.126	0.120	0.083	0.203	0.090	0.179	0.197	0.238	0.085	0.047	0.039	0.051	0.079	0.076
0.137	-	0.100	0.067	0.126	0.179	0.077	0.215	0.084	0.178	0.184	0.235	0.083	0.062	0.067	0.074	0.069	0.134
0.136	0.071	0.107	0.073	0.144	0.154	0.088	0.230	0.093	0.159	0.201	0.280	0.071	0.067	0.055	0.061	0.070	0.113
0.138	0.078	0.144	0.073	0.146	0.228	0.120	0.206	0.074	0.217	0.210	0.301	0.062	0.091	0.064	0.053	0.063	0.162
0.100	0.073	0.143	0.089	0.134	0.209	0.093	0.204	0.092	0.150	0.176	0.244	0.085	0.078	0.074	0.063	0.085	0.149
0.131	0.079	0.149	0.090	0.147	0.203	0.100	0.239	0.099	0.230	0.219	0.331	0.085	0.073	0.071	0.079	0.085	0.165
0.076	-	0.101	0.043	0.116	0.154	0.113	0.160	0.130	0.175	0.191	0.239	0.108	-	0.060	0.051	0.073	0.136
0.108	-	0.133	0.080	0.188	0.164	0.105	0.220	0.072	0.175	0.195	0.274	0.086	0.063	0.054	0.064	0.090	0.105
0.061	0.045	0.072	0.037	0.079	0.090	0.035	0.150	0.067	0.094	0.106	0.177	-	0.027	0.024	0.044	0.061	0.063
0.126	-	0.094	0.110	0.136	0.198	-	0.214	0.082	0.224	0.219	0.257	0.046	0.057	0.086	0.072	0.064	0.131
0.101	0.062	0.141	0.081	0.145	0.168	0.083	0.174	0.114	0.162	0.190	0.216	0.065	0.090	0.069	0.061	0.058	0.107
-	-	0.076	0.076	0.122	0.168	0.069	0.226	0.112	0.184	0.192	0.217	0.095	0.056	0.067	0.048	0.060	-

FIGURE CAPTIONS

Figure 1. Spectra of 6 low mass pre-main sequence stars included in the current survey. The spectra are arranged with one spectral order ($\sim$ 100 Å) on each page and cover a total wavelength range of 600 Å from 6100 - 6700 Å. The top four spectra on each page are data from the P60 echelle; the bottom four were taken with the Las Campanas 2.5m echelle. Note that the spectral orders of the two instruments differ slightly. The spectral resolution of the spectra is about 0.3 Å/pixel for the P60 data and 0.2 Å/resolution element for the Las Campanas spectrograms (at 6000 Å).

Figure 2. Atlas of spectral line identifications for the weakly active T Tauri star KM Orionis for the spectral region from 5900 - 6730 Å. The star is spectral type K2 with a $v \sin i$ of about 12 km s^{-1}. The absorption feature identifications were made using the Ultrecht Solar Atlas (Minnaert *et al.* 1965).

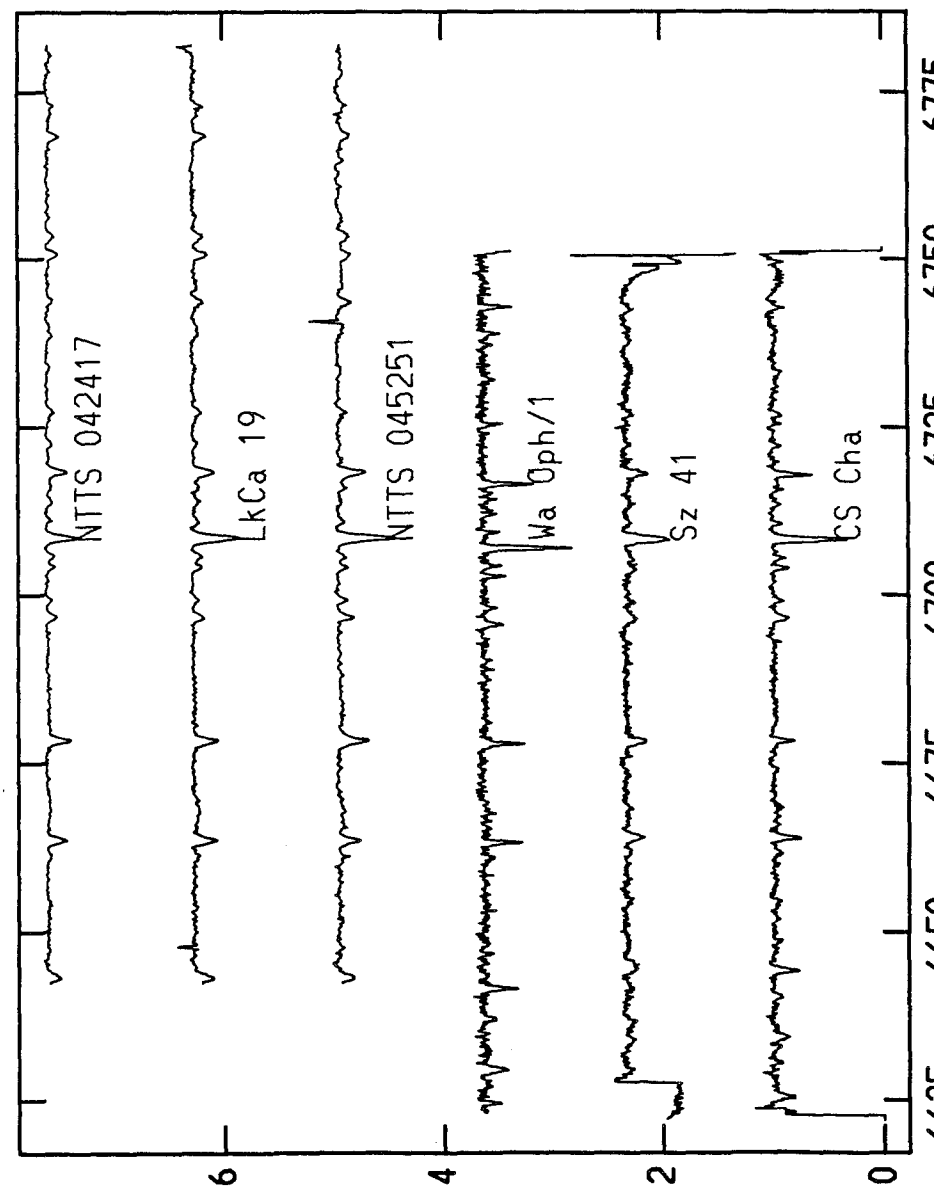
NTTS 042417
kCa 19
NTTS 045251
Wa Oph/1
Sz 41
CS Cha
6
4
2
0
6625
6650
6675
6700
6725
6750
6775

Figure 1

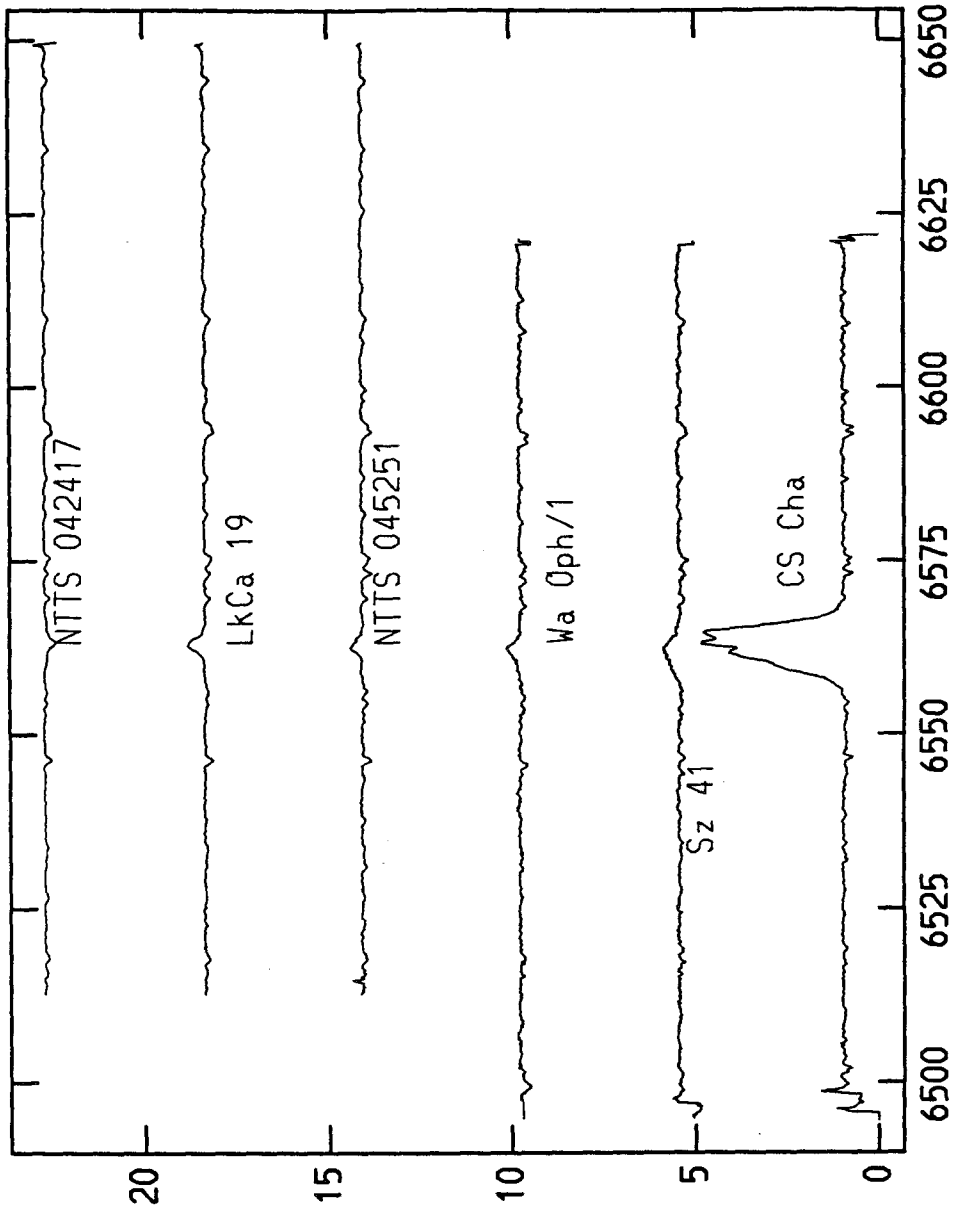

Figure 1 (continued)

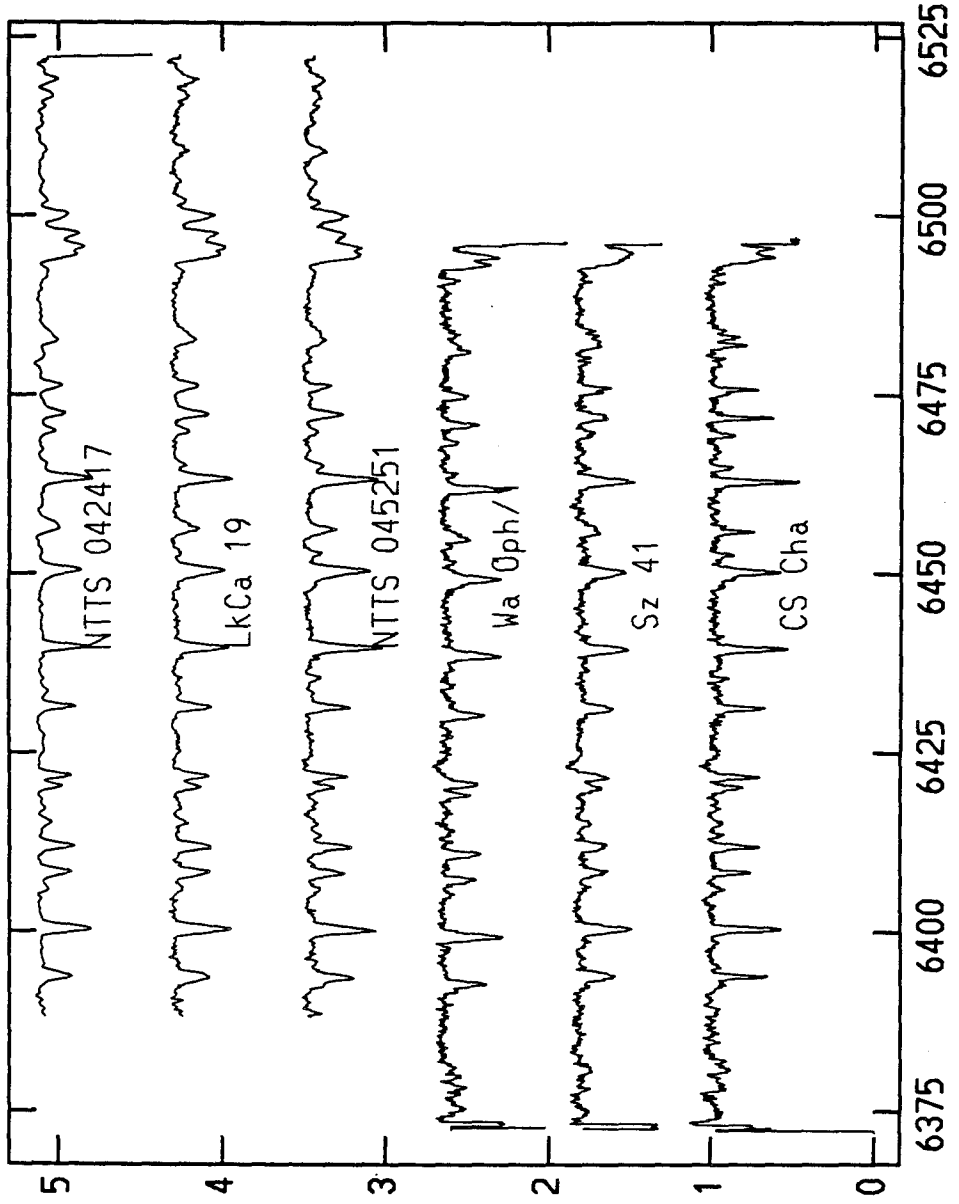

Figure 1 (continued)

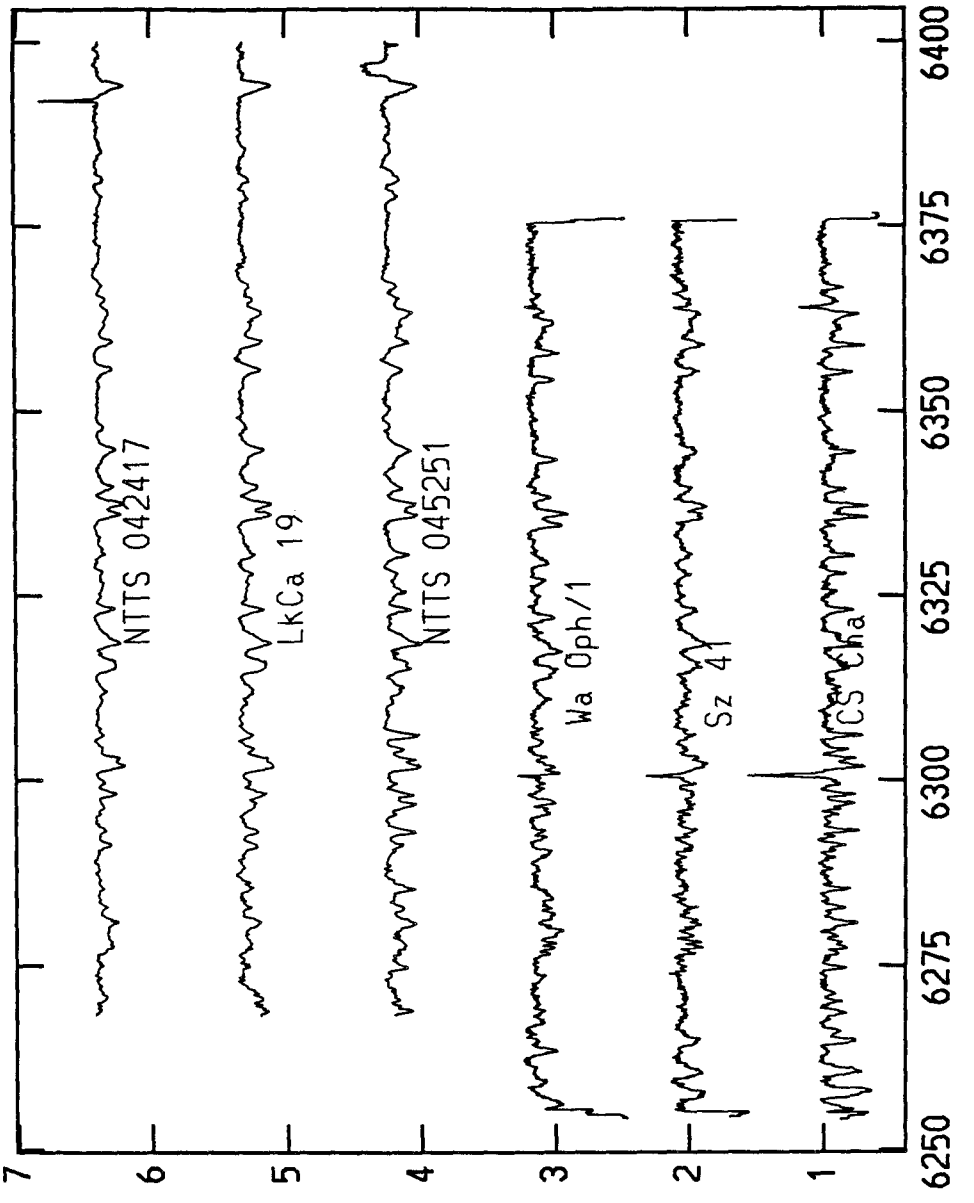

Figure 1 (continued)

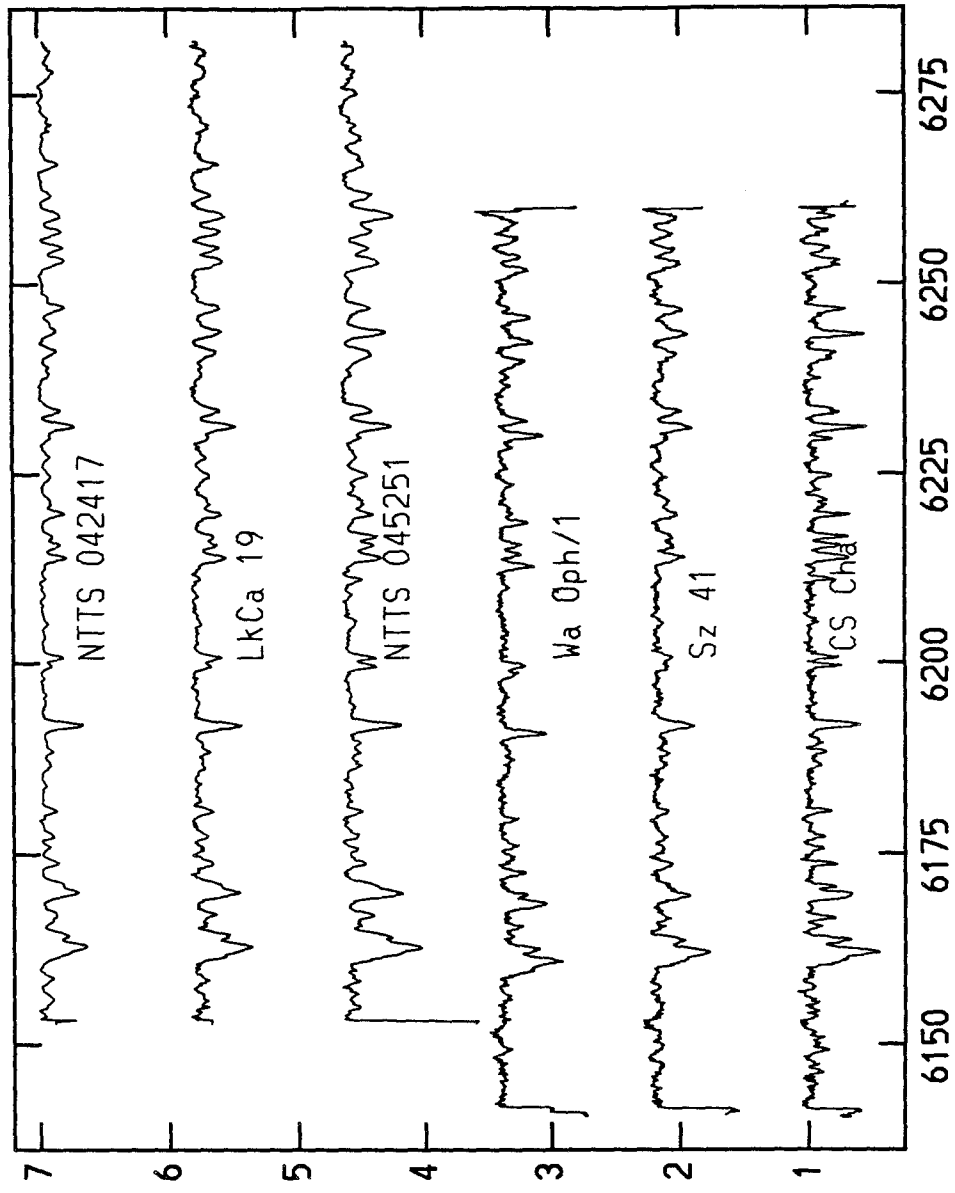

Figure 1 (continued)

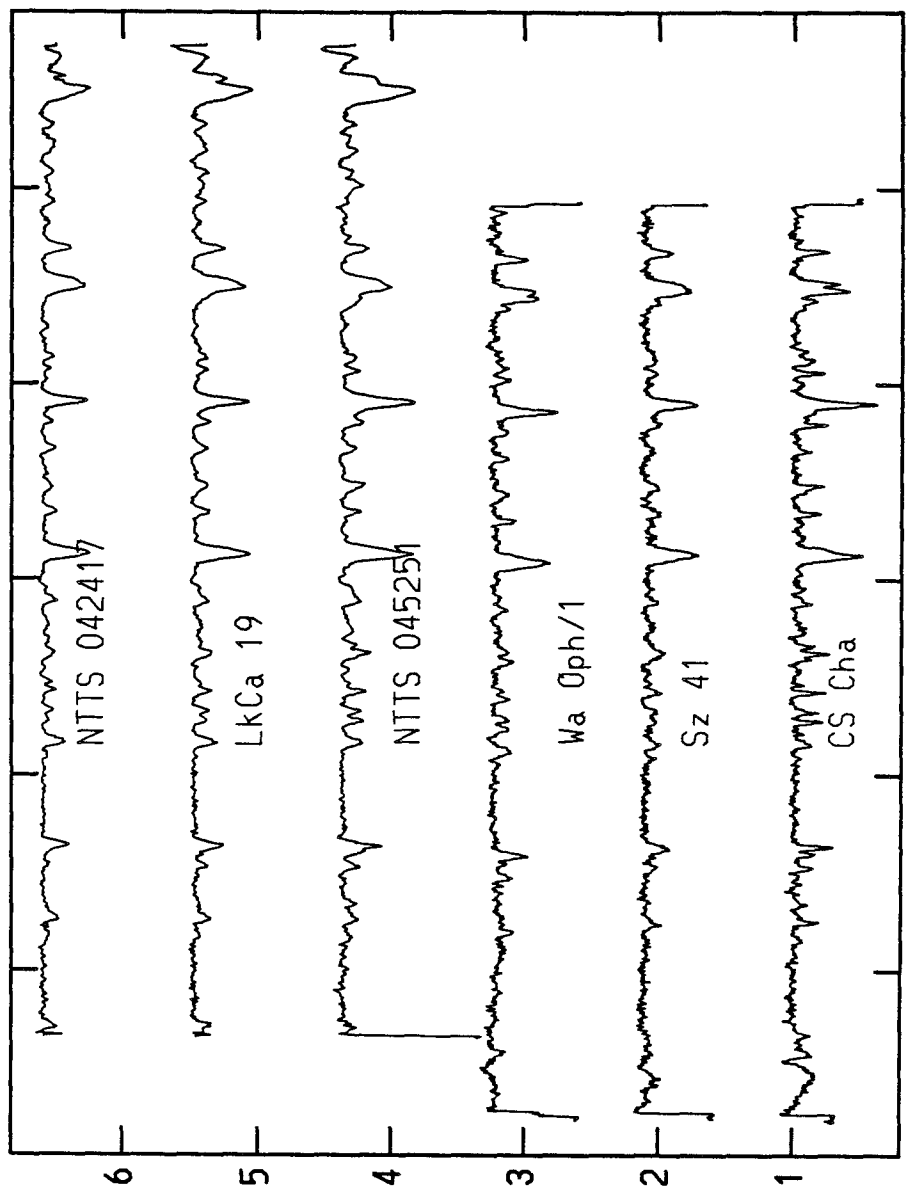

Figure 1 (continued)

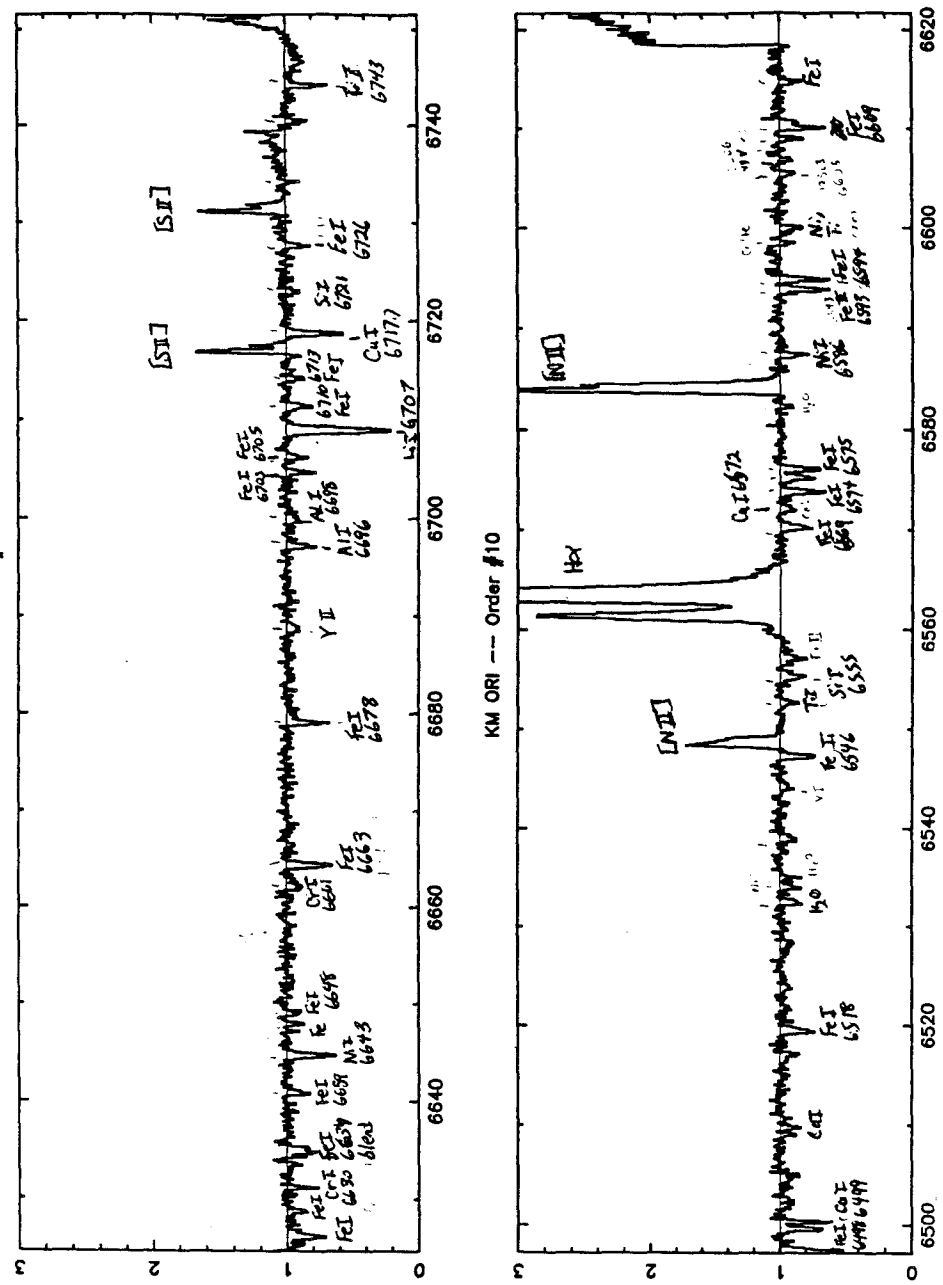
KM ORI -- Order #9
KM ORI -- Order #10
[SII]
[SII]
[NII]
[NII]
Hα
CaI 6717
CaI 6572
6640
6660
6680
6700
6720
6740
6500
6520
6540
6560
6580
6600
6620
0
1
2
3

Figure 2

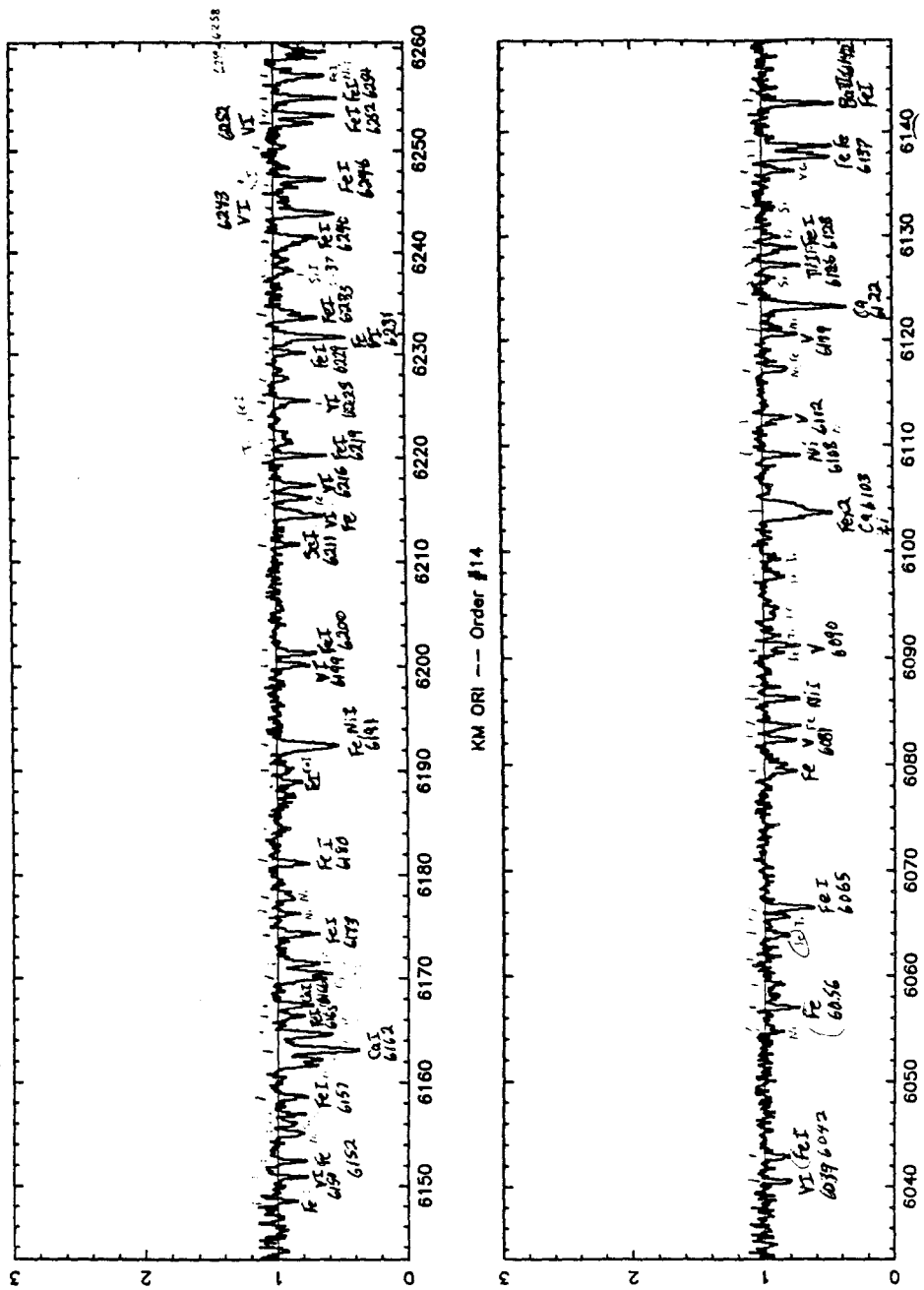

Figure 2 (continued)

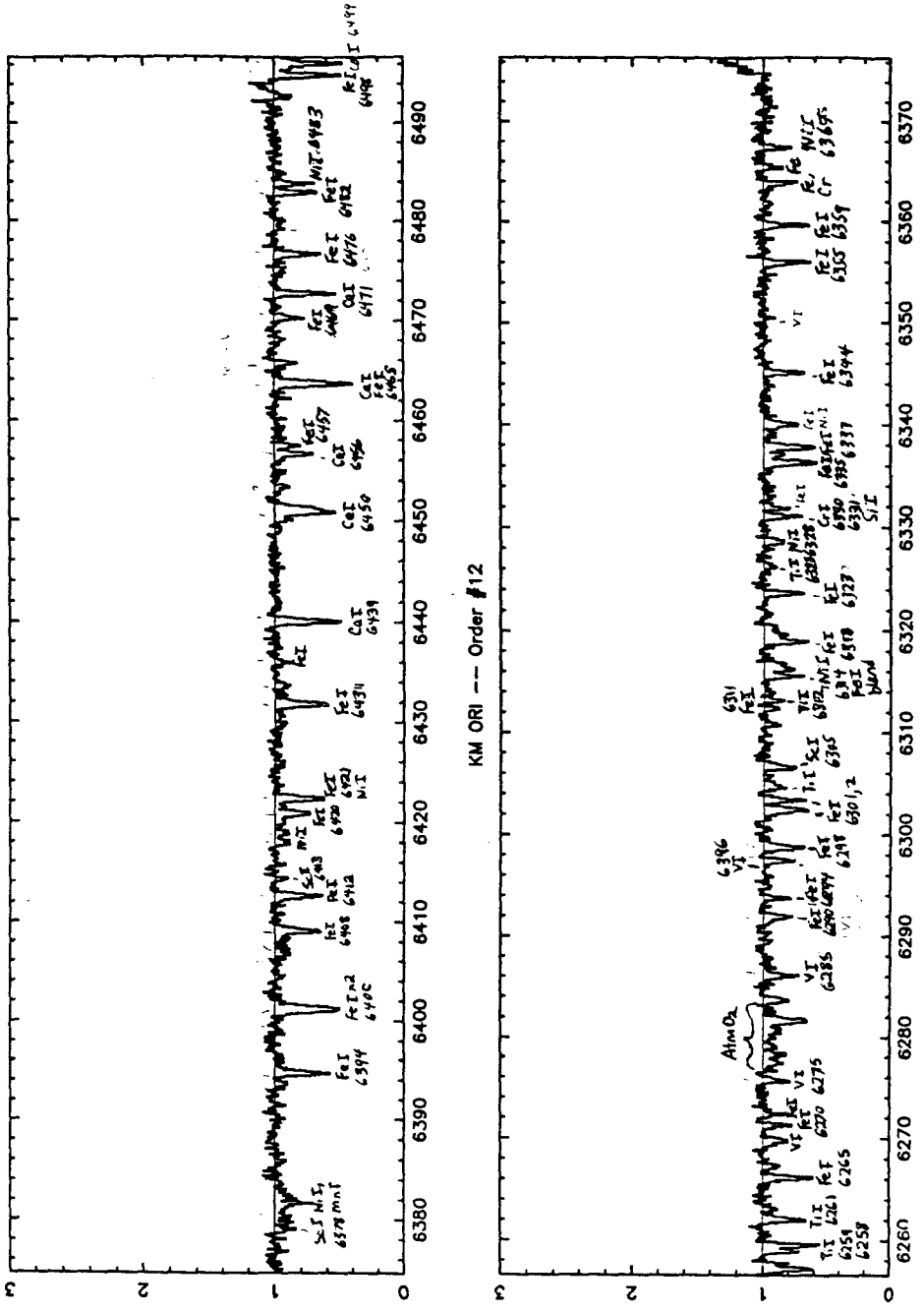

Figure 2 (continued)

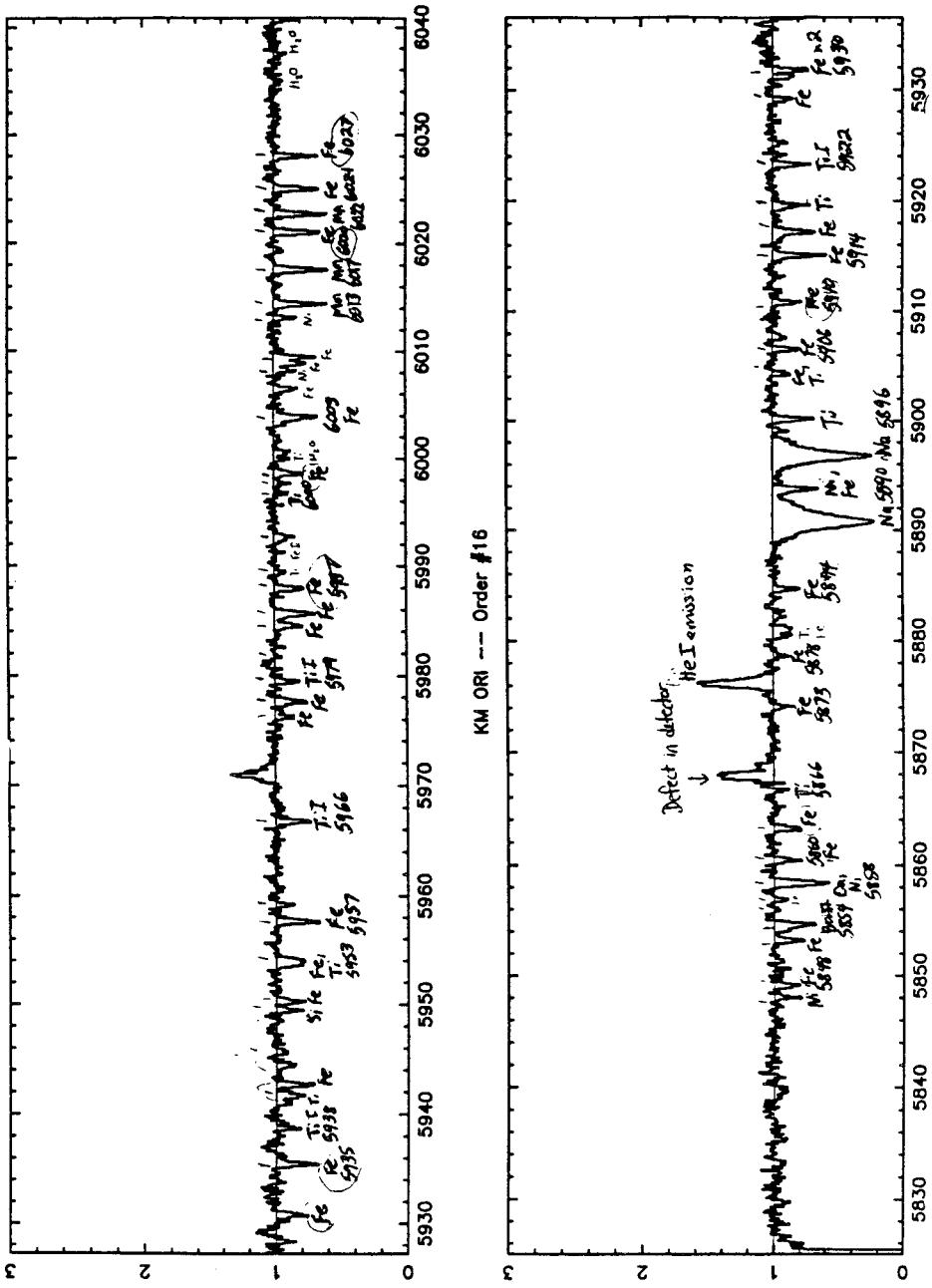

Figure 2 (continued)

Chapter III.

Atmospheric Parameters of Low Mass Pre-Main Sequence Stars

Abstract:

Using metallic line ratios from high signal-to-noise ratio echelle spectra of T Tauri stars and spectral standards, new effective temperatures are determined for a sample of 30 G - K pre-main sequence stars in five star-formation regions. Comparison of these values with previous spectral classifications using low-resolution spectra reveals large discrepancies in spectral type for some stars. Microturbulences derived for 17 "weak-line" T Tauri stars range as high as 3.2 $\pm$ 1.0 km s^{-1}; the mean microturbulent velocity of the sample is 1.69 $\pm$ 0.6 km s^{-1}. The temperature structure of T Tauri star photospheres is probed using plots of iron abundance versus line excitation potential and diagrams of neutral iron equivalent widths for PMS stars versus equivalent widths for spectral standards. These results suggest that T(τ) in "weak-line" T Tauri stars is similar to normal main sequence stars.

I. Introduction

Depite the plethora of T Tauri star spectroscopic data that has been obtained in the last few decades, little is known regarding the photospheres of these young, solar-type stars. Most of the high resolution spectral studies of the past ten years have focused on the most active members of the class, such as S CrA (Bertout *et al.* 1982; Appenzeller *et al.* 1986) and RU Lupi (Schwartz and Heuermann 1981; Boesgaard 1984). These investigations have concentrated almost exclusively upon the strong, time-variable emission lines in T Tauri (TTS) star spectra. Most of these well-studied young stars have quite complex spectra, with the Balmer lines of hydrogen in emission and often resonance and permitted metallic line emission as well. A smaller subclass of the active or "classical T Tauri stars" (CTTS) also have forbidden emission lines of [O I] and [S II] in their spectra. In addition, the photospheric absorption spectra are "veiled" by overlying continuum emission, making spectral classifications difficult or impossible at low resolution. As a consequence, the only known parameters of most T Tauri star photospheres are crude spectral types based on low resolution spectral classification (Herbig and Bell 1988), as well as surface gravities for some objects based on spectrophotometric radii determinations. (Cabrit *et al.* 1990). These data indicate that the class of pre-main sequence (PMS) objects known as T Tauri stars range over spectral types F - M and that many of these objects have surface gravities up to an order of magnitude lower than those of typical main sequence dwarf stars (*i.e.*, $R_* \approx 3R_\odot$). Since much of the T Tauri star research conducted to this point has emphasized study of the emission spectra of the CTTS as well as their spectral energy distributions (Cabrit *et al.* 1990), the importance of knowing the stellar temperature is limited quantifica-

tion of the photospheric contribution to the other sources of energy in the system. However, the use of modern solid state linear detectors capable of obtaining high signal-to-noise ratio absorption line spectra for relatively faint pre-main sequence stars opens up new possibilities for quantitative photospheric analysis of these objects. It has been discovered that the active objects are a minority of the population of low-mass PMS stars. Approximately 2/3 of PMS stars have only weak Balmer and Ca II emission, as well as prominent Li I 6707 absorption (Strom *et al.* 1989). These "weak-line" T Tauri stars (WTTS) are a population of stars coeval with the active T Tauri stars, but with photospheres that can be studied without corrections for veiling. Like the somewhat older but still young main sequence stars of the Pleiades and Alpha Per clusters (Duncan 1981; Balachandran *et al* 1989; Boesgaard and Friel 1990), weakly active PMS stars are a resource for understanding the present composition of the star-forming ISM, as well as providing insight into atmospheric processes in contracting stars.

However, even in less active low-mass PMS stars, the derivation of fundamental stellar parameters is not easy. When carrying out a compositional atmospheric analysis, effective temperatures are usually determined by relating the fluxes in certain wavelength bands to effective temperatures of photospheric models (Bell and Gustafsson 1989). For T Tauri stars, uncertainties in reddening due to possibly variable circumstellar extinction render most common color-Teff relations uncertain at best (Cohen and Kuhi 1979). In fact, low resolution spectral types are often used in conjunction with photometry to derive the extinction to these stars (Strom *et al.* 1989; Gauvin and Strom 1991). Another commonly employed means of determining stellar temperatures known as the "infrared flux method" (Blackwell *et al.* 1986) utilizes the ratio of the integrated stellar flux to the flux in an infrared band as a temperature indicator. Presence of excess IR emission from even the optically thin

disks which are thought to surround the majority of low mass pre-main sequence stars (Strom 1990) makes the IR flux method useless in finding stellar temperatures for T Tauri stars. Possible UV and optical excess from the hot accretion disk boundary layer thought to be responsible for the "veiling" in CTTS (Kenyon and Hartmann 1989; Hartigan *et al.* 1991) makes temperature determinations based on colors and fluxes especially uncertain in the more active stars. Thus, effective temperatures for solar-type PMS stars must be determined by spectroscopic, rather than photometric means. However, low-resolution spectral classification of T Tauri stars is difficult, especially in the more active stars. At low resolution, continuum veiling tends to make spectrum look hotter than it really is since it produces shallower photospheric features than a standard of the same spectral type. Resonance lines such as Na I λ5890 and λ5895 which are commonly used for MK classification are often at least partially filled by emission in CTTS. The hydrogen Balmer lines, used as temperature and gravity indicators in main sequence stars, are completely unfit for this purpose in T Tauri stars, since these lines are in emission in almost all low-mass PMS stars. However, high resolution, high signal-to-noise spectra of metallic lines in these stars provide possible solutions to the problem of accurate spectral classification. A common spectroscopic temperature determination technique known as "fine analysis" that uses the ionization equilibrium between Fe I and Fe II as an indicator of temperature is probably unusable for many T Tauri stars due to chromospheric Fe II emission which may partially fill in the photospheric Fe II lines. Curve-of-growth analysis using lines of neutral iron has also been used to determine PMS stellar temperatures (Maguzzu and Rebolo 1989) and, in one case, both temperature and microturbulence (Franchini, Castelli, Stalio 1991); however, it is a time-consuming method that typically requires extremely high S/N in the stellar continuum to be very precise. However, ratios between high and low exci-

tation lines of neutral metallic species are quite temperature sensitive, and when calibrated against relations of spectroscopic standards of known temperature, can yield effective temperatures accurate to within about 200 K. Boesgaard and Tripicco (1986, 1987) utilized this technique to determine effective temperatures for F stars lacking photometry. This method has also been used by Basri and Batalha (1990) to classify CTTS in Taurus-Auriga. The current study utilizes standard calibrated line ratios to find T_{eff} for 30 PMS stars.

Most of the previous work concerning T Tauri star photospheres has been based on low resolution MK spectral classifications. Many of these have been accumulated in a series of PMS object catalogues by Herbig and his collaborators. The first early collection of T Tauri star spectral types in the literature was the Herbig (1962) Catalog of Orion Population Stars with 126 entries. The Second or Herbig-Rao Catalog (HRC) (Herbig and Rao 1972) increased the number to 323. The third edition of this collection, the Herbig and Bell Catalogue (HBC) (1988), includes 742 T Tauri stars, weak T Tauri stars, and Herbig Ae/Be stars. All of the stars in the current sample were selected on the basis of stellar parameter information in the HBC. Cohen and Kuhi (1979) is the most comprehensive single source of T Tauri star spectral types. Using spectrophotometry of 7 Å resolution, CK used the relative strengths of resonance lines, metallic line blends, and TiO bands to classify 500 stars to a claimed accuracy of 2 spectral subclasses for K stars (a few hundred degrees). This study revised many previously assigned spectral types that were based on low dispersion, low signal-to-noise ratio photographic spectra. Improvement upon their work has been relatively piecemeal. Appenzeller *et al.* (1983) used methods similar to Cohen and Kuhi's to spectrally classify T Tauri stars in the southern hemisphere. Even some high resolution spectral studies of T Tauri stars depend upon concurrent low-resolution observations for spectral classification (Finkenzellar

and Basri 1987). New methods of spectral classification that take advantage of high-dispersion, high signal-to-noise spectra of T Tauri stars are required to better constrain the effective temperatures of these stars. The first published effort in this direction was performed by Basri and Batalha (1990), who used temperature sensitive line ratios of Fe I 6200 to Sc I 6210 and Fe I 5706 to V I 5708 to reclassify the spectral types of PMS stars in Taurus-Auriga. The current study improves upon their effort by using 4-6 line ratios calibrated against spectral standards to find the effective temperatures of 30 WTTS. At this point in time, only Franchini, Castelli, and Stalio (1991) have attempted to determine the microturbulent velocity (ξ_{mt}) in the atmosphere of a T Tauri star; they found $\xi_{mt} = 1.6 \pm 0.2$ km s^{-1} for Sz 19 using an empirical curve-of-growth for Fe I. Using an alternate method involving the minimization of scatter among Fe I abundances determined from several lines (Smith, Edvarsson, and Frisk 1986), the current study attempts to constrain the microturbulent velocity for the stars in the WTTS sample.

This chapter presents temperature and microturbulence determinations for 30 low and moderate activity PMS stars in several northern and southern star-forming regions. Section IIA discusses the method and results of applying line ratio temperature analysis to the PMS sample. Using 4-6 ratios of Fe I lines to V I lines calibrated against 13 spectral standards, the effective temperatures of 30 WTTS have been found with a one sigma uncertainty of less than 200 K in most cases, as compared to the $\pm$ two spectral subclass (330 K) uncertainty in previous determinations. Section IIB discusses two empirical techniques for comparing the temperature structure of WTTS to normal main sequence standards and presents the results of these methods as applied to the young star sample. Section IIC describes the technique used to place limits upon the microturbulence parameter and presents the microturbulent velocities found for 16 stars in the study. In Section III, the results

of these atmospheric investigations are discussed in the context of the normality of TTS photospheres and the controversy over the origin of TTS activity.

II. Analysis and Results

Thirty pre-main sequence stars and 14 spectral standards were observed with the echelle spectrographs at the Palomar 1.2m and the Las Campanas 2.5m telescopes. A resolution of 2 x 10^4 was obtained at Palomar with a spectral coverage of 4600 Å to 9600 Å using an 800 x 800 pixel TI CCD as the detector. The Las Campanas spectra have slightly higher resolution, but a shorter spectral range (3700 Å to 7000 Å) with the 2D-Frutti detector. Further details of the object selection, observations, and reductions are found in Chapter II.

A. Temperature Determinations

i) Spectral Standards

The current study uses metallic absorption line ratios to determine the spectral classification of 30 low-mass, pre-main sequence stars. In order to calibrate the ratios against effective temperature, thirteen spectral standards ranging in type from G1.5 to K7 were selected from the list of Bell and Gustafsson (1989). The Sun was also used as a spectral standard. The surface gravities of T Tauri stars are known to be lower than those of main sequence dwarfs, causing them to be classified as luminosity class IV; unfortunately, there are very few bright, solar metallicity subgiants with well determined temperatures in the lists of standards. Therefore, 11 of the chosen spectral calibration stars are luminosity class V, and only 3 (HR 1136, HR 6623, HR 7957) are subgiants. The work of Basri and Batalha (1990) in determining veiling for a number of Taurus-Auriga CTTS suggests that dwarfs are a

better match to the spectra of T Tauri stars than subgiants in any case. Unlike Basri and Batalha, who used Hyades dwarfs with presumably identical metallicity and moderately well determined temperatures as spectral templates for their analysis of TTS properties, the current study has chosen to calibrate temperature scales using a group of stars with diverse metallicities ($-0.3 \leq$ [Fe/H] $\leq +0.3$), but extremely well-determined temperatures.

Recent photometric temperature determinations for all of the chosen spectral standards have been obtained by Bell and Gustafsson (1989). In their paper, new color-temperature scales were derived using grids of line-blanketed theoretical models of solar-type stars. Temperatures were determined for 95 G and K stars of class II - V from the 13-color Johnson *et al.* (1975) and *JKL* photometry. Bell and Gustafsson also found temperatures for these stars using the "infrared flux method" which utilizes the ratio of the integrated stellar flux to the flux in an infrared band to indicate the stellar temperature. The Bell and Gustafsson effective temperatures of the standards are considered to be accurate to about 50 K. The stellar parameters of the objects chosen as standards for the current study are in Table 1. The Sun is also used as a standard throughout the current pre-main sequence star analysis. Equivalent widths for the relevant solar spectral lines are taken from Grevesse (1984). The solar effective temperature is assumed to be 5775 K.

Spectroscopic observations of the standards were obtained using the Palomar 60-inch echelle spectrograph (McCarthy 1988). For these very bright stars, signal-to-noise ratio of the spectra is typically in excess of 150. Continuum levels were set using the IRAF routine *continuum*, and equivalent width measurements were made using the measuring routines in *splot*. Deblending of some close line pairs (*e.g.*, V I λ6199, Fe I λ6200) was accomplished with the "d" ("deblend") function in IRAF's

splot package.

ii) Line Ratios

The present investigation uses line ratios to constrain the effective temperatures of T Tauri stars. The high spectral resolution of our observations allow utilization of pairs of individual neutral metal lines to determine temperature; previous low resolution studies (Cohen and Kuhi 1979) relied upon complicated metallic blends for spectral classification. The ratios of equivalent widths for absorption lines of widely differing excitation are quite sensitive to temperature variations. Using the LTE line abundance analysis program RAI10 (courtesy of M. Spite via A. Boesgaard) to generate theoretical equivalent widths for the (slightly blended) Fe I λ6200 and the V I λ6199 lines over a range of stellar effective temperatures, it is found that the predicted ratio of this line pair changes by a factor of ≥ 2 over a change in effective temperature of 1500 K. Figure 1 illustrates the variation of the λ6200 to λ6199 line ratio observed among 8 spectral standards as the effective temperature increases from 4500 K (HR 8086; K7 V) to 5840 K (HR 2047; G0 V). Previous uses of high-resolution line ratios for temperature determination include Boesgaard and Tripicco (1986) in which the Fe I λ6705 to Fe I λ6703 ratio was used to find the temperatures of several double-lined spectroscopic binaries; Boesgaard and Tripicco (1987) utilized Cr I λ6748 to Fe I λ6750 and Cr I λ6748 to Fe I λ6752 in addition to 6703/6705. Basri and Batalha (1990) were the first to apply the technique in spectral classification of PMS stars, utilizing the ratios of Fe I λ6200 to Sc I λ6210 and Fe I λ5706 to V I λ5708 to determine effective temperatures for Taurus-Auriga TTS. In all three studies, the relation between effective temperature and line ratio was calibrated using the ratios of stars with photometrically determined effective temperature. In the current study, the strategy for temperature determination is

to find several line ratios with roughly linear temperature dependences and use linear regression to fit the temperature versus ratio data derived from the 14 spectral standards. The empirical relation between ratio and T_{eff} for each line pair is applied to the equivalent width ratios measured for the PMS sample to determine the "ratio" temperature. The average of all the ratio temperatures for each star has been adopted as the effective temperature, and the standard deviation between the ratio temperatures is given as the formal uncertainty for T_{eff}.

Many ratios between Fe I lines of different excitation were tested as possible temperature indicators. However, only the ratio of Fe I λ6705 to Fe I λ6703 was found to be suitable; even so, the weakness of these two lines made their accurate measurement difficult in stars with large v sin i or low signal-to-noise ratio spectra. Therefore, it was decided in the current study to use lines of different neutral elements (iron and vanadium) for most of its ratios. According to Gratton and Sneden (1988), [Fe/V] = 0.0 for low mass disk stars with metallicities above [Fe/H] = -0.5; thus, it is assumed that differential enrichment of iron and vanadium in stars of differing metallicity will not affect the results. The line ratios selected are as follows: V I λ6199 (Excitation Potential(EP) = 0.29 eV) to Fe I λ6200 (EP = 2.61 eV), Fe I λ6200 to V I λ6216 (EP = 0.28 eV), V I λ6119 (EP = 1.06 eV) to Fe I λ6200, V I λ6119 to Fe I λ6219 (EP = 2.20 eV). Additional ratios used for some stars were Fe I λ6705 (EP = 4.61 eV) to Fe I λ6703 (EP = 2.76 eV) and Fe I λ6042 (EP = 0.0 eV) to V I λ6039 (EP = 1.06 eV). All of the pairs are found in either the same (6199/6200, 6200/6216, 6703/6705, 6039/6042) or adjacent echelle orders. The major uncertainty in measuring the equivalent widths is accurate placement of the continuum; however, this problem does not affect line pairs within the same order since errors in continuum placement generally affects the entire order equally. For the two ratios in which the line are selected from different orders (6119/6219,

6119/6200), the 10 mÅ uncertainty assumed for the equivalent width measurements translates to an $\approx$ 0.1 uncertainty in the ratio. The plots of T_{eff} versus equivalent width ratio for the 13 Bell and Gustafsson (1989) standards and the Sun are shown in Figure 2a) - 2e) for all ratios except λ6042 to λ6039. The line drawn through the points is the linear regression fit to the data. Parameters of the linear fit to each ratio-T_{eff} relation are contained in Table 2. The uncertainties attached to both the slope and y-intercept indicate the quality of the linear regression model in fitting the available data points. Because of the relatively small number of standards used in the fit, these uncertainties are probably underestimates. The implied temperature error due to the fit parameters is on the order of 20 K for most of the ratios, although it ranges as high as 75 K in 1 case (6703/6705).

The effective temperatures derived for 30 low-mass, PMS star in Taurus-Auriga, Orion, Chamaeleon, Ophiuchus, and other regions are presented in Table 3. Columns 2 - 4 and 6 contain the ratio temperatures determined using a linear regression fit to the T_{eff} versus line ratio data for 13 G and K standards. Column 5 contains temperatures derived by comparing the TTS ratios of V I 6039 to Fe I 6040 to those of the standards; for this particular line pair, interpolation of temperatures for a given ratio value is by eye since linear regression did not provide an appropriate fit to the temperature/ratio relation. Column 7 is the mean of the individual ratio temperatures and is also the value adopted as the effective temperature for each PMS star. The standard deviation of the ratio temperatures is also contained in column 7. The average standard deviation for the 30 stars is about 160 K, with values ranging from 50 K to 300 K. The size of the temperature uncertainty is highest for stars with large v sin i and low S/N spectra (*cf.* Table 2 Chapter II).

B. Photospheric Temperature Structure

In order to provide some confirmation of the normality of T Tauri star photospheres, neutral iron lines with a variety of equivalent widths and excitation potentials have been used to probe the temperature structure of the line-forming regions in WTTS photospheres. The current study has explored the merits of two strategies to accomplish this goal. The first involves plotting many WTTS iron line equivalent widths versus the equivalent widths of the same lines measured in a standard of the same spectral class. The "deep chromosphere" theory of T Tauri activity postulated that the photospheric temperature gradients of TTS are shallower than $T(\tau)$ in normal main sequence stars (Calvet *et al.* 1983). According to Finkenzellar and Basri (1987), the cores of the stronger absorption lines are formed at lower optical depth than weak lines; thus, stars which have an unusually large radial increase in the source function will have their intrinsically stronger lines partially "filled in" by chromospheric emission. Finkenzellar and Basri demonstrated this effect by dividing their T Tauri star spectrum by a template standard spectrum, leaving a residual "pseudo-emission" spectrum. A plot of many iron line equivalent widths for a T Tauri star versus the equivalent widths for a main sequence standard of the same spectral type will also provide evidence of line "filling" (see Figures 3 and 4). In these diagrams, temperature structure variation between a PMS star and a standard will manifest itself as a divergence of points away from the line of equal equivalent width towards the side of the standard star; the divergence increases as the intrinsic line strength increases. In other words, the ratio of W_λ(TTS) to W_λ(standard) decreases for increasing line strength since strong lines are filled with chromospheric emission. If the temperature structure is the same for the pre-main sequence and main sequence star, $W_\lambda(\mathrm{TTS})/W_\lambda(\mathrm{standard}) \approx 1$ for both weak and saturated absorption lines. A second technique for detecting discrepancies in PMS

T(τ) is to plot the abundances derived for several neutral iron lines versus the lower excitation potentials of the lines. In this case, the effect of

$$\frac{dT}{d\tau}(TTS) \leq \frac{dT}{d\tau}(model)$$

should be to depress the derived abundance for lines of lower excitation that are formed high in the photosphere. However, this method of finding T(τ) abnormalities is quite difficult since the stronger lines with low excitation potential are also those most affected by microturbulence effects. Underestimating the microturbulence in these stars tends to increase the derived abundances from the stronger lines, thus possibly cancelling out the effects of chromospheric filling in these lines. For this reason, the results of the [Fe/H] versus excitation potential plots are not discussed at length.

Unfortunately, factors other than differential photospheric temperature structure may have an impact on these empirical plots. In Figures 3 and 4, the line through the plot origin indicates the case in which the Fe I lines of the standard and PMS star are equal in strength. Figure 3a and 3b are theoretical calculations using RAI10 which show the impact of changing single photospheric parameters on the equivalent width[2] plots. Figure 3a demonstrates the effect that a spectral type mismatch of 200 K will have on the log W(FeI)$_{TTS}$ versus log W(FeI)$_{standard}$ plot. For a small effective temperature discrepancy, the data points are only slightly offset from the line of equal W(FeI). However, as the difference in spectral type between the TTS and standard increases, the scatter of the points will increase due to the differences in temperature sensitivity between the lines, and the locus of data points will be offset towards the star with lower temperature. Because of this effect, plots of this type can be used as an instrument of crude spectral classification. Log W(FeI)$_{TTS}$ versus log W(FeI)$_{standard}$ diagrams for the star LkHα 228 helped to

confirm that the spectral type is much earlier than previous spectral classification had indicated. Since iron lines with large equivalent widths are included in these diagrams, differences in microturbulence between the PMS star and the standard will also have a line strength dependent effect, as shown in Figure 3b. Here the effect of doubling the microturbulence from 1.8 km s^{-1} to 3.6 km s^{-1} has a dramatic role in increasing the line strengths in the star with higher ξ_{mt} even though all other parameters are identical between the two models. In this case, the stronger lines will probably belong to the TTS since they are expected to have greater microturbulence than less active main sequence standards (Steenbock and Holweger 1981). Veiling and abundance differences would each have similar effects on the Log W(FeI)$_{TTS}$ versus log W(FeI)$_{standard}$ plot, causing a displacement in the y-intercept, but not the slope of the line fitting the data points. The effects of veiling and abundance disparities are easily distinguished from temperature structure discrepancies; effective temperature and microturbulence mismatches are not. Another effect which can add scatter to this plot is a discrepancy between the v sin i of the PMS star and the standard. This is a potentially serious concern due to the relatively large v sin i's of T Tauri stars compared to other stars of the same spectral type. The major effect of rotational discrepancies is to blend some of the PMS star lines with nearby features, causing these lines to be stronger than the corresponding standard star feature, and therefore increasing the intrinsic point scatter. However, this same effect is useful since it identifies features that are contaminated by blending, allowing their exclusion from further abundance determinations. Finally, it is unfortunately true that the signal-to-noise ratio of the standards is far superior to the those of the WTTS spectra. The increased scatter introduced by the lower S/N of the TTS could mask many of the effects discussed above.

Figures 4a and 4b are plots of Fe I equivalent width for two low mass pre-main

sequence stars versus the equivalent widths for the same lines in main sequence standards of the same temperature. In Figure 4a, 18 neutral iron line equivalent widths for the Monoceros PMS star G-G 405 are plotted against those of HR 1136, a K0 spectral standard. Despite the large scatter probably due to the lower signal-to-noise ratio of the G-G 405 spectrum ($S/N_{G-G405} = 88$ compared to $S/N_{HR753} = 170$), the data points seem to follow relatively closely the line of equal W(FeI) indicating that the standard is a good match to the T Tauri star. The slight bias toward stronger lines in the T Tauri star could be an indication of higher metallicity in the younger star (see Chapter IV). No deviation in slope is seen among the lines with higher equivalent width which would indicate discrepancies in temperature structure between the two stars. Figure 4b shows the same type of diagram for the WTTS LkCa 19 and the standard star HR 1136. In this case, considerable deviation from equal W(FeI) is present for the lines with large equivalent widths, and an offset is present in the sense that most of the PMS star lines are deeper than those of the standard star. Further investigation reveals that LkCa 19 has an unusually high microturbulence for its spectral type (see Section IIC.) which causes the deviation from the expected slope. Table 4 lists the value of χ^2 assuming the line of equal equivalent widths as a fit for the W_λ - W_λ plots for each of the 30 WTTS in our sample. The dominant effect observed in these plots is unfortunately a large amount of scatter, as quantified for individual stars by Table 4. However, we do note that no systematic trend of lower PMS equivalent widths at higher line strength is observed in any of the sample TTS, indicating that chromospheric filling of strong lines is not detected in these stars. Plots of derived iron abundance versus lower excitation potential have also been performed for the PMS stars, using RAI10 with a grid of solar metallicity stellar atmospheres with $\log g = 3.8$ courtesy of Gustafsson (1988). None of the stars show a systematically lower abundance for

lines with low excitation potential; however, each of the lines used all had EP $\geq$ 2.0 eV, and, according to Finkenzellar and Basri (1987), the filling-in effect is most noticable for Fe I lines with EP $\approx$ 1.5 eV. In Figure 5, the abundance vs. excitation potential plot for P2441 is presented. No systematic trend of lower abundances for lower excitation lines is present, although the λ6246 line is unusually weak in this moderately active star.

C. Microturbulence

Microturbulence originally was a theoretical parameter of stellar line abundances analysis which was used to force agreement between abundances derived from unsaturated and saturated lines. Early abundance analyses indicated that models which included only thermal broadening and radiation damping mechanisms produced discrepancies in abundance between weak and strong lines of the same species (Gray 1976). Although microturbulence is still considered a free parameter in spectral analysis, it is thought to be a manifestation of small-scale convection in stellar atmospheres analogous to solar granulation. The microturbulent velocity is generally rather low in solar-type stars (1.0 km s^{-1} in the Sun), but at least one study suggests a link between chromospheric activity and enhanced microturbulence (Steenbock and Holweger 1981). In the few previous abundance studies of T Tauri stars (Strom *et al.* 1989; Basri, Martin, and Bertout 1991), the microturbulence has always been fixed at some arbitrarily chosen value, although the effect of changing the microturbulence on the abundance has been explored. The current study has the somewhat more ambitious goal of directly determining the value of the microturbulent velocity for at least some of the stars in the pre-main sequence sample.

Microturbulence determinations are generally straightforward, although the results may be complicated by uncertainties in other stellar parameters. The method of Smith, Edvardsson, and Frisk (1986), which we follow, involves repeatedly determining the abundances at a grid of microturbulence values for a set of neutral metallic lines of the same species but differing intrinsic strength. The correct microturbulence velocity is the line one that yields the minimum standard deviation of abundance for lines of all equivalent width, or, correspondingly, makes a zero slope for the linear fit through the abundance versus equivalent width data (Lemke 1989). The method works best for absorption lines with similar temperature sensitivities, because of possible effective temperature errors in the chosen model atmosphere. Twelve Fe I lines included in the Rutten and van der Zalm (1984) list of clean solar spectrum lines were chosen for the microturbulence determination. The chosen Fe I features are: λ6056.013, E.P. = 4.73 eV, log gf = -0.46; λ6165.363, E.P. = 4.14 eV, log gf = -1.63; λ6173.341, E.P. = 2.22 eV, log gf = -2.98; λ6200.321, 2.62 eV, log gf = -2.45; λ6219.287, E.P. = 2.20 eV, log gf = -2.42; λ6229.232, E.P. = 2.84 eV, log gf = -3.02; λ6336.830, E.P. = 3.69 eV, log gf = -0.69; λ6393.612, E.P. = 2.43 eV, log gf = -1.57; λ6703.576, E.P. = 2.76 eV, log gf = -3.13; λ6705.105, E.P. = 4.61 eV, log gf = -1.28; λ6726.673, E.P. = 4.61 eV, log gf = -1.12; λ6750.164, E.P. = 2.42 eV, log gf = -2.48. Despite care in selecting these features, variations in signal-to-noise ratio and v sin i from spectrum to spectrum sometimes compelled the author to eliminate lines that were contaminated by blending or defects in the spectrum. Iron abundances for the above lines have been found for the following microturbulence values: 0.5 km s^{-1}, 1.0 km s^{-1}, 1.8 km s^{-1}, 2.5 km s^{-1}, 3.0 km s^{-1}, 3.6 km s^{-1}, and 5.0 km s^{-1}. Figure 6 a) and b) are plots of iron abundance standard deviation versus microturbulence for KM Orionis and LkCa 19. A reasonable minimum to σ_{abun} is found at 1.8 s^{-1} for KM Ori, although the dip in $\sigma_{N(Fe)}$ is

rather shallow. The ξ_{mt} value implicated by Figure 6b) for LkCa 19 is considerably higher, at about 3.2 km s^{-1}.

The results of the microturbulence determination are presented in Table 5. The value of the microturbulent velocity is listed in Column 2. The uncertainties in Column 2 are simply the half width of the "dip" in the relation between σ_{abun} and microturbulence. Microturbulent velocities are only given for cases in which one broad minimum of $\sigma_{N(Fe)}$ more than 0.04 below the maximum values are found. Values of [Fe/H] which correspond to the derived microturbulence are in Column 3; these are differential logarithmic abundance relative to solar. Only 17 of the original sample of 30 stars proved amenable to this method of microturbulence determination. Sz 19 has a microturbulence value of 1.6 km s^{-1} $\pm$ 0.3 according to curve-of-growth analysis by Franchini, Castelli, and Stalio (1991); this value was adopted for use in the metallicity determinations in Chapter IV. In the other 13 PMS stars, it is assumed that noise, temperature errors, and large v sin is increased the scatter of abundances to the point where no single minimum in $\sigma_{N(Fe)}$ was found. For these stars, the value of ξ_{mt} is found that yields the same iron abundance as the other stars in the association with constrainable microturbulences. These velocities are in Column 4. Among the 18 stars with clearly determined ξ_{mt}, the mean value is 1.65 $\pm$ 0.62 km s^{-1}. For the whole sample (including the values in column 4), the mean is 1.76 $\pm$ 0.61 km s^{-1}. The microturbulences are higher for the stars in Orion (mean ξ_{mt} = 2.24 $\pm$ 0.4 km s^{-1}) than those in Chamaeleon (mean ξ_{mt} = 1.1 $\pm$ 0.37 km s^{-1}), probably because of the more massive PMS stars that were observed in Orion.

III. Discussion

The use of high-resolution spectral line ratios as temperature indicators for T Tauri stars appears to be considerably more accurate than low-resolution spectral classification. According to Herbig and Bell (1988), most spectral classifications of low-mass PMS stars which are included in the Herbig and Rao (1972) Second Catalog of Orion Population stars were performed with low resolution, poor signal-to-noise ratio photographic spectrograms. Many of these objects were only classified as "Ge" or K, because of the difficulty of distinguishing the known indicators of MK spectral type, especially in heavily veiled stars. Herbig (1977) employed an image intensifier with photographic plate on the Lick 120-inch to improve the spectral types of 50 T Tauri stars in several star forming regions. By comparing ratios of metallic line blends to those of MK standards, he was able to classify PMS stars of type K0 - M3 with considerable accuracy, including several stars in the current study. He also noted that the majority of stars for which a luminosity class was distinguishable appeared to belong to the class V or "dwarf" category, despite photometric studies that suggest surface gravities characteristic of subgiants (Cabrit *et al.* 1990). The most comprehensive survey of T Tauri star spectral types and, indeed, of many T Tauri star stellar parameters is the one by Cohen and Kuhi (1979). Utilizing the image-tube scanner on the Lick 3m telescope to obtain 7 Å resolution spectra for 500 Hα emission stars listed in the HRC, Cohen and Kuhi used metallic line blends, resonance lines, and TiO bands to determine the spectral types of T Tauri stars. Applying the spectral type to effective temperature conversions of Johnson (1966) for class V stars of type B5 - K7, they obtained effective temperature determinations accurate to $\pm$ 0.03 in log T_{eff}. This is equivalent to about $\pm$ 330 K at K0. Subsequent PMS star investigations have either used the classifications of Cohen and Kuhi (Strom *et al.* 1989) or employed similar low resolution spectral classification to determine effective temperatures for PMS stars (Appenzeller *et*

al. 1983). Even the outstanding high-resolution spectra of southern hemisphere T Tauri stars presented by Finkenzellar and Basri (1987) was supplemented by low resolution spectral data for spectral classification purposes.

However, with the advent of echelle spectroscopy has come a renewed interest in using high-resolution spectroscopy to determine the temperatures of T Tauri stars. Some of the most active stars, which had previously been categorized as "continuum stars" due to the lack of visible features at low resolution (such as DG Tau,AS353a, RU Lup), have been shown to have normal, albeit heavily veiled, photospheric features when observed at high signal-to-noise ratio and high resolution (Schwartz and Heuermann 1981; Basri and Batalha 1990). The biggest driver towards more accurate spectral typing of T Tauri stars has been the desire to investigate the nature of the "photospheric veiling" that causes the absorption lines of active T Tauri stars to appear shallower than inactive stars of identical spectral type. In order to determine the properties of the veiling, Hartigan *et al.* (1989) used the high-resolution spectrum of a standard star (convolved with the proper rotational function) added to a flat continuum of adjustable magnitude to model the spectrum of BP Tau. Their solution to the problem of finding the effective temperature of BP Tau was to compare χ^2 fits of standards with a variety of spectral types to the BP Tau spectrum; the standard which produced the minimum χ^2 was chosen as the appropriate spectral type to within 2 spectral subclasses. Despite the satisfactory results obtained by Hartigan *et al.* with the χ^2 fitting scheme, less complicated methods of determining the effective temperature are also available using high quality spectral data. High-resolution line ratios have been used in spectral classification by Basri and Batalha (1990), who needed highly accurate spectral types to determine the magnitude of continuum veiling in 35 T Tauri stars. In a later paper, Basri, Martin, and Bertout (1991) have used these spectral types to obtain lithium abundances for

a number of Taurus-Auriga T Tauri stars. Abundance determinations require high accuracy effective temperatures. A change in effective temperature of only 100 K can change the derived lithium abundance in a K0 star by 0.1 dex. Most classical studies of stellar abundances use photometric (optical and infrared color) temperature scales to determine T_{eff}. The current study indirectly uses these methods by establishing the relationship between line ratios and photometrically determined temperatures in the Bell and Gustafsson (1989) standard stars.

Table 6 compares effective temperatures derived for 30 WTTS to previous temperatures determinations for these stars. Column 2 contains the effective temperature from the spectral classification (using spectral type to T_{eff} table of Cohen and Kuhi 1979) of the star as it appears in the HBC; references to the original source of the spectral data are given below the table. In column 3 are additional temperature determinations from spectral classifications, if any, that appear in the literature. Effective temperatures determined from high-resolution spectra appear in bold-face type. Column 4 is a list of the effective temperatures adopted by the present investigation on the basis of metallic line ratios, and column 5 is the spectral type with which the adopted temperature most closely corresponds using the spectral type-to-effective temperature conversions of Cohen and Kuhi (1979). Finally, column 7 is the difference in degrees Kelvin between the newly derived effective temperature and the temperature corresponding to the mean of the previous spectral classifications.

The average difference between the effective temperatures derived in the current study and temperature determinations in the literature is about +120 K, but the scatter around this value is 340 K. It is not surprising that the low-resolution spectral classification could be inconsistent with our temperature determinations to

this degree, since they are only estimated to be accurate to ± 2 spectral subclasses (about 330 K at K0). In addition, the statistics for the entire sample are somewhat contaminated by the extremely large discrepancy between past and present spectral classifications of the two Cygnus stars, LkHα 191 and LkHα 228. In the case of LkHα 191, HBC lists a spectral type of K0,3 V ($\approx$ 5030 K), only about 250 K cooler than our adopted temperature of 5285 K. However, Cohen and Kuhi (1979) report the class as K6 ($\approx$ 4200 K). Careful examination of our high-resolution spectrum shows no evidence of TiO bands, and the line ratios clearly indicate photospheric temperatures in excess of 4200 K. Higher signal-to-noise spectra of this object should resolve the uncertainty about the spectral class of this object; however, it seems likely that the Cohen and Kuhi classification of K6 was in error, unless the spectral type of LkHα 191 has changed since 1979. LkHα 228 is an even more dramatic case of changes in spectral classification between high and low resolution spectral classification. The Cohen and Kuhi type is K1,2; the current study estimates the class at F8! Again, an examination of the high-resolution spectrum shows no evidence of spectral features characteristic of K stars. The Sc I λ6210 that is clearly visible in other K1,2 stars in our sample is not present at all down to a limit of a few milliangstroms. This case demonstrates most clearly the need for high resolution spectral classification of T Tauri stars before attempting investigations that are strongly dependent on accurate effective temperatures such as veiling or abundance studies. The fact that previous spectral classifications for WTTS could be seriously in error does not bode well for the spectral types of CTTS with their less distinct spectral features. However, our spectral types agree with Basri and Batalha (1990) to two spectral subclasses or better for the four stars of the current sample that overlap with their high resolution spectral classifications. The current study confirms their observation that temperatures determined from metallic line

ratios tend to be higher than those found from low resolution spectral classifications. Two stars that had previously been assigned the type of K7 (NTTS 045251 and SR 9) have been reclassified by the present study as K3 - K4. For SR 9, the type found by Basri and Batalha agrees with ours to within a spectral subclass. In addition, SR 9 is a star that is known to have extensive starspot coverage which could cause temporal variation in its spectral features and, thus, its derived spectral type. Considerable attention still needs to be directed towards comparisons of high and low resolution spectral classification of T Tauri stars in order to explain these discrepancies.

Even the high resolution temperature determinations attempted in the current investigation suffer from some possibly serious weaknesses. The use of main sequence standards of diverse age and metallicity as line ratio calibrators has been rejected by some other investigators such as Basri and Batalha (1990) and Hartigan *et al.* (1989). They prefer to use well-known standards to spectrally classify young Hyades dwarfs, which are then used as spectral standards for T Tauri stars. These young main sequence stars are probably also more similar in atmospheric structure and turbulence to the T Tauri stars than old disk standards. By using a group of stars that is uniform in metallicity, they eliminate the possibility of differential metal enrichment (*e.g.*, [Fe/V] $\neq$ 0.0) between standards with different metal abundances. However, the Hyades cluster is slightly metal-rich ([Fe/H] = +0.13; Cayrel, Cayrel de Strobel, Campbell 1985), which may not be the case for all pre-main sequence assiociations (see Chapter IV, Table 4); thus, some problems of differential enrichment between the standards and the PMS stars may still persist. Stellar parameters such as microturbulence and surface gravity are entirely unknown for most solar-type Hyades stars since most studies of cluster properties assume statistically average values for these parameters; in addition, the v sin i

values for many Hyades stars are much higher than the 20 - 30 km s^{-1} typical of T Tauri stars. In order to avoid the second layer of line ratio calibration caused by using the Bell and Gustafsson standards to find spectral types for young main sequence stars, future researchers should make use of the considerable photometric database in the literature on young main sequence clusters to determine effective temperatures before using these stars as templates for the T Tauri stars. Another weakness of the current study is the small number of standard stars observed, as well as their non-uniform temperature distribution. Of the 13 standards observed, only 3 (HR 8085, HR 8086, HR 753) are cooler than type K2. It is perhaps no wonder that our temperatures are hotter than previous determinations; our statistics are strongly biased towards G5 - K2 stars. In addition, plots of theoretical line ratios as a function of temperature suggest that linear regression may not be the best method of fitting these functions. The large scatter in 6705/6703 as a function of temperature for field stars found by Boesgaard and Tripicco (1986) confirms the large uncertainties incurred by using linear regression fits for some line ratios; however, their fits to Cr I λ6748/Fe I λ6750 and Cr I λ6748/Fe I λ6752 in Boesgaard and Tripicco (1987) have little scatter. A further *caveat* is the possible presence of spots on some of the stars observed. According to Bouvier, Bertout, and Boucher (1988), UX Tau A, CV Cha, RY Lup, and SR 9 all have periodic light curves which suggest large-scale starspot coverage. For these stars and perhaps others in the sample, line ratios involving low excitation lines such as those of V I which are enhanced in sunspots may vary with time, thus causing changes in spectral type. Finally, we must emphasize that the "effective temperatures" found by using line ratios are in reality only temperatures characteristic of the photospheric regions in which the line pair forms. The real utility of line ratios is in linking the known photometric temperature scales to spectral features that can be discerned even in

highly veiled stars.

The microturbulence results obtained by the present investigation have considerable relevance to the physics of T Tauri star atmospheres as well as to abundance determination efforts for WTTS. Although the mean microturbulent velocity found for the sample 16 WTTS (1.6 km s^{-1}) is larger than the typical value for main sequence solar-type stars, it is not outside of the normal range of variation for stars of type G - K (Nissen 1981). As expected for main sequence stars, the hotter PMS stars tend to have higher microturbulent velocities than the lower mass stars with some exceptions. The highest determined microturbulence (ξ_{mt} = 3.2 km s^{-1}) is that of LkCa 19, a K0 star in Taurus-Auriga. The spectrum of this star is almost boring in its normality, with small chromospheric emission features at Ca II H and K and Hα. However, recent X-ray observations from *Rosat* indicate that this star is an unusually bright source of X-ray emission (courtesy of M. Sternik, 1991). X-ray studies of other PMS stars with high microturbulence are necessary to confirm any correlation; however, this may be further evidence of the Steenbock and Holweger (1981) suggestion that microturbulence may be a manifestation of acoustic waves in the stellar atmosphere, and,thus, is fundamentally linked to mechanisms of stellar activity.

One of the most troubling questions which confronts researchers who would analyze the composition of PMS stars is how "normal" are T Tauri star photospheres compared to main sequence stars of similar spectral type. Are standard model atmospheres such as the ones of Kurucz (1979) and Gustafsson (1988, private communication) applicable to pre-main sequence stars or do these stars have fundamentally different photospheric temperature structures which in some way contributes to the activity of CTTS? Ten years ago, the consensis opinion was that

T Tauri star activity was caused by a deep chromosphere with a temperature minimum well-displaced from the one found in normal main sequence stars. Modelling by Calvet *et al.* (1983) suggested that the photospheric temperature structure in T Tauri stars had to be radically different from older stars to be able to produce the photospheric veiling observed in the most active members of the class. Indeed, the spectral ratioing work of Finkenzellar and Basri (1987) seemed to confirm that the veiling of T Tauri absorption line spectra was actually due to chromospheric emission lines "filling-in" the absorption features of moderately active stars. However, more recent studies by Hartigan *et al.* (1989, 1991) indicate that the veiling is actually caused by an almost featureless continuum which is sometimes many times brighter than the stellar photospheric continuum. The veiling also seems to be correlated with the presence of circumstellar material, suggesting that the excess continuum emission and many of the emission lines are coming from a boundary layer between the star and a surrounding accretion disk (Bertout 1989). In this latter scenario, the so-called "naked" or "weak-line" T Tauri stars lack an actively accreting disk which explains the absence of veiling or extremely strong emission features. The emission lines that are present in these stars are assumed to be due to chromospheric magnetic activity, such as flares and active regions. Although this activity is much stronger than the events observed on the Sun and other main sequence stars, the currently postulated T Tauri star photosphere is assumed to be very similar to photospheres of main sequence stars. The "disk" theory of T Tauri star activity is therefore a basic assumption behind our attempt to analyze pre-main sequence star atmospheres for composition using normal model photospheres.

The results of the $W(FeI)_{TTS}$ versus $W(FeI)_{Standard}$ and the Fe abundance versus excitation potential plots suggest that the absorption line-forming regions of the PMS stars in this study have relatively normal $T(\tau)$. Almost all of the 30

WTTS observed show no filling of Fe I lines with equivalent widths as high as 300 mÅ. The only star in the sample with possible chromospheric Fe I emission in one of the stronger Fe lines (λ6246) is P2441, a star which probably excites a Herbig-Haro object (Reipurth 1989) and is considerably younger than the other PMS stars studied. All of the WTTS in the sample show no hint of the behaviour noted by Appenzeller,Jankovics, and Jetter (1986) in the active, veiled stars S Cra and VV Cra; they found that only the *weaker* absorption lines in the solar spectrum could be identified as absorption features in the CTTS spectra. All of the stronger metallic features were either filled or in emission. The same effect is also seen in our spectrum of SR 4, an active K7 star observed during the current project which was not included in the WTTS sample due to the probability of photospheric veiling in its spectrum. Based on the current sample, it appears that the mechanism that causes filling of strong Fe I lines may also be linked to the phenomenon which causes veiling, since stars without veiling seem to have approximately normal photospheric temperature structure. Unfortunately, the empirical plots used in the current investigation are admittedly crude ways of exploring T(τ), especially considering the relatively low signal-to-noise ratio of these TTS spectra. A full analysis T(τ) in PMS stars should include a depth of formation analysis with high S/N spectra, possibly using young main sequence stars as templates.

This investigation finds no evidence that the photospheres of weak-line T Tauri stars are fundamentally different from those of ordinary main sequence stars. Despite their relatively high v sin i, starspots, flares, and X-ray brightness, most WTTS stars appear to have relatively normal photospheric temperature structure as indicated by plots of W_λ(WTTS) versus W_λ(standards). Their observed microturbulent velocities are not extrordinarily high compared to other solar-type stars, with values ranging from 0.5 km s^{-1} to 3.2 km s^{-1}. The effective temperatures

found in the current study are probably accurate to 200 K for most of the sample. With access to increasingly high resolution, high signal-to-noise ratio spectra of these objects, determination of extremely accurate spectral types using metallic line ratios should be relatively straightforward; high precision surface gravity derivations using line profiles will also become possible. From these results, I conclude that weak-line T Tauri stars are suitable candidates for atmospheric line abundance studies using conventional model photospheres.

IV. Summary

New effective temperatures have been determined for 30 low-mass pre-main sequence stars in five star formation regions. These temperatures are based on standard-calibrated line ratios of V I to Fe I and are accurate to 200 K in most cases. Some stars have been drastically reclassified by these observations relative to the spectral types assigned by low resolution studies. Microturbulent velocities have been determined for 16 of the stars in this sample, and the average value is 1.62 $\pm$ 0.61 km s^{-1}. The maximum microturbulence of 3.2 km $\pm$ 0.5 km s^{-1} was found for the Taurus-Auriga star LkCa 19. Empirical plots of EW_{TTS} versus $EW_{Standard}$ and Fe abundance versus line excitation potential show no abnormalities in T(τ) in the line forming region for Fe I lines with equivalent widths as high as 200 mÅ. We conclude that weak-line T Tauri stars have essentially normal photospheres, making them suitable targets for compositional analysis.

REFERENCES

Appenzeller, I., Jankovics, I., Krautter, J. 1983, *A.A.Supp.*, **53**, 291.

Appenzeller, I., Jankovics, I., Jetter, R. 1986, *A.A.Supp.*, **64**, 65.

Arribas, S., Crivellari, L. 1989, *A.A.*, **210**, 221.

Balachandran, S., Lambert, D. L., Stauffer, J. R. 1989, *Ap.J.*, **333**, 267.

Basri, G., Batalha, C. 1990, *Ap.J.*, **363**, 654.

Basri, G., Martin, E., Bertout, C. 1991, Submitted to *A.A.* (BMB).

Bell, R. A., Gustafsson, B. 1989, *M.N.R.A.S.*, **236**, 653.

Bertout, C., Carrasco, L., Mundt, R., Wolf, B. 1982, *A.A.*, **47**, 419.

Bertout, C. 1989, *Ann. Rev. Astron. Ap.*, **27**, 351.

Blackwell, D. E., Booth, A. J., Petford, A. D., Leggett, S. K., Mountain, C. M., and Selby, M. J. 1986, *M.N.R.A.S.*, **221**, 427.

Boesgaard, A. M., 1984, *AJ*, **89**, 1635.

Boesgaard, A. M., Tripicco, M. J. 1986, *Ap.J.*, **303**, 724.

Bouvier, J., Bertout, C., Boucher, P. 1988, *A.A.Supp.*, **75**, 1.

Cabrit, S., Edwards, S., Strom, S. E., Strom, K. M. 1990, *Ap.J.*, **354**, 687.

Calvet, N., Basri, G., and Kuhi, L. V. 1983, *Ap.J.*, **277**, 725.

Cayrel, R., Cayrel de Strobel, G., Campbell, B. 1985, *A.A.*, **146**, 249.

Cayrel de Strobel, G., Bentolila, C., Hauck, B., Duguennoy, A. 1985, *M.N.R.A.S.*, **221**, 427.

Cohen, M., Kuhi, L. 1979, *Ap.J.Supp.*, **41**, 743.

Duncan, D. K. 1981, *Ap.J.*, **248**, 651.

Finkenzeller, U., Basri, G. 1987, *Ap.J.*, **318**, 823.

Franchini, M., Castelli, F., Stalio, R. 1991, *A.A.*, **242**, 449.

Frisk, U. 1983, *Ph.D. Thesis*, Stockholm Univ..

Gauvin, L. S., Strom, K. M. 1991, *FCAD* preprint.

Gray, D. F. 1976, *The Observation and Analysis of Stellar Photospheres*, John Wiley and Sons, p. 416.

Grevesse, N. 1984, *Physica Scripta*, **T8**, 49.

Gustafsson, B. 1988, private communication.

Hartigan, P., Hartmann, L. W., Kenyon, S. J., Hewett, R., and Stauffer, J. R. 1989, *Ap.J.Supp.*, **70**, 899.

Hartigan, P., Kenyon, S. J., Hartmann, L. W., Strom, S. E., Edwards, S., Welty, A. D., Stauffer, J. R. 1991, *FCAD* preprint.

Hartmann, L. W., Kenyon, S. J. 1990, *Ap.J.*, **349**, 190.

Henize, K. G., Mendoza, E. E. 1973, *Ap.J.*, **180**, 115.

Herbig, G. H. 1962, *Adv.Ast.Ap.*, **1**, 47.

Herbig, G. H., Bell, R. 1988 *Publ. Lick Obs.* 1111.

Herbig, G. H., Rao, N. K. 1972, *Ap.J.*, **174**, 401.

Herbig, G. H. 1977, *Ap.J.*, **214**, 747.

Herbig, G. H., Vrba, F., Rydgren, A. E. 1986, *AJ*, **93**, 907.

Hyland, A. R., Jones, T. J., Mitchell, R. M. 1982, *M.N.R.A.S.*, **201**, 1095.

Johnson, H. L. 1966, *Ann.Rev.Astron.Ap.*, **4**, 193.

Johnson, H. L., Mitchell, R. I. 1975, *Rev.Mex.Astr.Astrofis.*, **1**, 299.

Kenyon, S. J., Hartmann, L. W. 1990, *Ap.J.*, **349**, 197.

Kurucz, R. L. Dudley Observatory Report 14 363.

Lemke, M. 1989, *A.A.*, **225**, 125.

Maguzzu, A., Rebolo, R. 1989, *Mem. S. A. It.*, **60**, 105.

McCarthy, J. A. 1988, *Ph.D. Thesis*, Caltech.

Nissen, P. E. 1981, *A.A.*, **97**, 145.

Penston, M. V., Hunter, J. K., O'Neill, A. 1975, *M.N.R.A.S.*, **171**, 129.

Reipurth,B. 1989, *A.A.*, **220**, 249.

Rutten, R. J., van der Zalm, E. B. J. 1984, *A.A.Supp.*, **55**, 171.

Rydgren, R. J., Vrba, F. J. 1984, *AJ*, **89**, 399.

Smith, G., Edvardsson, B., Frisk, U. 1986, *A.A.*, **165**, 126.

Steenbock, W., Holweger, H. 1981, *A.A.*, **99**, 102.

Sternik, M. 1991, private communication.

Stone, R. C., Taam, R. E. 1985, *Ap.J.*, **291**, 183.

Strom, K. M., Wilkin, F. P., Strom, S. E., Seaman, R. L., 1989a, *AJ*, **98**, 1444.

Strom, K. M., Strom, S. E., Edwards, S., Cabrit, S., Skrutskie, M. F. 1989b, *A.J.*, **97**, 1451.

Strom, S. E., Edwards, S., Skrutskie, M. F. 1989, *Cool Stars, Stellar Systems, and the Sun*, ed. G. Wallerstein, 275.

Schwartz, R. D., Heuermann, R. W. 1981, *AJ*, **86**, 1526.

Walter, F. M. 1986, *Ap.J.*, **306**, 573.

Walter, F. M., Brown, A., Mathieu, R. D., Myers, P. C., Vrba, F. J. 1988, *A.J.*, **96**, 297.

Table 1

HR Number	Spectral Type	T_{eff} (K)	log g	[Fe/H]	[Fe/H] Ref
7503	G1.5 V	5826	4.30	0.00	C
7504	G2.5 V	5664	4.40	0.00	C
2047	G0 V	5842	4.41	-0.09	N
Sun	G2 V	5775	4.40	0.00	-
6623	G5 IV-V	5527	4.10	0.30	C
7602	G8 IV	5098	3.56	-0.08	F
7462	K0 V	5253	4.50	-0.25	-
1325	K1 V	5114	4.65	-0.21	F
1084	K2 V	5156	4.61	0.05	F
753	K3 V	4775	4.6	-	-
1136	K0 V	4976	3.95	0.05	C
7957	K0 V	4996	3.34	-0.17	F
8085	K5 V	4463	4.50	-0.05	C
8086	K7 V	4252	4.60	-0.05	C

Data from Bell and Gustafsson (1989). Sources for [Fe/H] values: C = Cayrel de Strobel *et al.* (1985); F = Frisk (1983); N = Nissen (1981)

Table 2

Line Ratio	Number of Standards	Slope	Y-Intercept	χ^2
V I 6199/Fe I 6200	14	$-8.252 \times 10^{-4} \pm 5.263 \times 10^{-5}$	4.915 ± 0.275	0.106
Fe I 6200/V I 6216	13	$9.085 \times 10^{-4} \pm 6.340 \times 10^{-5}$	-3.448 ± 0.331	0.141
V I 6119/Fe I 6200	13	$-7.041 \times 10^{-4} \pm 4.053 \times 10^{-5}$	4.319 ± 0.211	0.058
V I 6119/Fe I 6219	13	$-4.750 \times 10^{-4} \pm 2.260 \times 10^{-5}$	2.963 ± 0.118	0.018
Fe I 6705/Fe I 6703	12	$6.861 \times 10^{-4} \pm 6.057 \times 10^{-5}$	-2.444 ± 0.310	0.084

Table 3

Star Name	$T_{6199/6200}$ (K)	$T_{6200/6216}$ (K)	$T_{6119/6200}$ (K)	$T_{6119/6219}$ (K)	$T_{6040/6042}$ (K)	$T_{6705/6703}$ (K)	Adopted T_{eff} (K)
Orion PMS Stars							
KM Ori	4845	4900	4902	4730	-	5097	4867 ± 119
LX Ori	4744	5239	4944	4627	4800	4640	4832 ± 210
TV Ori	4928	4481	4898	4667	-	4530	4701 ± 184
P 1270	5418	5165	5319	5299	5100	-	5260 ± 114
P 1404	5608	5579	5208	-	-	-	5465 ± 182
P 2441	5745	-	5701	5527	-	6138	5778 ± 223
HD 245059	5481	5513	5409	5456	5200	-	5412 ± 111
Chamaeleon PMS							
CS Cha	4716	4518	4497	4569	-	4571	4574 ± 77
Sz 19	5362	5017	5404	5304	-	5061	5272 ± 151
CV Cha	5340	4836	5205	5186	-	5113	5136 ± 167
SZ Cha	5164	4981	4858	4745	-	-	4937 ± 155
Sz 41	5097	4940	4614	4694	-	4512	4771 ± 216
Ophiuchus PMS							
He 3-1126	5544	5140	5555	5342	-	-	5402 ± 177
SR 9	4560	4788	4676	4501	-	4717	4648 ± 104
Wa Oph/1	5147	5333	5264	4974	-	4751	5094 ± 210
Wa Oph/2	4659	4874	5023	4810	-	4893	4851 ± 119
Haro 1-14/c	4745	4756	4725	4688	-	5019	4787 ± 118
Taurus PMS Stars							
NTTS 035120 SE	5778	-	5891	5892	-	5587	5787 ± 124
NTTS 035135	5106	-	5557	5442	5250	5462	5363 ± 163
NTTS 042417	5461	5573	5623	5732	5300	5176	5478 ± 191
NTTS 043124	5602	5601	5614	5482	-	-	5575 ± 54
NTTS 045251	4439	4409	4401	4715	4450	4775	4532 ± 153
LkCa 15	4943	4656	4766	4950	4750	4806	4770 ± 94
LkCa 19	5296	5230	5319	5232	-	5170	5249 ± 53
UX Tau A	4812	5360	5177	5172	5200	4800	5087 ± 208
Cygnus PMS Stars							
LkHα 191	5350	-	5549	5241	5000	5285	5285 ± 177
LkHα 228	5773	-	5908	5934	-	6269	5971 ± 183
Other PMS Stars							
AS 507	5266	5012	-	-	5100	4788	5042 ± 172
G-G 405	5270	5342	5329	5205	-	4853	5199 ± 180
RY Lup	4967	4932	5332	5438	-	-	5055 ± 300

Table 4

Star	Star SpT	Standard	Stan. SpT	χ^2 W(FeI)/W(FeI)
LkCa 15	K3	HR 753	K3 V	0.853
LkCa 19	K0	HR 1136	K0 IV	1.872
NTTS 045251	K4-K5	HR 753	K3 V	5.423
NTTS 035120 NE	G2	HR 7504	G2.5 V	4.500
NTTS 035135 SE	G8-K0	HR 1136	K0 IV	3.718
NTTS 042417	G8	HR 7602	G8 IV	2.977
NTTS 043124	G5-G8	HR 7602	G8 IV	4.483
UX Tau	K1	HR 1136	K0 IV	2.334
KM Ori	K2-K3	HR 1136	K0 IV	3.375
P2441	G2	HR 2047	G0 V	2.755
LX Ori	K2-K3	HR 1136	K0 IV	3.505
TV Ori	K3-K4	HR 753	K3 V	3.624
P1270	K0	HR 1136	K0 IV	3.334
P1404	G5-G8	HR 7602	G8 IV	2.709
HD 245059	G8-K0	HR 1136	K0 IV	3.830
Sz 41	K3	HR 1136	K0 IV	3.683
Sz 19	G5-G8	HR 7602	G8 IV	2.532
CS Cha	K4	HR 1136	K0 IV	3.307
CV Cha	K0-K1	HR 7602	G8 IV	2.467
SZ Cha	K2	HR 1136	K0 IV	4.087
SR 9	K3-K4	HR 7957	K0 IV	2.872
Wa Oph/2	K2-K3	HR 1136	K0 IV	3.603
Haro 1-14/c	K3-K4	HR 753	K3 V	4.548
Wa Oph/1	K1	HR 1136	K0 IV	3.697
He 3-1126	G8-K0	HR 1136	K0 IV	2.749
LkHα 228	F8	HR 2047	G0 V	2.930
LkHα 191	G8-K0	HR 1136	K0 IV	0.948
AS 507	K1-K2	HR 753	K3 V	1.179
G-G 405	K0-K1	HR 1136	K0 IV	0.457
RY Lup	K1-K2	HR 1136	K0 IV	2.876

Column 4: χ^2 of linear fit (m=1, b=0) to equivalent width FeI TTS versus equivalent width FeI Standard

Table 5

Star	Number of Lines	ξ_{mt} (km s^{-1})	[Fe/H]	$\approx \xi_{mt}$ Constraint (km s^{-1})
LkCa 15	9	1.8 ± 0.8	-0.092	-
LkCa 19	11	3.0 ± 1.0	-0.033	-
NTTS 045251	9	1.8 ± 1.0	-0.047	-
NTTS 035120 SE	-	-	-	2.0
NTTS 035135 NE	-	-	-	1.5
NTTS 042417	-	-	-	2.3
NTTS 043124	-	-	-	2.0
UX Tau	-	-	-	1.5
KM Ori	13	1.8 ± 0.5	0.045	-
P2441	9	2.5 ± 1.0	-0.069	-
LX Ori	10	1.8 ± 0.8	-0.051	-
TV Ori	7	1.8 ± 0.8	0.019	-
P1270	-	-	-	2.3
P1404	-	-	-	2.5
HD 245059	-	-	-	2.7
Sz 41	8	1.0 ± 0.5	0.134	-
Sz 19*	-	1.5 ± 0.2	0.130	-
CS Cha	10	1.5 ± 1.0	0.000	-
CV Cha	10	1.5 ± 0.8	0.219	-
SZ Cha	7	0.5 ± 0.5	0.171	-
SR 9	10	1.0 ± 0.5	0.101	-
Wa Oph/2	9	1.0 ± 0.5	0.168	-
Haro 1-14/c	10	1.8 ± 0.5	-0.030	-
Wa Oph/1	-	-	-	1.5
He 3-1126	-	-	-	1.5
LkHα 228	11	1.8 ± 0.8	-0.205	-
LkHα 191	-	-	-	2.5
AS 507	9	1.5 ± 1.0	0.200	-
G-G 405	9	2.5 ± 0.5	-0.239	-

* Microturbulence and [Fe/H] from curve of growth analysis by Franchini, Castelli, and Stalio 1989

Table 6

Name	HBC T_{eff} (K)	Other T_{eff} (K)	Adopted T_{eff} (K)	Adopted SpT	δ T_{eff} (K)
Orion PMS Stars					
KM Ori	5105[1]	-	4867	K2-K3	- 238
LX Ori	4475[1]	-	4832	K2-K3	+ 357
TV Ori	4198[1]	-	4701	K3-K4	+ 242
P 1270	5105[1]	-	5260	K0	+ 74
P 1404	5662[2]	-	5465	G5-G8	- 197
P 2441	5662[1]	5834[3]	5778	G2	+ 116
HD 245059	4775[4]	-	5291	G8-K0	+ 516
Chamaeleon PMS					
CS Cha	4591[5]	**3600**[6]	4574	K4	+ 329
Sz 19	5767[5]	**5500**[7]	5500	G5-G8	-
CV Cha	5445[8]	-	5136	K0-K1	- 309
SZ Cha	5236[9]	-	4937	K2	- 299
Sz 41	5170[10]	-	4771	K3	- 399
Ophiuchus PMS					
He 3-1126	5662[11]	-	5402	G8-K0	- 260
SR 9	4197[1]	**3900**[6], **4395**[15]	4648	K3-K4	+ 484
Wa Oph/1	4955[12]	-	5094	K1	+ 139
Wa Oph/2	5105[12]	-	4851	K2-K3	- 254
Haro 1-14/c	4775[13]	-	4729	K3-K4	- 46
Cygnus PMS Stars					
LkHα 191	4954[13]	4197[1]	5285	G8-K0	+ 710
LkHα 228	5029[1]	-	5971	F8	+ 941
Taurus PMS Stars					
NTTS 035120 NE	5662[14]	-	5768	G2	+ 108
NTTS 035135 SE	5236[14]	4950[14]	5363	G8-K0	+ 270
NTTS 042417	5105[14]	**5250**[15]	5478	G8	+ 300
NTTS 043124	5445[14]	-	5498	G5-G8	+ 51
NTTS 045251	4000[14]	-	4532	K4-K5	+ 532
LkCa 15	4395[16]	-	4770	K3	+ 375
LkCa 19	5236[16]	**4950**[15]	5249	K0	+ 156
UX Tau A	4955[17]	**5250**[15]	5087	K1	- 15
Other PMS Stars					
AS 507	5559[17]	-	5042	K1-K2	- 517
G-G 405	4678[17]	-	5199	K0-K1	+ 521
RY Lup	5105[18]	-	5055	K1-K2	- 50

Table 6 (continued)

References

1. Cohen and Kuhi 1979, 2. Penston, Hunter, and O'Neill 1975, 3. Rydgren and Vrba 1984, 4. Stone and Jaam 1985, 5. Appenzeller, Jankovics, and Krautter 1983, 6. Maguzzu and Rebolo 1989, 7. Franchini, Castelli, and Stalio 1989, 8. Henize and Mendoza 1973, 9. Rydgren 1988, 10. Hyland, Jones, and Mitchell 1982, 11. HD catalog, 12. Walter 1986, 13. Herbig and Rao 1972, 14. Walter *et al.* 1988, 15. Basri and Batalha 1990, 16. Herbig, Vrba, and Rydgren 1986, 17. Herbig and Bell 1988, 18. Herbig 1977

FIGURE CAPTIONS

Figure 1. Illustration of change in the ratio of V I λ6199 to Fe I λ6200 with effective temperature. The Figure shows a section of spectra from eight standards with increasing T_{eff} from HR 8086 (K7 V; top) to HR 2047 (G0 V; bottom). Notice that V I λ6199 (left of line pair at midspectrum) undergoes a drastic decrease in strength with increasing T_{eff} while Fe I λ6200 weakens only slightly.

Figure 2a) - e) Linear regression fits of variations in line ratio with effective temperature for 12 - 14 spectral standards. Fits are presented for a) V I λ6199/Fe I λ6200, b) Fe I λ6219/V I λ6119, c) V I λ6119/Fe I λ6200, d) Fe I λ6200/V I λ6216, e) Fe I λ6705/Fe I λ6703. Effective temperatures were assigned using photometric color-temperature transformations by Bell and Gustafsson (1989). Parameters of these fits are presented in Table 2.

Figure 3a), b) Plots of log W(FeI) vs. log W(FeI) for slightly differing model stellar atmospheres. The LTE line abundance analysis program RAI10 was used to synthesize equivalent widths for a number of neutral iron lines. In Panel *a)*, the model atmospheres differ in effective temperature by 200 K; the effect is a slight deviation from the line of equal W(FeI) for the stronger lines due to their lower excitation potential, and therefore, greater temperature sensitivity. In Panel *b)*, the two models differ in microturbulent velocity by a factor of 2 (1.8 km s^{-1} to 3.6 km s^{-1}). The observed effect on this plot is to substantially increase the strength of all of the iron lines in the model with higher microturbulence, with respect to the other model.

Figure 4a), b) Plots of pre-main sequence star log W(FeI) versus spectral standard log W(FeI). Figure 4 a) depicts Fe I equivalent widths of the K0-K1 weak-line T Tauri star G-G 405 plotted versus equivalent widths of HR 1136, a K0 IV standard. Despite scatter due to the lower S/N of the TTS spectrum, the fit of the equal W(FeI) line is relatively good. However, in Figure 4 b), the slope of the LkCa 19 log W(FeI) vs. HR 1136 log W(FeI) data points clearly deviates from 1 for the stronger lines. This effect is probably caused by the high microturbulence of the atmosphere of LkCa 19 (3.2 km s^{-1}; see section IIc.), although it could also indicate a deviation in the T(τ) between the two stars.

Figure 5. Iron abundance versus lower excitation potential of Fe I transitions for P2441. Plotted are log N(Fe) vs. EP (eV) for 16 lines of neutral iron in the G2 T Tauri star P2441. The agreement in abundances derived for lines with high ($\geq$ 4 eV) and low ($\leq$ 2.5 eV) indicates that a normal model photosphere is equally valid over this range of line-forming regions. Note that the equivalent width of Fe I λ6246, normally a very strong line, is abnormally weak in this star, possibly due to chromospheric filling.

Figure 6a), b) Standard deviation of [Fe/H] versus microturbulence for a) KM Orionis and b) LkCa 19. Iron abundances were derived for Fe I lines of varying strength at several different values of microturbulence. The microturbulence yielding the minimum standard deviation among the derived iron abundances is the correct value. For KM Orionis (Figure 6a), the microturbulent velocity is $\approx$ 1.8 km s^{-1}; for LkCa 19, it is about 3.2 km s^{-1}.

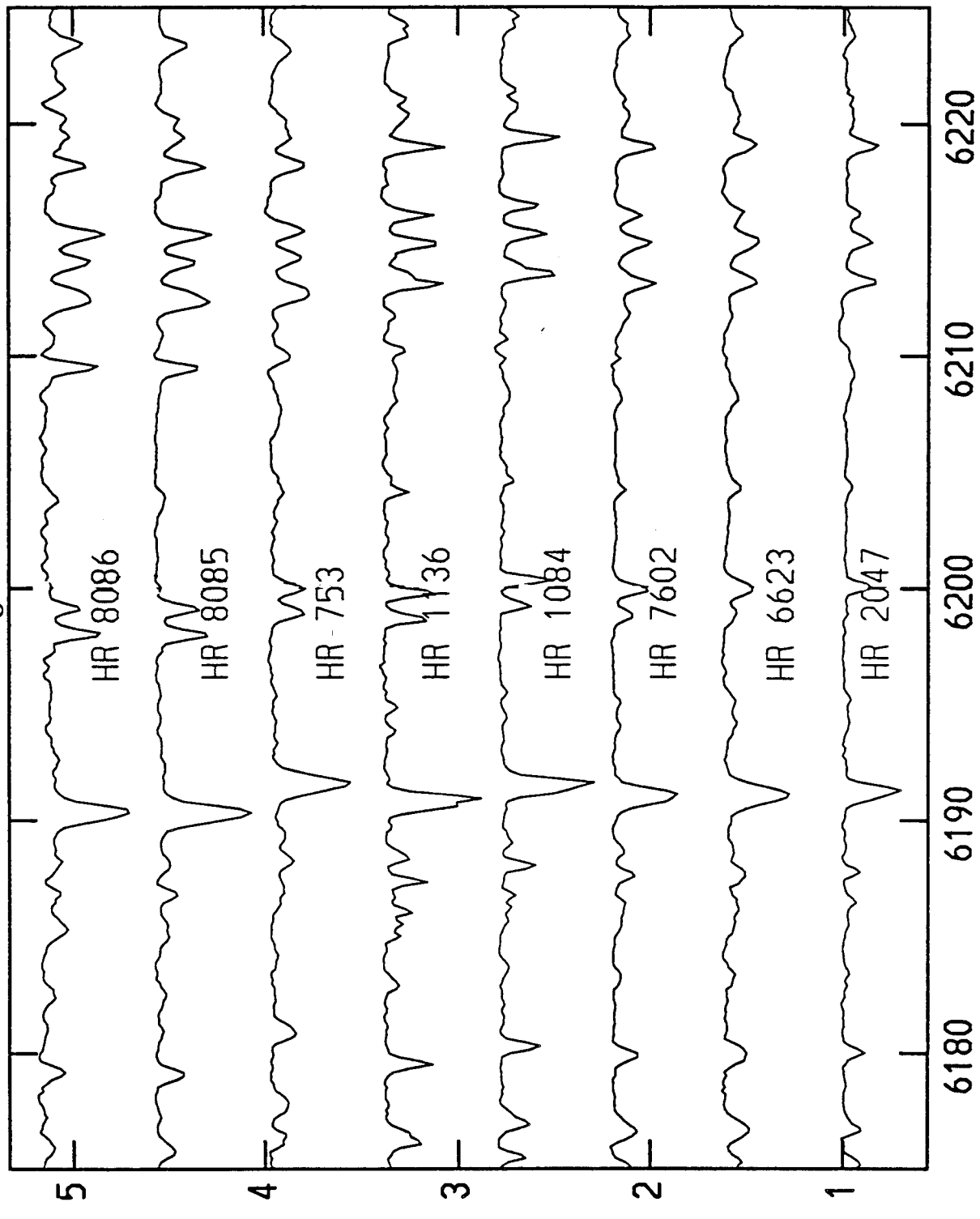
HR 8086
HR 8085
HR 753
HR 1136
HR 1084
HR 7602
HR 6623
HR 2047
5
4
3
2
1
6180
6190
6200
6210
6220

Figure 1

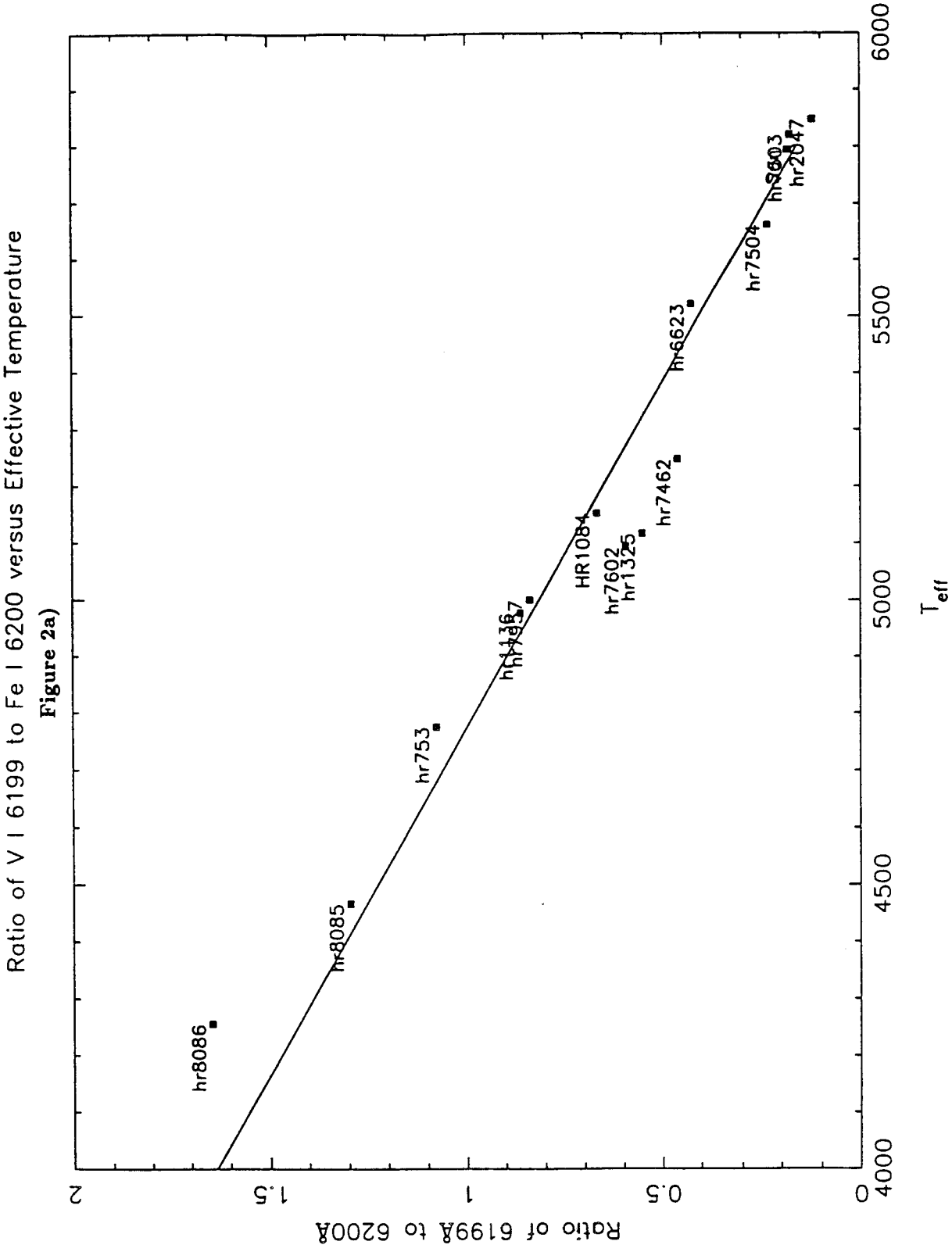
Ratio of V I 6199 to Fe I 6200 versus Effective Temperature
Ratio of 6199Å to 6200Å
T_{eff}
0
0.5
1
1.5
2
4000
4500
5000
5500
6000
hr8086
hr8085
hr753
hr7462
hr6623
hr7504
hr2047

Figure 2a)

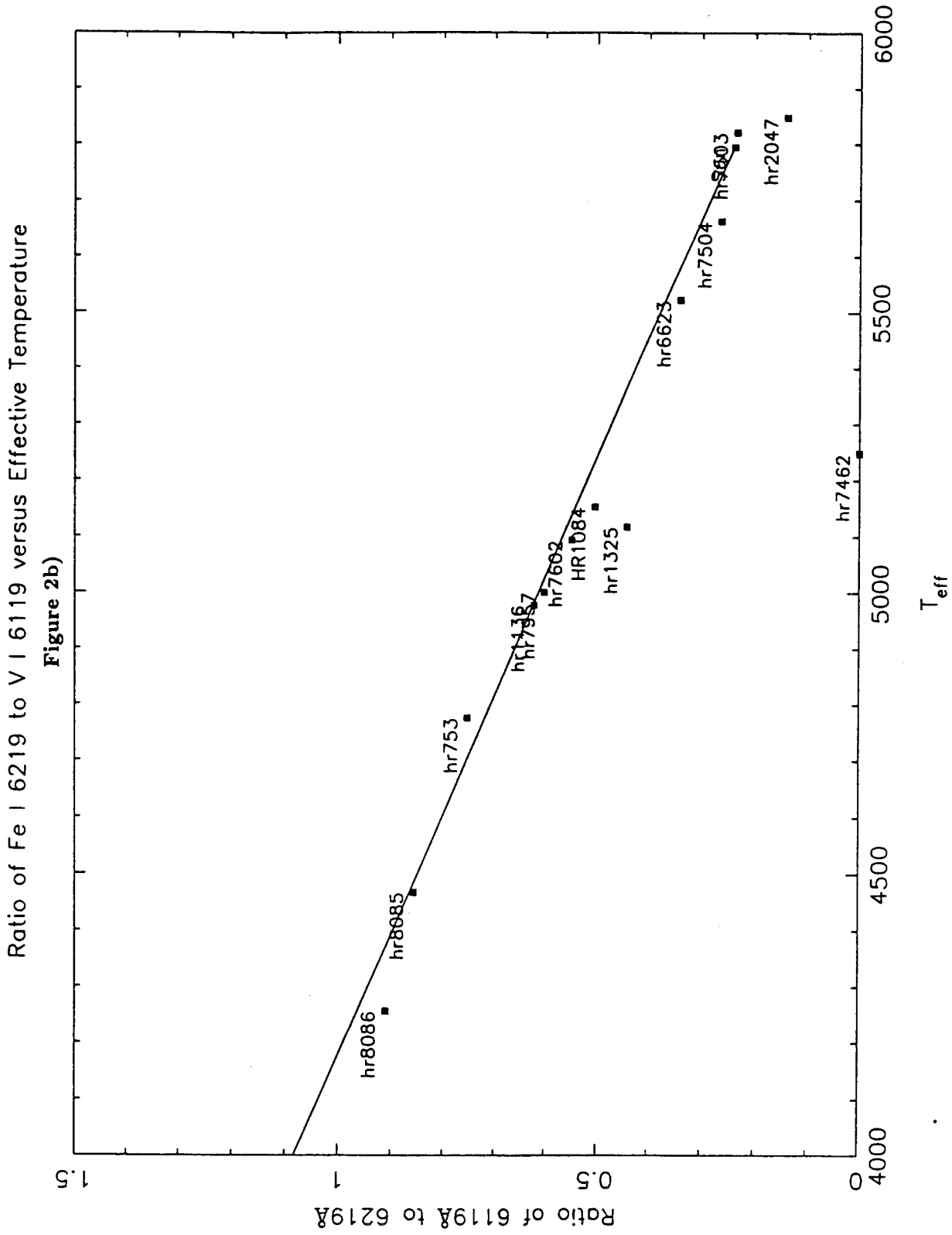
Ratio of Fe I 6219 to V I 6119 versus Effective Temperature
Figure 2b)
Ratio of 6119Å to 6219Å
T_{eff}
0
0.5
1
1.5
4000
4500
5000
5500
6000
hr8086
hr8085
hr753
hr1136
hr7602
HR1084
hr1325
hr6623
hr7504
hr2047
hr7462

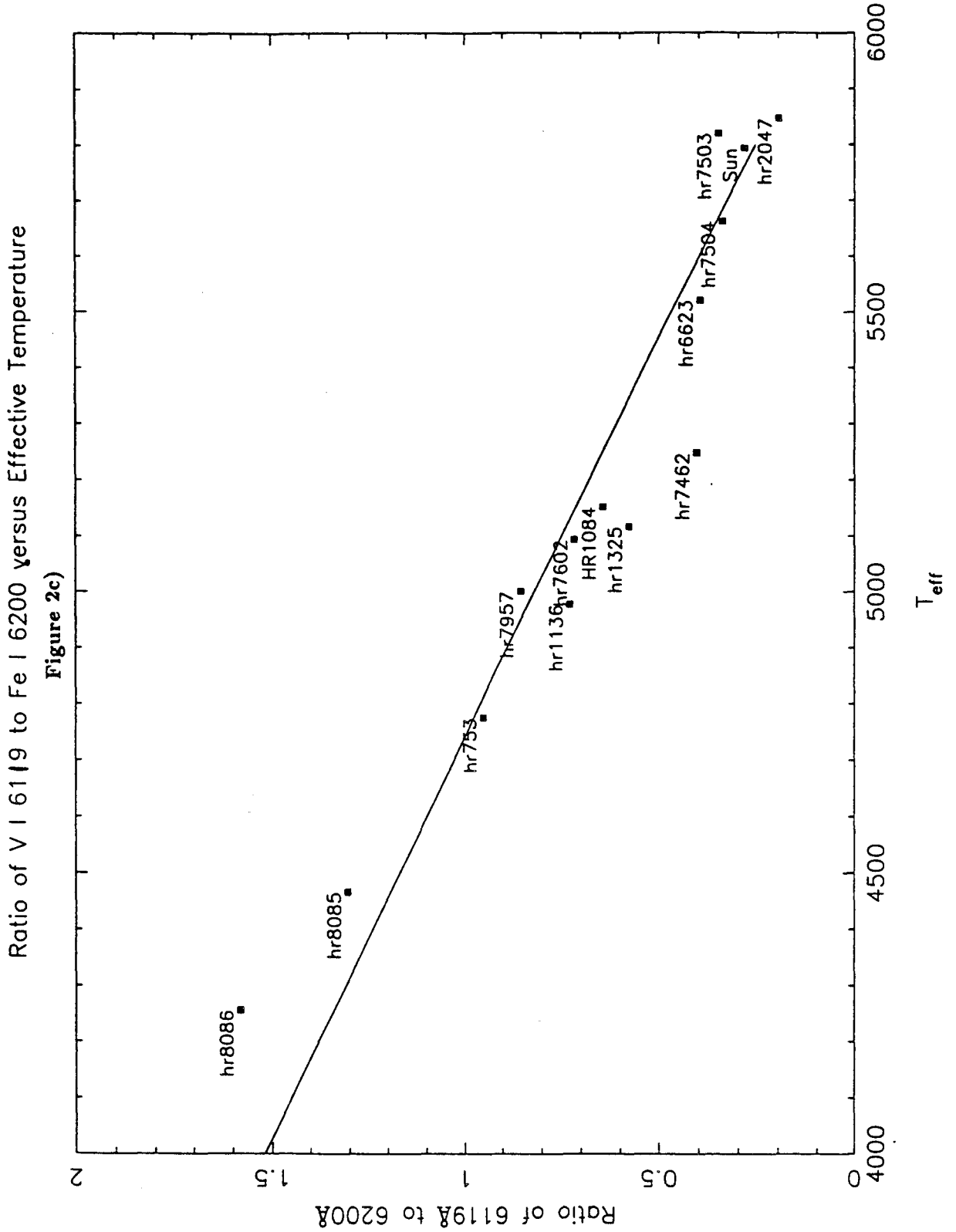
Ratio of V I 6119 to Fe I 6200 versus Effective Temperature
Ratio of 6119Å to 6200Å
T_{eff}
0
0.5
1
1.5
2
4000
4500
5000
5500
6000
hr8086
hr8085
hr753
hr7957
hr1136
hr7602
HR1084
hr1325
hr7462
hr6623
hr7504
hr7503
Sun
hr2047

Figure 2c)

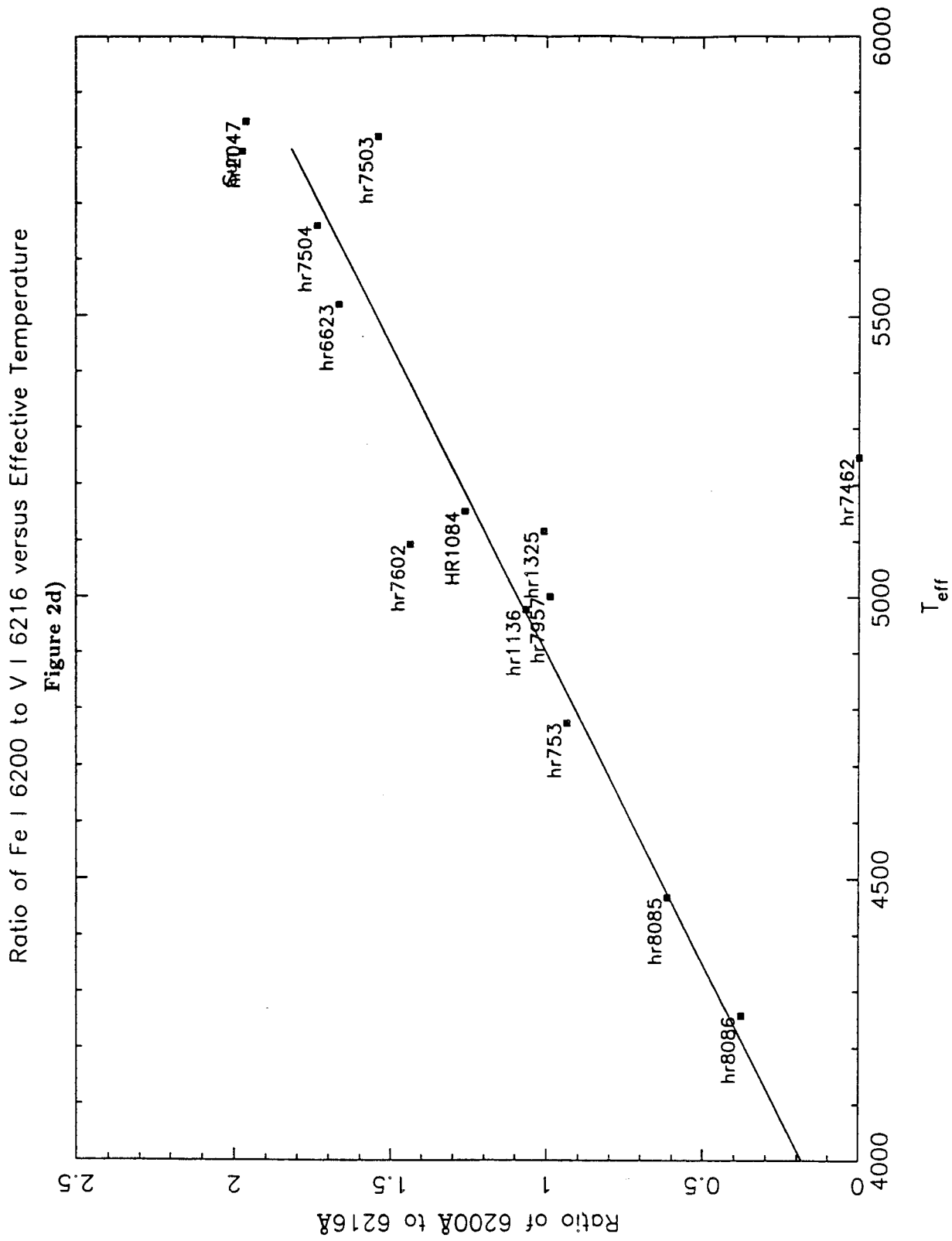
Ratio of Fe I 6200 to V I 6216 versus Effective Temperature
Ratio of 6200Å to 6216Å
T_{eff}
2.5
2
1.5
1
0.5
0
4000
4500
5000
5500
6000
hr7504
hr6623
hr7503
hr7602
HR1084
hr1136
hr1325
hr753
hr8085
hr8086
hr7462

Figure 2d)

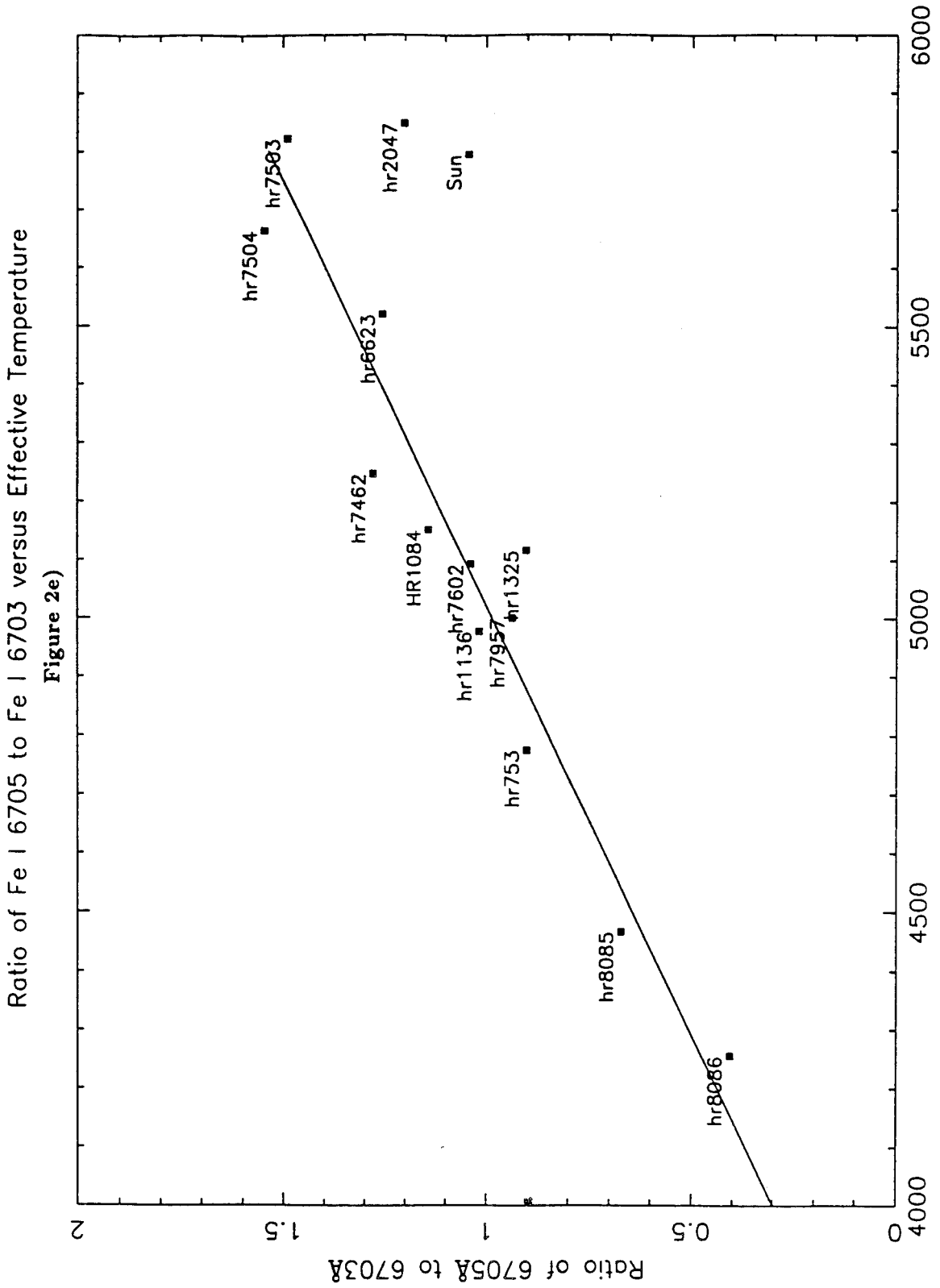
Ratio of Fe I 6705 to Fe I 6703 versus Effective Temperature
Ratio of 6705Å to 6703Å
T_{eff}
0
0.5
1
1.5
2
4000
4500
5000
5500
6000
hr8086
hr8085
hr753
hr7957
hr1136
hr7602
HR1084
hr7462
hr6623
hr7504
hr7503
hr2047
Sun
hr1325

Figure 2e)

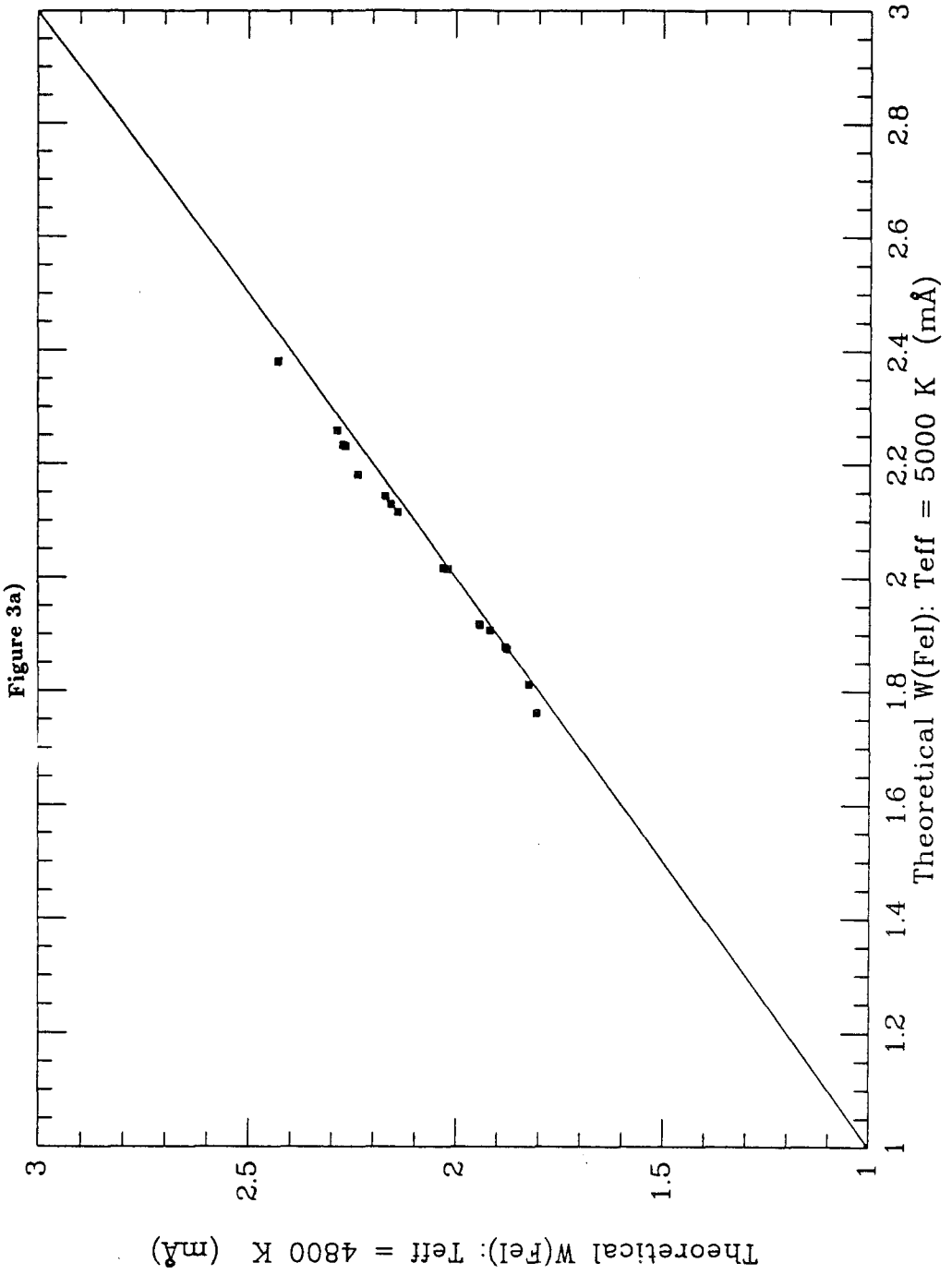
Figure 3a)
Theoretical W(FeI): Teff = 4800 K (mÅ)
3
2.5
2
1.5
1
1
1.2
1.4
1.6
1.8
2
2.2
2.4
2.6
2.8
3
Theoretical W(FeI): Teff = 5000 K (mÅ)

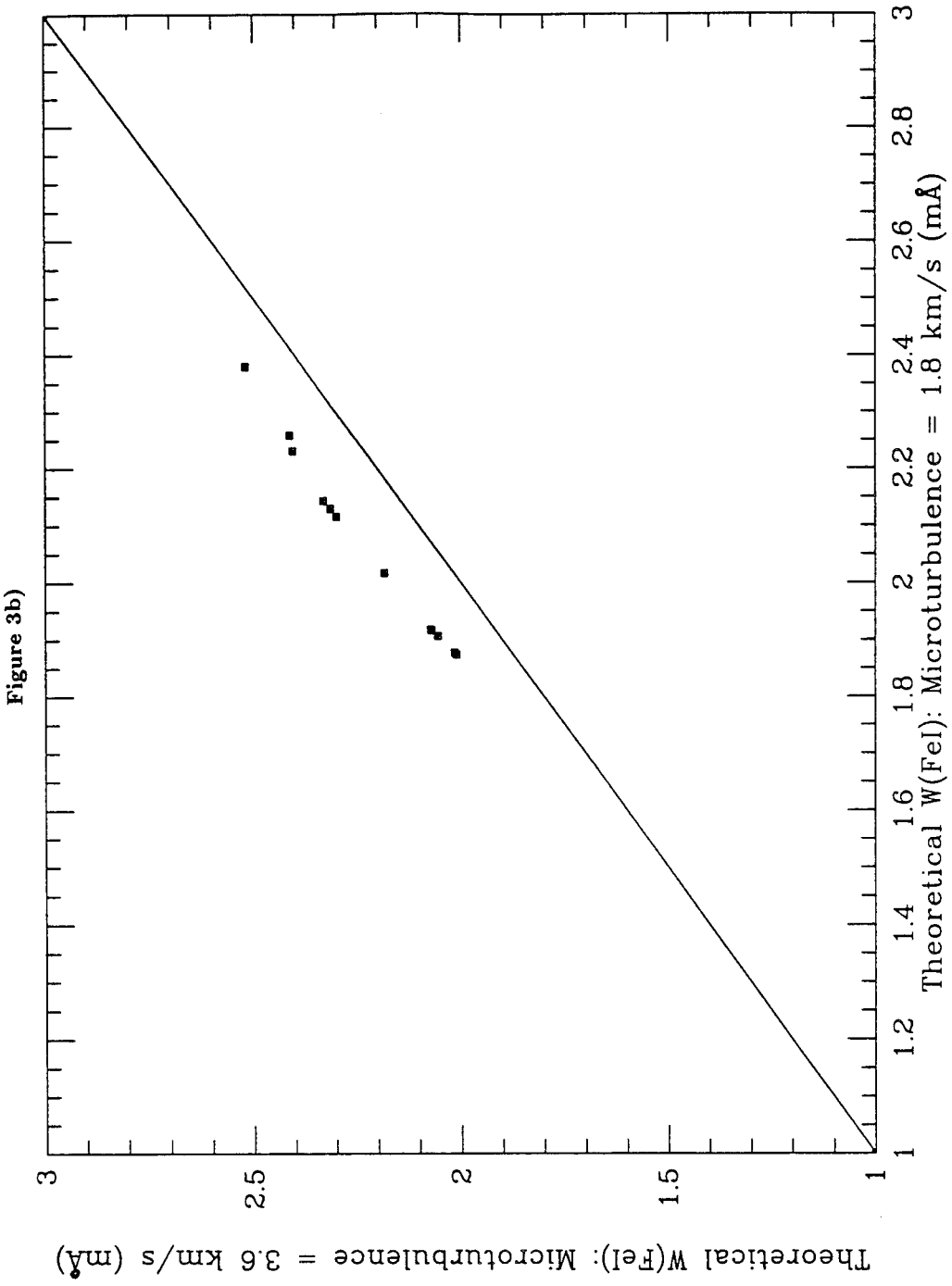
Theoretical W(FeI): Microturbulence = 3.6 km/s (mÅ)
3
2.5
2
1.5
1
1
1.2
1.4
1.6
1.8
2
2.2
2.4
2.6
2.8
3
Theoretical W(FeI): Microturbulence = 1.8 km/s (mÅ)

Figure 3b)

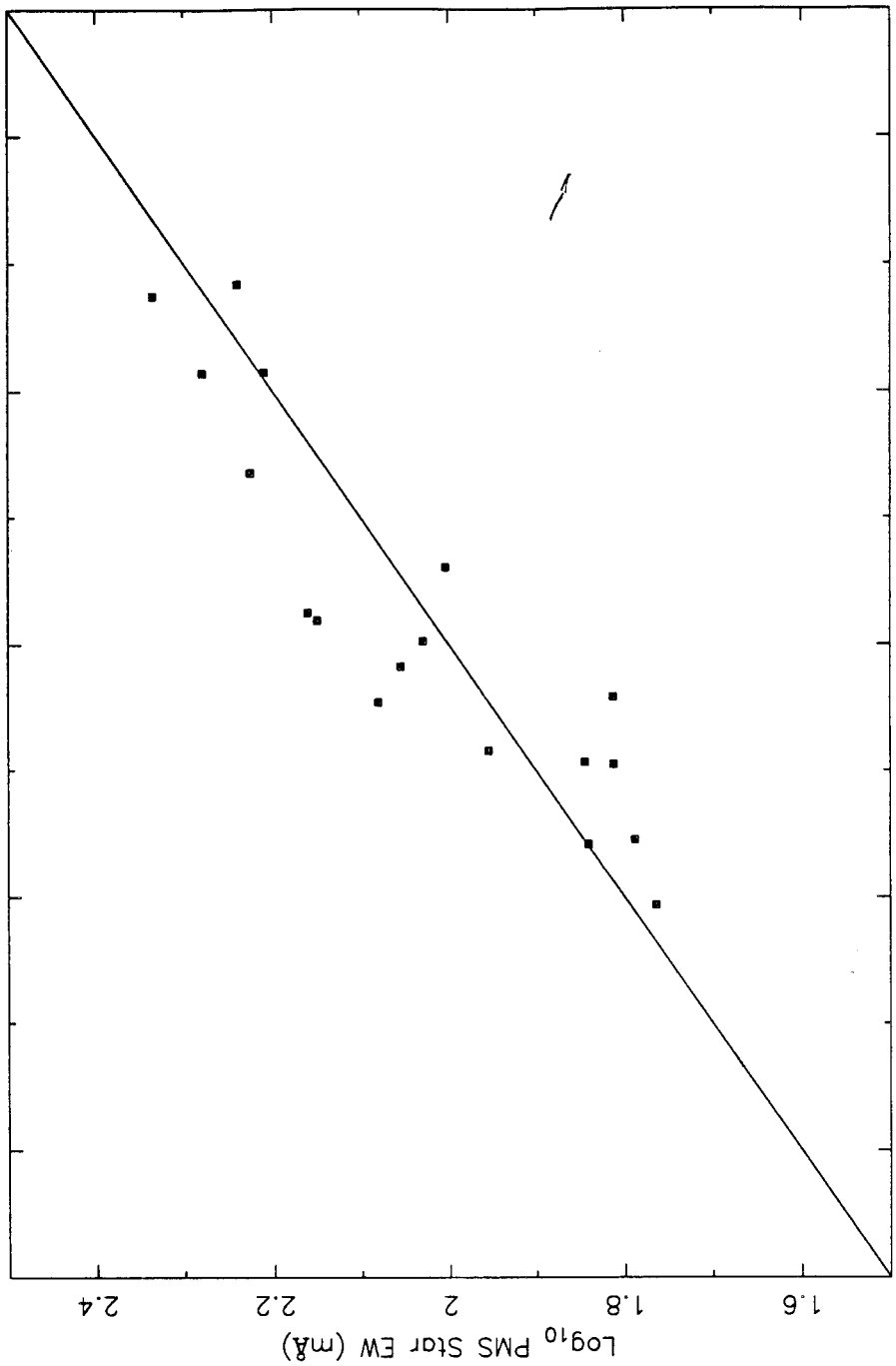

Figure 4a G-G 405 versus HR 1136

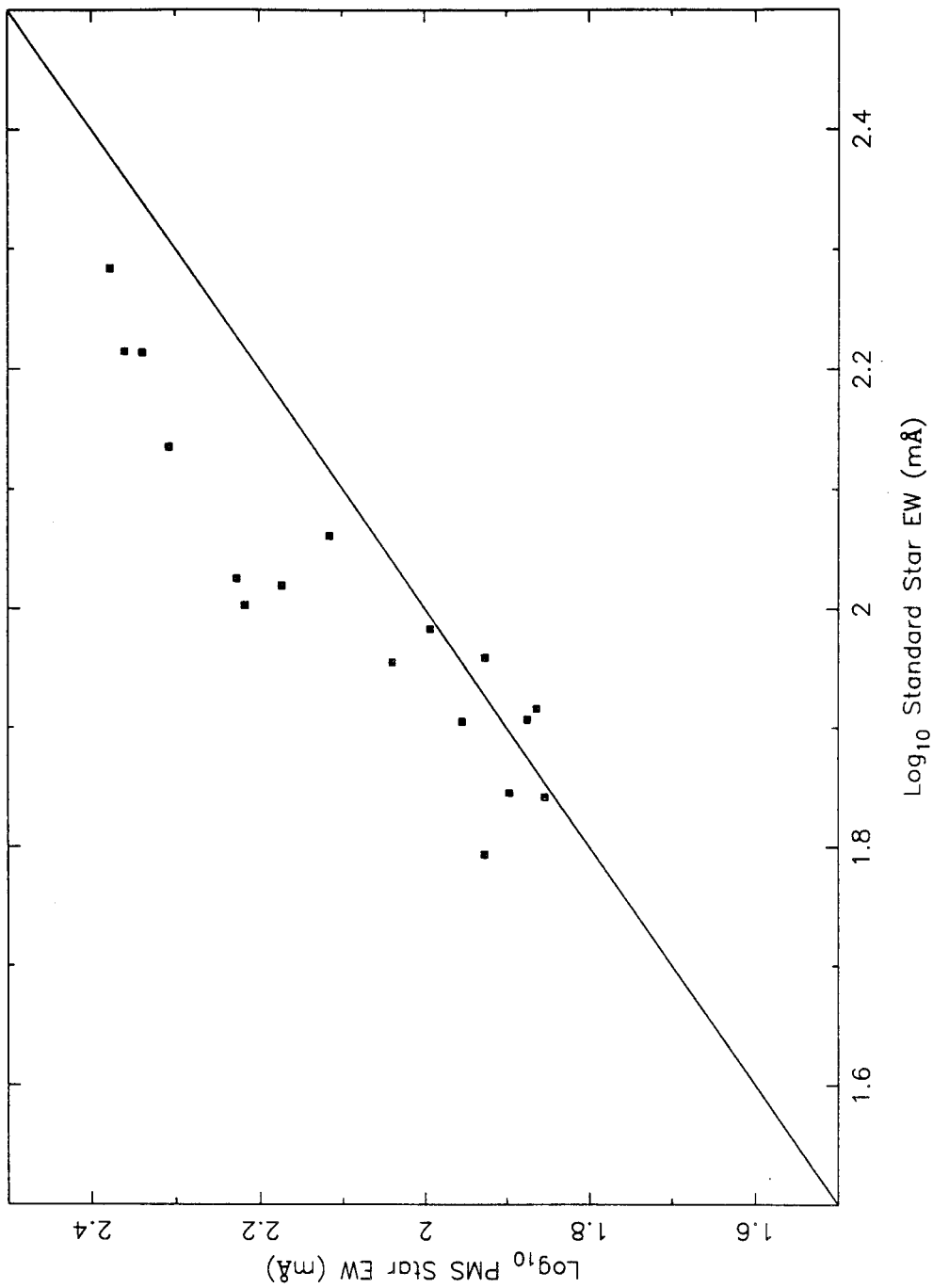

Figure 4b LkCa 19 versus HR 1136

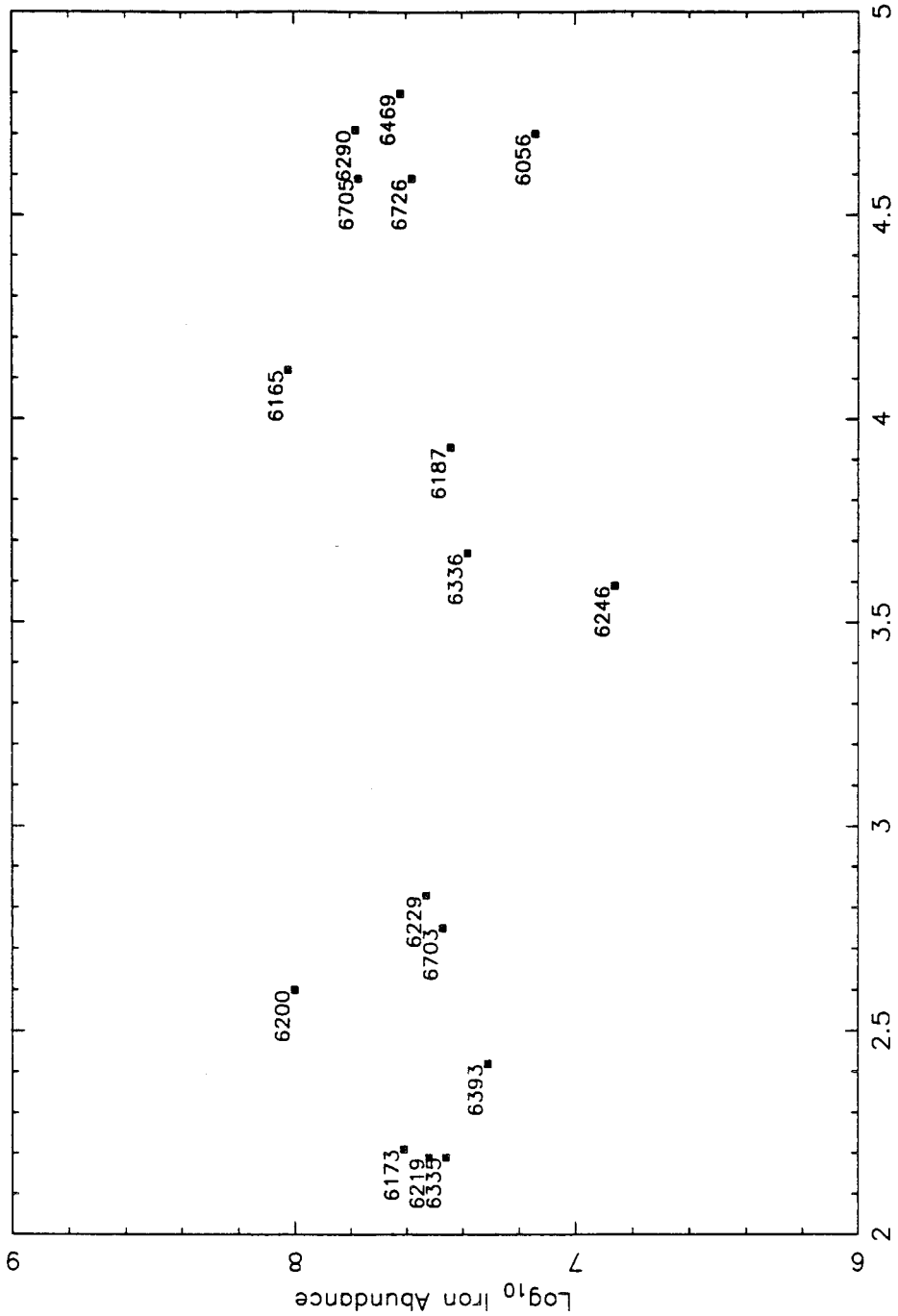
Log10 Iron Abundance
Lower Excitation Potential of Transistion (eV)
9
8
7
6
2
2.5
3
3.5
4
4.5
5
6165
6705
6290
6469
6726
6056
6187
6336
6246
6200
6229
6703
6393
6173
6219
6335

Figure 5.

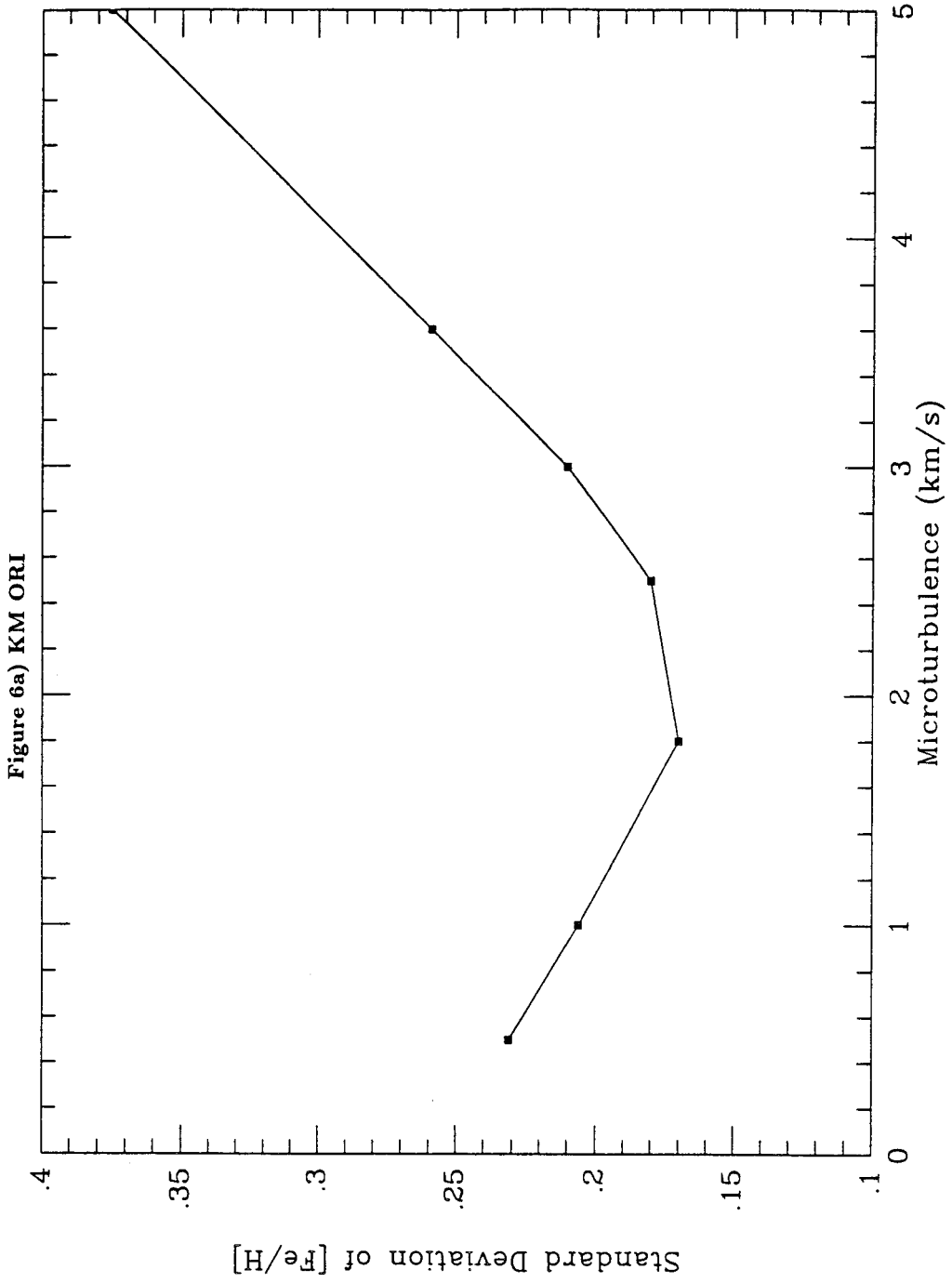
Figure 6a) KM ORI
Standard Deviation of [Fe/H]
.4
.35
.3
.25
.2
.15
.1
0
1
2
3
4
5
Microturbulence (km/s)

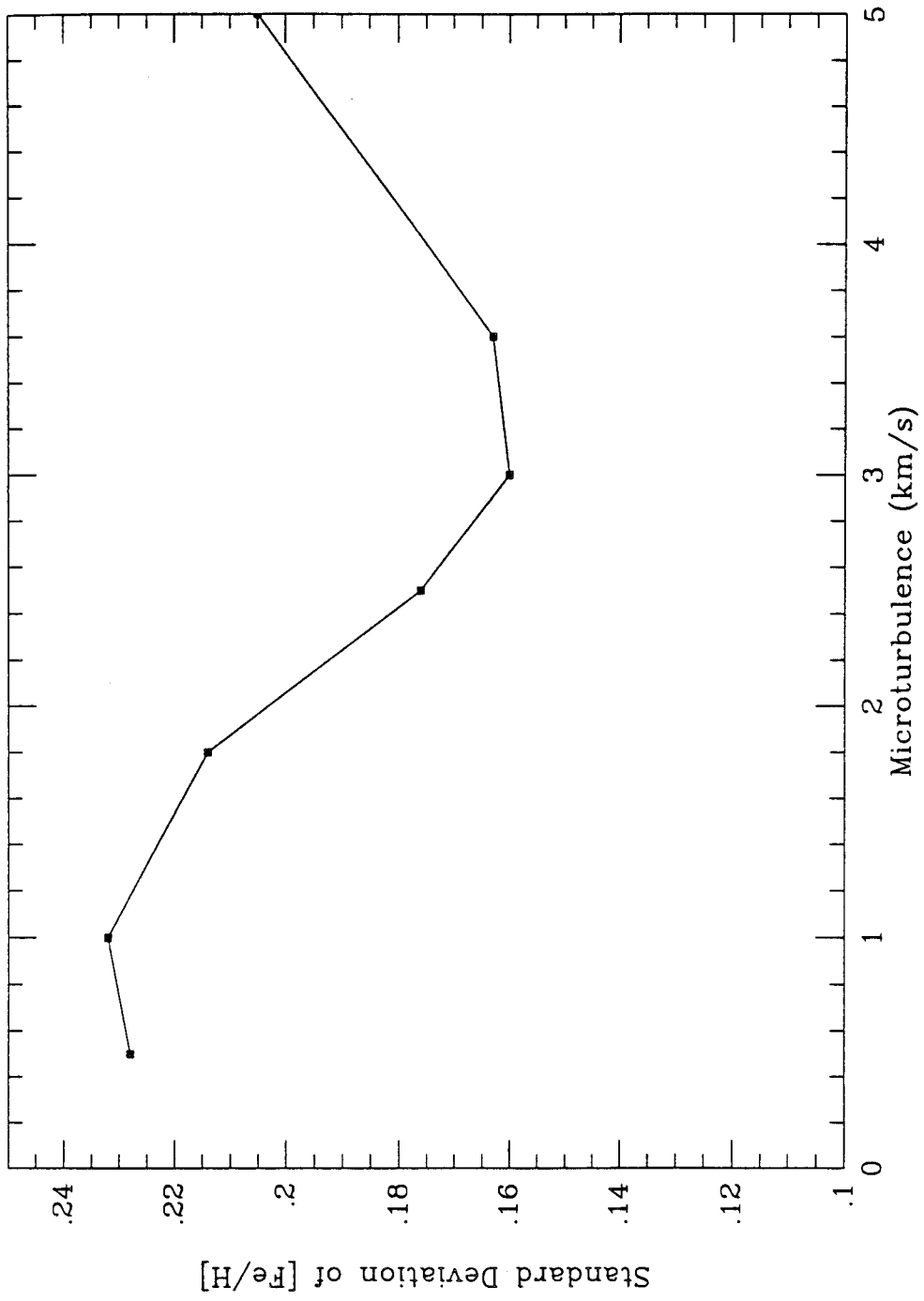

Figure 6b) LKCA 19

Chapter IV.

Metal Abundances in Nearby Pre-Main Sequence Star Associations

Abstract:

Using high-resolution echelle spectra, iron abundances have been determined for 30 pre-main sequence stars in several northern and southern hemisphere star-formation regions. Using samples of at least five stars in each cloud, bulk metallicities have been derived for the Taurus-Auriga, Orion, Chamaeleon, and Ophiuchus molecular clouds. [Fe/H] is slightly in excess of solar in Orion and Ophiuchus; Taurus-Auriga and Chamaeleon appear to have solar iron abundances. Abundances of aluminum, calcium, nickel, and titanium have also been found for some of the PMS stars. Within the uncertainties, all of these metal abundances have been found to be solar.

I. Introduction

Determination of metal abundances among stellar populations of varying age is a key observational tool for the study of galactic chemical evolution. During recent years, studies of nearby old disk stars have revealed that the metallicity of the star-forming interstellar medium increased by a factor of 2 (Carlberg *et al.* 1985) to 5 (Twarog 1980) during the period between 12 and 5 billion years ago. This age-metallicity relation decreases in slope for more recently formed stars in the solar neighborhood, indicating that the pace of chemical enrichment in the disk has slowed within the past four Gyr. Theoretical models of galactic chemical evolution have had varying success in fitting this empirical curve. All of these models depend upon assumed initial mass functions, star formation rates as a function of time, chemical composition of stellar ejecta ("yield"), and large scale galactic mass flows (Torres-Peimbert and Peimbert 1987). The central equation the simplest "one-zone" model of galactic chemical evolution is:

$$Z = p \ln \frac{m_{galaxy}}{m_{gas}}$$

where p ≡ yield of heavy elements, Z ≡ heavy element abundance (by mass), m_{galaxy} is the mass of the entire system, and m_{gas} is the mass of the residual gas (Searle and Sargent 1972). As more specific physical processes such as varying rates for different types of supernovae are introduced, the importance of the observed age-metallicity relation in constraining these models increases (Rocca-Volmerange and Schaffer 1990). The extension of the Twarog curve to stars much younger than the

Sun is required in order to provide a better observational foundation for studies of galactic chemical evolution.

However, the metal abundances of open cluster stars, which are among the youngest objects analyzed, seem to defy the extrapolation of the Twarog (1980) age-metallicity relation. Boesgaard (1989) explores the age-metallicity relation of the young disk in some detail. Metallicity studies of the Hyades (Cayrel, Cayrel de Strobel, and Campbell 1985; Boesgaard 1989; Boesgaard and Friel 1990), Pleiades (Boesgaard 1989; Boesgaard and Friel 1990), α Persei cluster (Balachandran, Lambert, and Stauffer 1989; Boesgaard and Friel 1990), Ursa Majoris stream (Boesgaard and Friel 1990), and other young clusters (Boesgaard and Friel 1990) reveal that age is not correlated with metallicity among stars younger than a few billion years. A good example of this is the Hyades (age $\approx$ 7 x 10^8 yrs.) [Fe/H] = +0.127 $\pm$ 0.022 as compared to -0.034 $\pm$ 0.024 for the Pleiades (age $\approx$ 7 x 10^7 yr) or Coma cluster (age $\approx$ same as Hyades) with [Fe/H] = -0.08 $\pm$ 0.04 (Boesgaard 1989). Some examples of even older, metal-rich open clusters (NGC 188, NGC 6791) have also been found (Janes, Tilley, and Lynga 1988). These results have been interpreted as evidence that the mixing time for chemically enriched gas to be incorporated into the star-forming interstellar medium is longer than 10^9 years (Boesgaard and Friel 1990). In the current study, metallicities are determined in four coeval associations of pre-main sequence stars. Discovery of a significant range in metal abundances between these very young clusters of the same age would provide further evidence of a long mixing timescale for the star-forming ISM.

One unique characteristic of pre-main sequence (PMS) star clusters is that they are still embedded in the interstellar clouds from which they formed. By comparing pre-main sequence atmospheric compositions to the ISM gas phase abundances de-

rived from ultraviolet absorption line studies of the same cloud, the amount of heavy elements locked up in interstellar grains within the cloud can be determined. During the almost 2 decades since the flight of *Copernicus* with the first high-resolution UV spectrograph, investigations of interstellar absorption features detected along a variety of "line-of-sight" through diffuse and moderately dense IS clouds have revealed that different elements show widely varying patterns of depletion with respect to solar abundance. It is presumed that these deficiencies in abundance are caused by the incorporation of metallic and volatile elements into interstellar grains (Jenkins 1987). The elements most affected are calcium, titanium, and aluminum; the abundance of these elements is as low as 1/1000 solar along certain lines-of-sight. Iron and nickel are also highly depleted, by factors of 10 or more. However, Na, K, and Mg are only depleted to 1/2 solar abundance, and sulfur and nitrogen are generally undepleted. Carbon and silicon depletion varies greatly according to the column density of hydrogen along the line-of-sight (Tielens and Allamandola 1987). Observed correlations between element depletion and condensation temperature (Field 1974) as well as first ionization potential (Snow 1975) suggest that a combination of grain condensation and accretion processes may explain the pattern of elemental depletions. Observations through clouds of varying column density reveal that the metallic elements Fe, Al, Ni, Ti, and Ca are increasingly depleted in regions with high hydrogen column density, with titanium being the element most sensitive to cloud density. It is unknown whether the correlation between column density and depletion is due to enhanced grain formation in dark clouds or by density inhibition of shocks which may destroy interstellar grains (Jenkins 1987). Although most of the UV ISM depletion studies have been conducted toward lightly or moderately reddened lines of sight due to instrumental limitations, some recent investigations have included the ρ Ophiuchus dark cloud (Snow and Joseph 1985) and the edge of

the Orion molecular cloud; both of these star-forming regions are included in the current study. Use of the Goddard High-Resolution Spectrograph (GHRS) aboard the Hubble Space Telescope is expected to expand the range of available lines of sight into deeply reddened regions in the near future. A common problem in all depletion studies is that the actual metallicity of the cloud is unknown; thus, solar abundance is assumed for all clouds, despite the variations in metal abundance seen among young main sequence clusters. Knowledge of individual cloud metallicities via compositional studies of associated young stars may improve the accuracy of depletion magnitudes by more than a factor of two (Joseph *et al.* 1986).

Until recently, solar-type pre-main sequence stars have been considered poor subjects for atmospheric abundance analysis. Most of the objects recognized as T Tauri stars prior to 1985 have intense Balmer line emission and excess continuum emission which "veils" (shallows) their photospheric absorption line spectrum. However, two fundamental discoveries during the late 1980's have changed the outlook toward abundance studies of PMS stars. First, a sizable population of "weak-line" or "naked" T Tauri stars have been found via X-ray studies of star-forming clouds (Walter *et al.* 1988). Although these stars have no veiling and weak emission lines, placement on the HR diagram shows them to be roughly coeval with the more active or "classical" T Tauri stars (CTTS) (Strom *et al.* 1989; Gauvin and Strom 1991), with ages generally less than 10^7 years. These WTTS are the direct ancestors of young main-sequence star cluster members, and they offer similar opportunities for analysis of coeval stars formed from the same interstellar material. Second, the "deep chromosphere" theory of T Tauri star activity has been largely abandoned in favor of the "disk/boundary layer" model (Bertout 1989). In the former theory, both excess continuum and emission lines in T Tauri star spectra were thought to be produced in a chromosphere of unusual optical depth and temperature structure

(Calvet *et al.* 1983). Assumption of this model implied that traditional atmospheric analysis of T Tauri stars would be meaningless, since the photospheric temperature structure of PMS stars would greatly differ from standard stellar atmopsphere models. However, the disk activity theory attributes all of the veiling continuum and most of the emission lines to a boundary layer between the slowly rotating T Tauri star and an accretion disk in Keplerian rotation about the star. Evidence for this model can be found in the work of Hartigan *et al.* (1989; 1991), in which the veiling continuum of CTTS is found to be a relatively flat continuum rather than a forest of chromospheric metallic lines. According to the disk activity model, T Tauri star photospheres should be completely similar to those of main sequence stars, although coverage by active regions and starspots is thought to be rather high in some cases (Bouvier, Bertout, and Boucher 1988). One major obstacle in the way of atmospheric analysis of these stars is a lack of accurate stellar parameters. Since many of the stars have unknown amounts of circumstellar extinction, traditional photometric temperature determinations are out of the question. Accurate spectroscopic temperatures can be found with the assistance of high-resolution spectra, and the current study uses the effective temperatures determined in Chapter III in the course of the abundance analysis. At this point in time, few abundance studies of PMS stars have been attempted, and all but one consist entirely of lithium abundance determinations (Bonsack and Greenstein 1959; Zappala 1972; Padgett 1989; Strom *et al.* 1989; Maguzzu and Rebolo 1988; Basri, Martin, and Bertout 1991; Duncan 1991). Only one iron abundance determination (for the Chamaeleon star Sz 19) has been previously done on a known PMS star (Franchini, Castelli, and Stalio 1991), which found that this young star was somewhat enriched in iron relative to the Sun. The derivation of abundances for other elements promises to assist in the extremely important lithium problem by identifying stars with unusual atmospheric

characteristics (e.g. high microturbulence) which may enhance the strength of Li I λ6707 as well as other metallic lines.

In this chapter, iron abundances are derived for 30 weak-line T Tauri stars in several star-forming regions. Samples of at least 5 stars are analyzed in each of the Taurus-Auriga, Orion, Chamaeleon, and Ophiuchus star-forming regions and used to derive the bulk metallicity of these clouds. Abundances of calcium, aluminum, titanium, and nickel are also derived for most of the stars. Metallicity dispersions within and between clouds are derived and discussed, and absolute depletions are obtained for the relevant elements in Ophiuchus and Orion.

II. Analysis

Spectra of 30 low-mass, pre-main sequence stars were obtained using the Palomar 1.2m echelle for the northern hemisphere stars and the Las Campanas 2.5m echelle spectrograph for the southern sky objects. The spectral range of these observations is $\approx$ 4600 to 9600 Å at a resolution of 20000 for the Palomar data and 3700 - 7000 Å and resolution of 30000 for the Las Campanas spectra. Lines of Fe I, Ti I, Ca I, Ni I, and Al I were selected from the orders between 5900 Å and 6700 Å where the signal-to-noise ratio of the spectra is greatest. Further details of the spectral reduction are found in Chapter II. Equivalent widths were measured on the reduced, continuum flattened spectra using the routines in the IRAF package *splot*. Comparison between spectra of the same object taken on different nights with the same instrument indicate an equivalent width uncertainty of about 12 %. The absorption features used in the analysis range in equivalent width from 30 - 250 mÅ. The equivalent widths for the pre-main sequence stars are listed in Table 3 of Chapter II. Solar equivalent widths used for the derivation of solar abundances

for each line were taken from the measurements of Furenlid and Meylan (1990) of the Kurucz *et al.* (1984) solar atlas.

The model atmosphere line abundance analysis was performed using the program RAI10 (courtesy of M. Spite via A. Boesgaard) with model photospheres provided by Gustafsson (1988, private communication). The grid of model atmospheres all assume solar metallicity and cover the temperature range between 4000 and 5800 K with steps of 200 K. All of the abundances were evaluated for models with $\log g = 3.8$; however, models with $\log g = 4.2$ were also available and were utilized to determine the gravity sensitivity of the abundance determinations. A solar model ($T_{eff} = 5770$; $\log g = 4.44$) was included with the grid. It was used to determine comparison solar abundances for the transitions in the study. Microturbulence values have been determined for 17 of the stars in the sample in Chapter III. For the stars without available microturbulence determinations, ξ_{mt} is assumed to be 1.8 km s^{-1}. The RAI10 program has the capability to evaluate blends with up to ten components, although in practice the metal lines chosen for this study were selected for their lack of blending. Broadening from radiation (natural), Van der Waals, and quadratic Stark effects are also included in the calculation. Transition probabilities for Fe I, Al I, Ni I, Ti I, and Ca I were obtained from Wiese (1979; 1984). The other $\log gf$ values come from Gurtovenki and Kostik (1981) and Thevénin (1984). Although RAI10 is capable of synthesizing spectral features, the output used in the current study is a list of calculated equivalent widths for given T_{eff} and abundances. Curves of growth were produced from this data and inverted to curves of constant abundance on an equivalent width versus effective temperature plot. Figure 1 is a sample of such a plot for Fe I 6705; the numbers beside the isoabundance contours are logarithmic iron abundances relative to Log N(H) = 12.00. Two-dimensional bicubic spline interpolation routines from *Numerical*

Recipes (Press *et al.* 1986) were then used to determine the logarithmic abundances for individual stars.

The lines chosen for the abundance determinations were selected on the basis of easy measurability in G - K star spectra, lack of obvious blending, and availability of reliable atomic parameters. Nearly all of the neutral iron lines were chosen from the database of Boesgaard and Burck (1988; private communication). Lines of other elements were selected from the list of "clean" solar lines by Rutten and van der Zalm (1984) and the features used in the abundance analysis of α Centari by Furenlid and Meylan (1990). The Fe I lines range in excitation potential from 1.48 eV to 4.61 eV. Table 1 is a list of the absorption lines used in the current study. Although a reasonable number of Fe I transitions were measured, few lines of the other interesting metals were usable due to their intrinsic weakness, the only moderate S/N of the PMS spectra, and rotational blending of the stronger features. In addition, blemishes and cosmic rays on individual spectra make some of the features in the list unusable for certain stars. The number of lines used in each iron abundance determination is noted in Table 3.

Table 2 shows the sensitivity of the elemental abundance determinations to uncertainties in various uncertainties in measurements and stellar parameters. The changes in [Fe/H] as a function of stellar parameter are calculated for LkCa 15, a K3 pre-main sequence star in Taurus-Auriga. The effective temperatures derived from spectroscopic line ratios in Chapter III are believed to be accurate to $\pm$ 200 K in most cases. Log$g$ = 3.8 is typical for G - K type PMS stars according to Cabrit *et al.* (1990) and Basri, Martin, and Bertout (1991), with a spread of a few times 0.1 dex. Microturbulence (ξ_{mt}) is more uncertain in these stars. Even the objects with ξ_{mt} determined in Chapter III have a potential error of $\geq$ 0.5 km s^{-1}, and the value

of 1.8 km s^{-1} used for the remainder of the sample is simply a guess based on the mean value found for the others. Equivalent width measurement errors, estimated at 12 %, also contribute to the uncertainty, especially for the weak features of Al I, Ti I, and Ni I.

III. Results

Table 3 gives the mean iron abundances for each star, both in terms of the absolute logarithmic abundance (relative to log N(H) = 12) and the abundance relative to solar ([Fe/H] = log $N(Fe)_*$ - log $N(Fe)_\odot$). The uncertainties listed with each value are the logarithimic standard deviations σ about the means. The standard deviations for individual stars vary greatly; those larger than the total uncertainty from random errors in measurement and stellar parameters appear to be correlated with low S/N and higher v sin i that are responsible for uncertain continuum placement and increased blending of weak metallic features. Stars are grouped according to star-formation region, and the mean iron abundance for each group and standard deviation between cluster members is listed in Table 4. According to the PMS evolutionary tracks of Cohen and Kuhi (1979), the oldest stars in the sample are NTTS 035120+3154 SW and NTTS 035135+2528 NE in Taurus-Auriga with ages of $\approx 2 \times 10^7$ years. Ages among the other stars range from 10^6 - 10^7 years. Figures 2 is a plot of [Fe/H] versus effective temperature for the stars of Taurus-Auriga, Orion, Chamaeleon, and Ophiuchus. The average error bar on the iron abundance is about 0.25 dex. The lack of temperature correlation in this diagram indicates that no grevious systematic temperature determination errors are present.

Abundances for calcium, aluminum, titanium, nickel, and vanadium are given in Table 5. The abundances listed in Column 5 are logarithmic values relative to

HR 1136, a K0 subgiant with near-solar metallicity (Cayrel de Strobel *et al.* 1985) which was observed with the Palomar 60-inch echelle. Atomic parameters for the lines used in these determinations are relatively uncertain, and the weakness of some of the features implies possibly significant equivalent width measurement errors for the spectra with S/N $\leq$ 100. However, by comparing the PMS abundances to those derived from a well-known standard observed at the same resolution, the uncertainties due to unresolved blends will be partially cancelled. The cluster average abundances are given in Table 6; no significant differences from solar abundances are apparent.

IV. Discussion

The mean iron abundances derived for four PMS association and, thus, for 4 molecular star-forming clouds are roughly solar, with some slight variations between groups. These values are presented in Table 5. The highest metallicity is found for six stars in the southern Orion cloud with $\overline{[Fe/H]} = +0.0917$ with a standard deviation (σ) of 0.0465 between the values of individual cluster members. similar to the Hyades $\overline{[Fe/H]} = +0.127 \pm 0.022$ (Boesgaard and Friel 1990). The mean iron abundance for the five Ophiuchus PMS stars is also about 2σ above solar abundance. The metallicities of the Taurus-Auriga and Chamaeleon objects are solar to within the uncertainties. These $\overline{[Fe/H]}$ values compare well with the iron abundances obtained for young main sequence clusters; however, the standard deviations of [Fe/H] within the T Tauri star associations are larger than those of the older clusters. The greater uncertainty in the PMS cluster abundances are a direct consequence of the larger stellar abundance uncertainties. The average abundance standard deviation among the Fe I lines used to derive individual stellar [Fe/H] is 0.25 dex in the current study. In comparison, $\overline{\sigma_{Fe}} = 0.090$ for the 14 Hyades stars analyzed

by Boesgaard and Friel (1990). The most important reason behind this difference is undoubtably the much higher signal-to-noise ratio of the Hyades observations (average S/N $\approx$ 500, compared to $\leq$ 100 for the current study). However, other contributing factors could be the smaller number of PMS stars included in the survey, uncertainty of PMS star stellar parameters (T_{eff}, log g, etc.), and possibly the higher activity level of the WTTS compared with the young main sequence stars (Cayrel *et al.* 1985). However, the near-solar metallicities obtained for this sample of PMS stars, in agreement with the young cluster studies, indicates that WTTS atmospheres are similar enough to ordinary stars to be analyzed using conventional model photospheres.

The only other high resolution study of iron abundance in a T Tauri star is the spectral synthesis analysis of Sz 19 by Franchini, Castelli, and Stalio (1991)(FCS). In the current analysis, the effective temperature found by FCS has been adopted. The microturbulence is assumed to be 1.8 km s^{-1}, within the uncertainties of the 1.6 $\pm$ 0.3 km s^{-1} determined by FCW. Surface gravity of $\log g = 4.0$ was used by FCW; $\log g = 3.8$ is assumed in the current study. Despite the similarity of the assumed stellar parameters, my results do not confirm the value of [Fe/H] = +0.24 $\pm$ 0.06 found in the previous work, although the current value of -0.03 $\pm$ 0.29 is (barely) consistent to within the uncertainties. The reason for this large discrepancy is probably a difference in continuum placement between the two investigations, possibly due to FCS's much higher S/N. Since Sz 19 is a relatively rapid rotator ($v \sin i \approx 35$ km s^{-1}), weak metallic lines in its spectra blend together, lowering the "continuum" level. Thus, moderate S/N curve of growth studies are at risk for underestimating abundances of rapidly rotating stars by a considerable degree. Spectral synthesis is the future analysis method of choice for such stars.

Not included in the calculation of $\overline{[Fe/H]}$ for the Taurus-Auriga cloud are the iron abundances for NTTS 042417+1744 and NTTS 043124+1824 due to the excessively large values derived for these stars. Both of these objects yield [Fe/H] $\geq +0.3$, which, if accurate, would qualify them as super metal-rich! The star HD 245059 in the northern Orion cloud also has an outstandingly large iron abundance ([Fe/H] = $+0.3307 \pm 0.20$) as derived in this study. The most likely explanation for the discrepant metallicities is an underestimate in the microturbulence values assigned to each of these objects. These stars were among the 13 weak-line T Tauri stars which eluded constraint from the microturbulence determinations in Chapter III. Thus, their metal abundances have been derived assuming $\xi_{mt} = 1.8$ km s^{-1}. The Taurus-Auriga star LkCa 19 (type K0) with microturbulence of 3.2 km s^{-1} also yields an [Fe/H] in excess of +0.3 if $\xi_{mt} = 1.8$ km s^{-1} is substituted for the correct value. As in Chapter III, it is possible to constrain the microturbulent velocities of the discrepant Taurus-Auriga objects by requiring their metallicities to conform to the "cloud" $\overline{[Fe/H]}$. With this assumption, the microturbulence of both stars is found to be ≈ 2.5 km s^{-1}. In the case of HD 245059, the difference in metallicity compared to stars of the southern (-6°) Orion molecular cloud could be due to an actual compositional difference; however, abundance analysis of other stars in that immediate region is required for conclusive evidence. A remotely possible explanation for all of the discrepant metallicities is the possibility that the stars with unusual abundances might not have formed in the nearby cloud; this is unlikely in the case of the Taurus-Auriga "naked T Tauri stars" (NTTS) (Walter *et al.* 1988).

The small differences in metallicity between coeval pre-main sequence stellar associations provides further evidence that mixing of chemically enriched material into the ISM has not occurred uniformly or on an extremely short time scale during

the present epoch of galactic chemical evolution. Boesgaard and Friel (1990) have constrained the "mixing time" of the ISM to $\geq 10^9$ yr based on their metallicities for young main sequence clusters. However, the small size of the metallicity differences between star-forming clouds indicates that molecular clouds are probably not chemically isolated from the rest of the galactic ISM throughout many cycles of star formation/destruction/ cloud re-collapse as suggested by Elmegreen (1987). One interesting possibility is that Orion and Ophiuchus have enhanced metal abundances because of the massive star formation and rapid subsequent enrichment of the ISM which also occurs in these birthplaces of low-mass stars. On the other hand, Taurus-Auriga is exclusively a site of low-mass star formation, where stars are slow to evolve to stages in which they lose chemically enriched material. An expansion of the current study to include more bimodal star-formation regions (such as Cygnus and Monoceros) as well as other Taurus cloud analogues (Lupus) will help to settle the question of whether chemical enrichment occurs internally or externally in molecular clouds.

Using the bulk cloud metallicities determined in this chapter, absolute depletions can be found for the lines of sight to η and π^5 Orionis (Shull 1979) as well as ρ Ophiuchi (Snow and Joseph 1985). The bulk metallicities derived for the Ophiuchus and Orion cloud complexes permit the derivation of absolute depletions for some metallic elements in these clouds. Ultraviolet observations of the lines-of sight to ϵ and π^5 Orionis indicate that iron is depleted by 1.2 - 1.5 dex and titanium by 1.1 - 1.5 dex relative to solar abundances in this region (Shull 1979). Since the [Fe/H] of Orion is $+0.09 \pm 0.05$, the total depletion of iron is actually 1.3 - 1.6 $\pm$ 0.05 dex, and titanium is depleted by 1.3 - 1.7 $\pm$ 0.2 dex. In Ophiuchus, the differences are even less significant: iron depletions go from -2.4 to -2.48 dex; aluminum from -1.7 to -1.6 dex; calcium from -5.2 to -5.3; nickel from $\leq$ -3.9 to -4.0; and titanium is

unchanged (Snow and Joseph 1985). These changes are small enough to be ignored for relative depletion studies within a given cloud complex. However, the current study indicates that metallicity differences between clouds are easily large enough to cause 0.2 dex errors in depletion investigations which include several clouds, such as those which address the correlation between depletion and n(H).

V. Summary

Iron abundances have been determined for 30 weakly active pre-main sequence stars of type G-K in several star-formation regions. Samples of at least 5 stars in Taurus-Auriga, Orion, Chamaeleon, and Ophiuchus enabled bulk metallicities to be found in each of these clouds. Small excesses of [Fe/H] over solar abundances are found in both Orion and Ophiuchus. Taurus-Auriga and Chamaeleon appear to have solar iron abundances to within the uncertainties. Abundances of aluminum, calcium, titanium, and nickel have also been derived for some of the PMS stars. Absolute depletion values for these elements, as well as iron, are determined for the lines-of-sight through the Orion and Ophiuchus clouds.

REFERENCES

Balachandran, S., Lambert, D. L., Stauffer, J. R. 1988, *Ap.J.*, **333**, 267.

Basri, G., Martin, E., Bertout, C. 1991, Submitted to *AA* (BMB).

Bertout, C. 1989, *Ann.Rev.Astron.Ap.*, **27**, 351.

Boesgaard, A. M. 1984, *A.J.*, **89**, 1635.

Boesgaard, A. M. 1989, *Ap.J.*, **332**, 410.

Boesgaard, A. M., Burck, E. E. 1988, private communication.

Boesgaard, A. M., Friel, M. J. 1990, *Ap.J.*, **351**, 467.

Boesgaard, A. M., Tripicco, M. J. 1986, *Ap.J.*, **303**, 724.

Bonsack, W. K., Greenstein, J. L. 1959, *Ap.J.*, **131**, 83.

Bouvier, J., Bertout, C., Boucher, P. 1988, *A.A.Supp.*, **75**, 1.

Cabrit, S., Edwards, S., Strom, S. E., Strom, K. M. 1990, *Ap.J.*, **354**, 687.

Calvet, N., Basri, G., and Kuhi, L. V. 1983, *Ap.J.*, **277**, 725.

Carlberg, R. G., Dawson, P. C., Hsu, T., Vandenberg, D. A. 1985, *Ap.J.*, **294**, 674.

Cayrel, R., Cayrel de Strobel, G., Campbell, B. 1985, *A.A.*, **146**, 249.

Cayrel de Strobel, G., Bentolila, C., Hauck, B., Duguennoy, A. 1985, *A.A.Supp.*, **59**, 145.

Cohen, M., Kuhi, L. 1979, *Ap.J.Supp.*, **41**, 743.

Duncan, D. K. 1981, *Ap.J.*, **248**, 651.

Elmegreen, B. G. 1987, in *Interstellar Processes*, eds. D. J. Hollenbach and H. A. Thronson, Jr. (Dordrecht:Reidel), p. 259.

Field, G. B. 1974, *Ap.J.*, **187**, 453.

Franchini, M., Castelli, F., Stalio, R. 1991, *A.A.*, **242**, 449.

Fuhr, J. R., Martin, G. A., Wiese, W. L., Younger, S. M. 1981, *J.Phys.Chem.Ref.Data*, **10**, 305.

Furenlid, I., Meylan, T. 1990, *A.A.*, **350**, 827.

Gauvin, L. S., Strom, K. M. 1991, *FCAD* preprint.

Gurtovenko, E. A., Kostik, R. I. 1981, *Ap.J.Supp.*, **46**, 239.

Gustafsson, B. 1988, personal communication.

Hartigan, P., Hartmann, L. W., Kenyon, S. J., Hewett, R., and Stauffer, J. R. 1989, *Ap.J.Supp.*, **70**, 899.

Hartigan, P., Kenyon, S. J., Hartmann, L. W., Strom, S. E., Edwards, S., Welty, A. D., Stauffer, J. R. 1991, *FCAD* preprint.

Janes, K. A., Tilley, C., Lynga, G. 1988, *A.J.*, **95**, 771.

Jenkins, E. B. 1987, in *Interstellar Processes*, eds. D. J. Hollenbach and H. A. Thronson, Jr. (Dordrecht:Reidel), p. 533.

Joseph, C. L., Snow, T. P., Seab, C. G., Crutcher, R. M. 1986, *Ap.J.*, **309**, 771.

Kurucz, R. L. 1984, *Smithsonian Ap. Obs. Rept.*, No. 362.

Maguzzu, A., Rebolo, R. 1988, *Mem. S. A. It.*, **60**, 105.

Padgett, D. L. 1989, in *Cool Stars, Stellar Systems, and the Sun*, Sixth Cambridge Workshop, (Astron. Soc. Pac. Conference Series), ed. G. Wallerstein, p. 354.

Press, W. H., Flannery, B. P., Teukolsky, S. A., Vetterling, W. T. 1986, *Numerical Recipes* (Cambridge University Press), p. 95.

Rocca-Volmerange, B., Schaeffer, R. 1990, *A.A.*, **233**, 427.

Rutten, R. J., van der Zalm, E. B. J. 1984, *Astron.Ap.Supp.*, **55**, 171.

Searle, L., Sargent, W. L. W. 1972, *Ap.J.*, **173**, 25.

Snow, T. P. 1975, *Ap.J.*, **202**, L87.

Snow, T. P., Joseph, C. L. 1985, *Ap.J.*, **288**, 277.

Spite, F., Spite, M. 1982, *A.A.*, **115**, 357.

Strom, K. M., Strom, S. E., Edwards, S., Cabrit, S., Skrutskie, M. F. 1989, *A.J.*, **97**, 1451.

Thévenin, F. 1990, *A.A.Supp.*, **82**, 179.

Tielens, A. G. G., Allamandola, L. J. 1987, in *Interstellar Processes*, eds. D. J. Hollenbach and H. A. Thronson, Jr. (Dordrecht:Reidel), p. 397.

Torres-Peimbert, S., Peimbert, M. 1987, in *Interstellar Processes*, eds. D. J. Hollenbach and H. A. Thronson, Jr. (Dordrecht:Reidel), p. 667.

Twarog, B. 1980, *Ap.J.*, **242**, 242.

Walter, F. M., Brown, A., Mathieu, R. D., Myers, P. C., Vrba, F. J. 1988, *A.J.*, **96**, 297.

Wiese, W. L., Fuhr, J. R. 1975, *J.Phys.Chem.Data*, **4**, 263.

Wiese, W. L., Smith, M. W., Miles, B. M. 1969, *Atomic Transition Probabilities: Na through Ca, NBS-22* Vol. II (USGPO) .

Zappala, R. R. 1972, *Ap.J.*, **172**, 57.

Table 1

Line Identification	E.P. (eV)	log gf	W_λ(Sun) (Å)	W_λ(HR 1136)(Å)
Fe I 6750.152Å	2.41	-2.620	0.075	0.100
Fe I 6726.668Å	4.59	-1.160	0.043	0.058
Fe I 6705.117Å	4.59	-1.170	0.043	0.068
Fe I 6703.573Å	2.75	-3.130	0.038	0.067
Fe I 6581.218Å	1.48	-4.790	0.018	0.083
Fe I 6469.210Å	4.84	-0.760	0.063	0.091
Fe I 6393.612Å	2.42	-1.590	0.151	0.199
Fe I 6336.830Å	3.67	-0.740	0.111	0.157
Fe I 6335.337Å	2.19	-2.230	0.106	0.157
Fe I 6290.974Å	4.71	-0.760	-	0.086
Fe I 6246.327Å	3.59	-0.680	0.133	0.202
Fe I 6229.232Å	2.83	-3.020	0.039	0.090
Fe I 6219.287Å	2.19	-2.433	0.095	0.127
Fe I 6200.321Å	2.60	-2.490	0.077	0.109
Fe I 6187.995Å	3.93	-1.800	0.049	0.081
Fe I 6173.341Å	2.21	-2.880	0.069	0.103
Fe I 6165.363Å	4.12	-1.580	0.045	0.091
Fe I 6056.013Å	4.73	-0.460	0.078	0.130
Al I 6696.020Å	3.14	-1.340	0.032	0.118
Al I 6698.669Å	3.14	-1.650	0.020	0.055
Ca I 6717.687Å	2.71	-0.390	0.103	0.197
Ca I 6471.660Å	2.52	-0.590	0.110	-
Ca I 6166.440Å	2.52	-1.260	0.071	0.115
Ca I 6122.217Å	1.89	-0.200	0.218	0.318
Ni I 6767.784Å	1.83	-2.170	0.074	0.106
Ni I 6643.629Å	1.68	-2.300	0.097	0.158
Ni I 6108.107Å	1.68	-2.720	0.066	0.097
Ti I 6743.124Å	0.90	-1.760	0.020	0.071
Ti I 6261.101Å	1.43	-0.590	0.049	0.092
Ti I 5978.543Å	1.87	-0.580	0.024	0.094
Ti I 5965.835Å	1.88	-0.490	0.031	0.080

Table 2

Element	δ[el/H] (δTeff +200 K)	δ[el/H] ($\delta \log g$ +0.4)	δ[el/H] ($\delta\xi_{mt}$ +1.2 km s^{-1})
Fe I	+0.07	+0.13	-0.44
Al I	+0.12	+0.07	-0.16
Ca I	+0.21	-0.10	-0.42
Ni I	+0.07	+0.27	-0.44
Ti I	+0.13	+0.16	-0.35

Table 3

Star Name	Number of lines	Log N(Fe)	[Fe/H]
Orion PMS Stars			
KM Ori	14	7.65 ± 0.24	+0.05 ± 0.24
LX Ori	14	7.67 ± 0.21	+0.06 ± 0.25
TV Ori	12	7.77 ± 0.26	+0.05 ± 0.30
P 1270	15	7.89 ± 0.17	+0.19 ± 0.26
P 1404	12	7.72 ± 0.31	+0.10 ± 0.29
P 2441	13	7.79 ± 0.24	+0.10 ± 0.32
HD 245059	12	8.00 ± 0.23	+0.33 ± 0.20
Chamaeleon PMS			
CS Cha	14	7.52 ± 0.22	-0.10 ± 0.22
Sz 19	12	7.56 ± 0.37	-0.03 ± 0.39
CV Cha	14	7.49 ± 0.16	-0.16 ± 0.20
SZ Cha	14	7.56 ± 0.20	-0.05 ± 0.19
Sz 41	14	7.73 ± 0.10	+0.11 ± 0.11
Ophiuchus PMS			
He 3-1126	12	7.68 ± 0.45	+0.06 ± 0.44
SR 9	14	7.80 ± 0.26	+0.12 ± 0.16
Wa Oph/1	15	7.75 ± 0.30	+0.08 ± 0.30
Wa Oph/2	14	7.72 ± 0.16	+0.11 ± 0.21
Haro 1-14/c	15	7.66 ± 0.18	+0.01 ± 0.20
Taurus PMS Stars			
NTTS 035120 SW	15	7.70 ± 0.26	+0.07 ± 0.33
NTTS 035135 NE	13	7.80 ± 0.37	+0.09 ± 0.37
NTTS 042417	14	7.98 ± 0.19	+0.34 ± 0.20
NTTS 043124	13	8.12 ± 0.30	+0.33 ± 0.20
NTTS 045251	14	7.69 ± 0.30	+0.01 ± 0.24
LkCa 15	14	7.69 ± 0.31	+0.01 ± 0.14
LkCa 19	13	7.57 ± 0.17	-0.05 ± 0.22
UX Tau A	12	7.68 ± 0.38	+0.04 ± 0.34
Cygnus PMS Stars			
LkHα 191	13	7.98 ± 0.23	+0.22 ± 0.31
LkHα 228	12	7.63 ± 0.26	+0.03 ± 0.26
Other PMS Stars			
AS 507	12	7.74 ± 0.20	+0.04 ± 0.31
G-G 405	16	7.67 ± 0.34	-0.01 ± 0.25
RY Lup	12	7.68 ± 0.33	-0.03 ± 0.33

Table 4

Star Formation Region	Number of Stars	Log N(Fe)	$\overline{[Fe/H]}$
Taurus-Auriga	6	7.69 ± 0.07	+0.03 ± 0.05
Orion	6	7.75 ± 0.08	+0.09 ± 0.05
Chamaeleon	5	7.57 ± 0.09	-0.05 ± 0.09
Ophiuchus	5	7.72 ± 0.05	+0.08 ± 0.04
All WTTS	30	7.73 ± 0.14	+0.07 ± 0.12

Table 5

Star Name	$[Al/H]_{HR1136}$	$[Ca/H]_{HR1136}$	$[Ti/H]_{HR1136}$	$[Ni/H]_{HR1136}$
Orion PMS Stars				
KM Ori	-0.05 ± 0.28	+0.06 ± 0.19	+0.35 ± 0.03	+0.29 ± 0.06
LX Ori	-0.17 ± 0.09	-	-0.12 ± 0.21	+0.09 ± 0.03
TV Ori	+0.14 ± 0.33	-	+0.01 ± 0.50	-
P1270	+0.18 ± 0.07	+0.34 ± 0.16	+0.09 ± 0.36	-0.05 ± 0.18
P1404	-0.20 ± 0.46	+0.13 ± 0.07	-	-0.33 ± 0.04
P2441	+0.01 ± 0.31	+0.16 ± 0.29	+0.01 ± 0.50	-0.03 ± 0.04
HD 245059	-0.09 ± 0.00	-0.10 ± 0.11	+0.27 ± 0.29	+0.27 ± 0.02
Chamaeleon PMS				
CS Cha	-0.26 ± 0.02	-0.08 ± 0.22	-0.45 ± 0.24	-
CV Cha	+0.05 ± 0.08	+0.03 ± 0.25	-	-0.26 ± 0.02
SZ Cha	-0.21 ± 0.11	+0.04 ± 0.35	+0.05 ± 0.10	+0.01 ± 0.25
Sz 19	+0.23 ± 0.17	+0.12 ± 0.25	-	-0.12 ± 0.32
Sz 41	-0.02 ± 0.13	+0.19 ± 0.37	+0.22 ± 0.29	+0.40 ± 0.19
Ophiuchus PMS				
SR 9	-0.07 ± 0.11	-0.04 ± 0.22	-0.03 ± 0.25	-
Wa Oph/1	+0.01 ± 0.24	+0.33 ± 0.27	-0.06 ± 0.23	+0.15 ± 0.07
Wa Oph/2	-0.23 ± 0.09	+0.09 ± 0.16	-0.05 ± 0.32	+0.04 ± 0.52
Haro 1-14/c	-0.14 ± 0.16	+0.22 ± 0.19	+0.23 ± 0.17	+0.19 ± 0.26
He 3-1126	-	+0.03 ± 0.38	-0.05 ± 0.42	-
Taurus PMS Stars				
NTTS 035120 SW	-	+0.17 ± 0.11	-0.02 ± 0.14	-0.14 ± 0.44
NTTS 035135 NE	-0.02 ± 0.20	+0.39 ± 0.29	-0.09 ± 0.24	+0.03 ± 0.52
NTTS 042417	+0.04 ± 0.01	+0.40 ± 0.26	+0.26 ± 0.27	+0.04 ± 0.16
NTTS 043124	+0.02 ± 0.21	+0.50 ± 0.13	+0.33 ± 0.44	+0.15 ± 0.08
NTTS 045251	-0.25 ± 0.16	+0.14 ± 0.16	+0.24 ± 0.16	+0.07 ± 0.46
LkCa 15	-0.16 ± 0.18	+0.40 ± 0.30	-0.21 ± 0.17	-0.17 ± 0.37
LkCa 19	+0.04 ± 0.15	-0.11 ± 0.32	+0.30 ± 0.28	-0.13 ± 0.40
UX Tau A	-	+0.15 ± 0.16	+0.15 ± 0.17	-
Cygnus PMS Stars				
LkHα 191	-0.25 ± 0.20	-	+0.26 ± 0.09	+0.37 ± 0.23
LkHα 228	-	+0.13 ± 0.29	+0.04 ± 0.48	-
Other PMS Stars				
AS 507	-0.35 ± 0.06	+0.13 ± 0.05	-0.04 ± 0.33	+0.07 ± 0.02
GG 405	-0.32 ± 0.13	+0.07 ± 0.34	-0.05 ± 0.38	+0.10 ± 0.12
RY Lup	-0.12 ± 0.22	+0.09 ± 0.05	-0.17 ± 0.23	-

Table 6

Star Formation Region	$\overline{[Al/H]}_{HR1136}$	$\overline{[Ca/H]}_{HR1136}$	$\overline{[Ni/H]}_{HR1136}$	$\overline{[Ti/H]}_{HR1136}$
Taurus-Auriga	-0.06 ± 0.11 (6)	+0.19 ± 0.17 (6)	-0.02 ± 0.12 (7)	+0.13 ± 0.18 (8)
Orion	-0.03 ± 0.14 (7)	+0.12 ± 0.14 (5)	+0.04 ± 0.21 (6)	+0.18 ± 0.20 (6)
Chamaeleon	-0.05 ± 0.18 (5)	+0.06 ± 0.09 (5)	-0.02 ± 0.27 (4)	-0.06 ± 0.28 (3)
Ophiuchus	-0.11 ± 0.09 (4)	+0.14 ± 0.12 (5)	+0.13 ± 0.06 (3)	+0.01 ± 0.11 (5)
All WTTS	-0.08 ± 0.15 (25)	+0.14 ± 0.16 (28)	+0.04 ± 0.20 (25)	+0.08 ± 0.20 (27)

FIGURE CAPTIONS

Figure 1. Plot of equivalent width versus $\log T_{eff}$ for Fe I λ6705 transition. Contours are isoabundance curves for iron generated by the *RAI10* line abundance analysis program. The numbers beside each contour are logarithmic iron abundances relative to $\log N(H) = 12.00$.

Figure 2. Plot of [Fe/H] ($\equiv \log N(Fe/H)_{star}$ - $\log N(Fe/H)_{\odot}$) versus $\log T_{eff}$ for 30 pre-main sequence stars of type G - K. Typical uncertainties are 0.25 dex for [Fe/H] and 200 K in T_{eff}. The extremely high points are probably due to underestimates of microturbulent velocity in the abundance analysis.

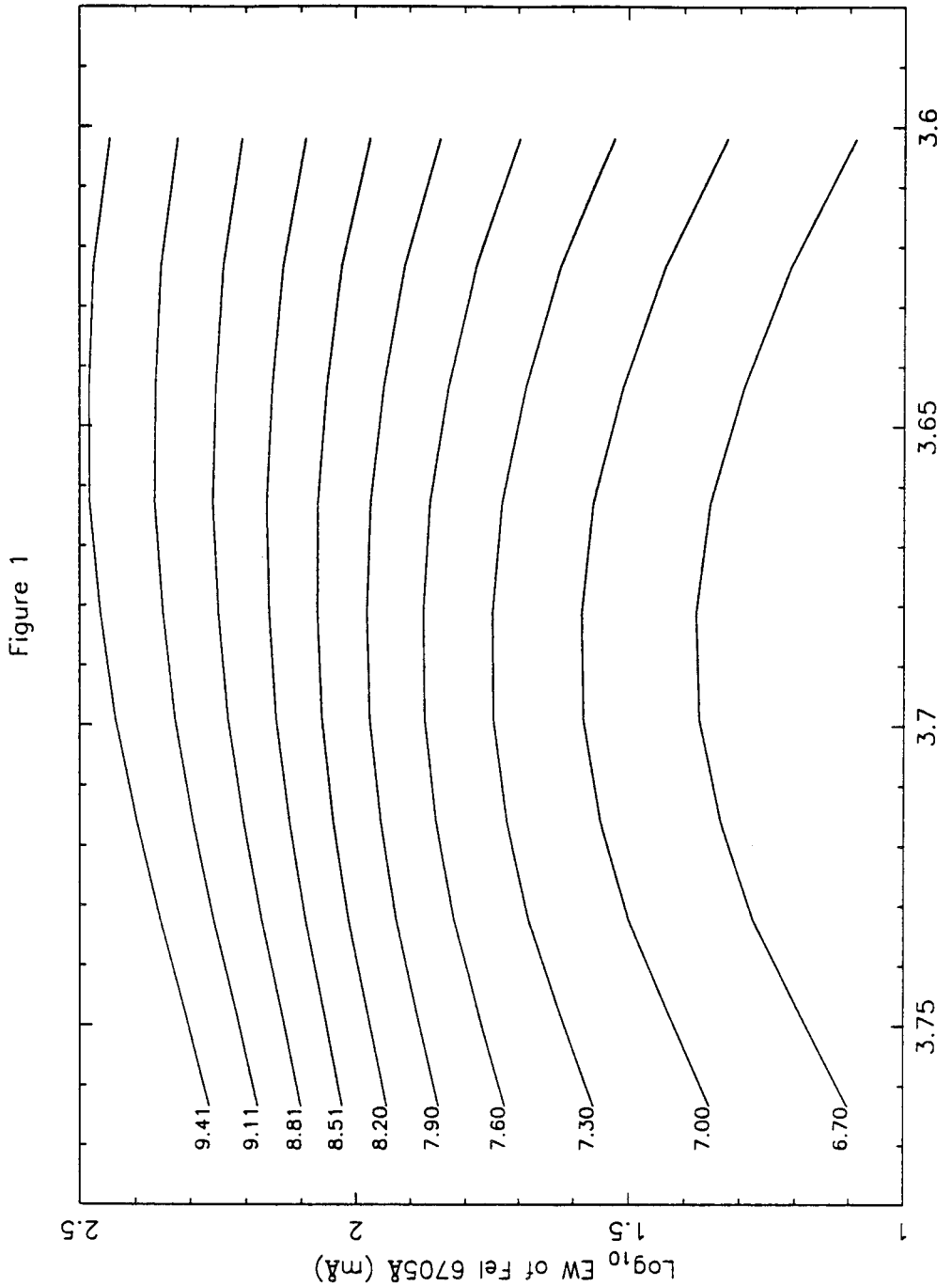
Log10 EW of FeI 6705Å (mÅ)
2.5
2
1.5
1
9.41
9.11
8.81
8.51
8.20
7.90
7.60
7.30
7.00
6.70
3.75
3.7
3.65
3.6
Log10 Teff

Figure 1

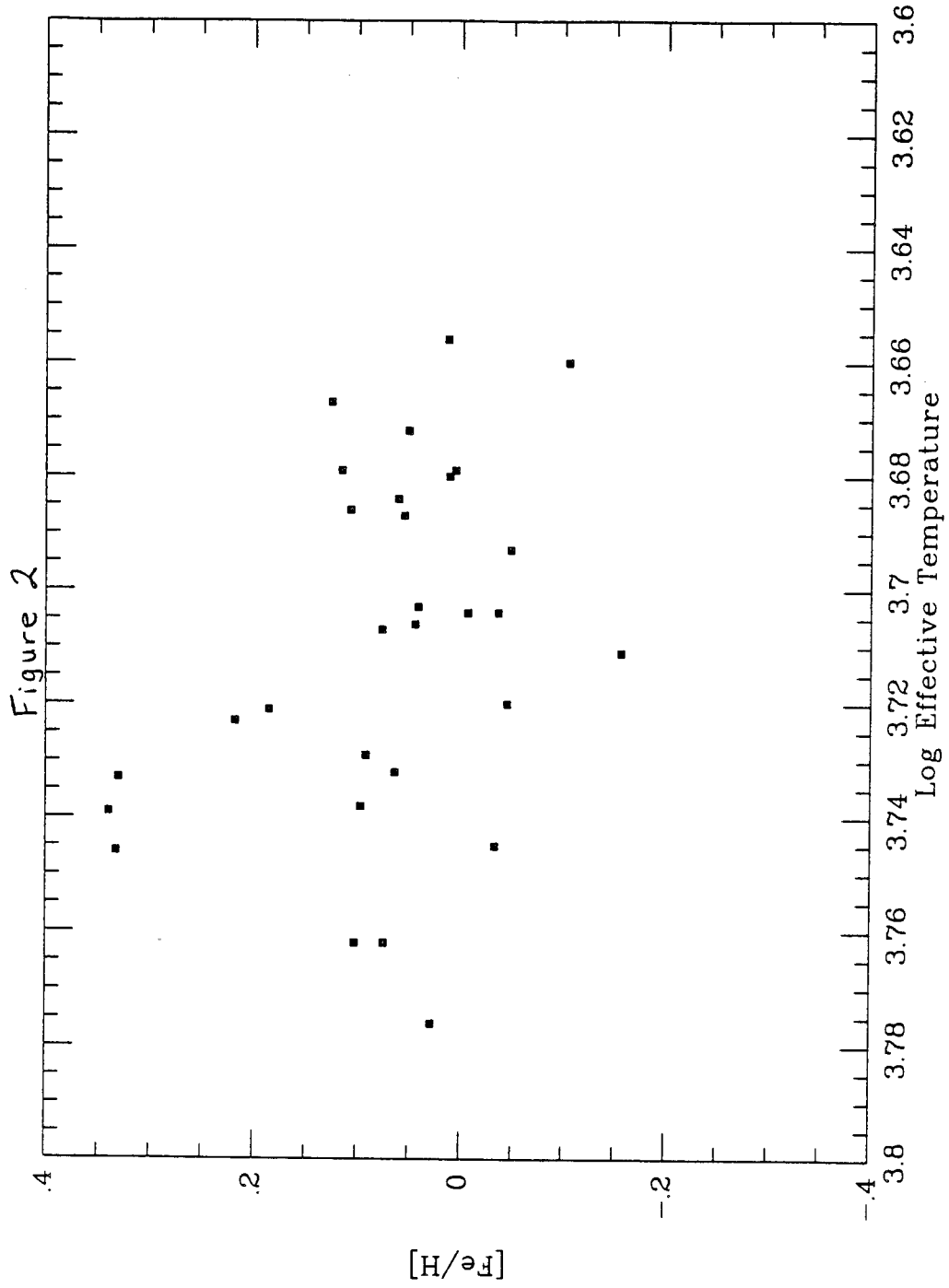
Figure 2
[Fe/H]
.4
.2
0
-.2
-.4
3.8
3.78
3.76
3.74
3.72
3.7
3.68
3.66
3.64
3.62
3.6
Log Effective Temperature

Chapter V.

Lithium Abundances in Low Mass Pre-Main Sequence Stars

Abstract:

Analysis of the neutral lithium 6707 Å blend in high resolution echelle spectrograms has yielded lithium abundances for 53 low mass pre-main sequence stars of types F8 - K7. Included in the sample are multiple members of six northern and southern hemisphere pre-main sequence (PMS) star associations. The mean lithium abundance of 37 weakly active pre-main sequence stars is log N(^{7}Li) = 3.60 $\pm$ 0.07 on a scale where log N(H) = 12. This value is $\approx$ 0.5 dex higher than the "canonical" maximum Population I lithium abundance of 3.1 $\pm$ 0.2 derived for young main sequence cluster stars and 0.3 dex larger than log N(Li) = 3.31 $\pm$ 0.04 for chondrites. Lithium abundances derived for individual PMS stars range as high as log N(^{7}Li) = 4.5. The star-to-star lithium abundance spread within the young star associations is larger than the observed variation between mean cluster abundances. The intracluster lithium abundance scatter appears uncorrelated with activity, rotation, or mass. No evidence for PMS depletion is found for stars in this sample, all of which have effective temperatures greater than 4500 K.

I. Introduction

Lithium is a critically important element in many areas of astrophysical research, including cosmology, galactic chemical evolution and stellar structure. As one of the lightest elements, lithium is thought to have been one of the few elements synthesized in the Big Bang. However, theorists disagree about exactly how much lithium was produced in the early universe. Standard Big Bang models predict abundances ranging from log N(Li)/N(H) = 1.9 to 3.0 depending on the choice of nucleon-to-photon ratio (Yang *et al.* 1984). Some inhomogeneous cosmologies with $\Omega_b = 1$ would produce larger amounts of lithium than the Standard Big Bang by factors of 5 to 50 (Malaney and Fowler 1989). Thus, an observational value for the "primordial" lithium abundance is extremely important as a constraint for various theories of primordial nucleosynthesis, as well as being a validity test for non-standard cosmologies. Lithium production is also expected in currently active nucleosynthetic processes, such as spallation reactions energized by galactic cosmic rays, supernova shocks, and stellar flares (Walker, Mathews, and Viola 1985; Brown *et al.* 1991); and s-process synthesis in AGB stars (Smith and Lambert 1989, 1990). Lithium abundances as a function of stellar age may thus provide a tracer of galactic chemical evolution once the base-level primordial abundance is established. However, lithium is also a fragile element, easily destroyed by nuclear reactions in stellar atmospheres. The responsible processes are ^{7}Li(p,α)^{4}He at T = 2.5 x 10^6 K and ^{6}Li(p,α)^{3}He at T = 2.1 x 10^6 K for the less abundant (by about a factor of 10) isotope. These temperatures occur within the outer convective zone of all late-type stars; thus, the lithium abundance measured in a stellar photosphere will be sensitive to the convective history of the star, as well as galactic lithium

enrichment and primordial lithium nucleosynthesis.

Because lithium is destroyed in convecting stellar envelopes, large lithium abundances are generally found only in young stars and non-convecting stars. Observational evidence for the destruction of lithium with time in stellar atmospheres can be found within the Solar System. The Sun itself has a lithium abundance of about 1.16 $\pm$ 0.1 (Steenbock and Holweger 1984). However, the solar system value measured from carbonaceous chondrites is 3.31 $\pm$ 0.04 (Anders and Grevesse 1989), implying that the solar atmosphere has been depleted in lithium by a factor of about 200 since the formation of the Sun. Population I F stars are good subjects for lithium determination studies, since they have shallow convection zones, spend little time on the fully convective Hayashi track during their pre-main sequence (PMS) phase, and are cool enough to allow the detection of the Li I 6707 Å line. Among Population I F field stars, the Li abundance ranges as high as 3.0 with a scatter that ranges down to the limit of detectability (about 2 mÅ or log N(Li) $\leq$ 1.0). Only about 50% of young F stars have abundances near 3.0, contrary to the original theoretical predictions that all F stars should preserve their original lithium abundances due to the absence of convection in their outer envelopes (Boesgaard and Tripicco 1986a; Balachandran 1989). An order of magnitude spread in abundances persists even among young main sequence cluster stars of similar mass; for example, lithium depletions of up to 1.0 dex below the maximum values are evident in the 46 F - K star α Per (t_0 = 5 x 10^7 yr) sample of Balachandran, Lambert, and Stauffer (1988). A similarly large spread in lithium abundances has been observed among Pleiades (t_0 = 7 x 10^7 yr) F stars observed by Duncan and Jones (1983). However, the maximum lithium abundances found among coeval F and G stars in the Hyades (Cayrel *et al.* 1984; Duncan and Jones 1983; Boesgaard and Tripicco 1986b; Boesgaard and Budge 1988), the Pleiades (Duncan and Jones 1983;

Boesgaard, Budge, and Ramsay 1987 Pilachowski, Booth, and Hobbs 1986), and α Per (Boesgaard, Budge, and Ramsay 1987; Balachandran, Lambert,and Stauffer 1988) are all extremely similar with maximum log N(Li) $\approx$ 3.1 $\pm$ 0.2. The lithium abundance at a given mass decreases with advancing age in Population I to the point where it is all but undetectable (W(6707) $\leq$ 0.002 Å) in several billion year old disk F and G stars (Herbig 1965; Duncan 1981; Boesgaard and Tripicco 1986a). However, two classes of older stars do have appreciable quantities of lithium in their atmospheres. As previously mentioned, a few AGB stars super-rich (log N(Li) $\approx$ 4.0) in lithium have been found both in the Galaxy (Brown *et al.* 1989) and the SMC (Smith and Lambert 1989, 1990). These stars are almost certainly producing lithium via the s-process in their atmosphere, possibly through the reaction ^{3}He(α, γ)^{7}Be(e^-, ν)^{7}Li (Cameron and Fowler 1971). In addition, a population of extremely metal-deficient halo dwarfs with effective temperatures between 6300 K and 5500 K have remarkably uniform lithium abundances of about 2.1 $\pm$ 0.15 (Spite and Spite 1982; Spite, Maillard, and Spite 1984; Hobbs and Duncan 1986; Rebolo, Molaro, and Beckman 1988). The discoverers of these objects contend that this lithium abundance represents the primordial value, implying that current galactic lithium values have been enriched by an order of magnitude via galactic chemical evolution. Current stellar evolutionary models support the notion that extremely metal-poor stars will have minimal convective depletion of lithium (Deliyannis, Demarque, and Kawaler 1988). However, there is still controversy as to whether more subtle mechanisms such as diffusion might cause substantial and uniform depletion of lithium during the 10 billion year main sequence lifetimes of these stars (Proffitt and Michaud 1991).

In agreement with theory, spectral observations of young low mass main sequence cluster stars reveal that the degree of lithium depletion at a given age is a

strong function of stellar mass. Theoretical pre-main sequence evolutionary tracks predict that late-type stars ($\leq 1\ M_{\odot}$) spend over 10^7 years on the fully convective Hayashi track, resulting in depletion of photospheric lithium as the surface material is mixed down to lithium-destroying temperatures. More massive stars follow a more horizontal path to the main sequence, avoiding the fully convective period almost entirely; thus, lithium is depleted more slowly in F stars than in K stars. Calculations of PMS convective Li depletion by Bodenheimer (1966), D'Antona and Mazzitelli (1984), Proffitt and Michaud (1989), and Pinsonneault *et al.* (1990) all predict relatively smooth declines of lithium abundance with time for stars of less than 1 $M_{\odot}$, with greater depletion occurring at lower masses. The exact mass below which PMS convective depletion becomes significant differs between the various models according to the choice of mixing-length parameters. The initial observational results in the Hyades (Cayrel *et al.* 1984) found a relatively tightly constrained relation with increasing lithium depletion for lower T_{eff} which seemed to confirm the theoretical expectations. Comparison between α Per (t_0 = 5 x 10^7 yr), Pleiades (t_0 = 7 x 10^7 yr), and Hyades (t_0 = 6 x 10^8 yr) lower main sequence demonstrate that the minimum effective temperature at which the initial lithium abundance is preserved in at least some stars increases from 5000 K for the youngest cluster to 6000 K for the oldest. This indicates that lithium destruction continues well beyond the PMS stage, even among F stars with negligible convection zones in their main sequence phases. In addition, Boesgaard and Tripicco (1986b) discovered a "lithium gap" of Hyades F stars with T_{eff} between 6300 K and 7000 K which have anomalously weak or undetectable lithium lines. This pattern is by no means universally present among young main sequence cluster stars. Lithium gaps seem well developed in Coma (Boesgaard 1989) and the Ursa Major Group (Boesgaard, Budge, and Burck 1988); however, no such pattern of depletion has

been found for the stars of α Per and the Pleiades. Since these last two cluster are both less than 10^8 years old, it is possible that lithium gaps develop on timescales greater than 10^8 years. Several mechanisms have been suggested as the explanation for the Hyades lithium gap, including diffusion (Delyannis, Demarque, and Kawaler 1990), rotationally-driven mixing (Pinsonneault *et al.* 1990) and meridional circulation (Michaud and Charbonneau 1991). The youngest main sequence clusters show considerable scatter of lithium abundance at a given temperature (σ log N(Li) $\approx$ 1.0 at 5700 K in the Pleiades) (Duncan and Jones 1983). For the Pleiades, this variation was orginally explained as a spread in formation time for cluster members or even multiple bursts of star formation within the cluster (Duncan and Jones 1983); however, similar scatter in Li persists among the much older stars of M67 (Hobbs and Pilachowski 1986) as well as almost every other cluster studied. The range of Li among coeval stars of the same mass may be explained by variation of initial angular momenta between cluster members; stars which have "spun-down" from large initial rotational velocities should undergo greater vertical mixing of surface material due to the shearing effects of differential rotation (Pinsonneault *et al.* 1990). However, this process must already be complete by the time G and K stars reach the main sequence since no correlation between lithium and v sin i was found in the Balachandran, Lambert, and Stauffer (1988) α Per sample. Variable chromospheric activity in the younger stars might also be responsible for some of the scatter, either by inducing variations in the line strength of Li I 6707 Å (Giampapa 1984) or by enhancing the microturbulence in the more active stars (Steenbock and Holweger 1981). However, no significant changes in the stength of the λ6707 feature during multiple rotation cycles of active main sequence dwarfs (Boesgaard 1991, private communication). Another more exotic suggestion is that the scatter is due to variations in the timescale of disk accretion during the PMS.

Stars with rapidly dissipating disks would have lower surface lithium than others with longer-lived disks providing fresh lithium to the stellar atmosphere (Pinsonneault *et al.* 1990b; Kenyon and Hartmann 1990). Because of the plethora of adjustable parameters in the problem of pre-main sequence lithium depletion, observational constraints on the degree of lithium depletion in the pre-main sequence will be important to the understanding of stellar evolution effects on photospheric lithium abundances. Accurate measurement of the lithium in young PMS stars holds the promise of establishing the current epoch N(^{7}Li) independent of diffusion and rotationally-driven mixing effects which may cause depletion of lithium in the atmospheres of well evolved stars. In addition, by comparing the lithium in PMS stars to chondritic abundances, the rate of lithium enrichment in the galaxy since formation of the solar system can be determined. If the ISM is enriched in lithium by stellar sources, some non-uniformity in current Population I lithium abundances as represented by PMS stars in different star formation regions may well be detectable, since the mixing timescale of the ISM is $\geq 10^9$ years (Boesgaard 1989; Boesgaard and Friel 1990). The current investigation addresses this issue by comparing the maximum lithium abundances in several widely separated star-forming clouds.

More than 30 years ago, Hunger (1957) recognized that the presence of an unusually strong line of Li I at 6707 Å was a distinguishing characteristic of T Tauri star absorption spectra. Bonsack and Greenstein (1960) made the first estimate of lithium abundance in pre-main sequence stars. They found that the ratios of lithium to calcium and iron in four classical T Tauri stars exceeded the solar ratio by a factor of 100, a value which was confirmed by Herbig (1965) and later by Zappala (1972) in his study of lithium abundances in pre-main sequence and young main sequence clusters Zappala's mean abundance for the pre-main sequence stars

in NGC 2264 was log N(Li) = 3.0, consistant with modern values for maximum lithium abundances in young main sequence clusters. However, despite the advent of modern solid-state detectors permitting high resolution spectroscopy of faint stars at reasonable signal-to-noise ratio, no studies of lithium abundance in T Tauri stars were published between 1972 and 1988, with the exception of Walter *et al.* (1987), an investigation of the fast-rotating pre-main sequence G star HDE 283572, and the Mundt *et al.* (1983) study of 5 "post-T Tauri stars" of type K in Taurus-Auriga. Both studies found a lithium abundance consistent with the maximum main sequence values of 3.0. In their study of weak-line or "naked" T Tauri stars in Taurus-Auriga, Walter *et al.* (1988) included Li I 6707 Å equivalent widths, but did not perform abundance determinations. Similar equivalent width measurements are included in Hartmann, Soderblom, and Stauffer (1987) for Taurus-Auriga stars of type G - M and Stauffer *et al.* (1989) for IC 2391. Shortly thereafter, a review of T Tauri star research (Bertout 1989) called for new lithium abundance determinations in T Tauri stars. Strom *et al.* (1989) (hereafter SWSS) responded first to this challenge with estimated lithium abundances for PMS stars in Taurus-Auriga and L1641 in Orion. Using the approximate spectral types from Cohen and Kuhi (1979) to determine effective temperatures, they found lithium abundances ranging from log N(Li) = 2.5 - 4.3 in K0-M0 T Tauri stars in Taurus-Auriga and the L1641 cloud in Orion. A more recent lithium study of 28 Taurus-Auriga PMS stars of type G8-K7 by Basri, Martin, and Bertout (1991; hereafter BMB), generally confirms the results of SWSS, finding an average log N(Li) = 3.6 $\pm$ 0.3. A detailed study of lithium in the moderately active T Tauri star BP Tauri (Duncan 1991) uses the subordinate line of ^{7}Li at 6103 Å to derive abundance, finding a smaller value by 0.4 dex than determinations based on the lithium resonance line at 6707 Å. Finally, Maguzzu and Rebolo (1989) have obtained lithium values for 26 T Tauri

stars in Ophiuchus, NGC 2264, and Taurus-Auriga, including some PMS stars of less than 1 $M_{\odot}$ which appear to have already undergone surface lithium depletion. Some of the preliminary results for the present chapter were presented at the 1989 Lawrence Livermore Workshop on The Lithium Problem and the 3rd Cool Stars, Stellar Systems, and the Sun Conference (Padgett 1989).

This chapter includes Li I 6707 Å equivalent width measurements of 53 weak and moderately active PMS stars in six major northern and southern hemisphere star-forming regions. Using new effective temperatures determined from spectroscopic line ratios for many of these stars, lithium abundances have been derived. Following the method of Smith and Lambert (1989, 1990), lithium abundances of a subsample of the targets are ratioed against potassium and calcium abundances in order to minimize the effects of microturbulence and line scattering processes that affect each of these lines. The relevance of improved microturbulence values (see Chapter III) upon pre-main sequence star lithium abundances is discussed. The possibility of correlation between lithium and such PMS characteristics as v sin i, X-ray flux, Hα luminosity, and infrared excess are also examined. In addition, comparisons are made between members of different star forming regions. Finally, we discuss the significance of our findings with respect to recent theoretical work on PMS lithium depletion and the question of whether lithium in Population I stars is of primordial origin.

II. Data and Analysis

Fifty-three PMS stars were observed using the echelle spectrographs at the Palomar 1.5m and Las Campanas 2.5m telescopes. The selection process as well as details of the observations and analysis are discussed in Chapter II. All of the stars

chosen for the investigation are either known "weak-line T Tauri stars" or moderately active stars without photospheric veiling. The spectral types of the target objects range from F8 - K7. Effective temperatures were derived using 4-6 pairs of temperature-sensitive line ratios calibrated against spectral standards with well known T_{eff} (see Chap. III). All calculations assumed solar metallicity and microturbulence of 1.8 km s^{-1}. Abundance determinations were performed using a grid of model photosheres provided by Gustafsson (1988, personal communication) T_{eff} = 4000 - 5800 K and log g = 3.8 and 4.2. The model atmosphere line abundance analysis program RAI10 (courtesy of M. Spite via A. Boesgaard) was employed to predict the equivalent width of the Li-Fe 6707 Å blend for different temperatures and abundances. The general procedure for abundance determination is discussed in some detail in Chapter IV. Table 1 of Chapter II lists the previously known stellar parameters for all stars in the sample.

A. Li I 6707 Å

The 6707 Å absorption line is composed of a ^{7}Li doublet, ^{6}Li doublet, and a weak iron line. The ^{7}Li I lines are located at 6707.761 and 6707.912 Å with ^{6}Li I lines 0.16 Å shortward of the ^{7}Li doublet. The first ionization potential of lithium is 5.39 eV, and the 6707 doublet is a resonance transition. A weak iron line at 6707.441 was also included in the synthesis. The log gf values for the ^{7}Li I lines are -0.0048 and -0.3063 respectively, and log gf for the iron line is -2.5229. The ratio of ^{6}Li/^{7}Li was set at 0.1 in all calculations, and solar iron abundance (7.67; Anders and Grevesse 1989) was also assumed. A trial run of RAI10 which only included the Fe I 6707 line shows that this transition contributes less than 20 mÅ of W_{6707} for even the lowest relevant stellar temperatures assuming a solar Fe abundance. If the iron abundance is increased to [Fe/H] = +0.3, the equivalent width of the 6707

Å line increases from 8 mÅ to 16 mÅ in K3 stars, which is less than a 5 % effect for the sample stars. Since the iron abundances derived for the PMS stars in the sample are all below this value (see Chap. IV), the decision to fix the iron at solar values for the 6707 Å line analysis introduces not more than a 5% equivalent width error for any one star.

The equivalent widths of Li I 6707 Å measured for each star are listed in Table 1. Equivalent widths were determined using the standard IRAF spectral reduction tools *continuum* and *splot*. The equivalent width uncertainty is the standard deviation of several equivalent width measurements for each star using slightly different continuum levels. This potential source of error is sensitive to the v sin i of the star since rotational blending of many weak features causes lowering of the effective continuum level in the spectrum. Placement of the continuum level is also affected by the signal to noise ratio of the spectrum since weak absorption features may become confused with large amplitude noise (see Chapter II for further explanation). Repeated observation of the lithium line for the "weak-line T Tauri star" (WTTS) SZ Cha on consecutive nights were found to be consistent to within 15%. Column 3 contains λ6707 equivalent width measurements for the target stars from the literature. Discrepancies between the current study and spectra obtained by previous authors are relatively limited, except in the case of several known "classical T Tauri stars" (CTTS). Because of the uncertain photospheric veiling in CTTS spectra, these stars are excluded from the formal lithium abundance determinations discussed in section III. Variation between past and present high resolution equivalent width measurements range up to 0.1 angstroms, implying Log N(Li) uncertainty of 0.1 dex for T_{eff} = 5000 K and 0.6 dex for T_{eff} = 5800 K.

Figure 1 shows a sample set of theoretical 6707 Å line curves of growth. This

line is extremely sensitive to changes in temperature over the range of T_{eff} from 4000 - 6000 K as Figure 1 demonstrates. A change in T_{eff} of 200 K, the average 1σ uncertainty in T_{eff} for the sample, will alter the derived lithium abundance by 0.20 dex for a K3 star. The temperature sensitivity of this neutral lithium resonance line makes accurate spectral classification crucial in assessing the lithium abundance of an individual star. Because of the unknown amount of circumstellar extinction associated with T Tauri stars, photometric temperature determinations are uncertain at best. The author chose to base her effective temperature determination on temperature sensitive line ratios. Most of the known PMS stars still have spectral classifications based on the low resolution spectral work of Cohen and Kuhi (1979). A few of the target stars in Taurus-Auriga have been reclassified by Cabrit *et al.* (1990) who used IR and high resolution optical spectroscopy to determine luminosities for 36 T Tauri stars. The current investigation uses the ratio of vanadium line to iron line equivalent widths to classify PMS stars with respect to a grid of spectral standards from Bell and Gustafsson (1989). Basri and Batalha (1990) use a similar method; however, they employ fewer ratios than the current study. Column 3 of Table 2 lists the derived effective temperatures for each of the target stars as well as the standard deviation of the temperatures determined in Chapter III. Table 6 of Chapter III compares the stellar T_{eff} obtained in the course of the current investigation to previous spectral classifications. Most of the adopted effective temperatures are accurate to better than 200 K which implies an 1σ error of 0.2 dex in lithium abundance; a few effective temperatures that were taken from the spectral classifications of Cohen and Kuhi (1979) are more uncertain. The effective temperature remains the dominant source of uncertainty in deriving lithium abundances from high resolution, high S/N WTTS spectra.

Although stellar surface gravity also affects line abundance determinations, the

Li I 6707 Å blend is insensitive to changes in log g. For Δ log g = 0.4 cm s^{-2}, the change in log N(Li) $\leq$ 0.01 for a K3 star. Because of this insensitivity to gravity, log g is fixed in the abundance determinations presented in this chapter. According to photometric surveys, T Tauri stars have larger stellar radii, and, thus, lower surface gravities than main sequence dwarf stars of the same spectral type. The work of Cabrit *et al.* (1990) and Gauvin and Strom (1991) show that surface gravity in low mass PMS stars ranges from log g = 3.0 to 4.5 with the mean at about 3.8. This value is typical of the PMS surface gravities determined by Basri, Martin, and Bertout (1991), which used the luminosities of Cabrit *et al.* (1990) together with their T_{eff} to obtain log g. Log g = 3.8 is also the surface gravity chosen for BP Tau by Duncan (1991) in his lithium analysis. In comparison, the solar surface gravity is log g = 4.44. Therefore, the value of log g is fixed at 3.8 for the stellar models used in the abundance determinations presented in this chapter.

Another stellar parameter of importance to the accurate derivation of lithium abundances is the microturbulent velocity of photospheric material. There is some empirical evidence to suggest that chromospherically active stars may have enhanced microturbulence in their photospheres (Steenbock and Holweger 1981). The current study has chosen the value of 1.8 km s^{-1} for the majority of the abundance determinations. This microturbulent velocity is somewhat higher than expected for inactive K dwarfs, but is close to the value found by Steenbock and Holweger for the chromospherically active K star ϵ Eridani (1.5 km s^{-1}); it is also close to the mean microturbulence value of 1.62 km s^{-1} found for 16 WTTS stars in the current sample in Chapter III. Coincidently, Basri, Martin, and Bertout (1991) chose this same microturbulent velocity in their derivation of lithium abundances in Taurus-Auriga pre-main sequence stars. In Figure 2, curves of growth for λ6707 are shown for ξ_{mt} = 1.8 km s^{-1} (solid) and ξ_{mt} = 3.6 km s^{-1}. Changes of $\pm$ 1.0 km s^{-1} will

only change log N(Li) by 0.04 for a K3 star; however, changes of several km s^{-1} can have a considerable effect. For example, a star with T_{eff} = 5000 and W_λ(6707) = 316 mÅ will have a derived lithium abundance of 3.3 for ξ_{mt} = 1.8 km s^{-1} and an abundance of 3.0 for ξ_{mt} = 3.6 km s^{-1}. Thus, an uncertainty of at least 0.1 dex is introduced by potential errors in assumed microturbulence. Unless otherwise stated, all lithium abundances quoted in this chapter assume ξ_{mt} = 1.8 km s^{-1}.

Unfortunately, only models with solar metallicity were available, so no determinations of the sensitivity of Li I 6707 Å to enhanced metallicity could be performed. Metallicity determinations for this sample of PMS stars (see Chap. IV) indicate that all have essentially solar abundances of iron to within the measured uncertainties. Therefore, errors due to stellar atmosphere metallicity are assumed unimportant in the present investigation.

Lithium abundance determinations for 39 PMS stars are listed in column 5 of Table 2. Considering all of the possible sources of error from measurement and stellar parameter uncertainty, these derived values of log N(^{7}Li) should be accurate to ± 0.4 dex, with a somewhat greater uncertainty for stars with poorly constrained effective temperatures. The listed abundance uncertainty includes only the effective temperature error, which is expected to be the dominant uncertainty in the lithium abundance determinations.

B. K I 7698 Å and Ca I 6717 Å

The K I λ7699 resonance line has often been used as an abundance calibrator for stars with uncertain atmospheric structure. Potassium's relatively low first ionization potential (4.34 eV) causes the resonance transition to be extremely sensitive to cooling in the upper photosphere. Because lithium also has a low ionization

potential (5.39 eV), the K I λ7699 line strength should be a useful indicator of atmospheric structure effects on the Li I λ line. The K I feature used in the study is located at 7698.980 Å and has a log gf = -0.1690. Cohen (1974) first used a qualitative comparison between the K λ7699 line strengths of normal (Li-depleted) and "Li-rich" K giants to verify that the large Li I 6707 Å equivalent widths were due to real abundance differences and not unusual atmospheric temperature structure or microturbulence. Previous studies had compared the Li I 6707 line to the sodium resonance lines (Spitzer 1949) and Ca I lines (Boesgaard 1970). The sodium resonance lines at 5890 and 5896 Å are a particularly poor choice for comparing to Li λ6707 in low-mass PMS stars. The sodium D lines are extremely saturated in K stars, are subject to interstellar and circumstellar absorption features, and sometimes show overlying emission in T Tauri stars. As was pointed out by Cohen (1974), the higher first ionization potential of calcium (6.11 eV) makes it less sensitive than lithium to abnormal temperature structure in the photosphere. Campbell and Smith (1987) have also used K I λ7699 to validate large abundances of sodium and aluminum derived from the resonance lines of these elements found in CN-rich giants. Potassium is an excellent comparison element for the alkali metals because it is not created or destroyed in any known process occurring in stellar atmospheres. More recently, Smith and Lambert (1989, 1990) also utilized Li/K to ascertain the reality of large lithium abundances in SMC AGB stars. By assuming that potassium abundances follow the same abundance pattern as iron relative to solar abundances (Gratton and Sneden 1987) and by determining the metallicity of the AGB stars, they were able to normalize their lithium abundances versus "known" potassium values. The current investigation employs the same methods in attempting to determine lithium abundances in low mass, pre-main sequence stars. Because of similarities between the condensation temperature and other properties

of these two elements, potassium has been used as a template for interstellar lithium depletion onto grains (Alcock, Fuller, and Mathews 1988). Because the core of the Li λ6707 line is formed at shallow depths ($\tau = 10^{-4}$, it will be deepened by line scattering processes unaccounted for in the RAI10 line analysis program (Duncan 1991). The K λ7699 line will be strengthened by the same processes since its core is also formed high in the photosphere; thus, the ratio of the lithium to potassium abundances should be independent of scattering effects. Figure 2 shows curves of growth for K λ7699 produced by RAI10. For a star with T_{eff} = 5000 K, ξ_{mt} = 1.8 km s^{-1}, W_{6707} = 200 mÅ, and log g = 3.8, a 500 K change in effective temperature will cause a 0.35 dex variation in derived potassium abundance, which indicates λ7699 is less temperature sensitive than λ6707. However, doubling the microturbulence from 1.8 km to 3.6 km s^{-1} has a serious impact on derived potassium abundances, as demonstrated in Figure 2 by the comparison between the 1.8 km s^{-1} curves of growth (solid lines) and the 3.6 km s^{-1} contours (dashed lines). Simply doubling the microturbulent velocity easily changes the derived potassium abundance by 0.6 dex in a 5000 K star. Thus, inaccuracies in model atmosphere microturbulence should be easily detectable by their effect on the λ7699 line. The K I λ7699 line is also considerably more sensitive to gravity than the Li I λ6707 feature; changing log g from 3.8 to 4.2 decreases the derived potassium abundance by 0.3 dex. A complicating factor in using λ7699 is its location in the midst of the atmospheric O_2 B band. The neighboring K line at 7696 Å was rejected because of blending with the band; however, the contamination is small ($\leq$ 10%) at 7699 Å. Unfortunately, the spectral range of the Las Campanas echelle extends to only 7000 Å in the red, so potassium information is limited to 12 PMS stars observed at Palomar. The ratio of W_{6707} to W_{7699} for the PMS sample is listed in column 5 of Table 1 and the ratio of N(Li) to N(K) is listed in column 7 of Table 2.

Unlike the K I λ7699 line, the Ca I λ6717 feature is not a resonance transition. However, its similar strength in K stars and proximity to the Li I λ feature makes it a still useful calibration for Li I, although perhaps less quantitatively accurate than the potassium resonance features. This strong calcium line at 6717.687 Å has a log gf = -0.390. Basri, Martin, and Bertout (1991) include W_{6707}/W_{6717} for most of their Taurus-Auriga sample in order to distinguish stars with unusual atmospheric structure or ξ_{mt} from truely lithium-rich PMS objects. Because Ca λ6717 is typically similar in strength to the lithium resonance line in early K stars, it is also sensitive to microturbulence. As the Ca λ6717 curves of growth in Figure 3 demonstrate, the calcium feature is less temperature sensitive than lithium over the T_{eff} region of interest. A 200 K increase in the effective temperature of a star with original T_{eff} = 5000 K and W_{6717} = 225 mÅ will increase the derived calcium abundance by 0.1 dex. This is due to calcium's higher ionization potential (6.11 eV) and excitation potential (2.7 eV). However, Ca I λ6717 is just as sensitive as K I λ7699 to microturbulence (0.6 dex abundance change when ξ_{mt} is doubled from 1.8 to 3.6 km s_{-1}). The 6717 line is also extremely gravity-sensitive; the derived calcium abundance changes by 0.6 dex(!) when log g increases from 3.8 to 4.2. These problems imply that the Ca I 6717 feature is best used for stars with very well determined gravities and microturbulences. Comparison with the Figure 2 reveals the similarity of the λ6707 curve of growth to K I λ7699. A potential disadvantage of Ca I λ6717 is its proximity to the [S II] λ6717 emission feature often associated with both circumstellar and background nebulosity. However, the spectral convenience of Ca λ6717 allows the feature to be measured for the entire PMS sample. Column 4 of Table 1 lists the ratio of W_{6707}/W_{6717} for all objects uncontaminated by [S II] emission. Column 6 of Table 2 lists the ratio of N(Li) to N(Ca) for these objects.

III. Results

A. Pre-Main Sequence Lithium Abundances

Figure 4a is a plot of W_{6707} versus T_{eff} for the all 53 PMS stars. The superposed curves are theoretical curves of ^{7}Li abundance as predicted by RAI10 using the log g = 3.8 Gustafsson models, expressed as the log N(^{7}Li) normalized to log N(H) = 12. For comparison, the solar lithium abundance is 1.16 ± 0.1 (Steenbeck and Holweger 1984) on this scale. Various star formation regions are represented as follows: Taurus-Auriga (12), Orion (14), Monoceros (7), Cygnus (3), Chamaeleon (6), and Ophiuchus (6), L1452 (1), L673 (1), L1529 (1), and an anonymous cloud in Andromeda (1). Figure 4b plots the derived lithium abundances versus effective temperature for the same sample. Of this group, 32 are known "weak T Tauri stars" (WTTS) (open squares), and 5 are moderately active "classical T Tauri stars" without apparent veiling. The remainder (italicized in Table 2) are stars with suspected veiling or very low S/N which were excluded from the cluster statistics. W134, a newly discovered PMS double-lined spectroscopic binary, was also excluded from the statistical sample. Table 3 lists the mean and standard deviation for the lithium abundances determined in the present investigation. The mean log N(Li) of the 37 sample stars is 3.60 with a standard deviation among the sample of 0.41 and an error in the mean of 0.07. *This determination is slightly in excess of the meteoritic solar system lithium abundance of 3.31 ± 0.04* (Anders and Grevesse 1989). It also coincides with the *maximum* observed lithium values among F and G stars in the Pleiades and Hyades (Duncan and Jones 1983), as well as K stars in α Per (Balachandran, Lambert, and Stauffer 1990). Interestingly, this multi-cloud PMS sample also agrees with the average log N(Li) = 3.6 ± 0.3 found for 28 PMS K stars in Taurus-Auriga (Basri, Martin, and Bertout 1991). The upper envelope of

abundances is defined by five objects which exceed log_{10}N(Li) = 4.5. The majority of the stars observed have derived lithium abundances in excess of 3.1 ± 0.2, the so-called "canonical" maximum value for Population I stars (Boesgaard and Steigmann 1985). Figure 4b plots N(Li) versus T_{eff}. Thus, *no evidence for lithium depletion is seen for this sample of G2 - K5 PMS stars with effective temperatures greater than 4500 K.* The scatter in lithium abundance is more than 1.0 dex for mid-K stars, similar to what has been seen in α Per and the Pleiades.

i) Taurus-Auriga

Among the PMS stars chosen for this investigation are 14 members of the Taurus-Auriga association. These objects are identified in Figure 5. Nine of these stars are included in the average cluster abundance. Five WTTS were selected from the list of Walter *et al.* (1988) and an additional two from the Lick Ca II emission survey. The remaining two weak-line objects are identified as T Tauri stars by Herbig and Bell (1988). The mean abundance of ^{7}Li for the 9 WTTS in the Taurus-Auriga sample is 3.34 ± 0.57. This very large dispersion is attributable to the large lithium abundances derived for LkCa 19, V773 Tauri, and NTTS 045251+3016. Figure 5 shows the lithium abundance versus effective temperatures for all 14 PMS stars. Eight of the stars have equivalent widths that correspond well with an estimated lithium abundance of between 2.7 and 3.3. Three of these stars (T Tau, DS Tau, and BP Tau) are CTTS with the potential to have veiled absorption spectra, so their lithium values are lower limits. The current study does not confirm the unusually high value of N(Li) (4.3) found for UX Tau A by Basri, Martin, and Bertout (1991), due in part to both the current study's smaller observed W_{6707} by 0.1 Å and the higher T_{eff} (by 200 K) chosen by BMB; instead, our value was 3.3. The remaining four objects with log N(Li)

less than 3.3 (NTTS035120+3154NE, NTTS035135+2528SE, NTTS042417+1744, NTTS043124+1824) are all WTTS with spectral types between G0 and K0. The upper envelope of lithium abundance (3.7 - 4.5) is occupied by four WTTS, only one of which (LkCa 15) has appreciable Hα emission. Of these objects, LkCa 19 is most striking for its large equivalent width of Li I 6707 Å, especially considering its relatively early spectral type. This star also has an anomalously high derived metal abundance [Fe/H] = +0.22 (Taurus-Auriga average metallicity is +0.03 $\pm$ 0.05 ; see Chapter IV) when microturbulence is assumed to be 1.8 km s^{-1}. In Chapter III, the actual microturbulence of LkCa 19 was found to be 3.2 km s^{-1}, which reduces its lithium abundance to about 4.0. Previous attempts to find the spectral type of LkCa 19 have classified it as K0 (Herbig, Vrba, and Rydgen 1986), K5 (Walter *et al.* 1988), and K2 (Basri and Batalha 1990). The mean of these spectral classifications corresponds to an effective temperature of about 4900 K, 300 K lower than the chosen value in the current study. If T_{eff} for LkCa 19 were lowered to 4900 K, its log N(Li) = 4.1, lower by 0.3 dex. Both NTTS045251+3016 and LkCa 15 were assigned higher effective temperatures than their Cohen and Kuhi (1979) spectral types would imply. If in error, these higher temperatures could explain their unusual lithium abundances. However, use of the original T_{eff} predict iron abundances for these two stars inconsistent with other Taurus-Auriga cluster members. V773 Tauri has an ill-defined spectral type due to its high v sin i, and the asymmetry of its spectral lines suggests that it could be a spectroscopic binary. SWSS measured the equivalent width of the V773 Tau 6707 line as 0.47 Å, which is 0.08 Å smaller than W_{6707} measured in the current investigation. Very high signal-to-noise spectra combined with spectral synthesis for the 6707 Å region will be necessary to characterize the surface lithium for this very interesting object, one of a few WTTS in Taurus-Auriga found to have circumstellar material bright at 1.3

mm (UX Tau A is another) (Beckwith, Sargent, and Chini 1990).

ii) Orion

The scatter in derived lithium abundance among the 12 Orion PMS is relatively small compared with the variation seen in other star-forming regions. Only one star (KM Orionis) has an abundance well above the mean. The mean log N(Li) is 3.64 $\pm$ 0.35 (error in the mean of 0.11) for the 12 objects included in the sample. Of the Orion PMS stars observed, LX Orionis, P2441, and SAN 6 have Hα emission strong enough to qualify as CTTS, but none of these objects show any qualitative signs of veiling. P2441 shows unusually strong signs of activity, including chromospheric filling of strong Fe I lines with emission, variable absorption features in its H alpha emission line, possible excitation of Herbig-Haro objects (Reipurth 1989), variation in spectral type with wavelength (Herbig and Bell 1988), and detection of 1.3 mm circumstellar dust emission (Stapelfeldt *et al.* 1991). Despite these possible indications of extreme youth compared with the other stars in the Orion sample, the lithium abundance derived for P2441 (3.3) agrees well with the average found for Orion PMS stars.

The maximum W_{6707} = 0.53 Å for the entire WTTS sample was measured for KM Ori, a K3 star with little or no stellar Hα emission and a strikingly deep 6707 Å absorption line. KM Orionis may indeed have an anomalously high lithium abundance, since its metallicity for the adopted T_{eff} ([Fe/H] = +0.05) is consistent with the other Orion stars analysed in Chapter IV. Increasing the microturbulence or decreasing the effective temperature for KM Ori would make its iron abundance significantly less than solar, in disagreement with other members of the Orion association. Unfortunately, the K I 7698 Å line was inaccessible with the Las Campanas

echelle, and no repeat observations of this star have been made from Palomar. [S II] emission from the Orion Nebula fills Ca I λ6717 in the spectrum of KM Ori. Thus, no calibrating lines were measured for this interesting object. Future observations will place a priority on obtaining K I λ7699 for KM Ori. Spectra taken at Las Campanas in 1988 and 1989 show a variation of 0.06 Å in W_{6707} between the two observations, suggesting the possibility of spots as a mechanism for strengthening the lithium resonance line (Strom *et al.* 1989; Basri, Martin and Bertout 1991); however, the study of Bouvier, Bertout, and Boucher (1988) found no photometric evidence for large spots on this star. A further possibility is that the lithium resonance line has a circumstellar absorption component which increases its equivalent width, although the Na I lines show no evidence of a similar effect. In addition, interstellar or circumstellar absorption lines are often offset in radial velocity from photospheric lines, but the KM Ori λ 6707 feature seems to be completely symmetric. Until these hypotheses can be tested, KM Orionis remains the best candidate for a truly lithium-rich pre-main sequence star in the present PMS sample.

iii) Southern SFR: Chamaeleon, Lupus, and Ophiuchus

Lithium abundance versus effective temperature for the southern star formation clouds of Chamaeleon, Lupus, and Ophiuchus is plotted in Figure 7. Six stars in the Chamaeleon cloud were analyzed for lithium abundance. Of these two are CTTS (Sz 19, CV Cha). Sz 19 is one of 26 PMS stars analyzed for lithium abundance by Maguzzu and Rebolo (1989). The current result (log N(Li) = 3.3) is lower than their value (3.7) by 0.4 dex due in part to the current investigation's lower W_{6707} (by 40 mÅ) for Sz 19. The average lithium value for these five stars is 3.52 $\pm$ 0.23 (error in mean = 0.10). These abundances are consistent with typical values from the other PMS clusters studied. However, the scatter is relatively small considering

the wide range of spectral types observed in the Chamaeleon SFR.

In the Lupus star forming region, there are remarkably few early type WTTS; most of the PMS stars are type M. Only one WTTS was analyzed for lithium abundance (RY Lup), in addition to three CTTS (RU Lup, GQ Lup, and Sz 98). The three CTTS are known to have heavy veiling, so their lithium lower limits are not included in the lithium abundance statistics.

Five PMS stars were observed in the Ophiuchus star formation region. The scatter of lithium abundances is rather high, especially considering that all the objects are WTTS. The mean lithium abundance is 3.74 $\pm$ 0.41. Haro 1-14/c has the highest derived lithium abundance with log N(Li) = 4.33. A slightly lower value of 4.0 was found for Wa Oph/1; however, this star has a more uncertain effective temperature and possibly lower surface gravity than Haro 1-14/c (Herbig and Bell 1988). The lithium abundances for He 3-1126 and Wa Oph/2 agree with each other with log N(Li) = 3.3. The chosen temperature for SR 9 is considerably higher (by 590 K) than previous spectral classifications would suggest, giving this star a moderately high lithium value of 3.8. Thus, in only a few weakly active PMS stars, the sample from the Ophiuchus star formation region covers almost the entire range of lithium abundances found in the complete young star sample.

iv) Other Regions

Figure 8 plots lithium against T_{eff} for the remaining stars of the PMS sample. The FU Ori type star V1057 Cygni is one of three PMS stars observed in the Cygnus region. Because of the great distance of this star formation region (1.5 Kpc) and the five magnitudes of foreground extinction, solar-type stars in Cygnus are typically quite faint ($m_v \approx 13$). For this reason, only two WTTS stars were

observed in this region. Despite the unusual and controversial nature of V1057 Cyg and a very uncertain spectral type, its derived lithium abundance is nearly identical to the LkHα 191 value of 3.6. Due to the large uncertainties associated with the stellar parameters of V1057 Cygni, this star is not included in the formal sample. A lithium abundance of 3.1 is derived for the late F star LkHα 228. This object was originally classified as a K1 star before line ratios revealed its considerably higher effective temperatures. In fact, the temperature determined for LkHα 228 could only be constrained as a lower limit, so the lithium value is a lower limit as well. The average of these two lithium abundances is 3.45 $\pm$ 0.23.

Five objects in the Monoceros star-formation region were observed. However, due to the faintness of low mass PMS stars at this distance, only one star (G-G 405) was observed at sufficient signal-to-noise ratio to determine an effective temperature from line ratios. The relatively high derived lithium value for G-G 405 corresponds well with the upper envelope of lithium abundances seen in other star formation regions. This star also qualifies as a CTTS, since the measured H α emission was 39 Å at the time of the lithium observation; however, its spectrum is without apparent veiling since its derived metallicity is quite high (see Chapter IV). W134, a bright PMS star observed in the vicinity of S Mon, was serendipitously discovered to be a double-lined spectroscopic binary with maximum separation of 150 km s^{-1}; unfortunately, this makes spectroscopic classification difficult. The properties of this star will be discussed in a forthcoming paper (Padgett and Stapelfeldt 1992). The remaining three CTTS (IP Mon, SS Mon, MO Mon) were analyzed for lithium abundance using effective temperatures from Cohen and Kuhi's (1979) spectral types. Both IP Mon and MO Mon have considerable photospheric veiling as measured by Basri and Batalha (1990) and thus were excluded from the formal lithium sample. The signal-to-noise ratio for our SS Mon spectrum ($\leq$ 30) is too

low for its high 6707 Å equivalent width (W_{6707} = 0.61 Å) to be meaningful. Observations by Maguzzu and Rebolo (1989) with considerably higher signal to noise give an equivalent width of 0.51 Å for SS Mon, which is somewhat less extreme. Because of the uncertainties in spectral type for W134 and SS Mon, only G-G 405 was included in the formal statistical sample.

The only star observed in Cepheus was AS 507. This surprisingly bright (m_v = 10.5) WTTS was originally classified as G8, which would have made it one of the most lithium-rich stars in the entire PMS sample. However, line ratios indicate the temperature is closer to that of a K1 star, reducing the derived lithium abundance to 3.4. Further observations of a larger sample of objects will be necessary to fully characterize the lithium abundance among pre-main sequence stars in this star formation region.

B. Abundance ratios: Li/K and Li/Ca

Because of the limited spectral range of the Las Campanas echelle in the red, spectra including the K I λ7699 line were obtained for only 16 Taurus-Auriga, Orion, and Cygnus stars. Figure 9 is a plot of W_{7699} versus T_{eff} with curves of constant potassium abundance. The equivalent widths of K I λ7699 for the spectral standards of roughly solar metallicity (filled squares) are plotted along with the pre-main sequence stars with available potassium spectra (open circles - star names). The fact that the spectral standards do not lie exactly along a contour of constant potassium abundance is likely due to the failure to include proper Stark broadening parameters for the 7699 Å feature. The greater stellar gravity of these main sequence dwarfs and subgiants also causes an overly high derived potassium abundance for the standards. Comparison of the PMS and standard stars reveals four WTTS which

have abnormally large W_{7699} for their spectral types: LkCa 19, NTTS 043124+1824, V773 Tauri, HD245059, and V1057 Cygni. All of these stars also have anomalously large metallicities for their clusters (see Chap. IV), with the exception of V1057 Cyg for which a metallicity determination was not attempted. These two facts suggest the following possibilities: these stars have ξ_{mt} much higher than 1.8 km s^{-1}; their surface gravities are considerably above log g = 3.8, or they have been assigned T_{eff} which are too high. For the case of LkCa 19, the microturbulence is found to be anomalously high (3.2 km s^{-1}; Chapter III), which explains its unusual equivalent widths. An additional possibility is that the temperature structure of the photosphere in these stars is unusual (however, see Chapter III for evidence against this hypothesis). Thus, the high lithium abundance derived for LkCa 19 (4.4) and V773 Tauri (4.5) are probably not correct, and the abundances for NTTS 043124+1824 and HD245059 are suspect as well. Following the method of Smith and Lambert (1989), it is possible to calibrate lithium abundances against the potassium resonance line. Since the cluster iron abundances for the Taurus-Auriga and Orion associations are essentially solar (see Chapter IV), and [Fe/K] $\approx$ 0.0 for disk stars (Gratton and Sneden 1986), one can assume that the potassium abundance is solar for each of the stars. Therefore,

$$\frac{N_{6707}(Li)}{N_{7699}(K)} = \frac{N_{actual}(Li)}{N_{\odot}(K)}$$

Using this method, the lithium abundance has been rederived for these four stars as follows: LkCa 19, log N(Li) = 3.5; NTTS 043124+1824, log N(Li) = 1.9; V773 Tauri, log N(Li) = 3.8 HD 245059, log N(Li) = 2.3. The depletion implied for the NTTS is rather startling compared to other Taurus-Auriga association members; however, this is one of the older cluster members according to PMS tracks.

V1057 Cygni also has an abnormally large W_{7699} for its poorly constrained spectral type. In the case of this well-known FU Ori star, these resonance lines may actually be formed in the disk photosphere rather than the stellar atmosphere,as is postulated for FU Ori itself. Figure 10 plots $N_{6707}(Li)/N_{7699}(K)$ versus temperature for the 16 PMS stars with available 7699 Å region spectra. An obvious correlation with temperature reflects the differences in temperature sensitivity between the two lines, and is not due to increasing lithium abundance at lower temperatures. However, the trend is much more striking than predicted by the ratio of theoretical equivalent widths for the two lines. The scatter remains quite large, contrary to what would be expected if it was entirely due to atmospheric effects. A smaller, but still significant range of values is seen in Figure 11, a plot of $N_{6707}(Li)/N_{6717}(Ca)$ for 25 PMS stars from the larger sample. There is also a significant increasing trend of $N_{6707}(Li)/N_{6717}$ with temperature that cannot be fully explained by the difference in temperature sensitivity of the λ6707 and λ6717 lines. The persistence of this temperature trend in both ratios of *derived abundances* indicates that there appears to be a real increase in the strength of Li I λ6707 with decreasing effective temperature in the current sample of G2 - K5 PMS stars that is not due to atmospheric structure or parameter effects. However, it is rather dangerous to draw any conclusions based upon the ratio of lines which are each on the flat part of the curve of growth, since small uncertainties in equivalent width may have large effects. In addition, the sample sizes are relatively small and need to be considerably increased before this phenomenon can be adequately demonstrated. The simplest explanation is that RAI10 (the line abundance analysis program used in this study) did not include some of the dominant broadening mechanisms for the K I λ7699 and Ca I λ6717 lines in the later-type K stars. Another possibility is that a circumstellar absorption component is contaminating the photospheric resonance features.

Obviously, further investigation will be required to settle this very intriguing question. Using the same normalization method as used with the potassium data, the lithium abundances of LkÇa 19, NTTS 043251+3016, and HD 254059 have been calibrated against calcium with the following results: LkCa 19, log N(Li) = 3.6; NTTS 043251+3016, log N(Li) = 2.8; HD 245059, log N(Li) = 2.8. The results for LkCa 19 and HD 245059 are consistent with the potassium calibrated results; however, the calcium-normalized lithium abundance for NTTS 043251+3016 is higher than the potassium calibrated value by 0.9 dex. Unfortunately, KM Ori, the most Li-rich star in the sample, was not observed at 7699 Å, and its Ca I 6717 Å is filled by [S II] from the Orion Nebula, so its anomalously high Li abundance must remain untested by these techniques for the present.

IV. Discussion

A. Uncertainties in the Derived Lithium Abundances for PMS Stars

Uncertainty in stellar parameters, especially effective temperature, remains the largest source of error when assessing the lithium abundance in the atmospheres of low-mass pre-main sequence stars. The lithium λ6707 line is extremely temperature sensitive for effective temperatures less than 6000 K, with the error in lithium abundance increasing by 0.1 dex for every +100 K of T_{eff} error. Table 6 of Chapter III lists various effective temperature determinations for some of the PMS sample. Although disagreement between low resolution and high resolution spectral classifications is no surprise, the scatter between temperature determinations using high resolution line ratio studies is still significant. Even some of the most weakly active stars included in the current study have relatively poorly constrained T_{eff} compared with the subjects of main sequence star abundance studies. The

use of 5 temperature sensitive line ratios to constrain T_{eff} in the present study is an improvement over the two used by BMB and there is ample room for further high spectral resolution line ratio studies of PMS stars. The extremely large differences in derived lithium abundance caused by variations in the adopted effective temperature is demonstrated by comparing the results of BMB with the current study. BMB derived a lithium value of log N(Li) = 4.3 for UX Tau, which was the highest abundance found in their investigation. However, the author finds a lithium abundance of 3.3 for the same star due to both a smaller measured W_{6707} (by 60 mÅ) and a 200 K cooler choice of T_{eff}. The current investigation's lithium abundance for LkCa 19 is higher by 0.7 dex than the BMB value due in part to a 200 K difference in adopted effective temperature, although the measured W_{6707} agrees to within 20 mÅ. Finally, our value of N(Li) for NTTS 045251+3016 is a full 1.2 dex higher than the value derived from the Walter *et al.* (1988) T_{eff} which is 550 K cooler than our determined temperature.

The use of line ratios to determine effective temperature is subject to a number of possible problems. The presence of starspots over a large fraction of the stellar surface could affect the line ratios used to determine effective temperature. The vanadium lines utilized in the line ratio pairs are enhanced in sunspots; however, the likely presence of large active regions with correspondingly high local temperature enhancements could serve to partially cancel out the effect of starspots. The unique position of low-mass PMS stars between dwarfs and sub-giants makes the choice of spectral standards to calibrate line ratios difficult. Basri and Batalha (1990) found that dwarf stars were preferable to subgiants as photospheric templates for veiling determinations, although PMS surface gravities are characteristic of subgiants. Despite previous suggestions that the temperature structure of pre-main sequence star photospheres could be substantially different from main sequence dwarfs (Calvet *et*

al. 1983), this doctoral investigation provides evidence that PMS photospheres do not appear to differ substantially from main sequence dwarfs (see Chapter III). The method of Hartigan *et al.* (1989) uses χ^2 fitting of PMS spectra with standards of similar type to constrain T_{eff}; however, this approach is sensitive to mismatches between microturbulence and metallicity. Probably the most accurate method of determining PMS effective temperatures is the empirical curve of growth analysis, which has already been applied to Sz 19 by Franchini, Castelli, and Stalio (1991). However, this is a labor intensive method which must be done on a star-by-star basis. Another approach to the problem of lithium temperature sensitivity is to use the subordinate lithium line at 6103 Å which is less affected by errors in T_{eff} since this line is not on the flat part of the curve of growth. This method seems particularly promising for late K - early M PMS stars such as BP Tau (Duncan 1991) since it also avoids using the saturated λ6707 line with its sensitivity to microturbulence and line scattering effects. Unfortunately, λ6103 is weak in early K and G stars, and is buried in the wings of an impressive Fe-Ca blend. Thus, the use of λ6103 is largely dependent on correctly subtracting the stronger Fe-Ca line, which relies heavily on properly determining ξ_{mt} and the abundances of Fe and Ca. The determination of accurate stellar effective temperatures for low-mass pre-main sequence stars is a critical requirement for the success of future T Tauri star abundance studies.

Errors in microturbulence for individual stars could account for some of the scatter in lithium abundances for PMS stars, as well as erroneously high derived abundance values for stars with high microturbulence. Past lithium abundance determinations for PMS stars, as well as the current study, have chosen to use a single value of ξ_{mt} (BMB, SWSS, MR) for G - M stars, despite the observed variation of microturbulence with effective temperature in the main sequence. In main sequence dwarfs of type K, microturbulences of up to 7 km s^{-1} have been measured

(Gray 1976), although the norm is closer to 1 km s^{-1}. Because the lithium λ6707 line is on the flat part of the curve of growth, a factor of two underestimate in the microturbulent velocity will cause a 0.5 dex overestimate of the lithium abundance for a star with T_{eff} = 5000 K and W_{6707} = 0.4 Å. The value of ξ_{mt} can be estimated by demanding that the relation of derived N(Fe) versus W_λ has zero slope (Chapter III). Another way to constrain the microturbulence is to use the average cluster iron abundance. By requiring that an individual star's metallicity match the average value determined from several members, ξ_{mt} can be approximated. Both of these methods are used in the microturbulence determinations in Chapter III. There is reason to expect higher microturbulences in PMS stars than main sequence stars of the same type. Steenbock and Holweger (1981) found evidence that microturbulence is enhanced in some chromospherically active late-type dwarfs. They derived a microturbulent velocity for ϵ Eri which was about 0.5 km s^{-1} greater than those for less active dwarfs of similar spectral type. They theorize that the microturbulent velocity is the spectroscopic signature of acoustic waves which may contribute to chromospheric and coronal heating; however, the actual mechanism for chromospheric and coronal heating is more likely related to variations in the stellar magnetic field (Zirin 1985). Since even WTTS have active chromospheres compared to normal main sequence stars, pre-main sequence stars might also have higher microturbulences than young main sequence stars. BMB point out that no T Tauri stars with v sin i less than 5 km s^{-1} have been found, possibly due to line broadening by microturbulence. However, among the PMS sample in Taurus-Auriga with measured chromospheric Ca II K flux (Walter *et al.* 1988), LkCa19, which according to the current study appears to have unusually an high microturbulent velocity does not have larger than normal Ca II fluxes. Although none of the usual spectral indicators of chromospheric activity were measured for the current

sample of T Tauri stars, the X-ray fluxes measured by *Einstein* are available for most of the Taurus-Auriga and Chamaeleon objects (Walter *et al.* 1988; Gauvin and Strom 1991). Recent data obtained by *Rosat* (Sternik 1991, personal communication) found that LkCa 19 was one of the brightest x-ray sources in Taurus, with an x-ray luminosity of 1.7 x 10^{31} ergs. Further work is required to confirm any correlation between microturbulence and x-ray luminosity as well as better constraining the atmospheric microturbulences of low-mass pre-main sequence stars.

A variety of other effects may have an impact on derived lithium abundances for PMS stars. Photometric studies have discovered that some T Tauri stars have considerable spot coverage; RY Lupi is one of the best studied examples of these spotted stars (Liseau *et al.* 1987). It is known from solar observations that lithium absorption is enhanced in spots because of the lower temperatures within these areas (Giampapa 1984). Quantitative analysis of the effect of large starspots on the lithium abundance have demonstrated that a 40% coverage of the stellar surface by spots could result in a 0.15 dex overestimate of the lithium abundance for a 5000 K star (SWSS, BMB); however, the effects of active regions or "plages" were not included in their simulations. According to Steenbock and Holweger (1984), non-LTE effects are not important in increasing W_{6707} for a given lithium abundance; in fact, these effects would most likely cause slight underestimates of lithium abundance by LTE line analysis programs. When identical surface gravities for all objects are assumed, there is the potential to introduce scatter in individual star abundance analyses. However, the gravities determined for weak- line stars in Taurus-Auriga and Chamaeleon are no more than $\pm$ 0.5 from the log g = 3.8 assumed in the abundance determination in Chap. III. Thus, no more than 0.02 dex of scatter should be introduced by gravitational uncertainties. A more relevant possibility is that line scattering from the upper photosphere may strengthen the core of the

lithium resonance line as it saturates, making abundance determinations based on this transition untrustworthy for late K stars. This was the conclusion reached by Wallerstein and Sneden (1983) for Li-rich K giants and shared by Duncan (1991) in his lithium analysis of BP Tau. This mechanism suggests that log N(Li) may be too high by 0.3 dex for the few K7 stars in the current sample, as well as a lesser amount for hotter objects. To avoid this problem, these researchers preferred using the λ6103 lithium line for abundance determination. This will be a difficult, but worthwhile goal in future lithium abundance studies of PMS stars with very high abundances derived using the λ6707 line.

Considering all the possible sources of error in the lithium abundance determinations, the evidence for PMS lithium abundances in excess of log N(Li) = 4.0 is not compelling, although values exceeding 3.6 are common and reliable in this data set. Nevertheless, there are still a few weak-line T Tauri stars (KM Ori, Haro 1-14/c, Wa Oph/1) with extremely large W_{6707} for their relatively well determined spectral types and microturbulences. Although no potassium lines were measured for these three objects, calibration of lithium using Ca I 6717 Å and assuming solar calcium abundance yields log N(Li) = 3.9 for Haro 1-14/c and 3.8 for Wa Oph/1. Because all three of these stars are bright with low v sin i, they will be ideal subjects for empirical curve of growth studies, spectral synthesis, and use of the Li I 6103 Å feature to test the validity of the remarkable lithium abundances yielded by the current investigation.

B. Astrophysical Reasons for the Spread of Lithium Abundances in PMS Stars

Differences in stellar angular velocity are often invoked as an explanation for the spread of lithium abundances among coeval stars of constant mass. This idea was first suggested by the solar evolution models of Endal and Sofia (1981) who showed that differential rotation between the Sun's outer convective zone and its interior would cause mixing to depths with temperatures sufficient to fuse all lithium. Futher theoretical work by Pinsonneault *et al.* (1989b) found that a range of initial angular momentum among stars with a constant initial lithium abundance would eventually produce a spread of surface lithium abundances among otherwise identical stars. Rapidly rotating stars are despun by processes on the stellar surface (such as stellar winds), causing a large velocity shear between the surface layers and the deep stellar interior; this shear causes turbulent mixing of surface material to depth. The predicted trend is for stars that have undergone the largest decrease in rotational velocity to be the most depleted. However, this correlation of lithium depletion with rotational velocity is not expected to develop until after the PMS stage. The observed relation between lithium abundance and projected rotational velocity in young low-mass stars has been quite different from this theoretical prediction. Balachandran, Lambert, and Stauffer (1991) found no definitive pattern of lithium versus v sin i in F - K α Per stars; however, they did note that all Li-depleted objects were also slow rotators. Although stars with large known v sin i's were rejected for the current investigation and most of the southern hemisphere objects lack measured v sin is, the current PMS sample contains objects with projected rotational velocities ranging from 10 - 40 km s^{-1}. Figure 12 plots v sin i versus N(Li) for the 18 objects in the sample for which v sin i has been determined. No trend is evident in this admittedly small group of objects; measurements of v sin i in a larger sample of low mass PMS stars are required for further investigation. One rather exotic explanation for the fast-rotating Li-rich stars seen in young main

sequence clusters is that these objects experience late accretion from circumstellar disks (Pinsonneault *et al.* 1989), restoring depleted lithium and adding angular momentum to the star. However, there appears to be no correlation between lithium abundance and mid-infrared luminosity (L_{MIR}) or sub-millimeter dust emission (presumably from circumstellar disks) in the few members of the sample with available photometry at these wavelengths. Indeed, some of the highest derived lithium abundances are found for WTTS without appreciable IR excesses (LkCa 19, CS Cha). Since the timescale for lithium depletion by 0.5 dex is 1 x 10^7 yr for a 1 $M_\odot$ star (Pinsonneault *et al.* 1990), the effect of late accretion on surface lithium abundances might not be evident until well after the PMS stage.

Another physical process that has been attributed as the source of both lithium abundance scatter and enhancement of lithium in young stars is the production of lithium in stellar flares. This mechanism was first invoked by Bonsack and Greenstein (1959) to explain the large lithium abundances found in T Tauri stars. A rather serious problem with this proposal is that spallation reactions should produce ^{6}Li in the same quantity as ^{7}Li (contrary to the observed ratio of 1:10), as well as a large overabundance of Be and B (Brown *et al.* 1991). In addition, calculations by Ryter *et al.* (1970) indicated that the energy required to synthesized the lithium found in a typical T Tauri star would exceed the total energy of gravitational collapse generated by the star! Guzik, Willson, and Brunish (1987) suggest that the excess ^{6}Li is consumed over time since it is destroyed via a more rapid process than ^{7}Li; however, the temperatures for destruction only differ by a factor of two. Studies of PMS beryllium, which is destroyed at somewhat higher temperatures than lithium (3.5 x 10^7 K; Boesgaard 1990), but is produced by many of the same types of processes (Boesgaard 1989), await HST or ground-based detectors with the ability to observe Be II 3719 at high resolution and signal-to-noise ratio. Given ultra-high

resolution, high signal-to-noise ratio spectroscopy on the Keck telescope to analyze ^{6}Li in the λ6707 feature, or UV spectroscopy of the 3130 Be line in faint PMS stars, this question can be fully resolved. The author of the present study instead attempts to find correlations between traditional indicators of stellar activity and the surface lithium abundance. A connection between stellar activity and lithium abundance would suggest that some lithium might be produced in flares or that lithium renewal is occurring via disk accretion. Lithium abundance versus equivalent width of Hα is shown in Figure 13. No correlation is seen; however, the largest dispersion of lithium abundances occurs among the stars with lowest Hα equivalent widths. A similar lack of any correlation is found in a plot of Hα luminosity versus lithium abundance (Figure 14). X-ray surface flux also seems to be uncorrelated with derived lithium abundance, as is shown in Figure 15. The relatively constant N(Li) seen among the stars with higher $L_{H\alpha}$ suggests that stars with active accretion may have a relatively constant lithium abundance. This scenario envisions a constant lithium abundance in the atmospheres of classical T Tauri stars which are continually repplenishing their lithium supply from a circumstellar disk. Then, as accretion ends, star-to-star differences in various stellar parameters begin to produce a range of lithium abundances. Another interpretation of possibly constant lithium abundances in active T Tauri stars is for the disk photosphere to be producing the absorption line spectrum. Since the disk abundances are undepleted, the λ6707 line would represent local cosmic lithium values. Testing this hypothesis will require sophisticated models of disk radiative transfer. A final possibility which does not involve disks *per se* is that stars with strong Hα may generate strong Li I resonance lines in an extended envelope or strong neutral wind.

Since lithium generally depletes with age, it is logical to assume that some spread in lithium abundance may be a result of non-coeval star formation within a

cluster. The idea of multiple star-formation episodes within a cloud was suggested by Duncan and Jones (1983) to explain the dispersion of N(Li) found for G and K stars in the Pleiades. Balachandran, Lambert, and Stauffer (1988) also discuss the possibility that the lithium scatter seen in α Per is due to two bursts of star formation. Figure 16 shows the relevant HR diagram for the current PMS sample, with evolutionary tracks from Cohen and Kuhi (1979) plotted as well. The luminosity data comes from a variety of sources: Cabrit *et al.* (1990) and Walter *et al.* (1988) for Taurus-Auriga, Gauvin and Strom (1991) for Chamaeleon, and Cohen and Kuhi (1979) for the remainder. A few of the WTTS in Taurus-Auriga and one in Chamaeleon may be $\geq 1 \times 10^7$ yr old. Figure 17 is a plot of lithium abundance versus age for 23 PMS stars. Once again, the magnitude of the scatter (≥ 1.0 dex) dominates the plot. However, the lower envelope of abundances clearly indicates greater depletion for some stars with $\log t = 7.5$ than any with $\log t = 6.0$. Obviously, a larger sample including deveiled CTTS would be helpful in establishing whether there is a trend of N(Li) with age for low-mass PMS stars.

C. PMS Lithium Depletion

Over the past decade, studies of lithium abundance in main sequence clusters have revealed patterns of lithium depletion as a function of effective temperature which change with the age of the cluster. Figure 18 is a plot of N(Li) versus temperature for the Pleiades ($t_0 = 7 \times 10^7$ yr; Duncan and Jones 1983) (starred squares), and α Per ($t_0 = 5 \times 10^7$ yr; Balachandran, Lambert and Stauffer 1988) (x's) stars of type G0 - K7, and the pre-main sequence stars in the current investigation (filled circles). The minimum effective temperature at which the "initial" cluster lithium abundance is preserved increases with age. Figure 19 shows the same plot for the low mass PMS sample of the current investigation (filled squares) combined with

the Taurus-Auriga PMS stars from BMB (starred squares) and the L1641 sample of SWSS (open triangles). The intercluster comparison is valid in this case because all PMS stars are expected to have ages less than 10^7 yr. One of the most interesting aspects of comparing the PMS sample with young main sequence stars is the apparent depletion of about 0.4 dex among the main sequence stars with T_{eff} greater than 5500 K. This depletion is not predicted by the standard evolutionary models (Pinsonneault *et al.* 1990) for the youngest stars in the sample, but is consistent with predictions for stars near 1 x 10^7 years old. Obtaining lithium abundances in a large sample of WTTS with effective temperatures greater than 5500 K should be a top priority for future work on PMS lithium depletion.

None of the stars from the current sample and few from SWSS show any signs of depletion below an average log N(Li) which increases slowly from about 3.4 at log T_{eff} = 3.75 to nearly 4.0 at log T_{eff} = 3.6. However, the Taurus-Auriga sample of BMB shows depletion of more than 1.0 dex for all stars with $T_{eff} \leq 4500$ K. Unfortunately, the current sample contains no stars with T_{eff} less than 4500, so the existence of a lithium depletion trend in the Taurus-Auriga association remains untested for the time being. The rapid change in maximum lithium abundances for stars with $T_{eff} \leq 5000$ between the age of Taurus-Auriga ($t_0 \leq 1$ x 10^7 yr) and α Per ($t_0 = 2$ x 10^7 yr) suggests an extremely efficient mechanism for lithium depletion in PMS stars of that mass range. Figure 20 plots N(Li) versus mass for the current PMS sample stars with photometry available to make mass estimates from the tracks of Cohen and Kuhi (1979). Combining our sample with that of BMB in Figure 20, three stars with mass below 1 $M_\odot$ show evidence of depletion. Curiously, the lithium scatter is also largest among stars of about 1 $M_\odot$. This could be due to deep convection manifesting itself as enhanced microturbulence. Underestimates in microturbulence would then be responsible for the highest derived lithium values.

More likely, it is due to the age spread of the cluster manifested as lithium abundance scatter.

D. PMS Lithium Abundances: Primordial or Enriched?

The average lithium abundance for our sample of 37 PMS stars (3.60 $\pm$ 0.07) is greater than the chondritic value of 3.31 $\pm$ 0.04 (Anders and Grevesse 1989) by a factor of 2. Although a few PMS stars have derived lithium values as high as log N(Li) = 4.5, these abundances could in most cases be due to uncertainties in effective temperature and microturbulence. A relatively small enhancement of 0.3 dex above solar system lithium values is indicated by the data, although lithium values derived from λ6707 for stars cooler than K3 are suspect due to the saturation of the lithium resonance feature. Thus, the PMS lithium data implies a possible enrichment of the interstellar lithium abundance since the formation of the solar system.

Table 3 contains the average lithium abundances for each of the star forming clouds surveyed in this investigation. Within the errors, all are the same. The standard deviation between the four PMS cluster averages is only 0.06 dex, compared with the intracluster σs of 0.2 - 0.6 dex. This homogeneity of maximum lithium abundance between widely separated molecular clouds implies either a constant lithium abundance throughout the disk ISM or extremely rapid mixing of enriched material into SFR. The abundance patterns seen are more consistent with a constant disk lithium abundance than with one varying with local enrichment. If enrichment is occurring, it is either on a VERY localized (intracluster) scale, or its effects are less than the scatter in this study. These results are consistent with studies of lithium in young main sequence cluster F stars that find a relatively

constant maximum abundance (3.1 ± 0.2) for all the clusters. Thus, the study of lithium abundances in PMS stars provides further evidence of the uniformity of the current interstellar medium lithium abundance. Whether or not this lithium is entirely primordial can probably only be settled by future studies of ^{6}Li and Be in the youngest members of the galactic disk population.

VI. Conclusions

1. Average PMS N(Li) for 37 low mass pre-main sequence stars using new T_{eff} and microturbulence determinations is about 3.60 with an error in the mean of 0.07 for T_{eff} between 4500 and 6000 K.

2. The ratio of Li/K is presented for 15 PMS stars in Taurus-Auriga and Orion. By assuming solar potassium abundances, lithium abundances were recalculated for four stars with anomalously large W_{6707} and W_{7699}. The potassium-normalized lithium values are much closer to the PMS mean, indicating that at least some exceptionally large PMS derived lithium values are due to atmospheric abnormalities. Li/Ca ratios show a large temperature dependence.

3. The average value of PMS lithium abundances exceed chondritic values by a factor of 2, possibly implying some large-scale lithium enhancement since the formation of the solar system. Star-to-star lithium variations are larger than intercluster variations.

4. The *average* lithium abundance for early K PMS stars is similar to the *maximum* values found in the youngest main sequence clusters (Pleiades and α Per). Depletion of about 0.4 dex is implied for stars of 1 $M_\odot$ during late pre-main sequence evolution. No systematic lithium depletion is detected down to T_{eff} of 4500 K in this PMS

star sample.

5. Lithium abundances in excess of 4.0 are derived for KM Orionis, Haro 1-16/c, Wa Oph/1, and CS Chamaeleon, even when the lithium values are calibrated against the Ca I λ6717 line. Observation of the Li I λ6103 line will be useful in verifying the large lithium abundances in these stars.

REFERENCES

Alcock, C., Fuller, G. M., and Mathews, G. J. 1987, *Ap.J.*, **320**, 439.

Anders, E., Grevesse, N. 1989, *Geochem.Cosmochem.Acta*, **46**, 2363.

Balachandran, S. 1989, Univ. of Texas Preprint.

Balachandran, S., Lambert, D. L., and Stauffer, J. R. 1988, *Ap.J.*, **333**, 267.

Basri, G., Bertout, C. 1989, *Ap.J.*, **341**, 340.

Basri, G., Batalha, C. 1990, *Ap.J.*, **363**, 654.

Basri, G., Martin, E., Bertout, C. 1991, Submitted to *AA* (BMB).

Beckwith, S., Sargent, A. I., Chini, R. S., and Gusten, R. 1990, *A.J.*, **99**, 924.

Bell, R. A., Gustafsson, B. 1989, *M.N.R.A.S.*, **236**, 653.

Bertout, C. 1989, *Ann.Rev.Astron.Ap.*, **27**, 351.

Bodenheimer, P. 1965, *Ap.J.*, **142**, 451.

Boesgaard, A. M. 1970, *Ap.J.*, **161**, 1003.

Boesgaard, A. M. 1989, *Ap.J.*, **332**, 410.

Boesgaard, A. M. 1991 private communication.

Boesgaard, A. M., Budge, K. 1988, *Ap.J.*, **332**, 410.

Boesgaard, A. M., Budge, K., and Ramsey, M. E. 1987, *Ap.J.*, **327**, 389.

Boesgaard, A. M., Friel, M. J. 1990), *Ap.J.*, **351**, 467.

Boesgaard, A. M., Steigmann, G. 1985, *Ann.Rev.Astron.Ap.*, **23**, 319.

Boesgaard, A. M., Tripicco, M. J. 1986a, *Ap.J.*, **303**, 724.

Boesgaard, A. M., Tripicco, M. J. 1986b, *Ap.J.*, **302**, L49.

Boesgaard, A. M., Tripicco, M. J. 1987, *Ap.J.*, **313**, 389.

Bouvier, J., Bertout, C., Boucher, P. 1988, *A.A.Supp*, **75**, 1.

Bonsack, W. K., Greenstein, J. L. 1959, *Ap.J.*, **131**, 83.

Brown, J. A., Sneden, C., Lambert, D. L., Dutchover, E. 1989, *Ap.J.Supp.*, **71**, 293.

Brown, L. E., Dearborn, D. S., Schramm, D. N., Larsen, J. T., Kurokuwa, S. 1991, *Ap.J.*, **371**, 648.

Cabrit, S., Edwards, S., Strom, S. E., Strom, K. M. 1990, *Ap.J.*, **354**, 687.

Calvet, N., Basri, G., Kuhi, L. V. 1983, *Ap.J.*, **277**, 725.

Cameron, A. G. W. 1982, In *Essays in Nuclear Astrophysics* eds. C. A. Barnes, D. D. Clayton, D. N. Schramm; Cambridge: Cambridge Univ. Press, p. 23.

Cameron, A. G. W., Fowler, W. A. 1971, *Ap.J.*, **164**, 111.

Campbell, B., Smith, G. H. 1987, *Ap.J.*, **323**, L69.

Cayrel, R., Cayrel de Strobel, G., Campbell, B., and Dappen, W. 1984, *Ap.J.*, **283**, 205.

Cohen, J. 1974, *P.A.S.P.*, **86**, 31.

Cohen, M., Kuhi, L. 1979, *Ap.J.Supp.*, **41**, 743.

D'Antona, F., Mazzitelli, I. 1984, *A.A.*, **130**, 319.

Deliyannis, C. P., Demarque, P., Kawaler, S. D., Krauss, L. M., Romanelli, P. 1988, Yale Physics preprint.

Duncan, D. K. 1981, *Ap.J.*, **248**, 651.

Duncan, D. K. 1990, Preprint STSci.

Duncan, D. K., Jones, B. F. 1983, *Ap.J.*, **271**, 163.

Endal, A. S., Sofia, S. 1981, *Ap.J.*, **243**, 625.

Franchini, M., Castelli, F., Stalio, R. 1991, *A.A.*, **242**, 449.

Finkenzeller, U., Basri, G. 1987, *Ap.J.*, **318**, 823.

Gauvin, L., Strom, K. M. 1991 FCAD preprint.

Giampapa, M. 1984, *Ap.J.*, **277**, 235.

Gratton, R. G., Sneden, C. 1987, *A.A.*, **178**, 179.

Gray, D. F. 1976, *The Observation and Analysis of Stellar Photospheres*, John Wiley and Sons, p. 416.

Gustafsson, B. 1988, personal communication.

Gunzick, J. A., Wilson, L. A., Brunish, W. M. 1987, *Ap.J.*, **319**, 957.

Hartigan, P., Hartmann, L. W., Kenyon, S. J., Hewett, R., and Stauffer, J. R. 1989, *Ap.J.Supp.*, **70**, 899.

Hartmann, L. W., Kenyon, S. J. 1990, *Ap.J.*, **349**, 190.

Hartmann, L. W., Soderblom, D. R., Stauffer, J. R. 1987, *AJ*, **91**, 575.

Herbig, G. H. 1965, *Ap.J.*, **141**, 588.

Herbig, G. H., Bell, R. 1988 *Publ. Lick Obs.* 1111.

Herbig, G. H., Vrba, F., Rydgren, A. E. 1986, *A.J.*, **93**, 907.

Hobbs, L. M., Duncan, D. K. 1987, *Ap.J.*, **317**, 796.

Hobbs, L. M., Pilachowski, C. A. 1986, *Ap.J.*, **309**, L17.

Hunger, K. 1956, *Zs.f.Ap.*, **39**, 36.

Kenyon, S. J., Hartmann, L. W. 1987, *Ap.J.*, **323**, 714.

Kenyon, S. J., Hartmann, L. W. 1990, *A.J.*, **93**, 907.

Liseau, R., Lindroos, K. P., Fischerstrom, C. 1987, *A.A.*, **183**, 274.

Maguzzu, A., Rebolo, R. 1989, *Mem. S. A. It.*, **60**, 105, (MR).

Malaney, R. A., Fowler, W. A. 1988, *Ap.J.*, **333**, 14.

Mazzatelli, I. 1990 in *Low Mass Star Formation and Pre-Main Sequence Objects*, ESO Conf. Proceedings No. 33, ed. B. Reipurth, p. 433.

Mazzatelli, I., Moretti, M. 1980, *Ap.J.*, **235**, 955.

Michaud, G. 1986, *Ap.J.*, **302**, 650.

Michaud, G., Charbonneau, P. 1991, *Space.Sci.Rev.*, **57**, 1.

Muller, E. A., Peytremann, E., de la Renza, R. 1975, *Solar Phys.*, **41**, 53.

Mundt, R., Walter, F. M., Feigelson, E. D., Finkenzellar, U., and Herbig, G. H. 1983, *Ap.J.*, **269**, 229.

Padgett, D. L. 1990 in *Cool Stars, Stellar Systems, and the Sun*, Sixth Cambridge Workshop, (A.S.P. Conference series),ed. G. Wallerstein, p.354.

Padgett, D. L., Stapelfeldt, K. R. 1992, in progress.

Pilachowski, C. A., Booth, J., Hobbs, L. M. 1987, *P.A.S.P.*, **99**, 1288.

Pinsonneault, M. H., Kawaler, S. D., Demarque, P. 1989, *Ap.J.*, **338**, 424.

Pinsonneault, M. H., Kawaler, S. D., Demarque, P. 1990, *Ap.J.Supp.*, **74**, 501.

Proffitt, C. R., Michaud, G. 1989, in *Cool Stars, Stellar Systems, and the Sun*, ed. G. Wallerstein, A.S.P. Conf. Ser. Vol. 9, p. 351.

Proffitt, C. R., Michaud, G. 1991, *Ap.J.*, **371**, 584.

Rebolo, R., Molaro, V., Beckman, J. E. 1988, *A.A.*, **192**, 192.

Reipurth, B. 1989, in *Low Mass Star Formation and Pre-Main Sequence Objects*, ed. B. Reipurth, ESO Conf. Proc. No. 33, p. 247.

Ryter, C., Reeves, H., Gradsztajin, E., Audouze, J. 1970, *A.A.*, **8**, 389.

Scalo, J. M. 1976, *Ap.J.*, **206**, 795.

Simon, T., Herbig, G. H., Boesgaard, A. M. 1985, *Ap.J.*, **293**, 551.

Smith, V. V., Lambert, D. L. 1989, *Ap.J.*, **345**, L75.

Smith, V. V., Lambert, D. L. 1990, *Ap.J.*, **361**, L65.

Spite, M., Maillard, J. P., Spite, F. 1984, *A.A.*, **141**, 56.

Spite, M., Spite, F. 1982, *A.A.*, **115**, 376.

Spitzer, L. 1949, *Ap.J.*, **109**, 549.

Stapelfeldt, K. R., Keene, J., Padgett, D. L. 1992, in progress.

Stauffer, J., Hartmann, L. W., Jones, B. F., McNamara, B. R. 1989, *Ap.J.*, **342**, 285.

Steenbock, W., Holweger, H. 1981, *A.A.*, **99**, 102.

Steenbock, W., Holweger, H. 1984, *A.A.*, **130**, 319.

Sternik 1991 private communication.

Strom, K. M., Wilkin, F. P., Strom, S. E., Seaman, R. L., 1989, *AJ*, **98**, 1444 (SWSS).

Wallerstein, G., Sneden, C. 1982, *Ap.J.*, **255**, 577.

Walker, T. P., Mathews, G. J., Viola, V. E. 1985, *Ap.J.*, **299**, 745.

Walter, F. M., Kuhi, L. V. 1984, *Ap.J.*, **250**, 254.

Walter, F. M., Brown, A., Linsky, J. L., Rydgren, A. E., Vrba, F. J., Roth, M., Carrasco, L., Chugainov, P. F., Shakovskaya, N. I., Imhoff, C. I. 1984, *Ap.J.*, **281**, 493.

Wlater, F. M., Brown, A., Linsky, J. L., Rydgren, A. E., Vrba, F., Roth, M., Carrasco, L. Chugainov, P. F., Shakovskaya, N. I., Imhoff, C. I. 1987, *Ap.J.*, **314**, 297.

Walter, F. M., Brown, A., Mathieu, R. D., Myers, P. C., Vrba, F. J. 1988, *A.J.*, **96**, 297.

Yang, J., Turner, M. S., Steigmann, G., Schramm, D. N., Olive, K. A. 1984, *Ap.J.*, **281**, 493.

Zappala, R. R. 1972, *Ap.J.*, **172**, 57.

Zirin, H. 1988, in *Astrophysics of the Sun*, Cambridge Univ. Press, p. 264.

Table 1

Name	W_{6707}(Li) (Å)	Previous W_{6707}(Li) (Å)	W_{6707}(LiI) W_{6717}(CaI)	W_{6707}(LiI) W_{7699}(KI)
Orion PMS Stars				
AN Ori	0.46 ± 0.01	-	-	1.56
KM Ori	0.52 ± 0.03	-	2.59	-
LL Ori	0.36 ± 0.01	-	-	1.36
LX Ori	0.42 ± 0.02	-	2.15	-
TV Ori	0.46 ± 0.03	-	1.60	-
P 1270	0.39 ± 0.01	-	2.16	-
P 1404	0.26 ± 0.01	-	2.05	-
P 1724	0.41 ± 0.03	-	1.98	1.33
P 2252	0.34 ± 0.01	-	-	-
P 2441	0.20 ± 0.01	-	1.22	-
P 2494	0.32 ± 0.01	0.40[c]	1.52	0.57
V466 Ori	0.32 ± 0.02	-	2.29	1.83
SAN 6	0.37 ± 0.01	-	2.00	1.05
HD 245059	0.32 ± 0.02	-	1.52	0.57
Lupus PMS Stars				
RU Lup	0.39 ± 0.03	-	-	-
RY Lup	0.35 ± 0.02	-	1.82	-
GQ Lup	0.42 ± 0.02	-	-	-
HK Lup	0.41 ± 0.02	0.51[e]	-	-
Chamaeleon PMS				
CS Cha	0.52 ± 0.01	0.55[e]	2.31	-
Sz 19	0.25 ± 0.02	0.29[e]	1.66	-
CV Cha	0.34 ± 0.03	-	-	-
SZ Cha	0.38 ± 0.01	-	1.91	-
Sz 41	0.45 ± 0.02	-	2.31	-
LkHα 332-20	0.44 ± 0.02	0.39[e]	-	-
Ophiuchus PMS				
He 3-1126	0.26 ± 0.01	-	1.58	-
SR 9	0.50 ± 0.01	0.49[e]	2.09	-
SR 4	0.49 ± 0.02	0.48[e]	2.15	-
Wa Oph/1	0.45 ± 0.01	-	2.37	-
Wa Oph/2	0.37 ± 0.01	-	1.81	-
Haro 1-14/c	0.52 ± 0.01	-	2.21	-

Table 1 (continued)

Name	W_{6707}(Li) (Å)	Previous W_{6707}(Li) (Å).	W_{6707}(LiI) W_{6717}(CaI)	W_{6707}(LiI) W_{7699}(KI)
Taurus PMS Stars				
NTTS 035120 NE	0.17 ± 0.02	0.26[a]	1.47	0.85
NTTS 035135 SE	0.22 ± 0.01	0.24[a]	1.41	0.73
NTTS 042417	0.29 ± 0.01	0.28[d]	1.42	1.06
NTTS 043124	0.23 ± 0.01	0.31[a]	1.34	0.47
NTTS 045251	0.54 ± 0.02	0.58[a]	1.79	0.97
LkCa 15	0.47 ± 0.01	0.47[b]	2.02	0.85
LkCa 19	0.46 ± 0.01	0.43[b],0.44[d]	1.87	1.00
UX Tau A	0.34 ± 0.02	0.35[c],0.40[d]	1.55	-
BP Tau	0.55 ± 0.02	0.45[d],0.55[e]	-	1.15
DS Tau	0.41 ± 0.02	0.42[c]	-	1.10
T Tau	0.29 ± 0.02	0.34[c],0.34[d]	-	0.83
V773 Tau	0.55 ± 0.03	0.47[c]	-	0.83
Cygnus PMS Stars				
LkHα 191	0.37 ± 0.01	-	-	1.14
LkHα 228	0.16 ± 0.02	-	1.51	0.73
V1057 Cyg	0.28 ± 0.03	-	-	0.78
Other PMS Stars				
AS 507	0.37 ± 0.04	-	1.72	1.74
G-G 405	0.42 ± 0.01	-	2.14	2.17
IP Mon	0.27 ± 0.03	-	-	-
MO Mon	0.34 ± 0.03	-	-	-
SS Mon	0.61 ± 0.04	0.51[e]	-	1.25
V360 Mon	0.42 ± 0.03	-	-	1.47
W 134 A	0.21 ± 0.03	-	-	0.85
W 134 B	0.17 ± 0.03	-	-	1.07

[a] Walter *et al.* (1988), [b] Hartmann and Stauffer (1987), [c] Strom et.al. (1989), [d] Basri, Martin, and Bertout (1990), [e] Maguzzu and Rebolo (1989)

Table 2

Name	WTTS?	T_{eff} (K)	Mass ($M_\odot$)	Log N(^{7}Li)	Log N(Li)/N(Ca)	Log N(Li)/N(K)
Orion PMS Stars						
AN Ori	Y	4497 ± 300	-	3.71 ± 0.3	-	-1.14
KM Ori	Y	4894 ± 119	1.1	4.41 ± 0.1	-	-
LL Ori	N	4864*	-	3.0	-	-
LX Ori	N	4832 ± 210	2.2	3.45 ± 0.2	-	-
TV Ori	Y	4701 ± 184	1.6	3.57 ± 0.2	-3.22	-
P 1270	Y	5260 ± 114	1.8	3.90 ± 0.1	-3.82	-
P 1404	N	5465 ± 182	2.0	3.22 ± 0.2	-3.50	-
P 1724	Y	4900 ± 350	-	3.50 ± 0.4	-	-2.00
P 2441	N	5778 ± 223	2.2	3.21 ± 0.2	-2.85	-
P 2494	Y	5236*	-	3.8	-	-2.55
V466 Ori	Y	5152 ± 119	1.5	3.24 ± 0.1	-	-1.78
SAN 6	N	5234 ± 375	-	4.07 ± 0.4	-	-2.48
HD 245059	Y	5412 ± 111	-	3.57 ± 0.1	-3.59	-3.28
Lupus PMS Stars						
RU Lup	Y	5236*	-	3.8:	-	-
GQ Lup	Y	4513 ± 55	-	3.41: ± 0.1	-	-
Sz 98	Y	4285*	-	2.3:	-	-
RY Lup	Y	5055 ± 300	-	3.31 ± 0.3	-3.31	-
Chamaeleon PMS						
CS Cha	N	4519 ± 105	1.2	3.83 ± 0.1	-2.57	-
Sz 19	Y	5500 ± 260	2.3	3.30 ± 0.3	-3.41	-
CV Cha	N	5270 ± 128	2.0	3.32 ± 0.1	-	-
SZ Cha	Y	4937 ± 155	1.7	3.31 ± 0.2	-3.17	-
Sz 41	Y	4771 ± 118	0.8	3.57 ± 0.1	-2.80	-
LkHα 332-20	Y	4954*	-	3.8	-	-
Ophiuchus PMS						
He 3-1126	Y	5402 ± 177	-	3.15 ± 0.2	-3.51	-
SR 9	Y	4648 ± 104	1.7	3.78 ± 0.1	-2.72	-
SR 4	N	4000*	1.5	2.47:	-	-
Wa Oph/1	Y	5094 ± 210	-	4.08 ± 0.2	-2.59	-
Wa Oph/2	Y	4851 ± 119	-	3.15 ± 0.1	-3.36	-
Haro 1-14/c	Y	4787 ± 118	-	4.22 ± 0.1	-2.38	-

Table 2 (continued)

Name	WTTS?	T_{eff} (K)	Mass ($M_\odot$)	log N(^{7}Li)	Log N(Li)/N(Ca)	Log N(Li)/N(K)
Taurus PMS Stars						
NTTS 035120 SE	Y	5787 ± 124	1.0	3.00 ± 0.1	-3.68	-3.08
NTTS 035135	Y	5363 ± 163	0.8	2.83 ± 0.2	-4.00	-3.16
NTTS 042417	Y	5478 ± 191	1.2	3.47 ± 0.2	-3.72	-2.64
NTTS 043124	Y	5575 ± 54	0.9	3.16 ± 0.1	-3.59	-3.70
NTTS 045251	Y	4532 ± 153	0.9	3.94 ± 0.2	-2.72	-1.77
LkCa 15	Y	4770 ± 94	-	3.80 ± 0.1	-2.89	-2.29
LkCa 19	Y	5249 ± 53	1.2	4.43 ± 0.1	-2.74	-2.08
UX Tau A	Y	5087 ± 208	1.1	3.28 ± 0.2	-3.57	-
BP Tau	N	4000*	-	3.0:	-	-
DS Tau	N	4395*	-	2.6:	-	-
T Tau	N	5236*	2.2	3.2:	-	-2.46
V773 Tau	Y	4775*	1.9	4.5:	-	-1.77
Cygnus PMS Stars						
LkHα 191	Y	5285 ± 177	-	3.73 ± 0.2	-	-2.36
LkHα 228	Y	5971 ± 183	-	3.13 ± 0.2	-3.27	-3.07
V1057 Cyg	N	5662*	-	3.6:	-	-
Other PMS Stars						
AS 507	Y	5042 ± 172	-	3.38 ± 0.2	-3.17	-
G-G 405	N	5199 ± 180	-	4.01 ± 0.2	-2.82	-
SS Mon	Y	4775*	-	4.9:	-	-
IP Mon	N	5309*	-	3.1:	-	-
MO Mon	N	5140*	-	3.4:	-	-
V360 Mon	N	5662*	-	4.8:	-	-
W134 A	Y	5662*	-	3.1:	-	-
W134 B	Y	5662*	-	2.9:	-	-

Star names in italics indicate active T Tauri stars which are not included in the statistical sample. Colon (:) after a lithium abundance indicates uncertain value due to veiling, low S/N spectrum, or poor spectral type.

* Stellar effective temperature obtained from spectral type listed in the Herbig-Bell Catalogue (1988)

Table 3
Average Abundances for Star Formation Regions

Star Formation Region	# Stars	log N(^{7}Li)*	σ	Log N(Li)/N(Ca)	Log N(Li)/N(K)
Taurus-Auriga	9	3.60 ± 0.20	0.57	-3.36 ± 0.47(8)	-2.55 ± 0.62(9)
Orion	12	3.64 ± 0.11	0.35	-3.40 ± 0.33(5)	-2.20 ± 0.67(6)
Chamaeleon	6	3.52 ± 0.10	0.23	-2.99 ± 0.32(4)	-
Ophiuchus	5	3.68 ± 0.23	0.45	-2.91 ± 0.44(5)	-
Sample PMS Stars	37	3.60 ± 0.07	0.41	-3.23 ± 0.44(21)	-2.44 ± 0.68(15)
$T_{eff} \leq 5000$ K	22	3.48 ± 0.09	0.40	-	-

Uncertainty listed with N(^{7}Li) is the error in the mean. Other uncertainties are standard deviations.

FIGURE CAPTIONS

Figure 1. Curves of growth for Li I λ6707 in Gustafsson model atmosphere for log g = 3.8 with ξ_{mt} = 1.8 km s^{-1} (solid lines) and ξ_{mt} = 3.6 km s^{-1}. Contours of constant effective temperature are shown for 200K intervals from 4000K (uppermost curve) to 5800K (lowest curve).

Figure 2. Same as Fig. 1, except for K I λ7699.

Figure 3. Same as Fig. 1 and 2, except for Ca I λ6717

Figure 4a. Equivalent width for the Li I λ6707 blend versus effective temperature for a sample of 46 low mass pre-main sequence stars in six different star forming regions. Contours of constant ^{7}Li abundance (log N(Li) against log N(H) = 12) produced by the RAI10 line abundance analysis program are shown. Mean abundance for the sample is log N(Li) = 3.60 $\pm$ 0.41.

Figure 4b. Lithium abundance versus effective temperature for entire sample of 53 low mass pre-main sequence stars. Filled squares represent stars with equivalent width of Hα emission *geq* 20 Å; open squares are weak T Tauri stars with Hα less than 20 Å.

Figure 5. Lithium abundance versus effective temperature for pre-main sequence stars in the Taurus-Auriga star-forming region. T Tau, BP Tau, and DS Tau are classical T Tauri stars (CTTS) with known photospheric veiling; thus, their

plotted lithium abundances are lower limits only and are not included in the formal statistical sample. V773 Tau is a fast rotator (v sin i *geq* 70 km s^{-1}, which accounts for its uncertain T_{eff}.

Figure 6. Lithium abundance versus effective temperature for pre-main sequence stars the Orion star formation region. LX Ori, P2441, and San 6 are CTTS without apparent veiling.

Figure 7. Lithium abundance versus effective temperature for pre-main sequence stars Chamaeleon (filled squares), Lupus (open circles), and Ophiuchus (filled triangles) star forming regions. GQ Lupi and RU Lupi are extreme CTTS with heavy veiling; thus, their lithium values are not included in the statistical analyses.

Figure 8. Lithium abundance versus effective temperature for pre-main sequence stars in the Cygnus (filled squares), Monoceros (open squares), and Cepheus (filled star) star-forming regions. The lithium abundances for V1057 Cygni (an FU Ori star), IP Mon, and MO Mon (both CTTS with veiling) are not included in the statistical sample. Neither is SS Mon, due to a very low signal-to-noise ratio spectrum. AS 507 is the sole representative of the Cepheus star forming region.

Figure 9. Equivalent width of the K I λ7699 line versus effective temperature for solar metallicity spectral standards (HR designations; filled circles) and pre-main sequence stars (open squares). Contours of potassium abundance (on the log scale where log N(H) = 12) are shown from 4.44 to 7.15. Solar potassium abundance is about 5.35 using the equivalent width from Gratton and Sneden (1987). Note

that the weak T Tauri stars NTTS043124+1824, LkCa 19, and HD 245059 have exceptionally strong K I λ7699 compared to standards of the same spectral type.

Figure 10. Ratio of lithium abundance (derived from Li I λ6707) to potassium abundance (derived from K I λ7699) plotted versus effective temperature for 16 pre-main sequence stars in the Taurus-Auriga and Orion star formation regions. Note the strong correlation with temperature due to the greater temperature sensitivity of the Li I resonance feature.

Figure 11. Ratio of lithium abundance (derived from Li I λ6707) to calcium abundance (derived from Ca I λ6717) plotted versus effective temperature for 25 pre-main sequence stars in all of the surveyed star formation regions. Note the correlation with temperature due to the greater temperature sensitivity of the Li I resonance feature. Scatter about the best fit to the temperature trend is about $\pm$ 0.4 dex.

Figure 12. Derived lithium abundance versus projected rotational velocity for 18 pre-main sequence stars in Taurus-Auriga, Chamaeleon, Orion, and Ophiuchus. Velocities were obtained from Herbig and Bell (1988) and Gauvin and Strom (1991). The largest lithium abundances are found among stars with low values of v sin i.

Figure 13. Derived lithium abundance versus equivalent width of H α emission measured in the current work plotted for 30 pre-main sequence stars without photospheric veiling. Note that the scatter is largest among the weak T Tauri stars.

Figure 14. Derived lithium abundance versus H α luminosity for 15 pre-main

sequence stars in the Taurus-Auriga and Chamaeleon star forming regions. Values of H α luminosity are derived using photometry from Cabrit *et al.* (1990) and Gauvin and Strom (1991).

Figure 15. Derived lithium abundance versus x-ray surface flux for 14 pre-main sequence stars in the Taurus-Auriga and Chamaeleon star-forming regions. X-ray values are from Walter *et al.* (1988) and Gauvin and Strom (1991). A new x-ray surface flux has been derived for LkCa 19 (highest lithium abundance and x-ray flux in Taurus-Auriga) using the ROSAT value courtesy of Michael Sterzik (1991, personal communication).

Figure 16. Hertzspring-Russell diagram for 29 PMS stars in the current study with available photometry. Temperatures were derived using line ratios in the current study (see Chapter III), and luminosities were obtained from Cabrit *et al.* (1990), Gauvin and Strom (1991), and Cohen and Kuhi (1979). Solid curves are the evolutionary tracks for stars of 0.8 to 3.0 solar masses; dashed curves are isochrones for low mass stars from 10^5 to 10^7 years old. Tracks and isochrones are from Cohen and Kuhi (1979).

Figure 17. Derived lithium abundance versus age for 22 pre-main sequence stars in Taurus-Auriga, Ophiuchus, and Chamaeleon. Ages were obtained from Cabrit *et al.* (1990), Maguzzu and Rebolo (1989), and Gauvin and Strom (1991). No real correlation between age and lithium abundance is demonstrated.

Figure 18. Derived lithium abundance versus effective temperature for the current sample of pre-main sequence stars (filled circles), Pleiades stars (open stars;

age $\approx$ 7 x 10^7 yr) (Duncan and Jones 1983), and α Persei stars (crosses; age $\approx$ 5 x 10^7 yr) (Balachandran, Lambert, and Stauffer 1988). Note that PMS stars are not depleted at lower temperatures as the young main sequence cluster stars are.

Figure 19. Derived lithium abundance versus effective temperature for current PMS sample (filled circles), the Taurus-Auriga stars of Basri, Martin, and Bertout (1991) (starred squares), and the L1641 Orion weak T Tauri stars of Strom *et al.* (1989) (filled triangles).

Figure 20 Log of derived lithium abundance versus stellar mass ($M_\odot$) for 22 PMS stars in the current sample with masses determined from the Cohen and Kuhi (1979) PMS tracks. Star forming regions are designated as follows: Taurus-Auriga - open triangles; Orion - filled triangles; Chamaeleon - filled squares; Ophiuchus - filled pentagon.

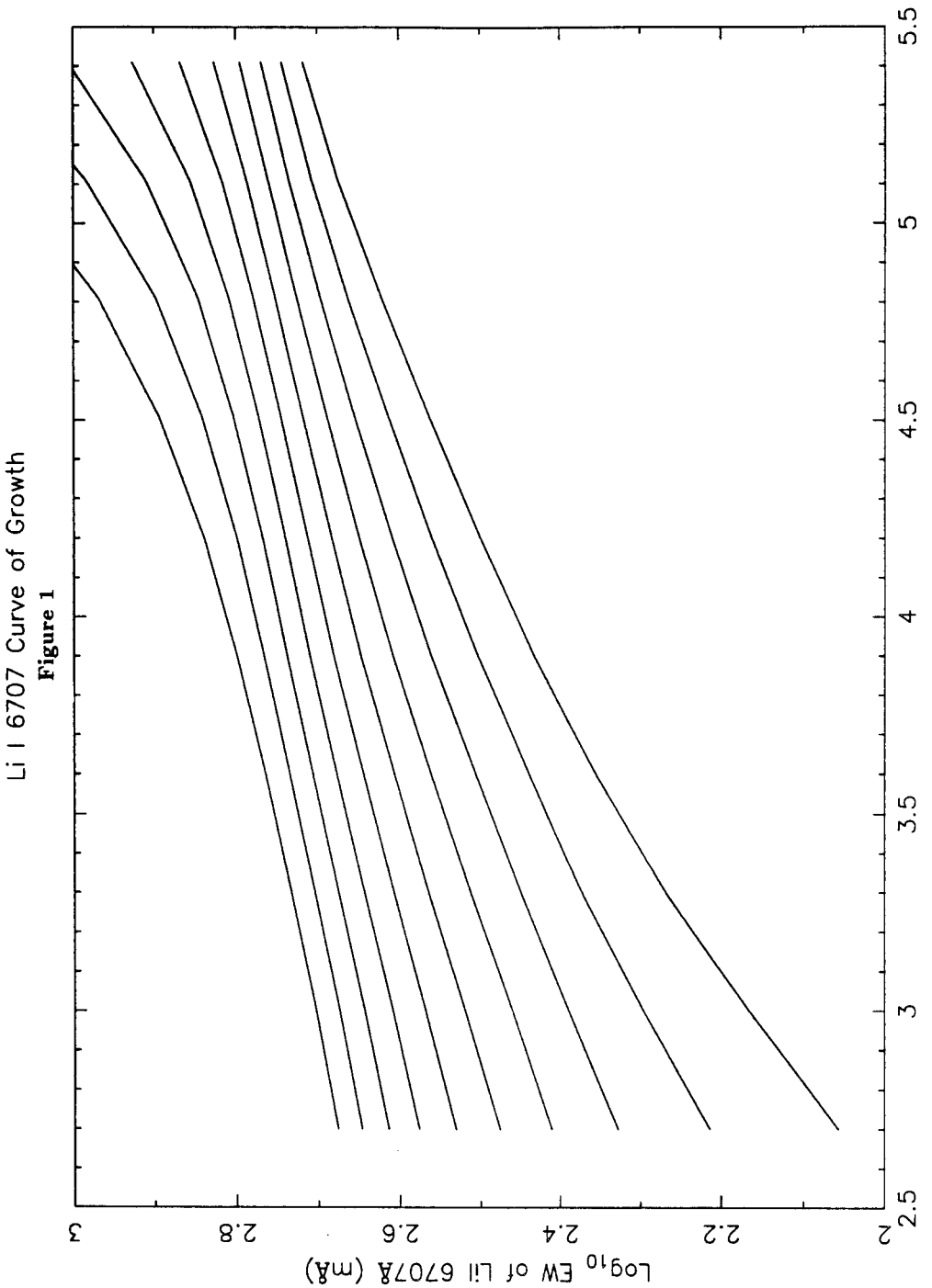
Li I 6707 Curve of Growth
Log10 EW of LiI 6707Å (mÅ)
Log10 N(Li)
3
2.8
2.6
2.4
2.2
2
2.5
3
3.5
4
4.5
5
5.5

Figure 1

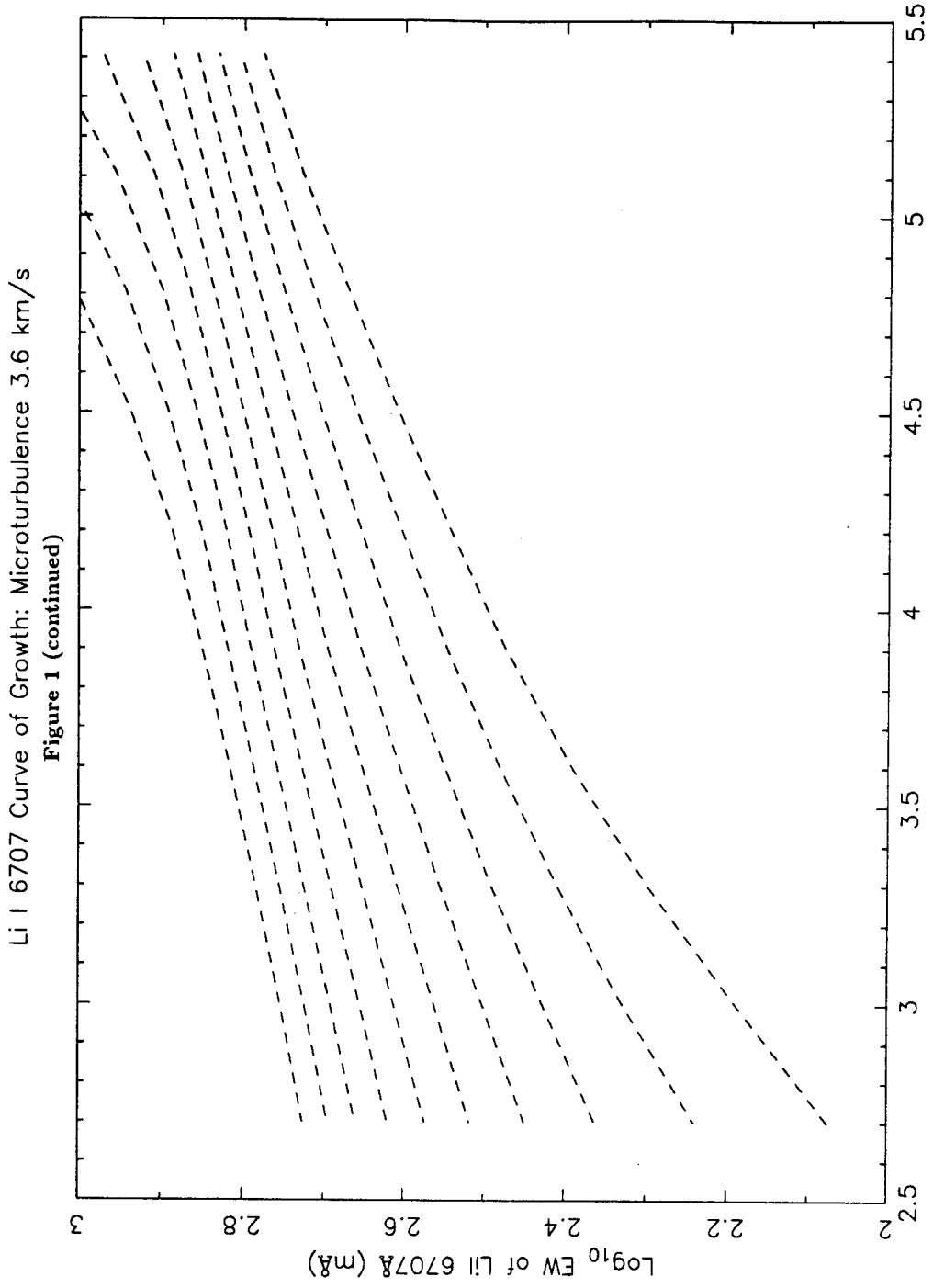

Figure 1 (continued)

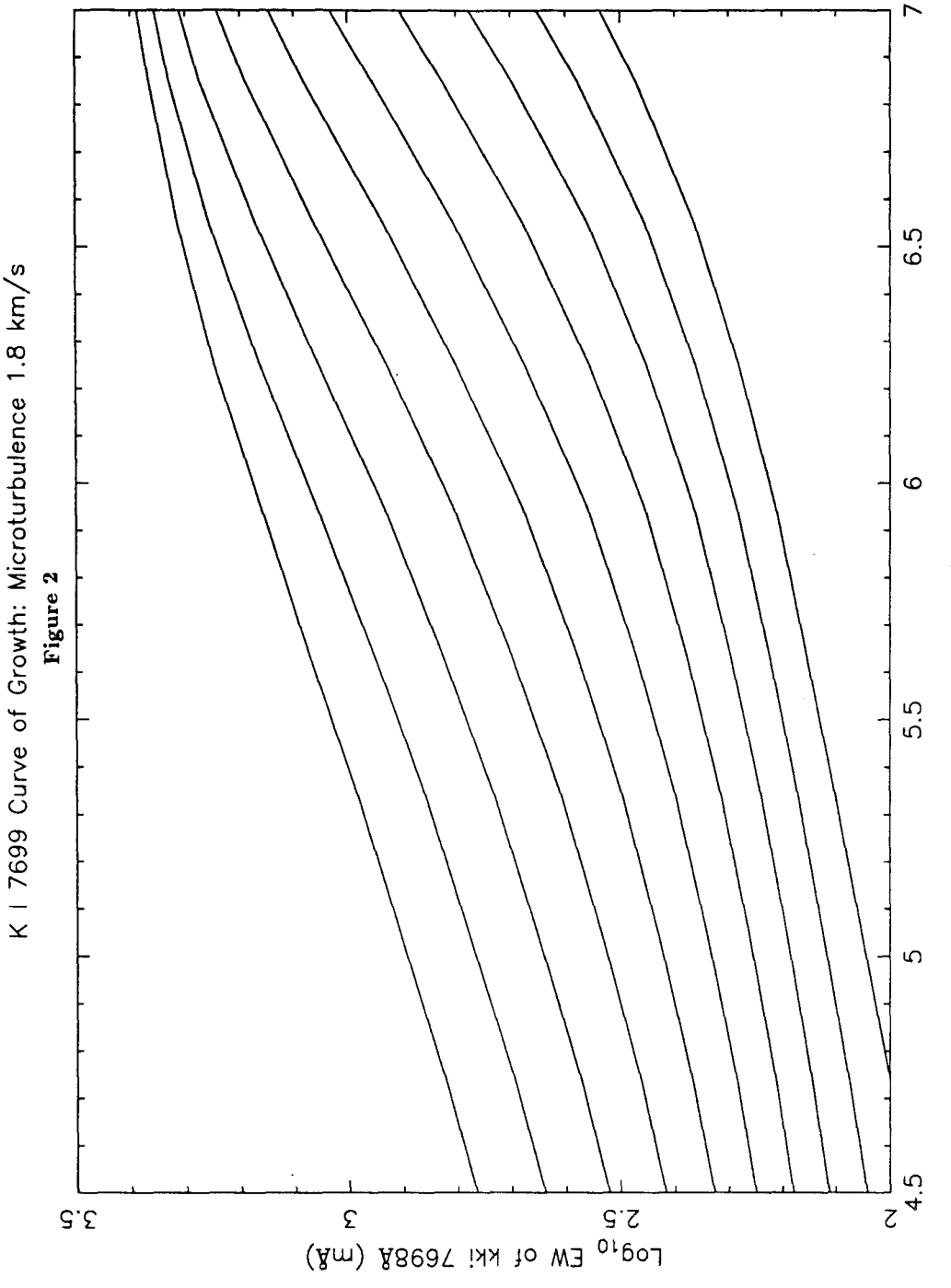
K I 7699 Curve of Growth: Microturbulence 1.8 km/s
Log10 EW of kKi 7698Å (mÅ)
Log10 N(kk)
2
2.5
3
3.5
4.5
5
5.5
6
6.5
7

Figure 2

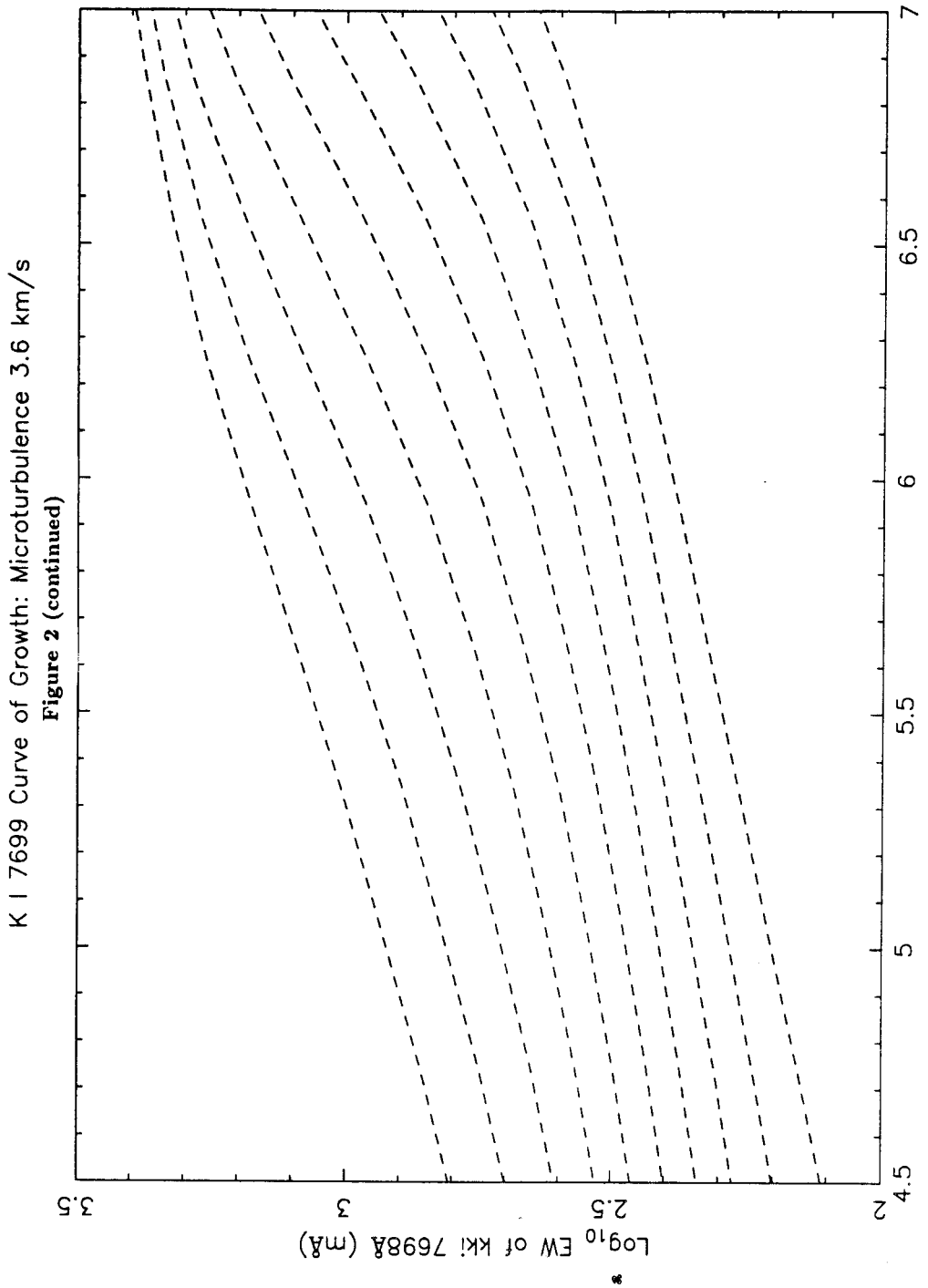

Figure 2 (continued)

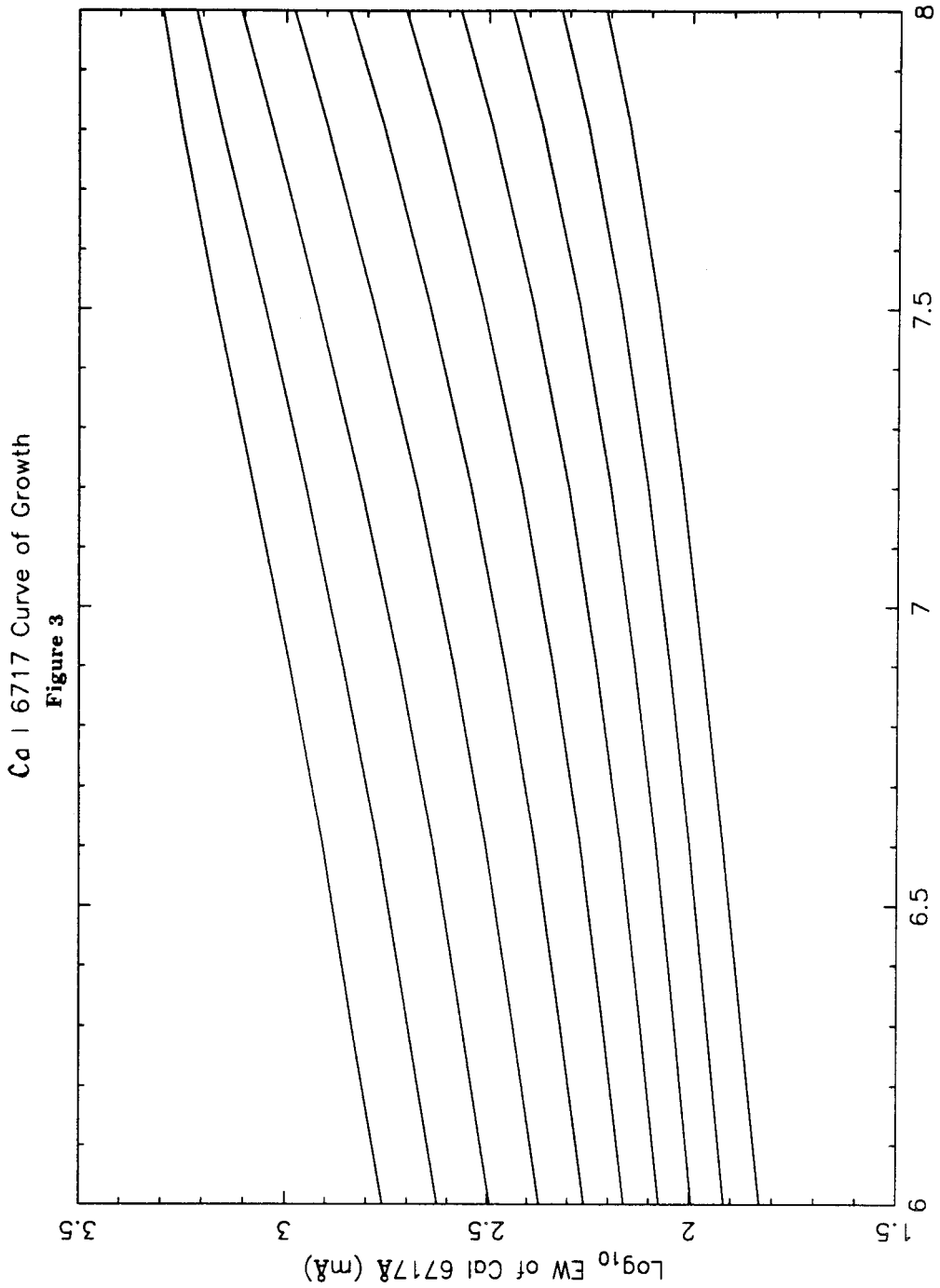
Ca I 6717 Curve of Growth
Log10 EW of CaI 6717Å (mÅ)
1.5
2
2.5
3
3.5
6
6.5
7
7.5
8
Log10 N(Ca)

Figure 3

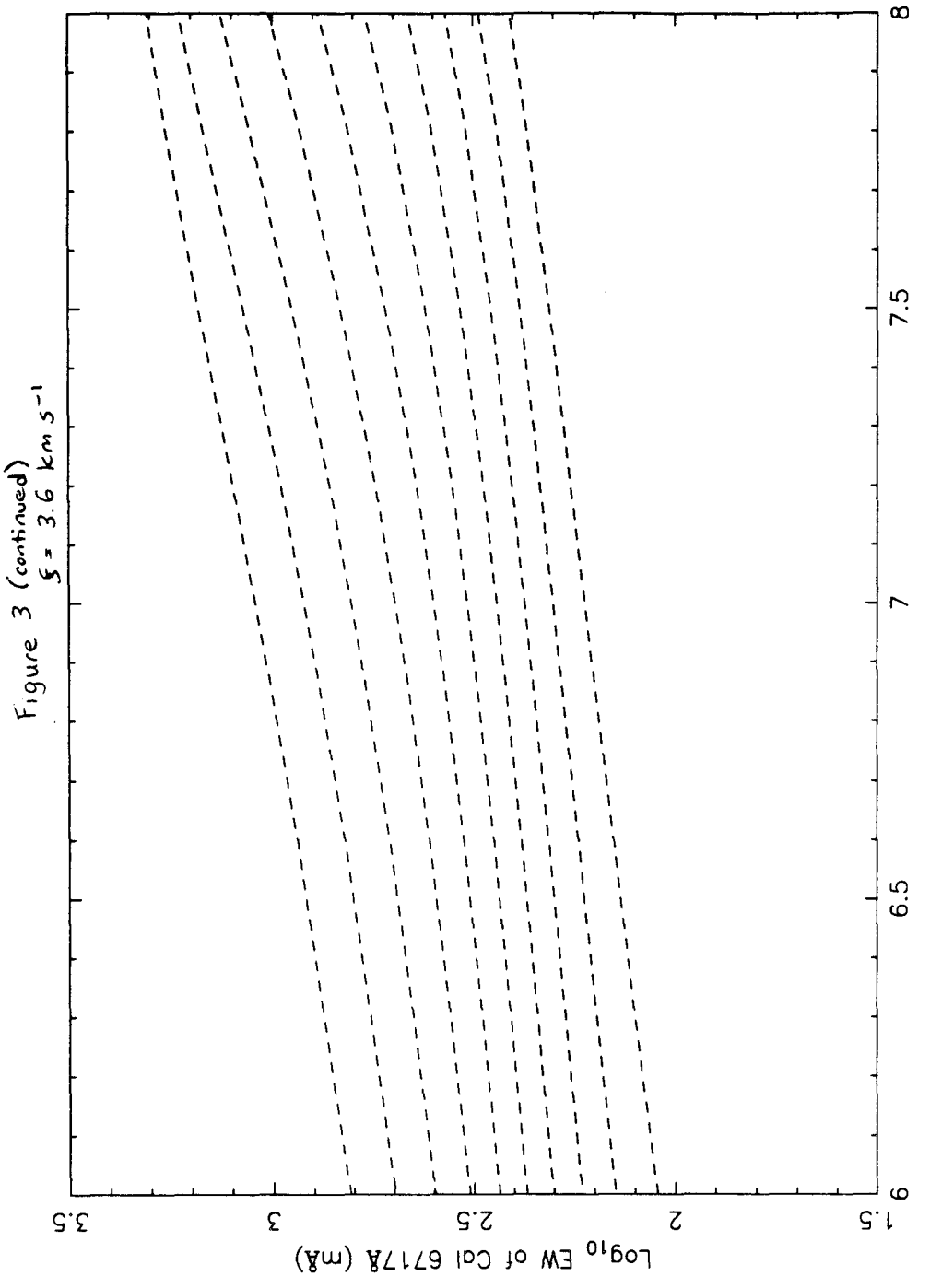

Figure 3 (continued)
$\xi = 3.6$ km s^{-1}

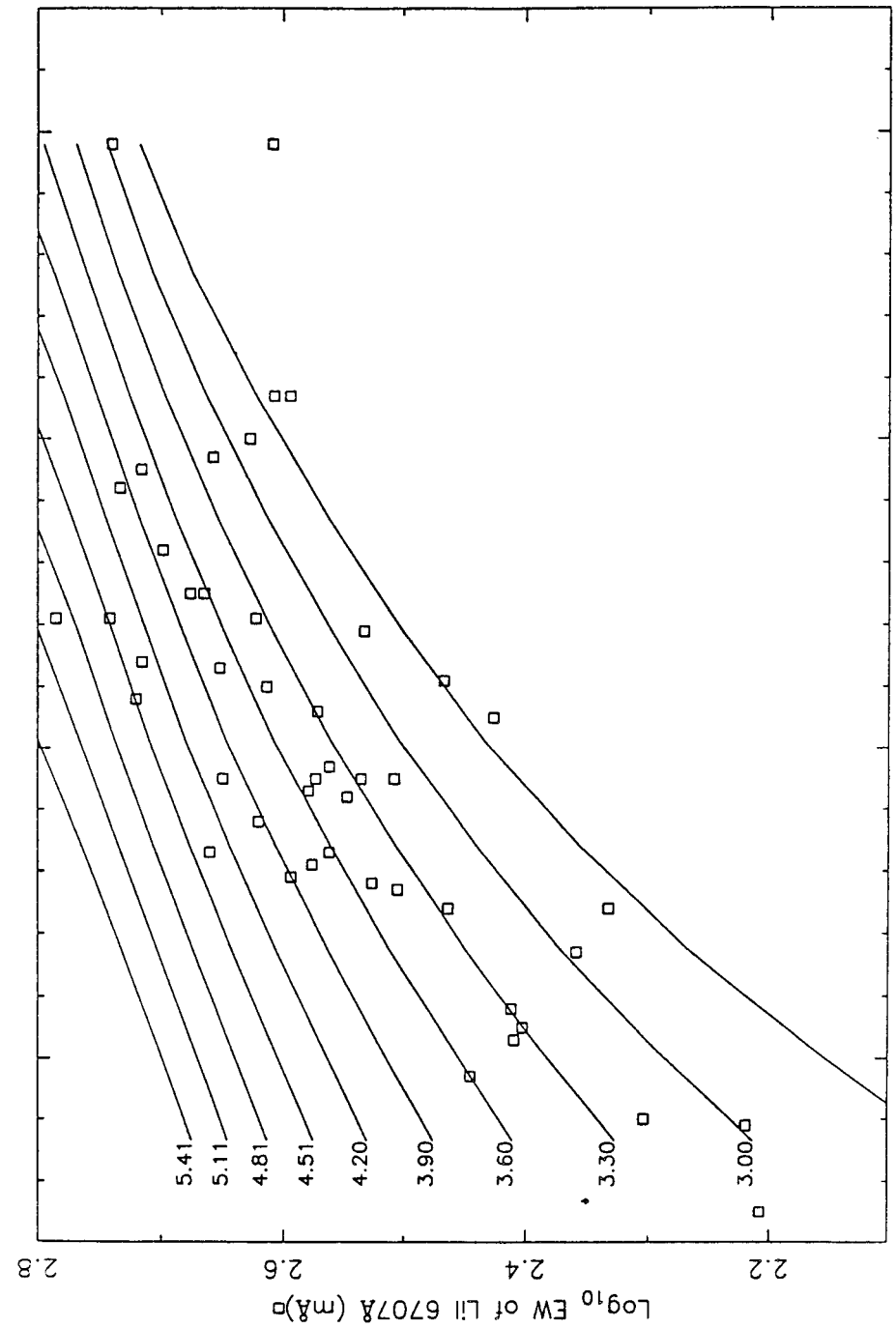
Log10 EW of LiI 6707Å (mÅ)
2.2
2.4
2.6
2.8
Log10 Teff
3.6
3.65
3.7
3.75
2.70
5.41
5.11
4.81
4.51
4.20
3.90
3.60
3.30
3.00

Figure 4a

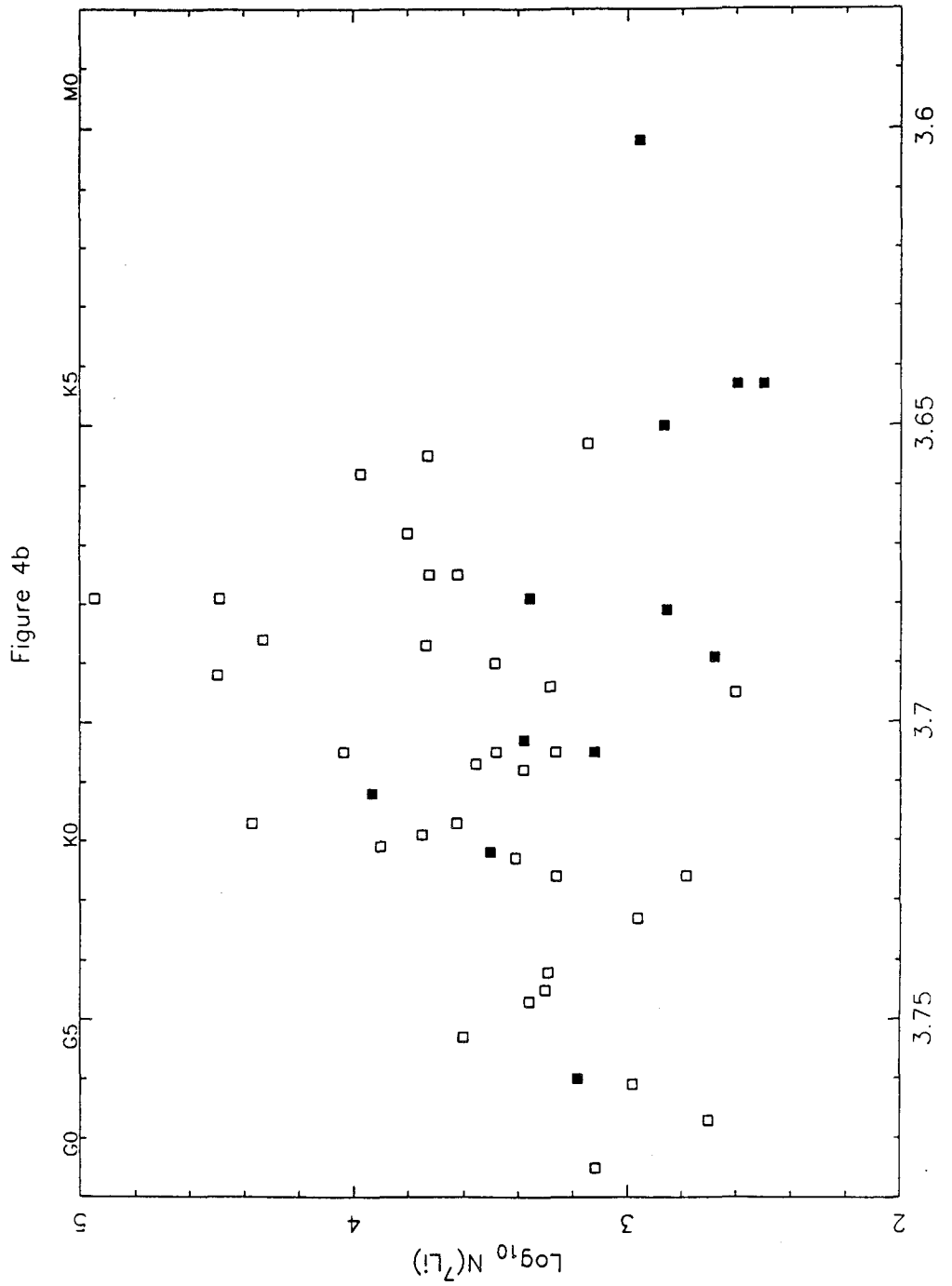

Figure 4b

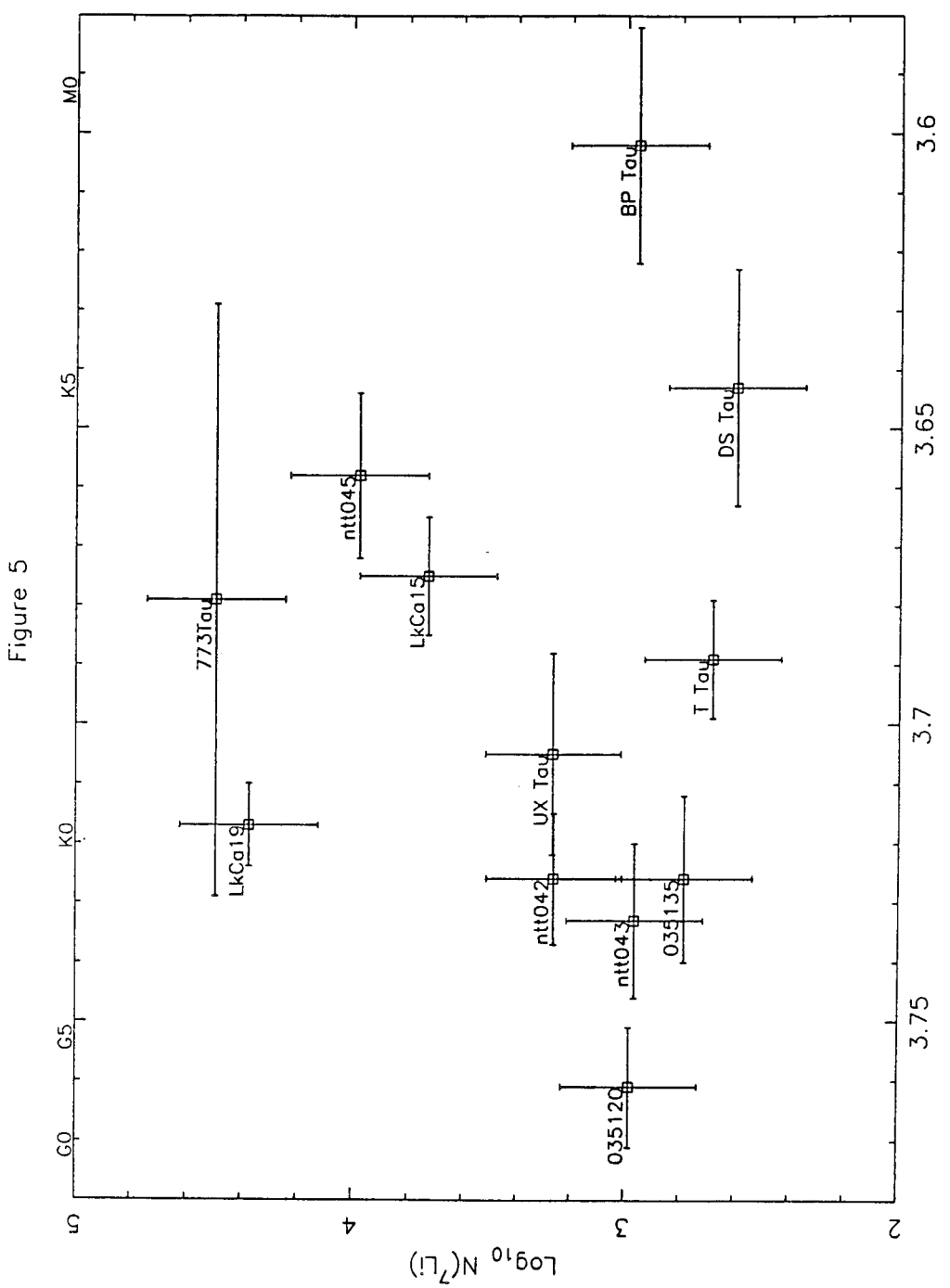
Log10 N(7Li)
Log10 Teff
G0
G5
K0
K5
M0
5
4
3
2
3.75
3.7
3.65
3.6
BP Tau
DS Tau
T Tau
UX Tau
LkCa15
ntt045
LkCa19
773Tau
035120
ntt043
035135
ntt042

Figure 5

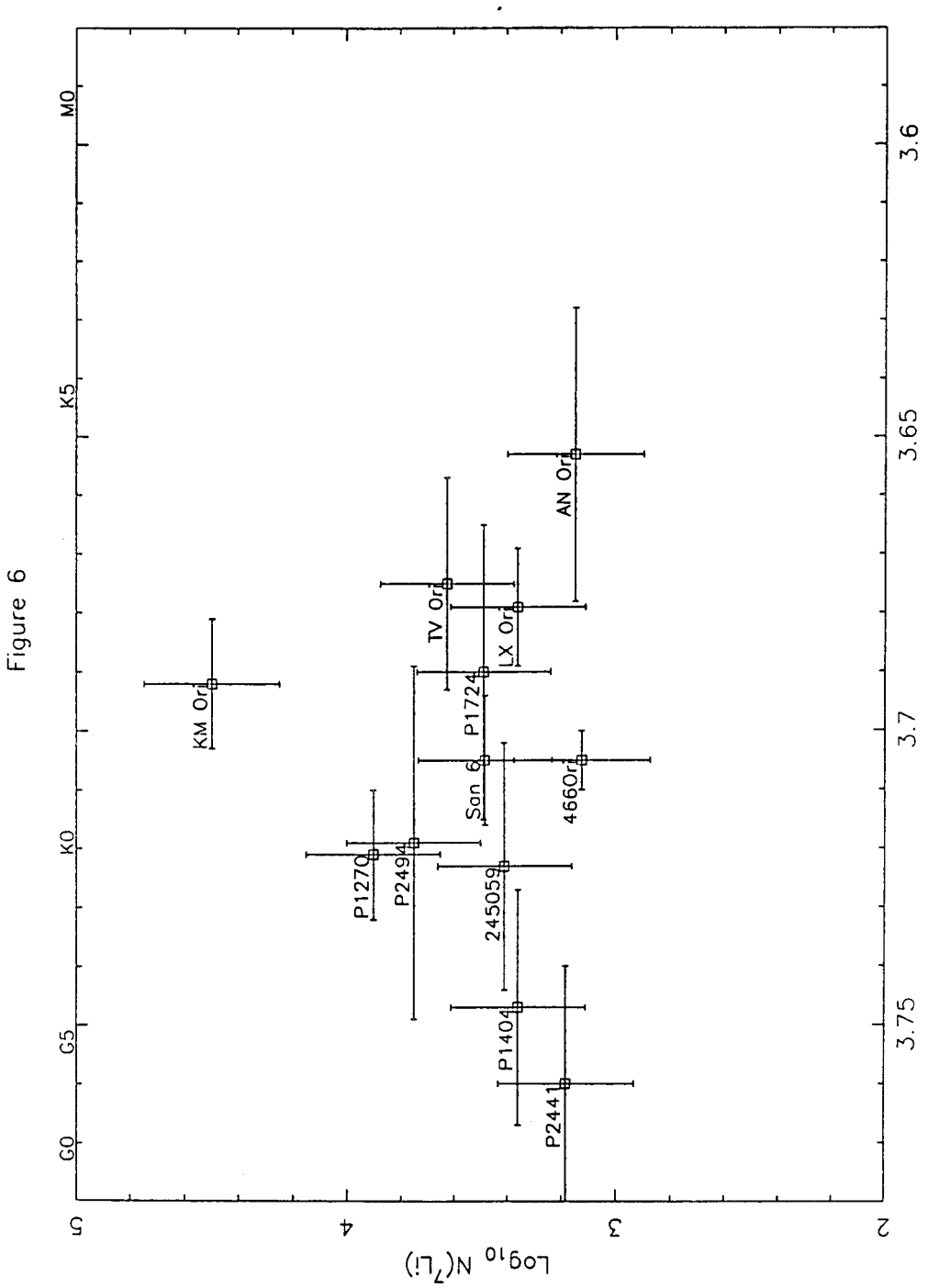
Log10 N(7Li)
5
4
3
2
G0
G5
K0
K5
M0
3.75
3.7
3.65
3.6
Log10 Teff
KM Ori
P1270
P2494
San 6
P1724
TV Ori
LX Ori
AN Ori
466Ori
245059
P1404
P2441

Figure 6

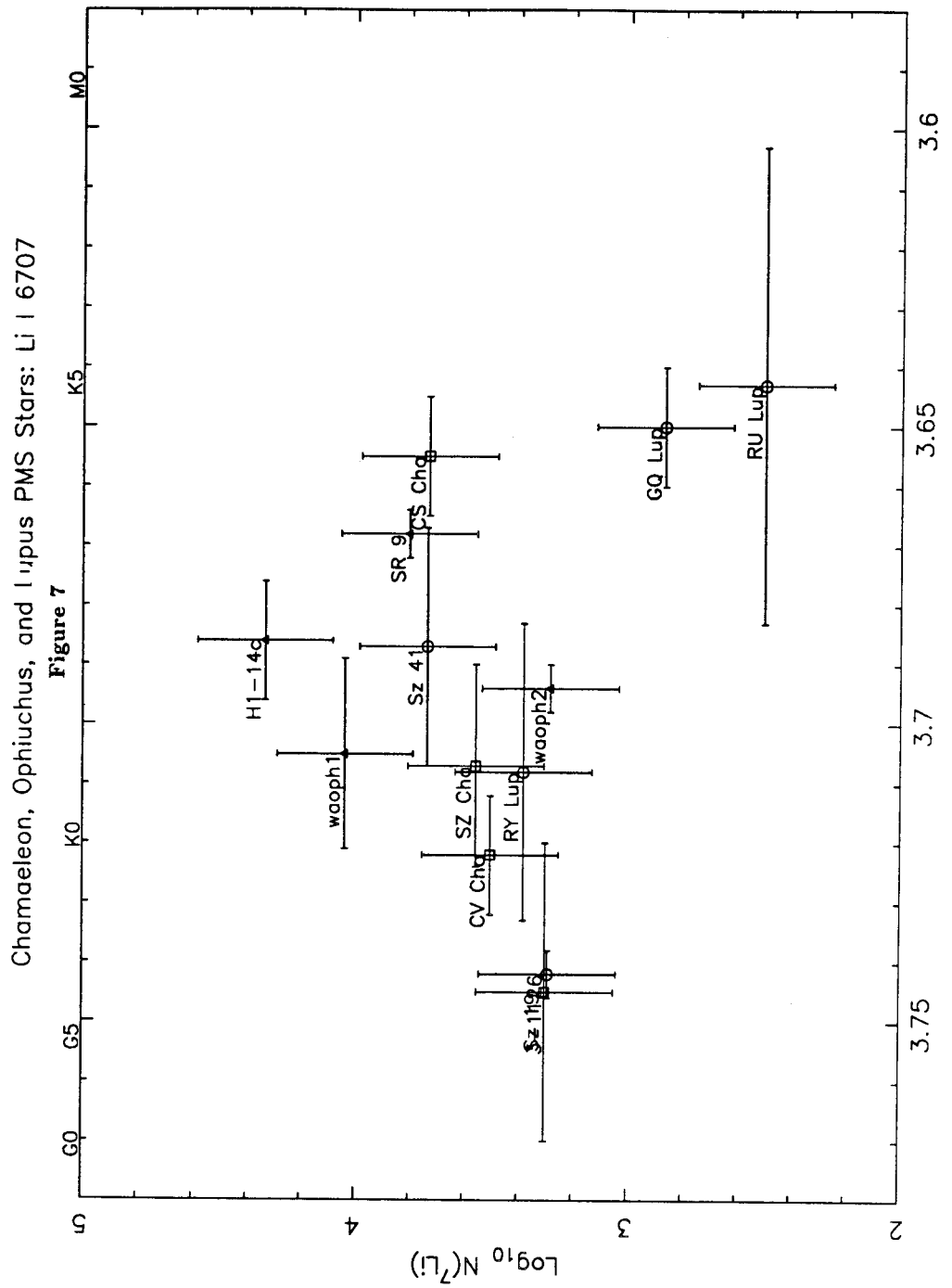
Chamaeleon, Ophiuchus, and Lupus PMS Stars: Li I 6707
G0
G5
K0
K5
M0
5
4
3
2
Log10 N(7Li)
3.75
3.7
3.65
3.6
Log10 Teff
H1-14
waoph1
Sz 41
SR 9
CS Cha
waoph2
SZ Cha
RY Lup
CV Cha
GQ Lup
RU Lup

Figure 7

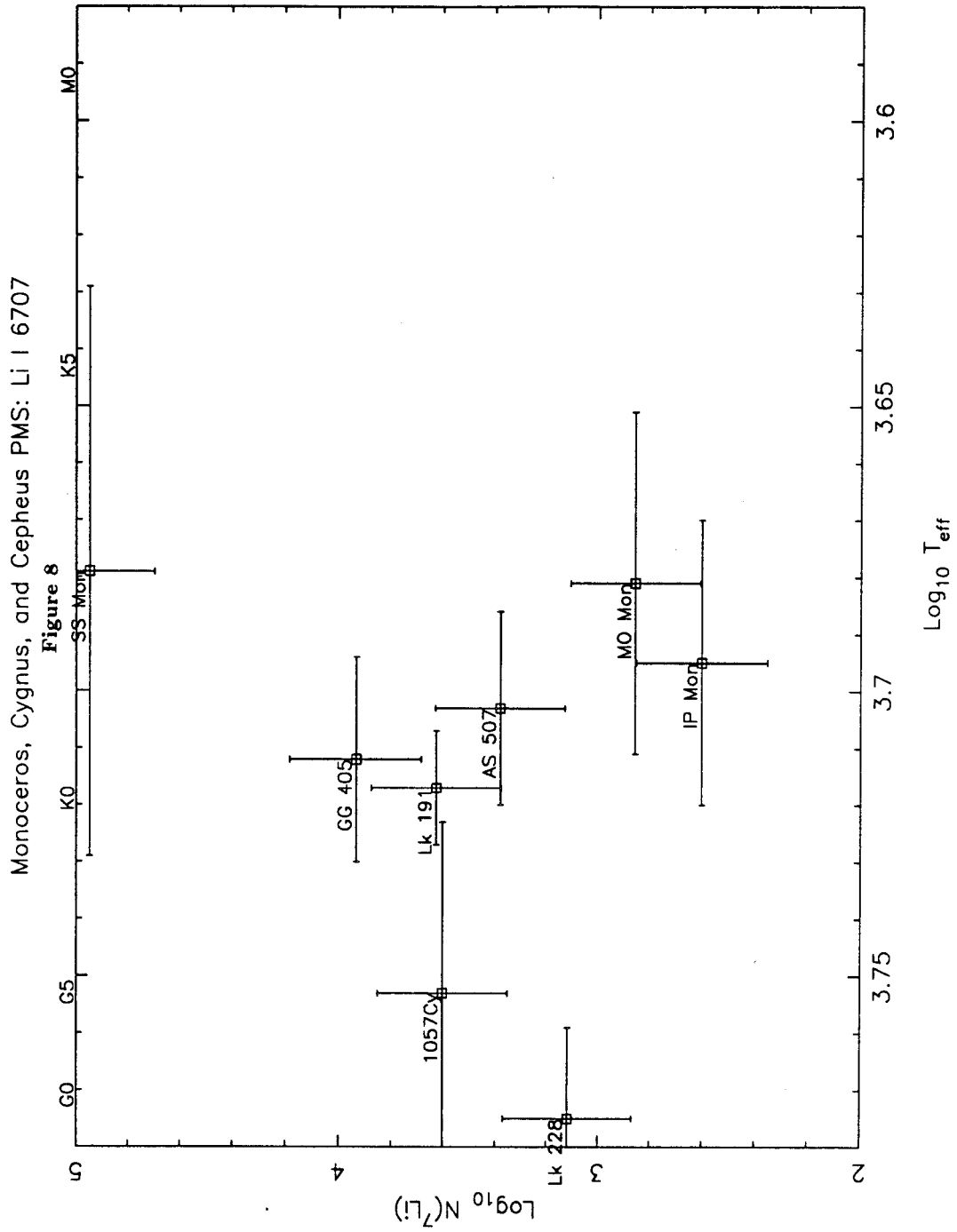
Monoceros, Cygnus, and Cepheus PMS: Li I 6707
Log10 N(7Li)
Log10 Teff
G0
G5
K0
K5
M0
5
4
3
2
3.75
3.7
3.65
3.6
SS Mon
GG 405
Lk 191
AS 507
1057Cyg
Lk 228
MO Mon
IP Mon

Figure 8

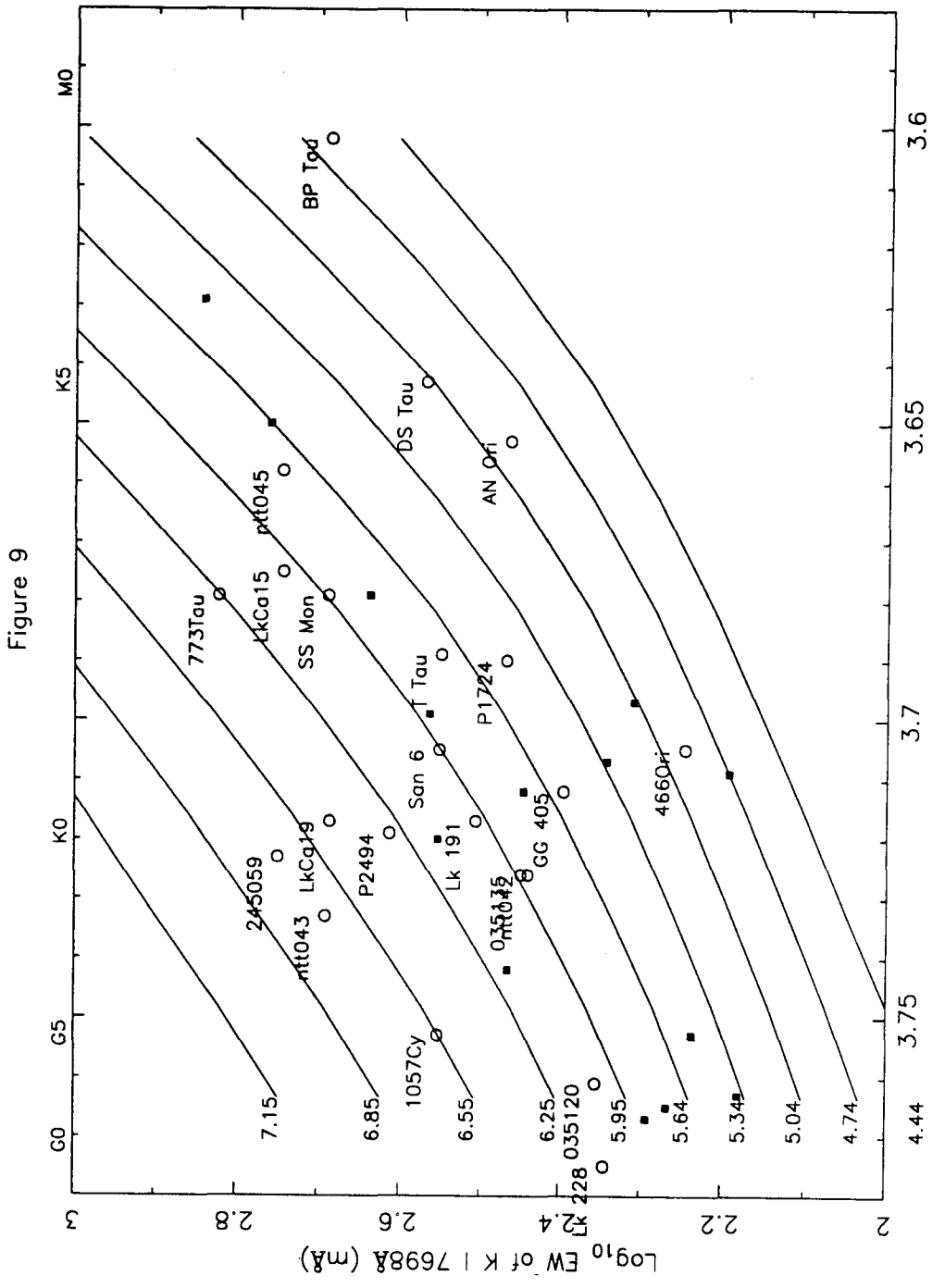
Figure 9
Log10 EW of K I 7698Å (mÅ)
Log10 Teff
G0
G5
K0
K5
M0
3
2.8
2.6
2.4
2.2
2
3.75
3.7
3.65
3.6
4.44
4.74
5.04
5.34
5.64
5.95
6.25
6.55
6.85
7.15
BP Tau
DS Tau
AN Ori
P1724
T Tau
San 6
GG 405
Lk 191
P2494
LkCa19
SS Mon
LkCa15
773Tau
1057Cy
035120
Lk 228

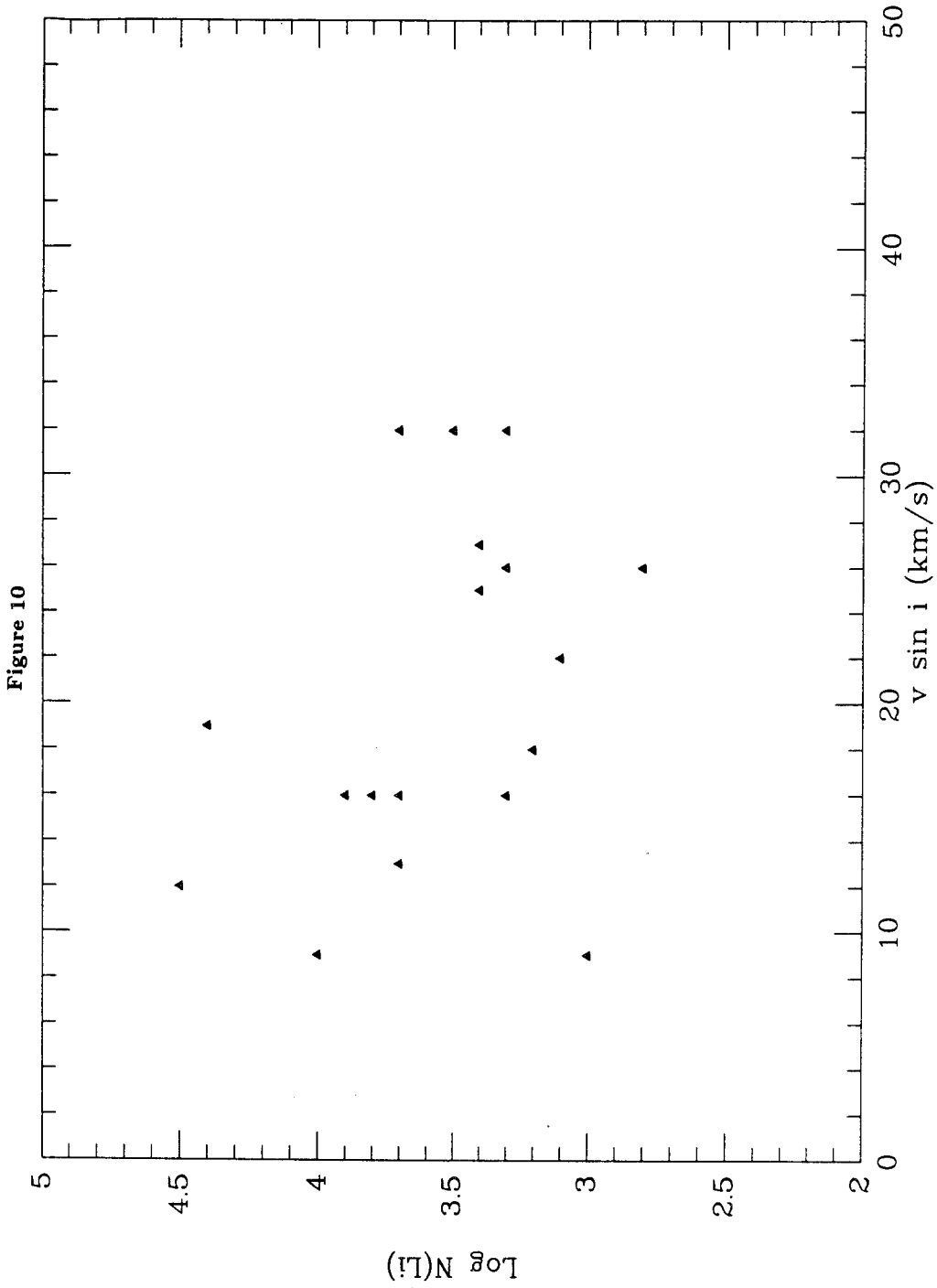

Figure 10

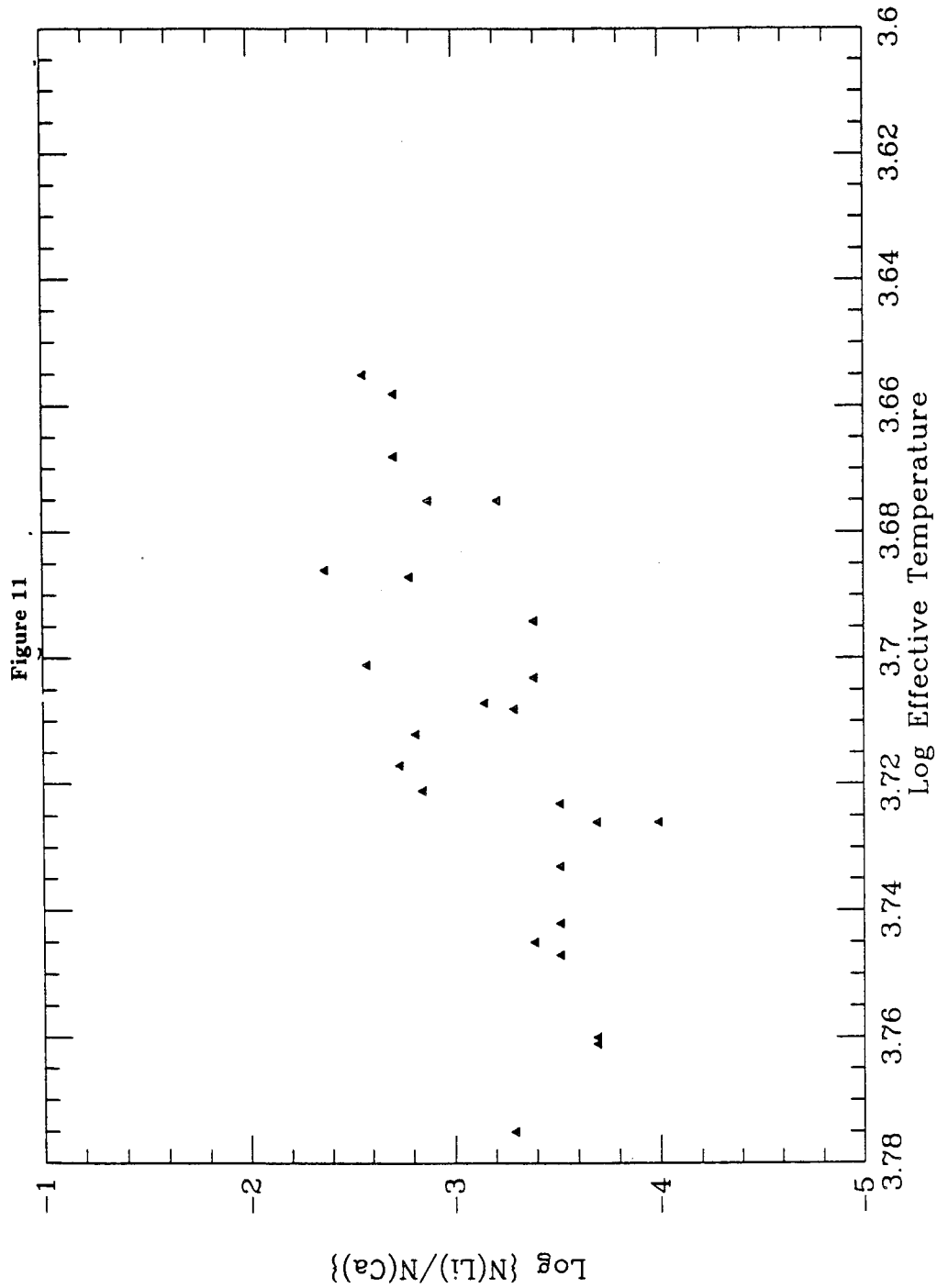
Log {N(Li)/N(Ca)}
-1
-2
-3
-4
-5
3.78
3.76
3.74
3.72
3.7
3.68
3.66
3.64
3.62
3.6
Log Effective Temperature

Figure 11

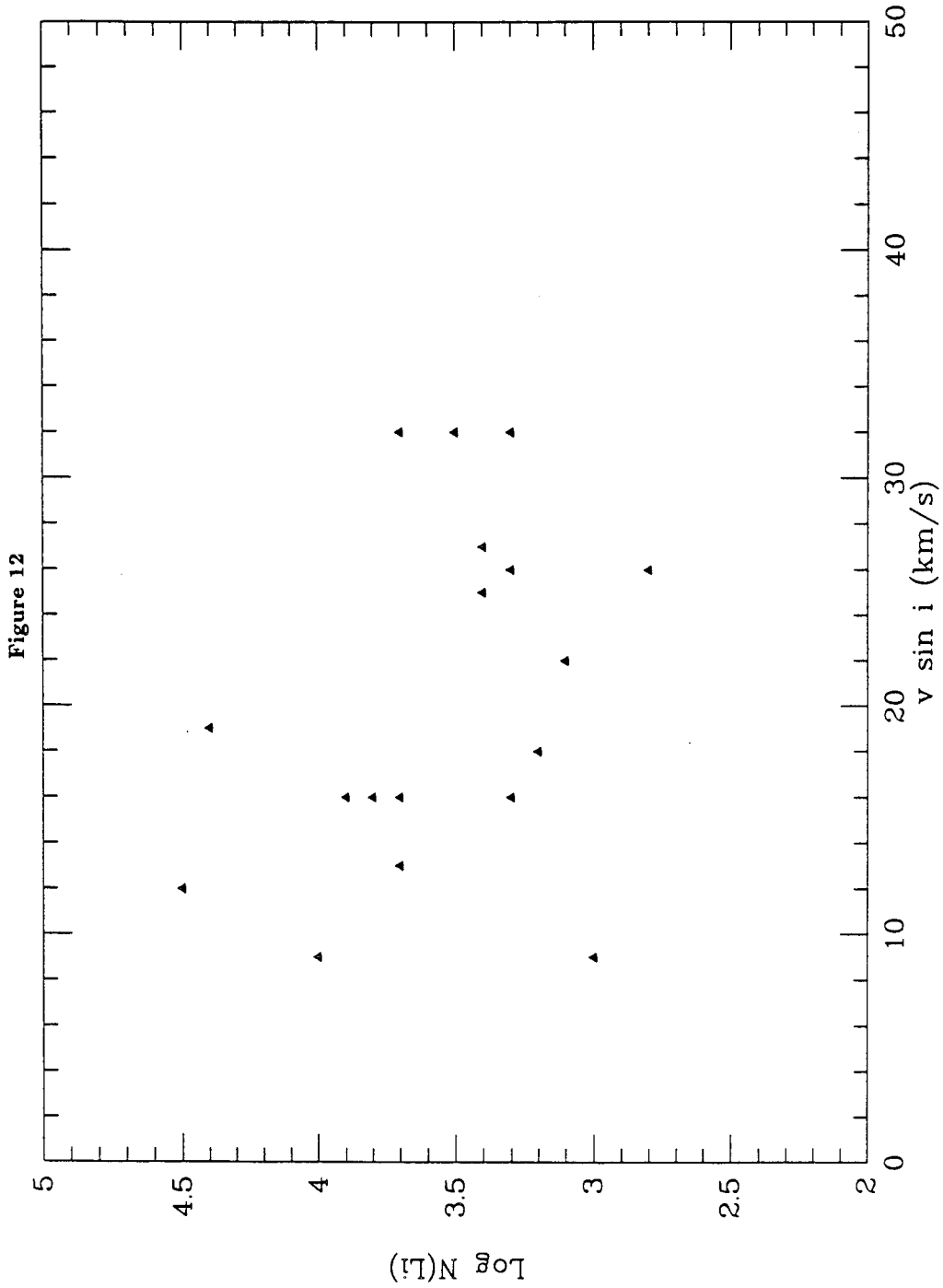

Figure 12

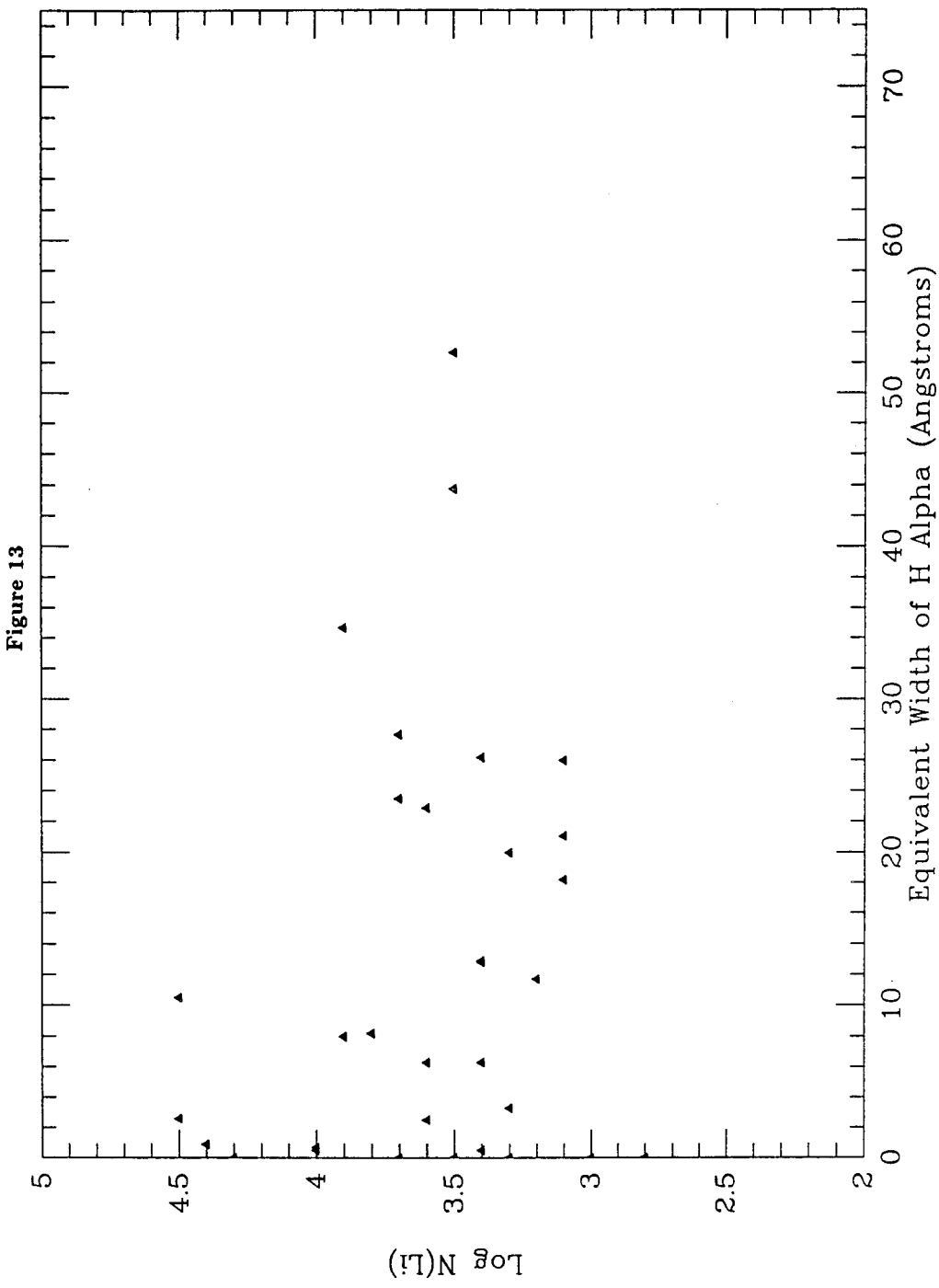
Log N(Li)
5
4.5
4
3.5
3
2.5
2
0
10
20
30
40
50
60
70
Equivalent Width of H Alpha (Angstroms)

Figure 13

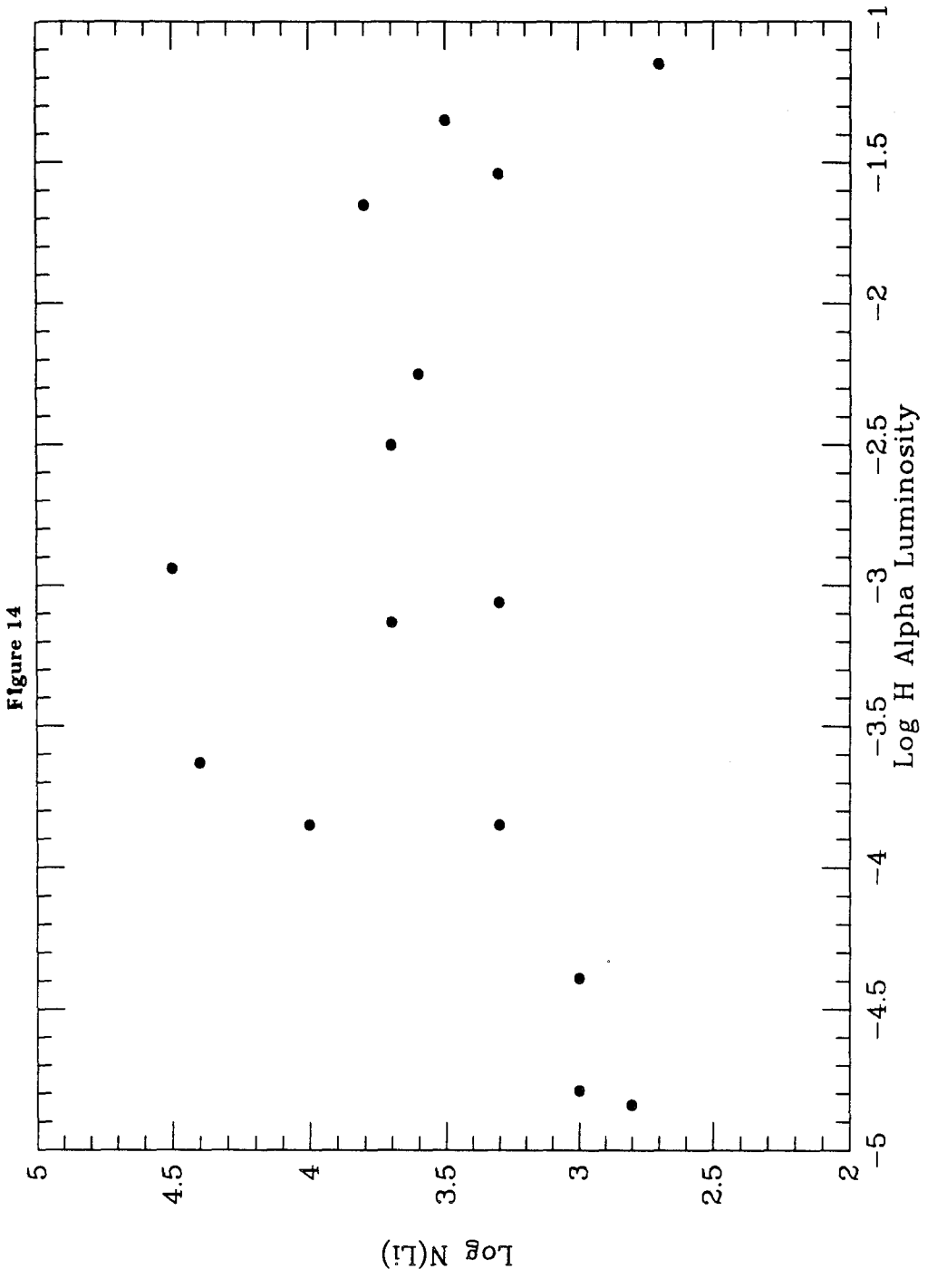

Figure 14

Figure 15

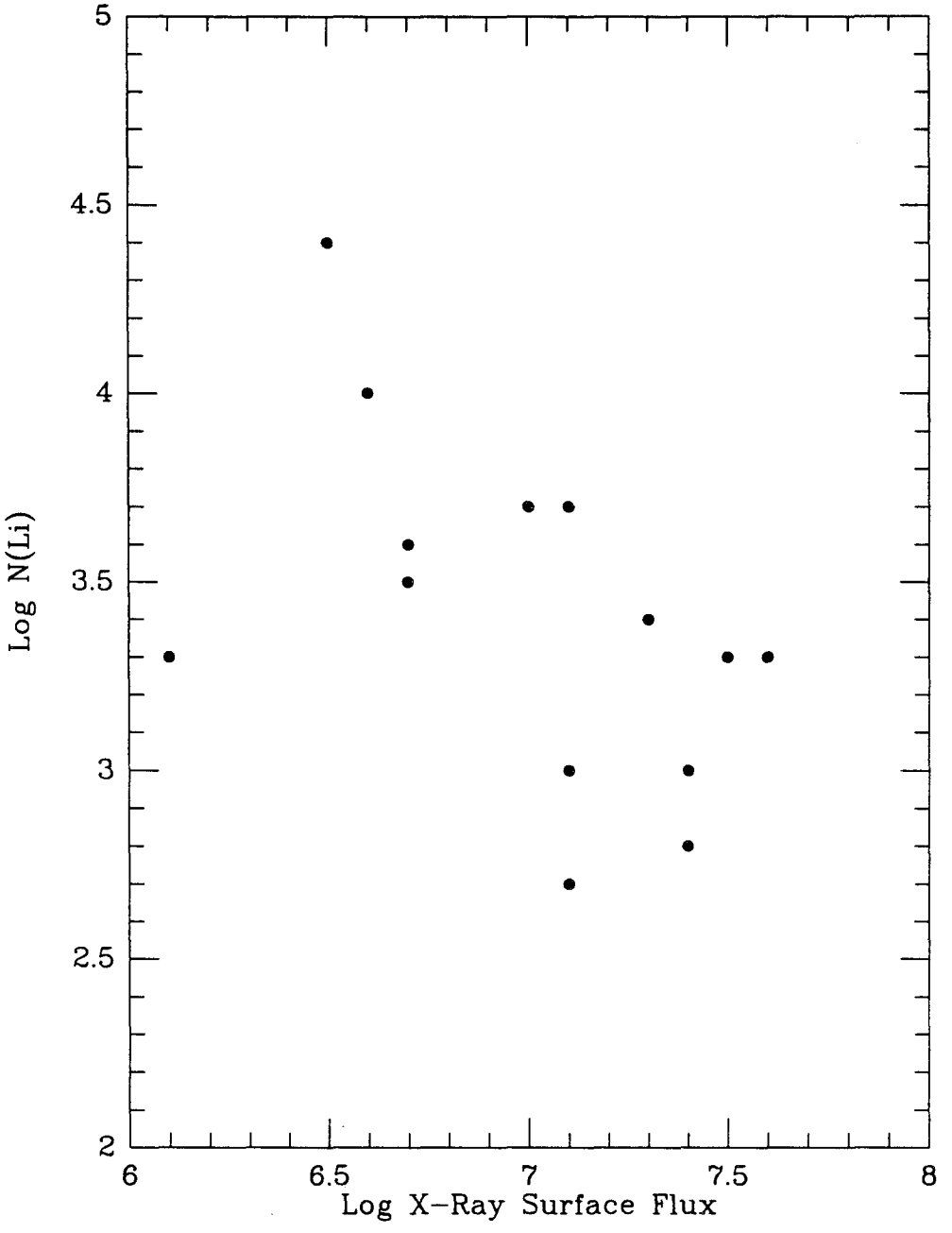

Figure 16

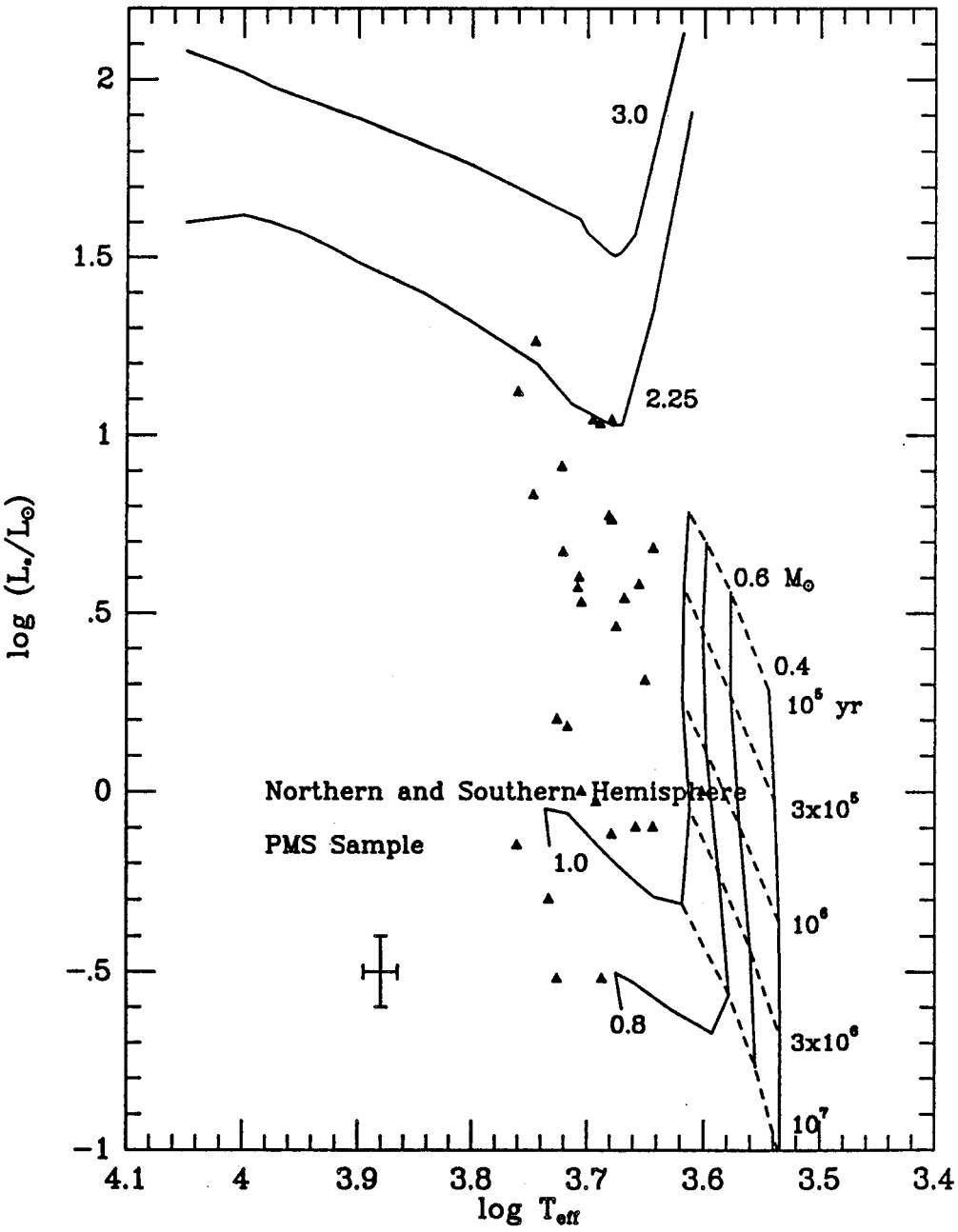
3.0
2.25
1.0
0.8
0.6 M⊙
0.4
10⁵ yr
3x10⁵
10⁶
3x10⁶
10⁷
Northern and Southern Hemisphere
PMS Sample
log (L*/L⊙)
log T_eff
2
1.5
1
.5
0
-.5
-1
4.1
4
3.9
3.8
3.7
3.6
3.5
3.4

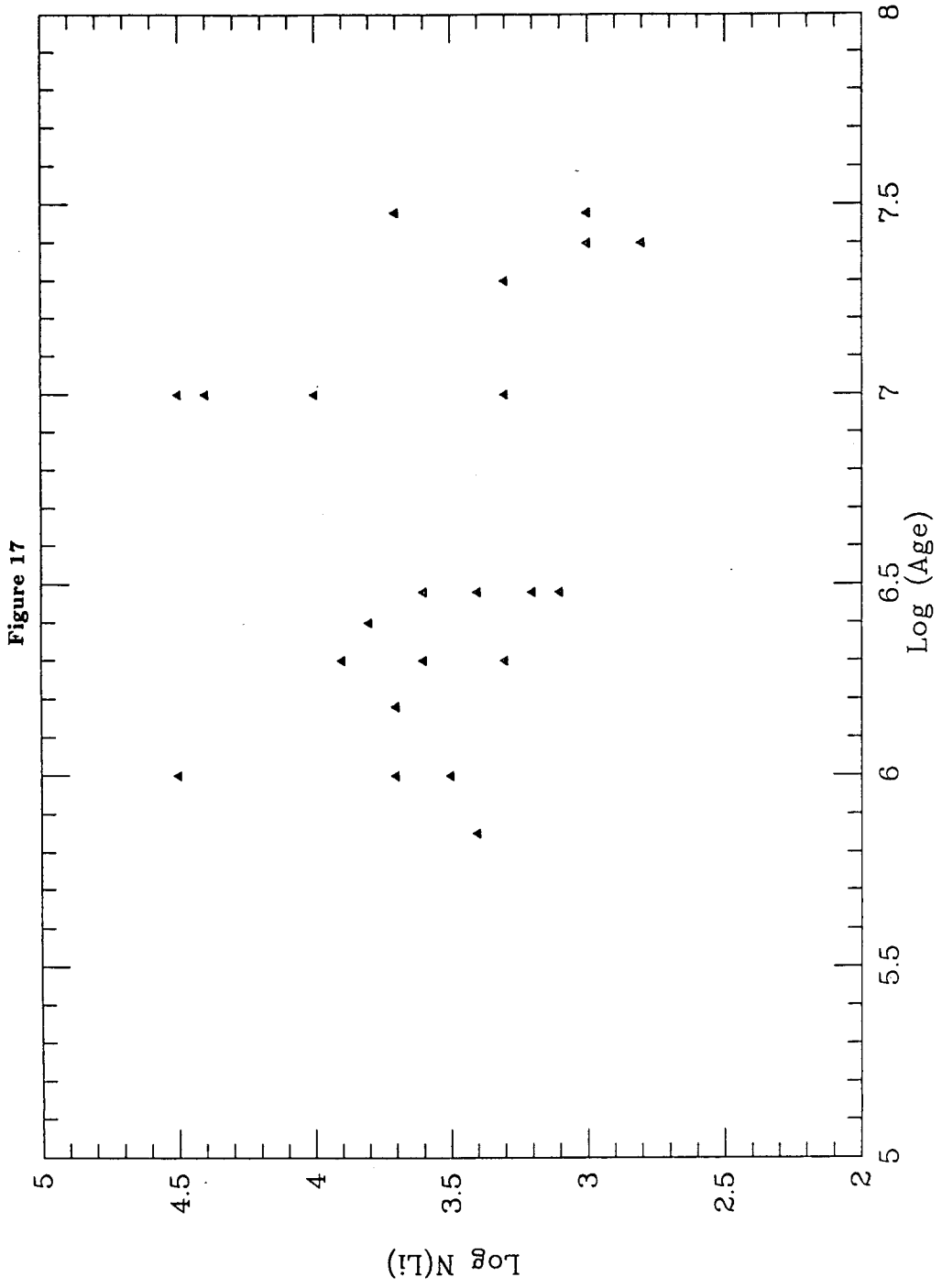

Figure 17

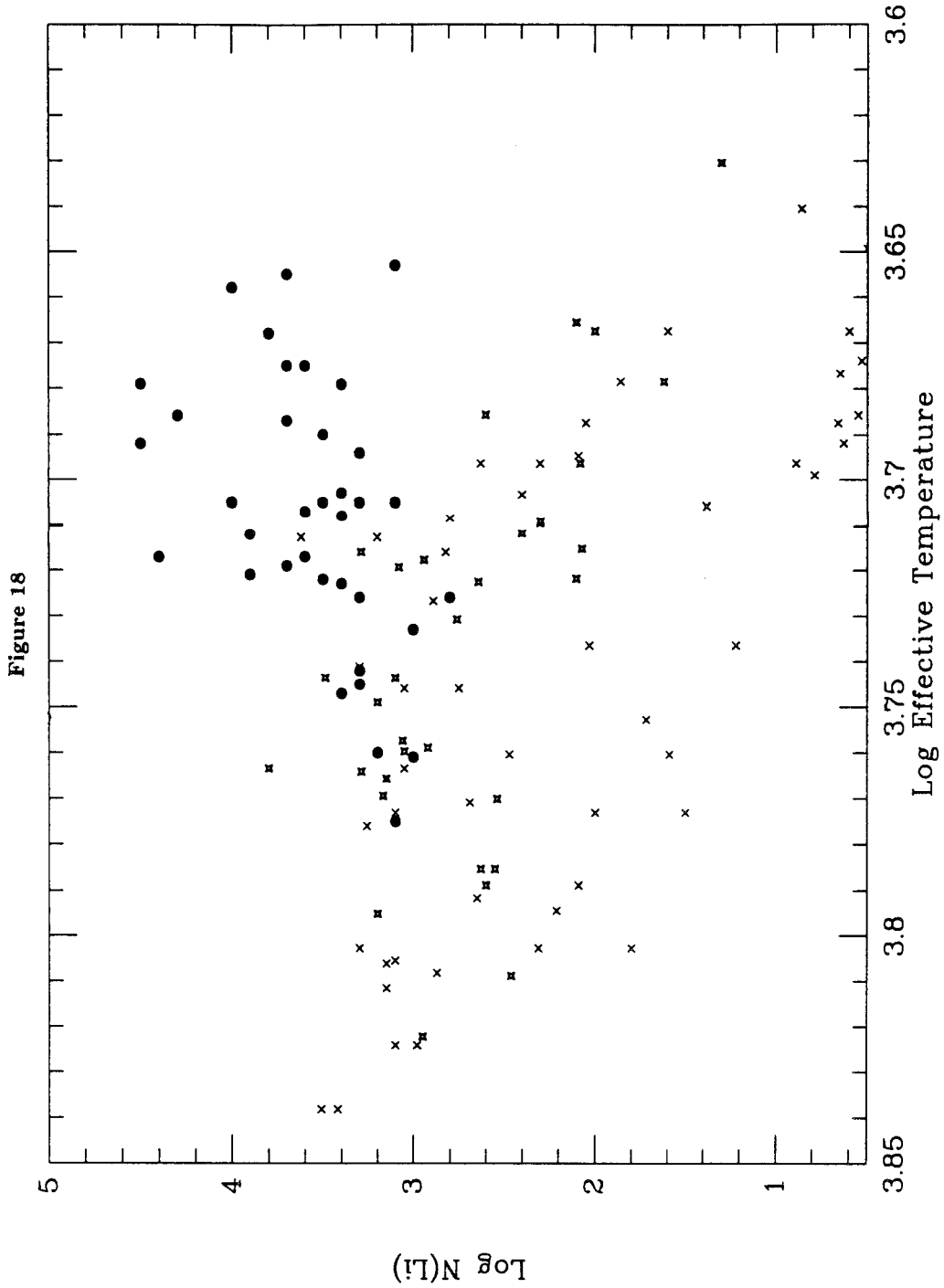

Figure 18

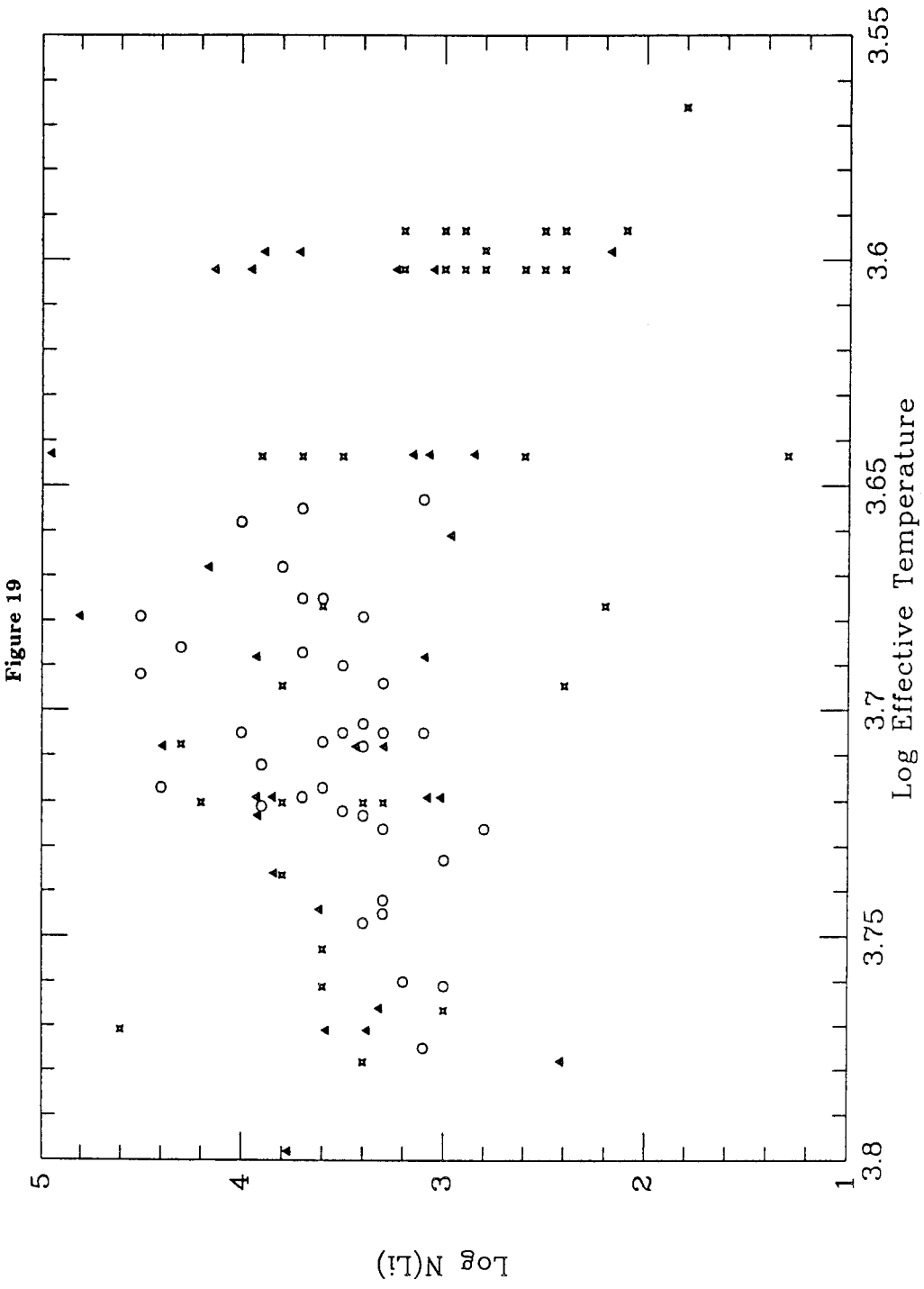

Figure 19

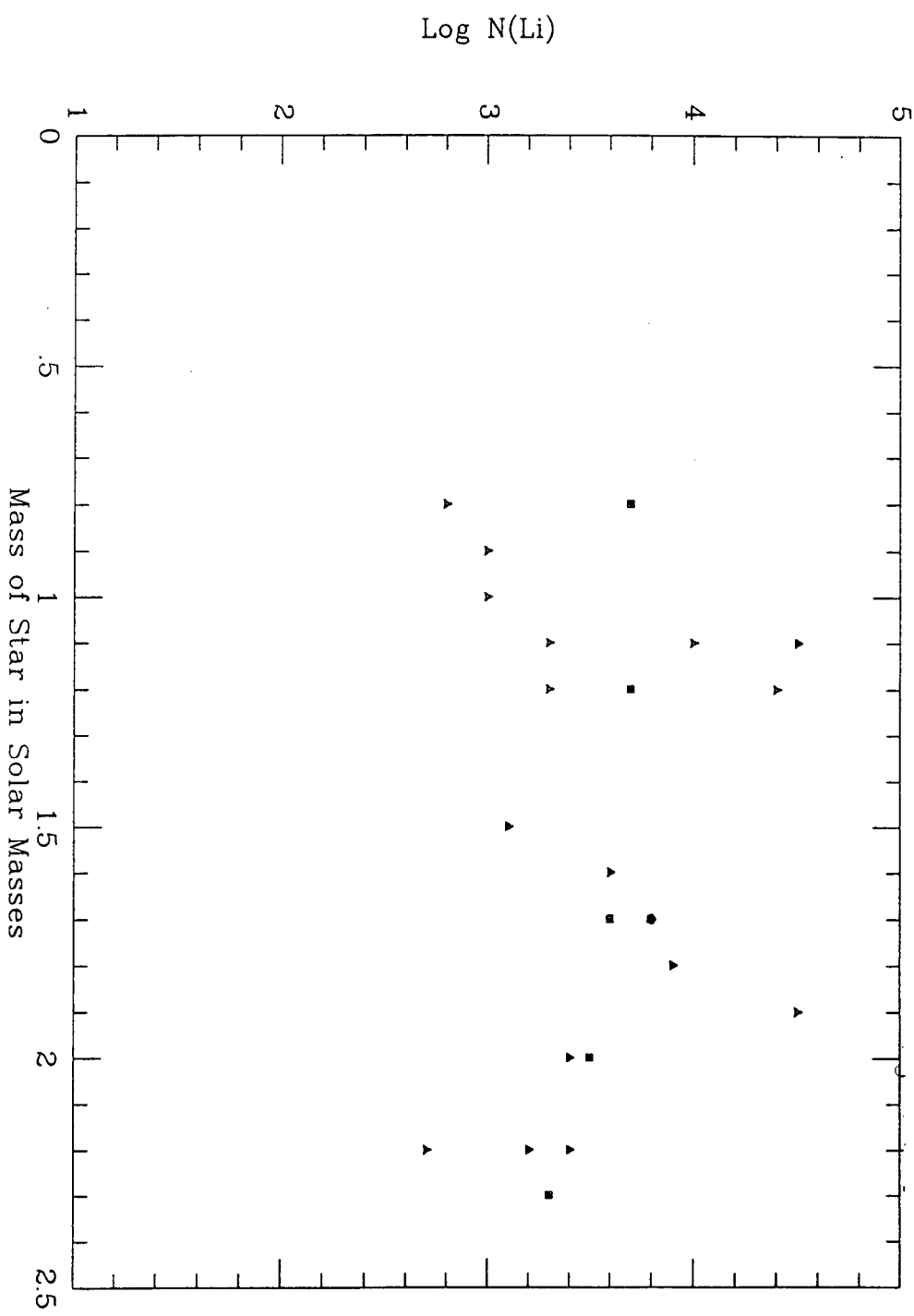

Figure 20